Centro Andaluz de Biología del Desarrollo

CSIC
CONSEJO SUPERIOR DE INVESTIGACIONES CIENTÍFICAS

JUNTA DE ANDALUCIA

DOCTORAL THESIS

Glycogen Synthase Kinase-3:
A Role in Ageing and Metabolism

Centro Andaluz de Biología del Desarrollo
Universidad Pablo de Olavide

Annmary Paul Erinjeri

Director:
Dr. Marta Artal Sanz

Seville, 2018

INDEX

● ● ●

ABSTRACT

Prohibitins (PHBs) are a class of conserved mitochondrial proteins that profoundly influence ageing. PHB depletion shortens the lifespan of wild type animals, while it causes a dramatic extension in metabolically compromised *daf-2(e1370)* mutants. This opposing lifespan phenotype is attributed to alterations in mitochondrial function and metabolism, but the exact function of PHBs is yet to be deciphered. This project was developed to better understand the function of the essential mitochondrial prohibitins in the regulation of ageing. To elucidate novel signalling mechanisms mediating the metabolic adjustments that lead to opposite ageing outcomes in response to PHB depletion, we performed a kinase RNAi screen using prohibitin deletion mutants. First, we characterized prohibitin deletion mutants. As these mutants are sterile, they are maintained balanced heterozygous. We accomplished a sorting protocol for selection of homozygous PHB mutants. We used vital Nile Red (NR) staining as a read-out as PHB depletion reduces NR staining. In order to quantify the intensity of NR staining, we developed an image analysis protocol. From the screen, we identified the conserved Glycogen Synthase Kinase-3 (GSK-3), as a strong suppressor of the reduced NR staining phenotype caused by prohibitin deletion mutants.

Beyond its role as a regulator of insulin-dependent glycogen synthesis, GSK-3 also controls critical cellular functions. We investigated how GSK-3 influences longevity in conditions of compromised insulin signalling and mitochondrial impairment. We demonstrate that GSK-3 depletion decreases wild type lifespan but does not affect *phb-2* mutants. However, the long lived *daf-2* and *phb-2;daf-2* mutants show strong suppression in lifespan upon loss of GSK-3. We show that GSK-3 is ubiquitously expressed via CRISPR-Cas9 endogenous gene tagging. We examined several parameters, including alterations in energy stores - glycogen/triglycerides, mitochondrial respiration and lipid composition to deduce how metabolic alterations upon GSK-3 depletion influence lifespan and found that these varied in a genetic background specific manner. Additionally, we also prove that the activity of GSK-3 is essential in the intestine for normal ageing and especially for the long lived *daf-2* mutants. Our data thus, delineates a novel role for GSK-3 in metabolism and its interplay with IIS and mitochondrial metabolism in ageing regulation.

• • •

ABBREVIATIONS

°C - Degree Celsius
age-1 - AGEing alteration
AMPK - AMP-activated protein kinase
Amp - Ampicillin
ATGL - Adipose triglyceride lipase
ATP - Adenosine triphosphate
bp - Base pair
cDNA - Complementary DNA
CGC - Caenorhabditis Genetics Centre
CK1 - Casein kinase I
CRISPR - Clustered regularly interspaced short palindromic repeats
daf - Dauer formation
dInR - *Drosophila* insulin like receptor
DNA - Deoxyribonucleic acid
DNC - Dorsal Nerve Cord
dsRNA - Double stranded ribonucleic acid
E. coli - *Escherichia coli*
EMS - Ethyl methanesulfonate
ETC - Electron transport chain
EtOH - Ethanol
FOXO - Forkhead box O
FUdR - Fluorodeoxyuridine
GFP - Green Fluorescent Protein
GSK-3 - Glycogen Synthase Kinase-3
GST - Glutathione-S-transferase
HSF-1 - Heat shock transcription factor-1
IGF-1R - Insulin-like growth factor-1 receptor
IIS - Insulin/ insulin-like growth factor-1 signalling
IPTG - Isopropyl- β-D- thiogalactopyranoside
IR-A - Insulin receptor-A
IR-B - Insulin receptor-B

kDa - KiloDalton
KH_2PO_4 - Potassium dihydrogen phosphate
KOH - Potassium hydroxide
LB - Luria–Bertani
$MgSO_4$ - Magnesium sulphate
MQ - MilliQ
mRNA - Messenger Ribonucleic acid
Na_2HPO_4 - Disodium hydrogen phosphate
NaCl - Sodium chloride
NAD^+ - Nicotinamide adenine dinucleotide
NaOH - Sodium hydroxide
NBRP - National BioResource Project
NGM - Nematode growth medium
NR - Nile Red
ORO - Oil -Red-O
PBS - Phosphate buffered saline
PCR - Polymerase chain reaction
PDK - Phosphatidylinositol-dependent kinase
PHA-4 - Defective pharyngeal development protein 4
PHB - Prohibitin
PI3K - Phosphatidylinositol-3-kinase
PTGS - Posttranscriptional gene silencing
RISC - RNA-induced silencing complex
RNAi - Ribonucleic acid interference
ROS - Reactive oxygen species
rpm - Revolution per minute
siRNA - Small interfering RNAs
SKN-1 - SKiNhead
Tet - Tetracycline
TOR - Target of rapamycin
Tyr - Tyrosine
UTR - Untranslated region
VNC - Ventral Nerve Cord
YA - Young Adult

1. *Caenorhabditis elegans* as a model organism

Caenorhabditis elegans (*Caeno* meaning recent; *rhabditis* meaning rod; *elegans* meaning nice) is a tiny, free-living, transparent nematode. It feeds on bacteria and can be easily isolated from rotting vegetable matter (Barriere and Felix 2014). They are up to 1mm long in length and are usually observed under a dissecting or a compound microscope (Brenner 1974). It is easy and cheap to propagate large quantities of worms in the lab, either on a nutritive agar with a layer of *E. coli* cells or in liquid medium. Cholesterol is added because *C. elegans* is unable to synthesize sterol *de novo*. This method has been standardized amongst laboratories to enhance reproducibility of experiments (Houthoofd et al. 2003). Worms are usually grown at 15°C or 20°C. Worms develop much slower at lower temperatures, whereas at higher temperatures the rate of development is faster but reproductive health is often compromised.

Originally derived from mushroom compost isolate, Dr. Sydney Brenner introduced the N2 strain that is being used as wild type, in the late 1950s. Though he had initially developed the nematode as a model organism to help answer questions in development and neurobiology (Brenner 1974), over time, *C. elegans* has been developed and studied in laboratories worldwide in all research areas including metabolism, gene regulation, protein biology, ageing, evolution, etc. The *Caenorhabditis* Genetics Center (CGC), University of Minnesota (Gershon and Gershon 2002; Stiernagle 2006) provides nematode strains to the *C. elegans* community and it is recommended that experiments should be performed with stocks provided by the CGC. *C. elegans* has three Nobel prizes to its credit - awarded to Dr. Brenner, Dr. Horvitz, and Dr. Sulston in 2002 for their discoveries concerning genetic regulation of organ development and programmed cell death (apoptosis), awarded to Dr. Fire and Dr. Mello for their work on RNA interference *(RNAi)* in 2006 and awarded to Dr. Chalfie in 2008 for development of green fluorescent protein (GFP) as a biological marker (Corsi et al. 2015).

1.1 Life cycle of *C. elegans*

The lifecycle of *C. elegans* at 25°C is 3 days. During its normal development, the worm undergoes embryogenesis, hatches from an egg and then progresses

through four larval (L1 to L4) stages to an egg-laying adult (Figure 1). Worms increase in size as they progress through the larval stages. The end of each stage is marked by a period of inactivity - lethargus. During this period, the worms cease pharyngeal pumping. Lethargus ends with the molting (ecdysis) of the old cuticle. Reproductive adult hermaphrodites produce progeny for a period of 2-3 days, ~ 12 hrs after the L4 molt. Without food, animals arrest at the L1 stage. When they resume feeding, they grow normally to adulthood.

Under conditions of environmental stress, namely, alterations in population density, food availability and ambient temperature, an arrested developmental variant of the worm is formed called the dauer larva (from the German *dauern*, to last or to endure). The decision to form dauer is taken at the late L1 larval stage. Dauers were first described by Cassada and Russell (Cassada and Russell 1975) and exhibit different morphological and behavioural features. Dauer larvae are thinner in comparison to all the other larval stages (Corsi et al. 2015) (Figure 1) and have a specialized cuticle. Dauer larvae do not pump, their oral orifices are closed by an internal plug and their pharynxes are constricted. They can be easily differentiated from L3 larvae under a dissecting microscope (Hu 2007). Dauer larvae can survive for up to a year if prevented from desiccation (Wood and Johnson 1994). Once favourable conditions are sensed, dauers resume development maintaining their normal lifespan. Therefore, the dauer stage is considered a non-ageing developmental stage.
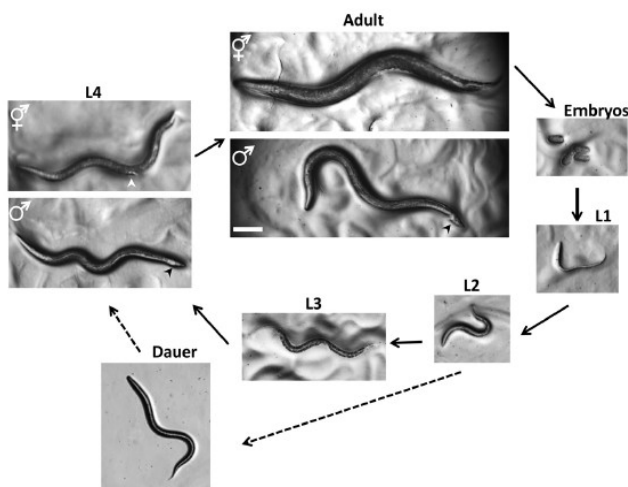
Figure 1: Life Cycle of *C. elegans.* Bar 0.1 mm (Corsi et al. 2015).

The worm exists mostly as a self-fertilizing hermaphrodite, though males arise at a frequency of <0.2%. It is hard to distinguish between hermaphrodites (females) or males until the L4 stage (Figure 1). In adults, females are characterized by a wider girth and tapered tail, whereas, males have a slimmer girth and a fan-shaped tail (Figure 1, Adult, black arrowhead).

1.2 *C. elegans* tissue system

C. elegans has a defined tissue system. During hermaphrodite development, 1090 somatic cells are generated; of which 131 undergo apoptosis at distinctive times. There are 959 somatic nuclei in an adult hermaphrodite of which 302 are neurons and 95 are body wall muscle cells. On the other hand, the adult male has 1031 somatic nuclei, of which 381 are neurons (extra neurons are mostly for male mating behavior). The adult male despite having more cells, is slightly slender and shorter (approx. 0.8 mm) as compared to the hermaphrodite. The animal is composed of a series of concentric tubes (Figure 2C). The epidermis encloses a pseudocoelomic fluid-filled cavity that houses the main organ systems.
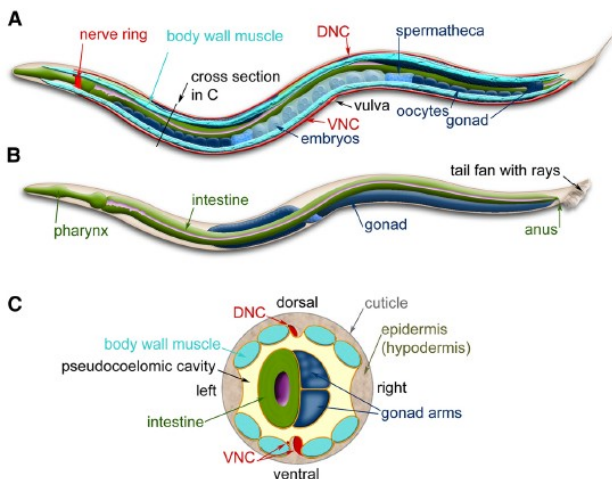
Figure 2: Anatomical features of *C. elegans.* **A.** Hermaphrodite worm. **B.** Male worm. **C.** Cross-section of the hermaphrodite in **(A)** shows the four body wall muscle quadrants surrounded by the epidermis and cuticle with the intestine and gonad housed within the pseudocoelomic cavity (Images modified from www.wormatlas.org).

Epidermis - The epidermis of the embryo through a series of cell fusions makes large multinucleate epidermal cells that secrete the cuticle. The cuticle is a protective layer of specialized extracellular matrix (ECM), composed of collagen, lipids and glycoproteins and establishes body shape and provides anchoring points for muscle contraction (Figure 3A). Mutations in genes required for cuticle formation produce visible phenotypes, example - the Roller

(Rol) phenotype (a result of mutations in collagen genes wherein animals move in a corkscrew fashion) or the Dumpy (Dpy) phenotype (wherein worm has normal width but reduced length). At the end of each larval stage, *C. elegans* sheds its cuticle and secretes a new one to house the growing organism.
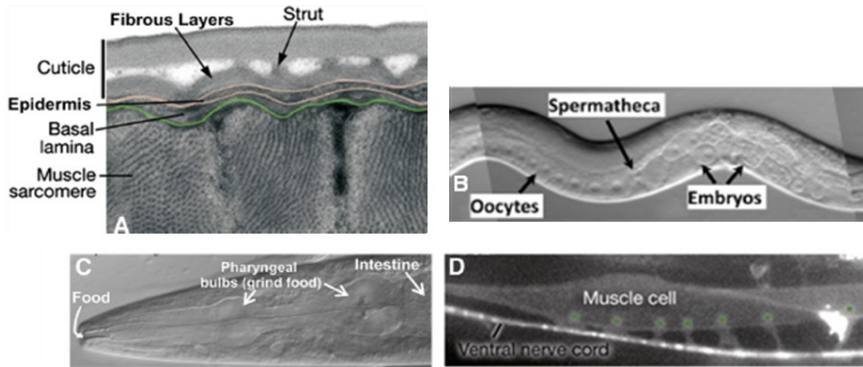
Figure 3: Tissue morphology of *C. elegans*. **A.** Cross section of the outer layers of the worm show muscle cells below the epidermis and cuticle. Transmission electron microscopy (TEM) image **B.** Developing oocytes in the gonad (rectangular cells - clear, circular nucleus inside) followed by the spermatheca (where oocytes are fertilized), and multiple embryos in the uterus **C.** Anterior view of the worm showing the mouth, the pharynx, and the start of the intestine **D.** Single body wall muscle cell with 6 muscle arms extending to the ventral nerve cord (lateral view) (Images from www.wormatlas.org).

Muscles - Body wall muscles that run along the length of the body (Figure 2A and 3D) are four quadrants that are connected to the epidermis. The regular contraction and relaxation of these muscles leads to the sinusoidal movement of the animal. Apart from body wall muscles, *C. elegans* has muscles that control eating - pharyngeal muscles; egg laying - vulval and uterine muscles and the contractile gonad sheath, mating - male specific tail muscles and defecation - enteric muscles.

Digestive System - Bacteria enters through the mouth (anterior region of the animal) and passes through the pharynx, a two-lobed neuromuscular pump that grinds the food before it is passed on to the intestine for digestion (Figure 3C). The *C. elegans* intestine consists of 20 large, polyploid epithelial cells arranged in pairs that form a tube running the length of the animal. The intestine is attached to the posterior pharynx (Figure 4A).

The primary function is digestion of food and absorption of nutrients. It also is a storage organ involved in synthesis and storage of macromolecules. It contains a large number of storage granules that change in size, shape and number during development (Figure 4C). The intestine is also involved in initiation of innate immune responses to pathogens. In hermaphrodites, the intestine is also involved in synthesis and secretion of yolk particles. The intestine is also thought to be the major organ in which fatty acid metabolism takes place.
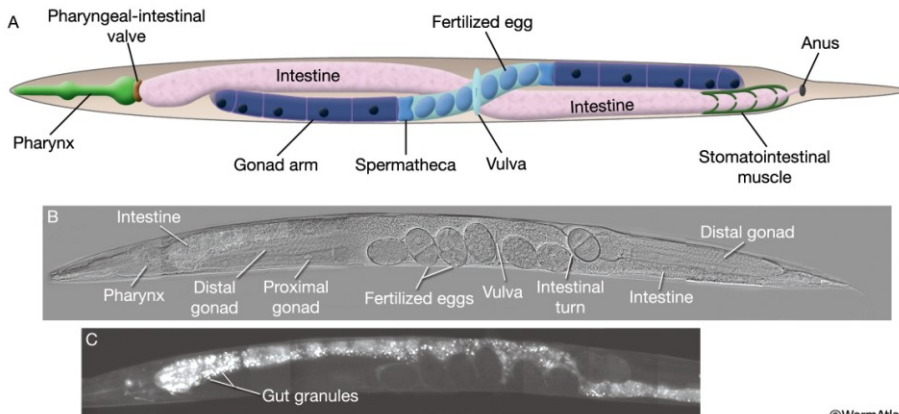
Figure 4: The intestine of *C. elegans* . **A.** The intestine is positioned on the left side of the body anterior to the vulva and on the right side of the body posterior to it (ventral view). **B.** Adult intestine runs parallel to the gonad along the length of the body (ventral view). DIC image. **C.** Autofluorescent birefringent granules fill the intestine throughout its length. This is the same animal as in B. Epifluorescent image. Images from Wormatlas.

Nervous system - The nervous system of the adult hermaphrodite has 302 neurons whereas an adult male has 383 neurons (Figure 5). This simplicity was a key feature when Dr. S. Brenner proposed *C. elegans* as a choice for a new model organism (Brenner 1974).
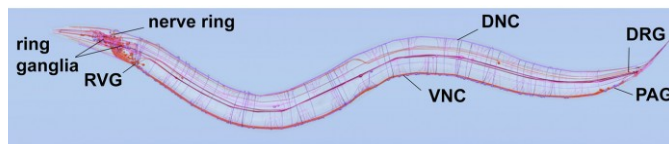
Figure 5: *C. elegans* nervous system. Image shows some major nerve bundles, ventral nerve cord (VNC), dorsal nerve cord (DNC), nerve ring and ganglia - ring ganglia, retrovesicular ganglion (RVG), pre-anal ganglion (PAG), dorsal-root ganglion (DRG) (Image is from the OpenWorm browser utility (openworm.org)).

A majority of neuronal cell bodies are arranged in the head, in the ventral cord and in the tail. Neurons have a simple structure with one or two neurites (or processes) exiting from the cell body with the exception of some, for example - mechanosensory neurons, that have branched neuritis.

Reproductive system - The somatic gonad, located at the centre of the body, consists of two mirror-image U-shaped tubes in hermaphrodites (Figure 2A,B), whereas in males the gonad consists of a single U-shaped lobe (not shown). Both gonads house the germline where the oocytes and sperm develop (Figure 3B, 6A). The somatic gonad and the germline develop together during larval stages until animals reach maturity at the young adult stage. Oocytes can be fertilized by sperm from the hermaphrodite or sperm obtained from males through mating. In the *C. elegans* germline, one can observe all stages of meiosis at once as the germline is a visible gradient of development (Figure 6). This property makes it extremely useful for germline studies (Figure 6B).
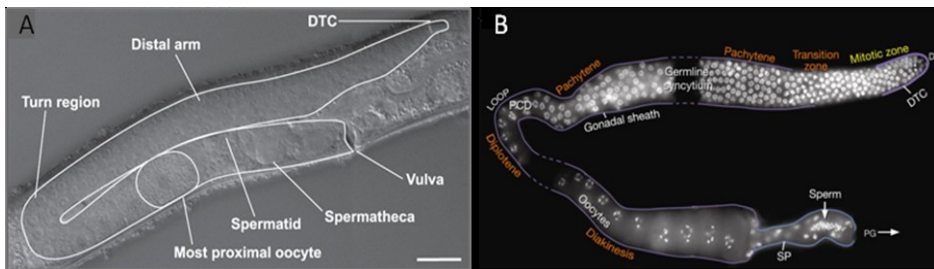
Figure 6: *C. elegans* germline. **A.** Micrograph of a single early adult gonad arm, with gonad arm and proximal-most oocyte outlined. When the first oocyte is ovulated, sperm are pushed into the spermatheca (Atwell et al. 2015). **B.** Single gonad arm dissected from a hermaphrodite showing germ cell DNA (DAPI stained). Meiosis begins in the Pachytene region (upper right) and continues around the loop of the gonad until oocytes are formed. Stored sperm are located in the spermatheca of the gonad (bottom right). PCD - Programmed cell death. Images from WormAtlas (www.wormatlas.org).

Secondary sexual mating structures are the vulva in the females and the fan-shaped tail in males. The vulva located on the ventral side of the hermaphrodite is the means for sperm entry from the male and egg laying from the uterus. Both sexes are diploid for the five autosomal chromosomes. The hermaphrodites have two X chromosomes and males have a single X chromosome. *C. elegans* has no Y chromosome and the genotype of males is referred to as XO. The majority of offspring produced by self-fertilization are

hermaphrodites. Only 0.1-0.2% of the progeny are males due to rare meiotic non-disjunction of the X chromosome. But upon male fertilization, male sperm outcompetes that of the hermaphrodite and 50% of males arise. This feature is extremely useful for genetic crosses.

1.3 Nomenclature

In *C. elegans* nomenclature, gene names, allele designations, reporter genes are written italicized. Gene names consist of 3-4 letters, a hyphen and an Arabic number, followed by the mutation (allele) names, usually 1-3 letters and an Arabic number. Non-italicized three-letter abbreviations are used to indicate the phenotype, which is synonymous with the gene name; but the first letter is capitalized. For example, *daf-2(e1370)* refers to the mutation e1370 in the gene *daf-2*, in which mutation causes a Daf (defective in dauer formation) phenotype. The protein product is written in non-italic capitals (DAF-2). Genes that have been identified through bioinformatics approaches get systematic gene identification (*e.g.* ZK154.3) until further studies facilitate a gene name. In case of strain names, 2 or more capital letters and a number, for example, CB429 and TU38 are used to designate a strain containing one or more genetic differences. The letters indicate the laboratory that constructed the strain. Strains created in our laboratory are pre-fixed with the letters MRS. A more comprehensive guide to worm nomenclature description can be found at http://www.wormbase.org/about/userguide/nomenclature.

1.4 Unique attributes of *C. elegans*

A combination of several features apart from the ones discussed earlier, make *C. elegans* attractive as a premiere model organism for research. Animal populations can be cryo-preserved for years, thus, a large number of strains can be maintained. Males can be induced by short exposures to higher temperatures. Animals can be synchronized by hypochlorite (bleach) treatment of gravid adults - only eggs survive this treatment as they are protected by an egg-shell. As the worm is transparent, developmental biologists have used it to examine biological problems at the single-cell level. The same also facilitates studies in living animals utilizing fluorescent protein reporters (Chalfie et al. 1994). Worms are non-pathogenic.

The entire *C. elegans* genome (100Mb) has been sequenced and annotated (*C. elegans* Sequencing Consortium, 1998). It has 20104 predicted protein coding genes (WormBase release WS264, year 2018)(Gerstein et al. 2010). The dedicated website WormBase (www.wormbase.org) provides an incredible bioinformatics resource (Bieri et al. 2007; Lee et al. 2018). Another online resource on *C. elegans* research is the Wormbook (www.wormbook.org) (Girard et al. 2007) that also houses *C. elegans* methods (WormMethods) and the *C. elegans* Newsletter (The Worm Breeder's Gazette).

1.5 Limitations of *C. elegans*

Phylogenetically, worms are evolutionarily distant from humans (Johnson 2003; Gruber et al. 2015) and have a simple body plan that lacks defined organs/tissues (Plowman et al. 1999; Gruber et al. 2015; Tissenbaum 2015). The nematode, *C. elegans,* lacks many genes from the hedgehog signalling cascade which are important for organ patterning during development in vertebrates (Corsi et al. 2015). Similarly, they lack some protein kinases that are present in humans. Manipulating an organism only 1mm in length is challenging especially at the individual tissue level and in studies involving biochemistry (Johnson 2003). Moreover, there are no *C. elegans* cell culture lines. Electrophysiology studies of *C. elegans* neurons and muscles, though possible, are very demanding and indirect measurements such as calcium imaging are used as read out of neuronal activity (Corsi et al. 2015; Tissenbaum 2015). Regarding ageing studies, there is little information regarding late life pathology of worms. Worms are scored as dead when they fail to respond to touch, but the rate of deterioration due to age is not the same for all tissues of worms - muscle degradation is faster whereas nervous system is more resilient (Johnson 2003; Antebi 2007).

2. Technologies for *C. elegans*

The usefulness of the nematode is further enhanced by technological developments. In particular, I describe those utilised in this Thesis, including alteration of gene expression, genome editing techniques, manipulation of large numbers of worms and automated imaging techniques. These advances bypass laborious efforts and project the worm as a model for studying a wide range of biological processes with ease.

2.1 RNA interference (RNAi)

RNAi is an evolutionarily conserved process that leads to posttranscriptional gene silencing (PTGS) activated by double-stranded RNA (dsRNA) or small interfering dsRNA (siRNA)(Figure 7)(Hannon 2002). RNAi has been hypothesized to function as a naturally occurring cellular antiviral defence mechanism against foreign dsRNA invasion (Grishok 2005). In the nematode, it has emerged as an important tool for studying in vivo gene function (Fire et al. 1998) as RNAi has the capacity to cross cellular boundaries. Initially used for knocking down functions of individual genes, it has now been utilised in several organisms on a global level by the production of large scale RNAi libraries that target the whole genome. Sequences of identified genes can be known immediately and lethal mutations are easier to identify. The inclusion of RNAi into research has hastened the pace at which new gene functions are being discovered (Kamath and Ahringer 2003; Boutros and Ahringer 2008).
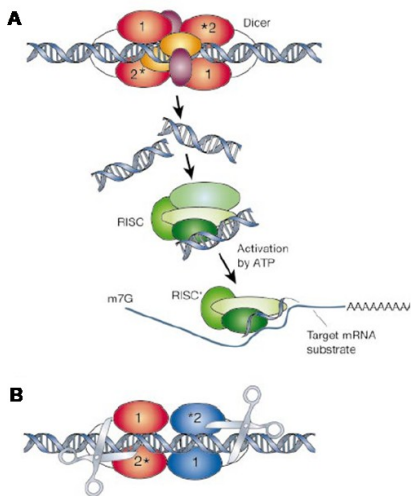
Figure 7: Molecular mechanism of RNAi. **A.** RNAi is initiated by the Dicer enzyme, which processes dsRNA into ~22-nucleotide siRNAs which are incorporated into a multicomponent nuclease, RISC (coded in green). RISC must be activated from its dormant form, containing a double-stranded siRNA to an active form, RISC*, by unwinding of siRNAs. RISC* then uses the unwound siRNA as a guide to substrate selection. **B.** Representation of Dicer binding and cleaving dsRNA (Hannon 2002).

There are four methods for dsRNA delivery in *C. elegans* - feeding the worm with bacteria producing dsRNA (Timmons et al. 2001), injection of dsRNA into any region of the worm (Fire et al. 1998), soaking the worms in dsRNA (Tabara et al. 1998) or *in vivo* production of dsRNA from transgenic promoters (Tavernarakis et al. 2000). The RNAi in *C. elegans* is systemic, a distinctive trait not seen in *Drosophila* or mammalian cells, meaning that when dsRNA corresponding to the transcript of a gene of interest is introduced into one tissue, it leads to RNA silencing even in distant cells. Long dsRNAs are

introduced into *C. elegans* via ingestion of expressing *E.coli* and are intracellularly diced into small-interfering RNAs (siRNAs) leading to an efficient knockdown because many different siRNAs are generated from each dsRNA. RNAi by feeding is a less labor-intensive procedure than injection, thus, making it convenient for performing RNAi on a large number of worms or for testing a large number of different genes and also, is considerably less expensive than injection or soaking that requires the in vitro synthesis of dsRNA.

The systemic effects of RNAi are a huge advantage for large-scale genome wide RNAi screens. For large-scale RNAi studies, two RNAi feeding libraries covering the whole genome have been made and are currently available. Both libraries use bacterial feeding for dsRNA delivery - the method of choice for large-scale screens and routinely used for experiments that target individual genes as well. The two libraries differ in the type of template that is used to produce dsRNA and the number of targeted genes. The first library, from the Ahringer group has 16,757 clones. It was made by cloning gene-specific genomic fragments between two inverted T7 promoters (Kamath and Ahringer 2003). The second library, from the Vidal group has 11,511 clones and was made by the Gateway cloning of full-length open reading frame (ORF) cDNAs into a double T7 vector. There is some overlap between the two libraries and together they target about 94% of *C. elegans* genes and efforts are underway to create feeding strains for the remaining ones. Individual clones and whole libraries are available from Geneservice. The Vidal library is also available from Open Biosystems (Ahringer 2006; Antoshechkin and Sternberg 2007; Boutros and Ahringer 2008). Using genome-wide RNAi feeding libraries (Kamath and Ahringer 2003), genes have been identified that are required for longevity (Dillin et al. 2002), signal transduction (Keating et al. 2003), development (Fraser et al. 2000) and metabolism (Ashrafi et al. 2003), amongst others.

Large scale RNAi screens are usually carried out either in 96-well liquid culture (rapid and employs liquid-handling devices) or solid media (on agar plates, more time consuming but allows detailed phenotypic scoring) (Figure 8). Worms can be subjected to RNAi at any stage and assayed later, or mothers can be treated and their progeny scored (Boutros and Ahringer 2008).
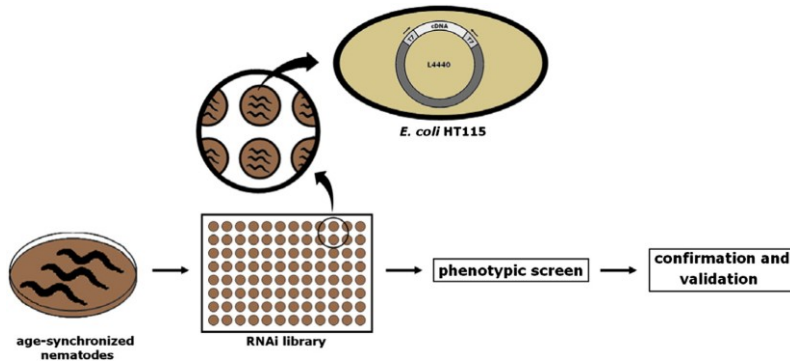
Figure 8: Phenotype based high-throughput RNAi screen strategy. Age-synchronized worms are moved to microtiter plates housing the desired RNAi libraries. Each well contains a different clone of HT115 *E. coli* bacteria and produces a specific dsRNA which is taken up by the nematodes and induces a knockdown of the corresponding gene. Positive hits from the screen are confirmed by sequencing. RNAi feeding can be started at any developmental stage and the scoring of the screen depending on the experiment design can be any developmental stage (Sin et al. 2014).

RNAi by feeding method involves cloning of a DNA fragment corresponding to the gene of interest into a vector for the expression of dsRNA. L4440 feeding vector is used for this purpose which has T7 promoter sites next to both sides of the multiple cloning sites (MCS). After a specific DNA fragment is cloned into the vector, dsRNA is produced in the bacteria by transcription with T7 polymerase. The plasmids are then transformed into the bacterial strain HT115 (DE3), an RNase III-deficient strain of *E. coli* in which expression of T7 RNA polymerase can be induced by addition of isopropyl-β-D-thiogalactopyranoside (IPTG). The efficiency of RNAi by feeding is improved by RNase III deficiency because the dsRNA produced is more stable in the bacteria. The worm eats the bacteria and the dsRNA produced is absorbed by the worms through the intestine and distributed throughout the animal (Timmons and Fire 1998; Timmons et al. 2001). RNAi efficiency varies spatially and temporally. Late-stage embryos (whose eggshell may be impermeable to dsRNA), neurons, males, and early larval stages have been observed to exhibit resistance to RNAi by feeding (Kamath et al. 2001; Timmons et al. 2001). RNAi phenotypes might also vary in a gene- and method-dependent manner. Soaking, dsRNA feeding or injecting methods are not effective in neurons. In some neurons, only injected plasmids producing dsRNA knockdown gene function reproducibly for some genes tested (Tavernarakis et al. 2000).

2.1.1 Tissue specific RNAi

Tissue-specific RNAi is done by generating worms that are proficient for RNAi only in a tissue of interest, using a transgenic mutant strain that carries an *rde-1* mutation (RNAi resistant). The wild-type *rde-1* is then expressed under the control of a tissue-specific promoter (in non-neuronal tissues) (Qadota et al. 2007). Worms are then fed bacteria expressing dsRNA for a gene of interest, which reduces activity of that gene only in the specific tissue in which *rde-1* is expressed (Figure 9). This technique aids researchers to determine spatial requirements for gene function or to study genes with pleiotropic effects in different tissues.
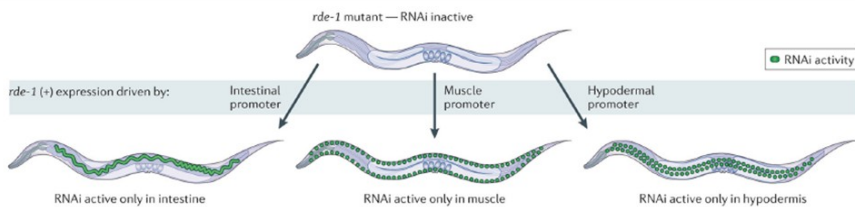
Figure 9: Tissue specific RNAi. *rde-1* mutants are RNAi-deficient. When wild type *rde-1* (+) is expressed under the control of a tissue-specific promoter (intestinal, muscle or hypodermal), worms become RNAi-proficient in the tissue where *rde-1* (+) is expressed (Xu and Kim 2011).

2.2 Genome editing in *C. elegans*

Gene expression pattern is routinely monitored in the worm using the reporter genes fluorescent protein to study gene function. This requires injection of corresponding transgenes into animals - transgenesis (Chalfie et al. 1994). Here, exogenous DNA is introduced into the developing oocytes of adult hermaphrodite animals via DNA microinjection or DNA-coated microparticle bombardment, which then generate transgenic worms among their progeny (Rieckher et al. 2009). In microinjection, transgenic worms are obtained by injecting the appropriate DNA fragments or plasmids and their progeny will carry and inherit the exogenous DNA as an extrachromosomal array that contain many copies of the co-injected DNA. However, extrachromosomal arrays can be lost during cell divisions, leading to a variable transmission rate (Mello et al. 1991). Microinjection is widely used and enables transgenic expression of genes, genome editing by the clustered regularly interspersed short palindromic repeats (CRISPR)-Cas9 system, or transcription of dsRNA for

RNAi. DNA bombardment involves DNA coated gold microparticles that are 'shot' into the worms at high speeds, using a specialized biolistic bombardment instrument or 'gene gun'. A bulk of transformed worms generated are integrants containing low number of transgene copies, resulting in stable transmission of transgenic DNA over future generations (Praitis et al. 2001). However, these methods have limitations such as the high copy number associated with extrachromosomal arrays and the random site of integration associated with bombardment. Newer and more accurate techniques include the Mos1-mediated Single Copy Insertion (MosSCI) method (Frokjaer-Jensen et al. 2008) and the CRISPR-Cas9 system (Friedland et al. 2013; Waaijers and Boxem 2014) that have rapidly progressed in *C. elegans* and now facilitate targeted mutations in any location in the genome in any genetic background.

2.2.1 CRISPR-Cas9

CRISPR-Cas9 system for genome engineering has advanced the study of gene function, as it allows precise targeted mutations in endogenous genes, allowing one to examine the relationship between gene function and phenotype. It also facilitates insertion of coding sequence for a fluorescent protein and allows monitoring the expression and localization of endogenous proteins (Hsu et al. 2014).The CRISPR–Cas9 system compared to other approaches is theoretically simpler and has high target specificity. In brief, a single protein (Cas9) is used to generate a DNA break, which is then targeted to a DNA sequence using a single short RNA (Figure 10) (Frokjaer-Jensen 2013)

Figure 10: Overview of CRISPR–Cas9 system. The CRISPR–Cas9 enzyme is guided to the target site by a single guide RNA. The target sequence is determined by the 20 nucleotides in red followed by the PAM sequence (NGG). The double stranded break (DSB) is generated 3 bp upstream of the PAM(Frokjaer-Jensen 2013).

In bacteria, Cas9, an endonuclease is guided to specific DNA sequences by two small RNAs - called CRISPR RNAs (crRNAs) and trans-acting crRNAs (tracrRNAs).

The crRNAs and tracrRNAs can be engineered to form a chimeric single guide RNA (sgRNA). The Cas9 nuclease has two independent nuclease domains that each cut one DNA strand, leading to a double stranded break (DSB) (Jinek et al. 2012). Once the sgRNA is loaded into the Cas9 protein, this complex cleaves DNA that is complementary to a 20-bp stretch (the "protospacer") of the sgRNA. To cleave DNA, the 20-bp guide sequence must be followed by another nucleotide and then the GG – the protospacer-adjacent motif (PAM) motif.

Three CRISPR-Cas system types (I, II, and III) exist that use unique mechanisms for nucleic acid recognition and cleavage. The CRISPR-Cas9 technology originates from type II CRISPR-Cas systems, which provide bacteria with adaptive immunity to viruses and plasmids. It has a distinctive property very useful for genome engineering applications - these require only a single protein for RNA-guided DNA recognition and cleavage - making it the backbone of CRISPR-Cas9 technology (Doudna and Charpentier 2014).

The CRISPR-Cas 9 system has been adapted to several model organisms including *C. elegans*. In order to achieve heritable changes in the worm genome, Cas9 protein and sgRNA have to be expressed in the germ line. John Calarco was amongst the first to demonstrate Cas9 activity in *C. elegans*, and used this to generate mutations by non-homologous end joining (NHEJ) (Friedland et al. 2013), followed by the demonstration of homologous recombination-mediated gene conversion (Tzur et al. 2013).

DSB repair through NHEJ often leads to generation of small insertions or deletions - indels, which might disrupt gene function (Figure 11A,B). On the other hand, homologous recombination repair allows gene modification and addition of specific tags in the genome. This involves supply of a repair template that contains sequences identical to the DNA flanking the target cut site. Hence, a sequence of choice can be inserted (Figure 11E-G). In case, homologous regions are far apart in the genome, endogenous sequences can also be replaced with a desired sequence, for example to create a deletion mutant (Figure 11C,D) or to replace a gene with a specific mutant variant (Figure 11H-J)(Waaijers and Boxem 2014).
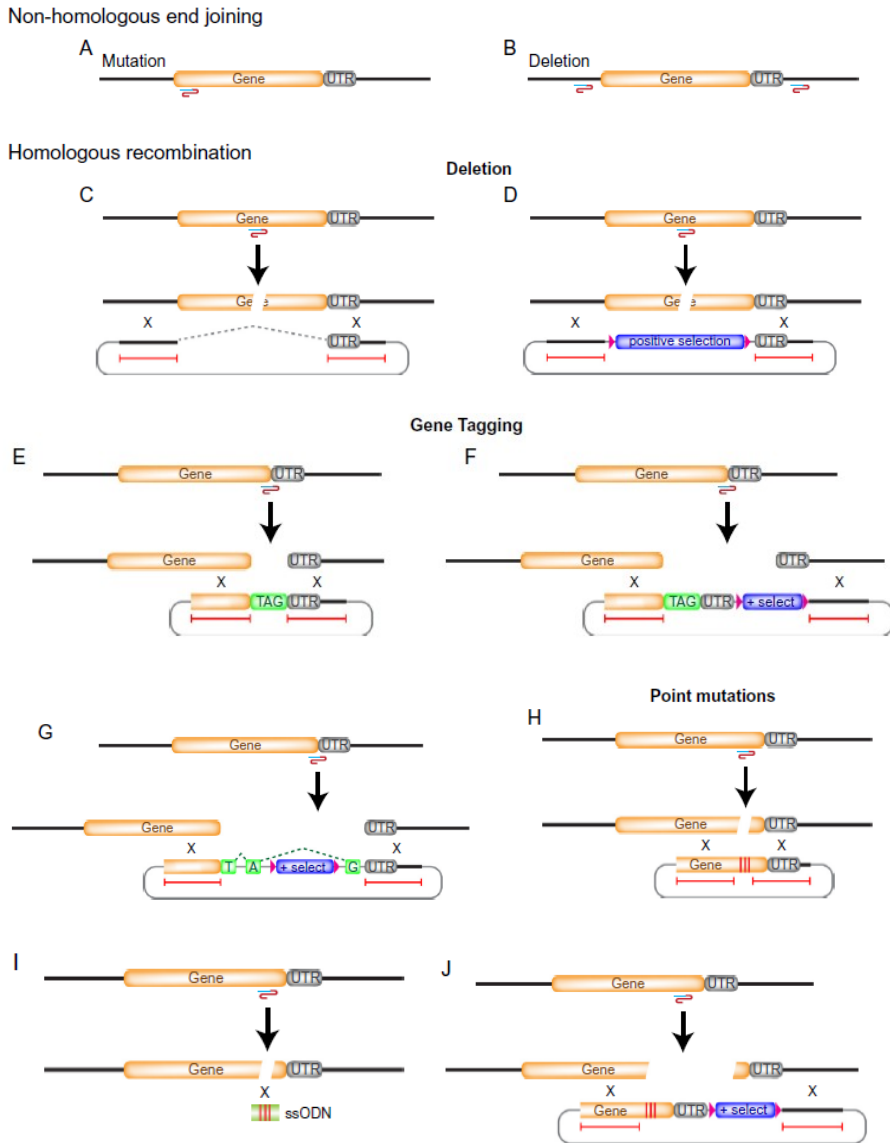
Figure 11: Genome engineering strategies using CRISPR-Cas9. Target sites are indicated by sgRNA. (A- B) Non-homologous end joining can be used to generate mutations and deletions. (C–J) Homologous recombination being used to generate deletions, insert gene tags, or engineer point mutations. Homologous regions are indicated by the red lines in the repair constructs. Re-cleavage after repair is prevented by having the target sequence in the repair template or the PAM sequence mutated (Waaijers and Boxem 2014).

Despite the ease of using CRISPR-Cas9 to insert exogenous sequences into a genome, several limitations exist. It is time consuming and expensive to generate the repair template and guide RNA constructs for each desired insertion. Also, one has to exhaustively screen through candidates to identify the modified organisms. To identify CRISPR modified animals, commonly used strategies such as selectable marker-based strategies and co-CRISPR have been optimized and used successfully for insertion of relatively simple sequences, such as translational GFP fusions.

This thesis has used, a PCR-free high-efficiency modular plasmid assembly called SapTrap method developed by the Jorgensen Lab. This simplifies the production of targeting vectors for tag insertion, as well as the selection of successfully modified strains, thus, improving genomic tagging in worms using CRISPR (Schwartz and Jorgensen 2016). SapTrap method produces single plasmid targeting vectors that, when co-injected with a Cas9 expression plasmid, insert genetic tags with high frequency.

To simplify the repair template production for CRISPR-Cas9 mediated insertion, this technique uses a selectable marker for direct identification of modified worms. Here, a LoxP-flanked *C. briggsae unc-119* selectable marker is positioned within a synthetic intron of the tag, such as GFP. The LoxP sites allow excision of the *unc-119* cassette by CRE recombinase (a recombinase that mediates site specific recombination, leaving behind one LoxP site) expression. To allow concurrent expression of both gfp and *unc-119*, the *unc-119* gene is inserted in the opposite orientation relative to gfp. Using this cassette, a complete repair template can be generated simply by adding homology arms to each side of the gfp tag. We utilized a SapTrap compatible GFP knockout (KO) cassette as tag plus marker donor plasmid that can be utilized to study gene function in specific tissues (Munoz-Jimenez et al. 2017). It is based on FLP-mediated gene knockout. FLP is a site-specific recombinase from yeast that acts at FLP-recombinase targets (FRTs); if two FRTs are in the same orientation, FLP will excise the sequence between the FRTs (Hubbard 2014). This GFP KO cassette has Frt sites in introns 1 and 2. If crossed to a transgenic strain expressing FLP, the second GFP exon will be excised by recombination between the two Frt sites. This will cause a frame shift in the third exon leading to

generation of a premature termination codon and degradation of any atypical GFP::*gene of interest* transcript by nonsense-mediated mRNA decay.

Next, to reduce the plasmid assembly workload, a single plasmid was designed using Golden Gate strategy, using the restriction enzyme SapI, to encode both the sgRNA transcript and the repair template for an individual insertion event. The repair template is split into five sections and supplied independently to the reaction - 5' and 3' homology arms, combined tag and selectable marker, and the N- and C- terminal connectors. As the sgRNA targeting sequence and homology arms are supplied in the Sap Trap assembly as synthetic, annealed oligonucleotides, PCR is not required. A donor plasmid library supplies the rest - fluorescent and non-fluorescent tags, a selectable marker and optional regulatory sequences that allow tagging at either termini - N or C (Schwartz and Jorgensen 2016). This reduces the expense and time taken to produce vectors for genome editing and can provide repair templates that can tag a protein in a tissue-specific manner. Eventually, Sap Trap could be used for genome-wide projects to verify the expression pattern or to generate knockouts of all genes in the *C. elegans* genome.

2.3 High-throughput whole animal screening strategies

The transparency and small size of the worm coupled with the systemic RNAi methodology has assisted the design of high-throughput and high-content whole worm screens utilising fluorescent protein reporters/dyes (Hamilton et al. 2005; Artal-Sanz et al. 2006; O'Rourke et al. 2009a; Lejeune et al. 2012; Wahlby et al. 2012). The small size is also compatible with flow cytometric systems such as the COPAS (complex object parametric analysis and sorting) Biosort System 'Worm Sorter' (Pulak 2006) , laFACS (live animal FACS) (Fernandez et al. 2012) and automated pipetting devices like MultiFlo (BioTek) (Leung et al. 2011), which in turn, have made screenings in multiwell plates more convenient. Most high-content RNAi approaches using worms were first employed for drug discovery screenings (Kwok et al. 2006) using solid media and were laborious. Hence, a liquid based workflow (Lehner et al. 2006; O'Rourke et al. 2009a) was adopted using automated robotic liquid handlers and imaging platforms. These have been used to search for antimicrobial compounds (Moy et al. 2009), to identify pharmaceutical interventions against ageing (Gill et al. 2003; Petrascheck et al. 2007; Petrascheck et al. 2009;

Maglioni et al. 2015), and to look for disease modifiers (Gosai et al. 2010) and have further advanced existing genome-wide screening strategies (Gill et al. 2003; Moy et al. 2009; O'Rourke et al. 2009a; Gosai et al. 2010).

2.3.1 Worm sorting

The COPAS (Worm sorter) facilitates the analysis, sorting, and dispensing of *C. elegans.* Sorting parameters are based on the physical parameters of axial length of the object (worm length), optical density of the object (optical extinction), and the intensity of fluorescent markers (green/yellow/red). Once analyzed, worms are selected and dispensed according to user criteria into multi-well plates for high throuput screening (User Manual ; Pulak 2006). While the earlier mentioned laFACS and MultiFlo are cheaper options - laFACS is limited to sorting only L1 larvae due to the nozzle size limitation, whereas, the MultiFlo requires a tightly synchronized population, not suitable for sorting herterogenous populations. The COPAS on the other hand is apt for isolation of sub-populations of worms from a heterogeneous population on the basis of fluorescence, optical densities and for stage/size specific sorting (Pulak 2006).

Previously, the COPAS has been used to carry out large scale fluorescence based stage-specific (L1 to adult) sorting of integrated or extrachromosomal strains based on absence or presence of fluorescence such as GFP+/GFP- (Rea et al. 2005; Gosai et al. 2010; Twumasi-Boateng et al. 2014), mCherry+/ mCherry- (Miedel et al. 2012; Gamerdinger et al. 2015). Further, to sort worms using dual fluorescence (reduced green to red ratio) after EMS to screen for mutants defective in dopaminergic cell fate (Doitsidou et al. 2008; Nagarajan et al. 2014) and to screen for mutants with increased GFP expression profiles following EMS (Kuroyanagi et al. 2006).

The worm sorter comes equipped with the Profiler feature that gives a list of successive point measurements along the object passing through the flow cell and builds a fluorescence profile. Based on these measurements, it can detect fluorescence intensity peaks along the length of the object. This feature has been used for accurate acquisition of GFP strains to make post-embryonic developmental chronograms (Dupuy et al. 2007) and sorting L4 worms with different transgenic arrays (GFP expression in pharynx from worms that had GFP expression in coelomocytes or both) (Duverger et al. 2007).

COPAS has also been used for sorting balanced mutants for molecular biology purposes at the L3 and L4 larval stages where selection of homozygous worms that lacked pharyngeal GFP was done from a mixed population that expressed pharyngeal GFP (Latorre et al. 2015; Ruegger et al. 2015). An image based high-content assay to measure germ cell fate reprogramming has sorted balanced strains at the young adult stage. Here, worms that lacked GFP and expressed mCherry in the pharynx were sorted from a mixed population that carried both GFP and mCherry in the pharynx (Benson et al. 2014). The COPAS, thus, provided a solution to a major bottleneck that prevented use of balanced strains on a large scale basis. It also reduces time and human errors and facilitates new experiments previously considered difficult.

In this thesis, we have utilized the worm sorter, for sorting a balanced strain. This involved sorting and selecting homozygous worms at the L1 larval stage that lack GFP expression in the pharynx from a heterozygous balanced population expressing pharyngeal GFP.

2.3.2 Imaging strategies

A complicated aspect in screening strategies is the integration of effective and automated analysis of the acquired data, which is often, in the form of images. Automated image based high content platforms allow measurement of different properties at the same time unlike high throughput where there is only a single readout (Buchser et al. 2004). Acquired images can be stored, making it accessible for re-analysis or for screening of other phenotypes. Fluorescence microplate readers have been used previously for automated real-time fluorescence detection in worms (Gill et al. 2003; Leung et al. 2011). For quantitation of complex phenotypes in worms, several software programs have been designed and implemented. The open-source cell image analysis program CellProfiler has been used for automated quantification of worm survival (Moy et al. 2009), the Cellomics ArrayScan VTI and its BioApplication, the SpotDetector program has been utilized to develop a high-quality drug discovery platform (Gosai et al. 2010) and also to screen for pro-longevity interventions targeting the mitochondria (Maglioni et al. 2015) . The image-analysis toolbox "WormToolbox" from the CellProfiler project caters to a variety of assays irrespective of the imaging system used (Wahlby et al. 2012; Wahlby et al. 2014). This is an open-source, image analysis software designed

specifically for *C. elegans* . A challenging aspect of measurement of single worms is that they might overlap during imaging. WormToolbox has got past this block, as it is able to computationally untangle worms from within a cluster of worms so that data for these worms can be obtained. Apart from size, shape and fluorescence measures, the machine-learning algorithm in CellProfiler Analyst can be used to spot slight and complex differences in various measurable phenotypes (Wahlby et al. 2012).

In this thesis, an automated image acquisition protocol has been designed using the INCA Analyzer 2000 (GE Healhcare), a microscope that facilitates high-content screening. Also, worm segmentation protocols were developed using the Developer Toolbox software (version 1.9.2) (GE Healthcare), accompanying the INCA Analyzer 2000.

For complex phenotypes lacking robust methods of quantification, such as in ageing worms (paralysis, uncoordinated locomotion, less/loss movement) 'worm tracking systems' exist. These include high-throughput softwares like the Multi-Worm Tracker (MWT) and the Parallel Worm Tracker (Ramot et al. 2008; Swierczek et al. 2011) for automated movement behavior analysis and tracking, for measurement of thrashing (Buckingham and Sattelle 2009), DevStaR (Developmental Stage Recognition) for quantification of developmental stages (White et al. 2013), WormScan for measuring mortality, movement, fecundity and size (Mathew et al. 2012) etc. An upgrade of this is the Lifespan Machine that allows automated collection of lifespan data (Stroustrup et al. 2013). As these strategies are further refined, they will open the doors for novel and more complex *C. elegans* based high-throughput screenings.

3. Ageing

The Oxford Dictionary defines 'Age' as the length of time that a person has lived or a thing has existed and 'Ageing' as the process of growing old. Ageing is a fundamental, time-dependent degenerative process transcending species and evolutionary boundaries and is inevitable. Understanding the cause of ageing is one of the major challenges for this century, as age related deterioration is the primary cause factor for afflictions like cancer, Alzheimer's disease, neurodegenerative disorders, cardiovascular diseases, diabetes etc.

Tentative hallmarks of the ageing process with an emphasis on mammalian ageing are - genomic instability, shortened telomeres, epigenetic alterations, loss of proteostasis, deregulated nutrient sensing, mitochondrial dysfunction, cellular senescence, stem cell exhaustion and altered intercellular communication (Lopez-Otin et al. 2013). Ageing is also accompanied with significant alterations in metabolic and physical activity. Though ageing was not thought to be a regulated process, genetic and genomic studies have helped accelerate ageing research by revealing that ageing is subject to regulation from signalling pathways and transcription factors. Mechanistic insights into the genetic regulation of ageing arise from studies done in model organisms like yeast, worms and flies. An important goal of ageing studies is to achieve life span extension along with an increased quality of life, with minimal side effects (Collins et al. 2008; Kaletsky and Murphy 2010; Kenyon 2010b; Lopez-Otin et al. 2013; Gruber et al. 2015)

3.1 *C elegans* in ageing research

C. elegans is a leading model organism to understand the genetic control of longevity owing to its ease of handling and a short and invariant lifespan (~ 17 days at 20 °C). This invariance and the ease of genetic manipulation allows for identification of mutants that shorten or lengthen lifespan (Collins et al. 2008; Tissenbaum 2015). In worms, lifespan (synonymous to the total rate of ageing) is defined as the number of days, the worm remains responsive to external stimuli (Sutphin and Kaeberlein 2009).

Ageing in the worm (Figure 12) is accompanied with several phenotypic features - torpor, cessation of mobility and reproductive capacity, reduction in the ability to sense/respond to environmental stimuli and accumulation of auto-fluorescent deposits (lipofuscin) in cells - that are also seen in other animals (Kaletsky and Murphy 2010). Decline in pharyngeal pumping rate and defecation rates are also observed (Houthoofd et al. 2003).

Hence, aged worms look and behave old, just as people do. The first evidence for a gene that influenced ageing in the worm, came with the discovery of *age-1* (Friedman and Johnson 1988) and since then over several 100 genes including the insulin receptor *daf-2* (Kenyon et al. 1993) have been discovered that modulate longevity in *C. elegans*.
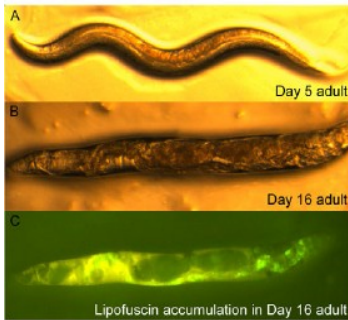
Figure 12: Ageing in *C. elegans*. **A.** The morphology of a young day 5 adult worm is different when compared to **B.** an aged day 16 worm. **C.** Lipofuscin accumulation in a day 16 adult worm. Lipofuscin serves as an auto fluorescent ageing biomarker in both worms and humans. (Kaletsky and Murphy 2010)

3.2 Pathways that regulate ageing

Ageing is subject to regulations by several signalling pathways and transcription factors. Though these were first described in organisms like yeast, worms and flies, a huge number extend lifespan in mammals as well. These include the well described insulin/insulin-like growth factor- 1 (IGF-1) signalling pathway, nutrient sensing pathways such as TOR, AMPK and sirtuin regulated signalling, germline signalling and epigenetic mechanisms. Apart from ageing, these pathways also control biological processes, such as development, reproduction, metabolism, etc. Though these pathways have different transcription factors, they influence nematode longevity in a conserved manner through overlapping processes, for example through modulations in lipid metabolism. Here, the insulin/IGF-1 signalling pathway has been discussed in more detail, for other pathways influencing ageing, refer Table 1.

3.2.1 Insulin/IGF-1 signalling pathway

Around two decades ago, it was discovered that mutations in *age-1* (Friedman and Johnson 1988) and *daf-2* (Kenyon et al. 1993) are capable of doubling the lifespan of worms. Further studies revealed the significance of the insulin/insulin-like growth factor- 1 (IGF-1) signalling (IIS) pathway in regulation of ageing. The IIS was one of the first pathways identified in this regard (Kenyon 2005). The lone insulin/IGF-1 receptor in worms is encoded by *daf-2*, and *age-1* is the catalytic subunit of the downstream phosphoinositide 3-kinase (PI3K) (Kimura et al. 1997). Apart from lifespan extension, *age-1* and *daf-2* mutants also exhibit resistant to oxidative stress, hypoxia, heat stress, heavy metals and bacterial pathogens (Lithgow et al. 1995; Barsyte et al. 2001). These observations supported the idea that the ageing process is under

genetic control (Kenyon 2010b). The IIS pathway also acts as a food and stress sensing pathway all through development. When food is in abundance, worms progress through the larval stages and into adulthood. But on encountering conditions of stress - food limitations or overcrowding, they enter the dauer state, marked by delayed reproductive maturity and increased stress tolerance. When favourable conditions return, the dauers develop into reproductive adults (Cassada and Russell 1975). *daf-2* mutants have a prominent dauer- constitutive phenotype (Riddle et al. 1981).

Both the long lived and the dauer phenotypes of *daf-2* worms are dependent on DAF -16, the downstream FOXO forkhead transcription factor (Riddle et al. 1981; Kenyon et al. 1993). Ligand binding to the insulin receptor DAF-2 leads to activation of its tyrosine kinase activity. This in turn initiates a cascade of phosphorylation events that activate several downstream kinases such as AGE-1/PI3K, PDK-1, AKT-1/2, and SGK-1 which phosphorylate DAF16 leading to its inactivation and retention in the cytoplasm, thus, blocking transcription of target genes. When IIS pathway is absent or there is a mutation in *daf-1* or *age-1*, DAF - 16 enters into the nucleus where it turns on survival genes that double lifespan of the worms (Lin et al. 1997; Lee et al. 2001). Loss of the *daf-2* or *age-1* also slows down the age-related downfalls. Hence, the IIS pathway regulates longevity. Inhibiting IIS modulates lifespan also through changes in gene expression of the heat-shock transcription factor HSF-1 (Hsu et al. 2003); SKN-1, a Nrf-like xenobiotic-response factor (Tullet et al. 2008); and PQM-1 (a gene encoding the C2H2-type zinc finger and leucine zipper-containing protein) (Tepper et al. 2013). These transcription factors, up regulate or down regulate various genes that mediate effects on lifespan (Kenyon 2010b).

The IIS pathway is an evolutionarily conserved pathway that regulates lifespan across many species (Kenyon 2005)(Figure 13). *Drosophila melanogaster* has a single insulin-like receptor (dInR) and reducing IIS signalling or increasing the activity of FOXO (the Drosophila orthologue of DAF-16) specifically in adipose tissue extends lifespan (Clancy et al. 2001; Tatar et al. 2001; Hwangbo et al. 2004). Mammals have several *daf-2* homologs [IGF-1 receptor (IGF-1R), insulin receptor (IR)-A and IR-B] that are able to form multiple homodimer and heterodimer pairs (Benyoucef et al. 2007). Despite these differences in insulin receptor expression, the functional consequences are similar, as reduced IIS

also extends life span in multiple mammalian species. In mice, a striking inverse correlation between IGF-1 levels and lifespan has been observed amongst inbred strains (Yuan et al. 2009). Likewise, longevity in dogs is also inversely proportional to body size (Greer et al. 2007b). Perturbation of insulin/IGF-1 activity can also increase lifespan in humans. Mutations known to impair IGF-1 receptor function are overrepresented in certain cohorts of centenarians (Kojima et al. 2004; Suh et al. 2008).

Figure 13: Evolutionary conservation of the IIS pathway. IIS pathway in *C. elegans*, *Drosophila melanogaster* and mammals. Orthologous signalling components are depicted at level with each other across the three pathways (O'Neill et al. 2012)

Studies on the tissue-specificity of the IIS pathway with respect to longevity have established differing results. While restoring DAF-2 and AGE-1 expression specifically in neurons seems sufficient to decrease the lifespan of the long-lived *daf-2* and *age-1* mutants, the same is not true in the intestine (Wolkow et al. 2000). However, another study established that AGE-1 expression in the intestine can decrease the long lifespan of the *age-1* mutant (Iser and Wolkow 2007). Also, in a *daf-2;daf-16* mutant, tissue-specific restoration experiments demonstrated that reestablishment of DAF-16 expression in the intestine extends the lifespan, whereas in neurons, the same exhibited only modest effects on lifespan (Libina et al. 2003). The IIS pathway acts both in a cell-autonomous and non-autonomous manner, which might explain the complexity associated with lifespan regulation by

the IIS pathway (Apfeld and Kenyon 1998; Wolkow et al. 2000; Libina et al. 2003; Iser and Wolkow 2007; Zhang et al. 2013).

3.3 Mitochondria in ageing

Mitochondria are ubiquitous intracellular organelles, primarily involved in adenosine triphosphate (ATP) production through oxidative phosphorylation (a series of electron transferring reactions via the electron transport chain (ETC) located in the mitochondrial inner membrane), which is the main source of intracellular energy. These organelles also serve as sites for key processes - beta oxidation, the tricarboxylic acid cycle, and apoptosis regulation. Hence, mitochondrial function is central to cell homeostasis and survival and has long been linked to ageing. Mitochondrial oxidative phosphorylation declines with age in diverse organisms (Pulliam et al. 2013).

The first evidences that disrupting mitochondrial function could directly control lifespan came from studies in *C. elegans.* Loss-of-function mutations in *clk- 1* (*clk-1* encodes a protein required for the biosynthesis of ubiquinone - an essential cofactor in the ETC), and also mutation of the iron sulfur protein (ISP-1) of the mitochondrial complex III were found to extend worm lifespan (Lakowski and Hekimi 1996; Feng et al. 2001). Eventually, genetic screens in *C. elegans* identified that knockdown of more components of the ETC extended lifespan (Dillin et al. 2002; Lee et al. 2003) . A bulk of these results that altered expression of ETC components and impaired mitochondrial function, still, led to an increase in lifespan. A scenario opposite to human ageing that is generally associated with a decline in mitochondrial function (Short et al. 2005). Likewise, mouse models with increased mitochondrial mutations, exhibit accelerated ageing (Trifunovic et al. 2004; Kujoth et al. 2005). A reason for these opposing observations could be the scale of mitochondrial dysfunction achieved, as a mild knockdown of various mitochondrial ETC components leads to increased lifespan in *C. elegans*, a higher-efficiency knockdown, that increases mitochondrial impairment, shortens lifespan (Rea et al. 2007). There is also genetic evidence in mammalian models that mild impairment of mitochondrial function might extend lifespan (Liu et al. 2005).

Based on work in *C. elegans*, it has been described that several pathways are activated after a mild mitochondrial impairment (Chang et al. 2015). A known

mediator is the mammalian hypoxia inducible factor 1 (HIF-1α, encoded in worms by *hif-1*). Activation of *hif-1* is required for the extended lifespan of several long-lived mitochondrial mutants. Other mediators include the p53 ortholog CEP-1, the homeobox protein CEH-23, the apoptotic factor CED-3 and skinhead-1 SKN-1, the *C. elegans* ortholog of the mammalian transcription factor NF-E2 (Nrf2) (Chang et al. 2015; Finkel 2015).

Additionally, it has been shown that the lifespan of several ETC mutants are also mediated by the transcription factors UBL-5, DVE-1, and ATFS-1, which regulate the mitochondrial unfolded protein response (UPR^{mt}). UPR^{mt} is a mechanism that monitors protein homeostasis and maintains proper protein function within the mitochondria (Yoneda et al. 2004; Durieux et al. 2011). Briefly, UPR^{mt} signalling is initiated when the amount of unfolded proteins in the matrix exceed the capacity of the mitochondrial chaperones. The ClpXP protease degrades unfolded proteins to peptides, which are then exported by the putative mitochondrial inner membrane ATP-binding cassette (ABC) transporter protein HAF-1 to the cytosol. The presence of these peptides in the cytosol leads to the activation and nuclear translocation of the the bZIP transcription factor ATFS-1 (via unknown mechanisms). Additionally, UBL-5, a ubiquitin-like protein, and the transcription factor DVE-1 are translocated from the cytoplasm into intestinal nuclei and form a complex (Benedetti et al. 2006; Haynes et al. 2007). These promote ATFS-1 binding and transcriptional up regulation of mitochondrial chaperone genes that lead to their import into mitochondria, hence, restoring homeostasis. The UPR^{mt} in *C. elegans* can be visualized by the induction of the mitochondrial chaperones, *hsp-6*::GFP and *hsp-60*::GFP (Yoneda et al. 2004).

3.3.1 Mitochondrial Prohibitins

A class of mitochondrial proteins that influence longevity differentially by modulating energy metabolism are prohibitins (Artal-Sanz and Tavernarakis 2009b), and named as prohibitin because the first prohibitin (PHB1) was identified in mammals as a potential tumour suppressor that inhibited proliferative activity (McClung et al. 1989). Later, it was shown to be an artefact of the 3'UTR (Jupe et al. 1996b; Jupe et al. 1996a). The second prohibitin (PHB2) was identified via its binding, to the IgM antigen receptor(Terashima et al. 1994). PHB1 was also shown to bind to the IgM

receptor and hence, Terashima et al., named these proteins as B-cell receptor complex associated proteins (BAP) - BAP32/PHB1 and BAP37/PHB2.

Prohibitins are ubiquitously expressed, evolutionarily conserved proteins that localize to the mitochondria. PHB1 and PHB2 having the molecular weights of 32kDa and 34kDa respectively, together form the mitochondrial prohibitin complex (PHB). They associate with each other to form a high molecular weight ring like structure of 1MDa (Back et al. 2002) with a diameter of 20-25 nm in the inner mitochondrial membrane. About 12 to 16 PHB heterodimers contribute to this ring like structure(Figure 14) (Back et al. 2002). Loss of either PHB1 or PHB2 leads to absence of the entire prohibitin complex (Nijtmans et al. 2000). PHB1 and PHB 2 have around 50% amino acid sequence identity and 60% similarity. The mitochondrial prohibitin complex has been identified in yeast (Steglich et al. 1999; Nijtmans et al. 2000), *C. elegans* (Artal-Sanz et al. 2003) and in human fibroblasts (Nijtmans et al. 2000).
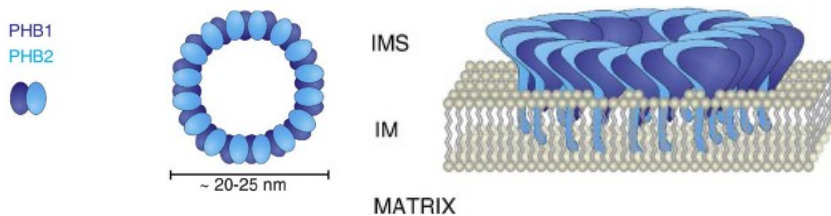

Figure 14: The prohibitin complex. PHB1 and PHB2 compose the mitochondrial prohibitin complex. These heterodimers assemble into a ring-like prohibitin complex with alternating subunit composition. The prohibitin complex is located in the mitochondrial inner membrane. Intermembrane space- IMS, inner membrane – IM (Merkwirth and Langer 2009)

Despite extensive research, the exact molecular mechanism of the prohibitin complex is yet to be deciphered. Nevertheless, they have been implicated in several cellular processes: cell-cycle regulation, cell signalling, senescence, nuclear transcriptional activation, apoptosis, mitochondrial biogenesis and may also regulate inflammation, obesity, neurodegenerative disorders in mammals (Artal-Sanz and Tavernarakis 2009a; Merkwirth and Langer 2009; Theiss and Sitaraman 2011). Apart from the initial role proposed for prohibitins in cell cycle progression (McClung et al. 1989; Nuell et al. 1991), a variety of roles have been proposed for PHBs in the mitochondria. They maintain mitochondrial morphology (Artal-Sanz et al. 2003; Kasashima et al. 2006; Merkwirth et al. 2008) and cristae structure (Griparic et al. 2004; Ahn et al.

2006; Merkwirth et al. 2008) and additionally function as a scaffold that recruits membrane proteins to a specific lipid environment (Osman et al. 2009). The PHB complex regulates membrane protein degradation by the mitochondrial m-AAA protease (Steglich et al. 1999). It also functions as a chaperone that stabilizes unassembled membrane proteins (Nijtmans et al. 2000; Nijtmans et al. 2002) and also has a role in mitochondrial genome stabilization (Wang and Bogenhagen 2006; Bogenhagen et al. 2008; Kasashima et al. 2008). Recently, PHB-2 has been established to be a mitophagy receptor that is essential for Parkin mediated mitophagy in mammalian cells and *C. elegans* (Wei et al. 2017).

Prohibitins have been found in circulation (Mengwasser et al. 2004) and on the plasma membrane (Terashima et al. 1994). Several experiments have shown that PHBs localise predominantly to the mitochondria (McClung et al. 1995; Nijtmans et al. 2000), but nuclear localisation of PHB1 (Wang et al. 2002; Fusaro et al. 2003) and PHB2 (Sun et al. 2004) has also been shown by several investigators.

In the yeast, *Saccharomyces cerevisiae*, depletion of PHB decreases replicative lifespan of the cells, accompanied with defects in mitochondrial membrane potential and extended cell division time (Coates et al. 1997; Berger and Yaffe 1998). In contrast, in multicellular organisms like *C. elegans* (Artal-Sanz et al. 2003), depleting PHB proteins leads to developmental arrest and germline (sterility and small brood size) and somatic defects (reduced body size and abnormal somatic gonad) (Artal-Sanz et al. 2003). Also, in *C. elegans* embryos, PHB-2 is required for paternal mitochondrial clearance (Wei et al. 2017). In mice, PHBs are essential for development and neuron-specific PHB2-deficient mice exhibit premature death (Park et al. 2005; Merkwirth et al. 2008; Merkwirth et al. 2012). PHB depletion also shortens lifespan of petunia flowers whether on the plant or detached (Chen et al. 2005).

A striking feature of PHB depletion in the nematode is with respect to ageing. Depletion of PHBs decreases the lifespan of wild type animals, whereas, the same in metabolically compromised long lived *daf-2 (e1370)* IIS mutants leads to a dramatic extension in lifespan (Figure 15A,B). Additionally, loss of PHB also increases the lifespan of TGF-β pathway mutants (*daf-4, daf-7*) that controls diapause and ageing. Apart from this, PHB deficiency also further extends the

lifespan of several mitochondrial *(gas-1, mev-1, clk-1, isp-1)* and dietary-restricted *(eat-2)* mutants (Artal-Sanz and Tavernarakis 2009b). Thus, PHB deficiency leads to an opposing ageing phenotype depending on the compromised metabolic background. This is seen to be conserved in both mice (Ising et al. 2015) and yeast (Schleit et al. 2013).
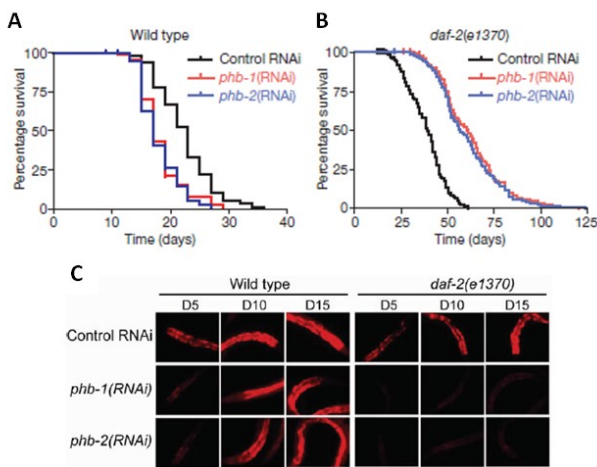

Figure 15: Prohibitin depletion phenotypes in *C. elegans*. PHB deficiency leads to opposing lifespan phenotypes. Survival curves depicting **A**. wild type and **B.** IIS defective *daf-2(e1370)* mutants when subjected to *phb-1/-2(RNAi)*. Reduced Nile Red staining upon PHB knockdown, **C**. Wild type animals (left panel) and *daf-2* mutants (right panel) subjected to RNAi with either *phb-1* or *phb-2* (Anterior side of the animals is shown) (Artal-Sanz and Tavernarakis 2009b).

The ageing process is accompanied by marked alterations in fat metabolism and fat utilization is strongly linked to mitochondrial energy metabolism. Alterations in the levels of fat content, as measured by vital Nile Red staining, also varies differentially upon PHB depletion. Early in adulthood, PHB deficiency reduces Nile Red accumulation in both wild type and *daf-2 (e1370)* mutants. However, this reduction is only maintained in the PHB depleted *daf-2 (e1370)* mutants through ageing (Artal-Sanz and Tavernarakis 2009b). Hence, prohibitin depletion affects vital NR staining in a genetic background and age-specific manner (Figure 15C). Despite the lipid staining NR dye establishing functions for several metabolic genes (Ashrafi et al. 2003; Mak et al. 2006), its usage *in vivo* has come under controversy as it fails to correlate to triglyceride levels (O'Rourke et al. 2009b). This has been addressed in further detail in section 4.1.2.1 of the thesis. Inspite of this, we have evidences that PHB deficiency broadly influences metabolism. Utilising advanced metabolomics, our lab has shown that PHB deficiency in wild type animals and the IIS *daf-2*

(1370) mutants leads to pronounced alterations in fatty acid composition, carbohydrate and amino acid metabolism (Lourenco et al. 2015).

4. Lipid and carbohydrate metabolism in *C elegans*

Lipid and carbohydrate synthesis and breakdown (Figure 16) are highly conserved processes and the worm has orthologs for most of the key metabolic enzymes, thus major metabolic pathways are present in *C. elegans.* Conserved metabolic pathways include lipid uptake and transport, fat synthesis pathways, pathways of β-oxidation in the mitochondria and peroxisomes, glycolysis, gluconeogenesis and amino acid metabolism.
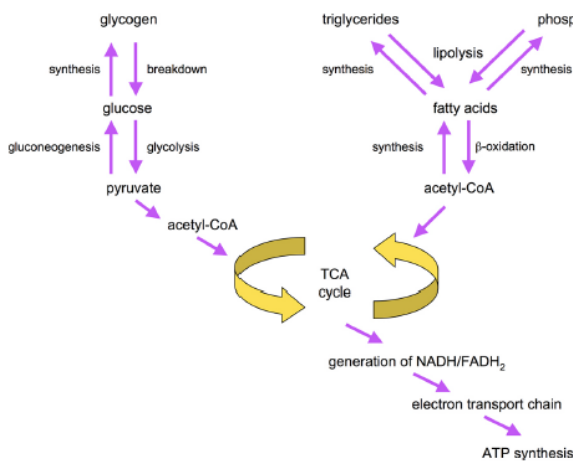
Figure 16: Overview of fat and sugar synthesis and breakdown pathways. Carbohydrate and fat stores, glycogen and triglycerides respectively are broken down by cells to generate acetylCoA and NADH and $FADH_2$ through the tricarboxylic acid cycle (TCA) cycle. NADH and $FADH_2$ are further used to generate ATP through oxidative phosphorylation. Image from Wormbook

Research in worms has been ongoing to illustrate genes involved in and affecting lipid synthesis, storage and breakdown. Also, there have been investigations regarding the developmental consequences that occur when specific lipids are incorrectly synthesized or when lipid homeostasis is deregulated (Ashrafi et al. 2003; McKay et al. 2003; Van Gilst et al. 2005a; Van Gilst et al. 2005b; Taubert et al. 2006; Ashrafi 2007; Brock et al. 2007; Braeckman et al. 2009; Lemieux and Ashrafi 2015; Watts and Ristow 2017).

4.1 *C. elegans* fat

Just like mammals have adipocytes for storage of fat, *C. elegans* stores fat in lipid droplets, mostly in their intestinal and hypodermal cells. Lipid droplets are subcellular organelles that store neutral lipids (Walther and Farese 2012). They have an enriched core of hydrophobic lipids such as triacylglycerides (TAGs)

and cholesterol esters and are surrounded by a monolayer of phospholipids (Zhang et al. 2010b). Apart from this, substantial fat deposits are also found in maturing oocytes of the germline as well as fertilized embryos (Figure 17)(Ashrafi 2007; Lemieux and Ashrafi 2015).
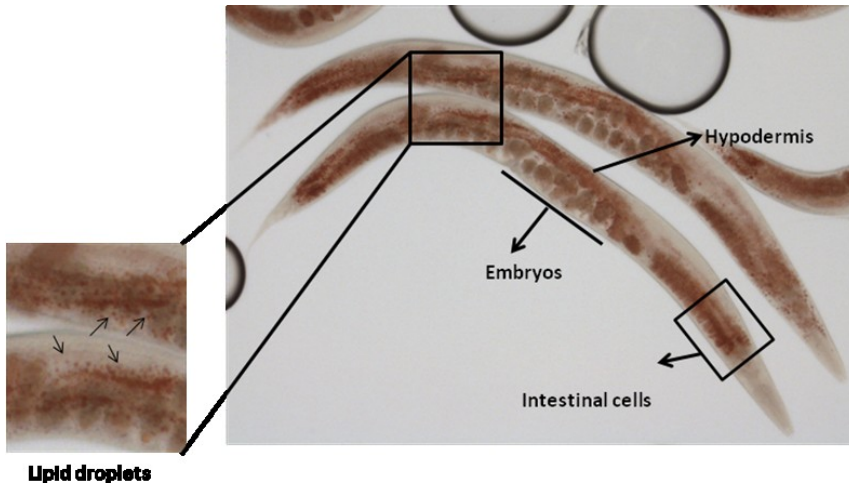

Figure 17: Visualization of lipid droplets using Oil- Red-O staining. Oil-Red-O stain in the transparent body of a wild type animal (Head of the animals are towards bottom right).

TAGs are also a component of yolk (similar to mammalian lipoproteins), which is synthesized in the intestine and transferred to developing oocytes during reproduction. This manner of triglyceride mobilisation during reproduction in the nematode is called vitellogenesis. Members of the vitellogenin (*vit*) family function to transport stored lipids in the form of yolk to the oocytes from the intestine (Kimble and Sharrock 1983; Schneider 1996). The *C. elegans* has 6 *vit* genes, *vit-1* to *vit-6*. The *vit-1, -2, -3, -4* and *-5* genes, contribute to the pool of YP170 - the major yolk protein , whereas, the *vit-6* encodes a protein that is processed into YP115 and YP88 (Blumenthal et al. 1984; Spieth and Blumenthal 1985).

4.1.1 Composition of *C. elegans* fat

40-55% (approximately) of total lipids are composed of triacylglyceride fat stores. This is dependent on diet and growth stage. Also, approximately 35% of the dry body mass of the worms is lipid (Braeckman et al. 2009). While the triglyceride stores vary depending on diet, phospholipids levels do not vary

(Brooks et al. 2009). Phospholipid pools are composed of 55% ethanolamine glycerophospholipid, 32% choline glycerophospholipid, 8% sphingomyelin (approximately). The remaining 5% are lyso-choline glycerophospholipids, cardiolipin, inositol glycerophospholipids. Relative abundance of these might change with changes in growth temperature (Ashrafi 2007). The nematode also has a wide range of saturated, monounsaturated and polyunsaturated fatty acids (PUFAs) including arachidonic (20:4n-6) and eicosapentaenoic acid (20:5n-3) as well as monomethyl branched chain fatty acids (mmBCFAs) (Watts and Browse 2002).

4.1.2 Visualization and quantification of *C. elegans* fat

As C*. elegans* is transparent, fat stores can be directly visualized with ease in intact animals. Diverse methods ranging from staining techniques, advanced non invasive microscopy methods, biochemical extractions and quantifications have been employed for this purpose. Only the techniques utilized in this thesis have been described here, however, a summary of all methods with their respective pros and cons can be found in Table 2.

4.1.2.1 Vital dye methods

An easy manner of visualizing fat depots in the worm is supplementing their *E. coli* bacterial diet with vital dyes, like Nile Red or BODIPY-labelled fatty acids (BODIPY-FA). This method leads to accumulation of these fluorescent dyes in various sub cellular compartments, some of which are lipid droplets while others are lysosome related organelles (Schroeder et al. 2007; O'Rourke et al. 2009b; Mullaney et al. 2010; Zhang et al. 2010a). However, staining methods using Nile Red and BODIPY-labelled fatty acid do not distinguish between animals with low fat levels and animals that fail to uptake these dyes (Ashrafi 2007). A major advantage of vital dye labelling is that sample preparation time is minimal, lower variability between samples and *in vivo* studies are facilitated. Also, vital dyes are not known to produce any adverse effects on the growth rate, brood-size, pharyngeal pumping, dauer formation and recovery or lifespan of the worms. These qualities make it profitable for quantitative, robust, high-throughput screening strategies.

Nile Red

Nile Red is a lipophilic dye that fluoresces in hydrophobic environments making it a useful indicator of lipid droplets in cells, tissues, or, in the case of *C. elegans*, in living animals. Nile Red produces a peak emission of 560–580 nm when in environments that have a high concentration of triacylglycerides or very low-density lipoproteins. When in environments that have more of mono- or diglycerides, phospholipids, free fatty acids, Nile Red produces a red shifted peak emission of 620–640 nm (Greenspan and Fowler 1985).

As mentioned earlier, *C. elegans* stores its fat mainly in the gut or intestinal epithelial cells apart from the hypodermis and in the embryos. The intestinal cells of the worm contain gut granules - cell type specific compartments that have been proposed to be lysosome-related organelles (LRO) (Hermann et al. 2005) that are birefringent and auto fluorescent (Schroeder et al. 2007). These granules are different from lysosomes since they lack the key molecular marker LMP-1, the *C. elegans* LAMP homolog of true lysosomes (Schroeder et al. 2007; O'Rourke et al. 2009b). But the understanding of these organelle structures or the properties of these fat storage structures is very poor.

In the worm, LROs are sites of accumulation of age-related auto-fluorescence (Gerstbrein et al. 2005), sites for cellular reservoir for zinc (Roh et al. 2012) and have also been reported to be sites for storage of cholesterol (Wang et al. 2014). It was also observed that these gut granules are the site of accumulation of vital dyes such as Nile Red and BODIPY-FA when these dyes are fed to worms mixed within the bacteria. The *C. elegans* metabolism field has extensively used this fluorescent lipophilic dye, Nile Red to indicate fat stores, based on the staining of granules in the worm's main fat storage organ, the intestine and the lipophilic properties of the above mentioned dyes. Hence, it was concluded that Nile Red stores were the main sites of fat stores. It was observed that Nile Red stains eggs, hypodermis, germ line etc. poorly – tissues that were known to have a higher content of triglycerides as measured by other techniques. Additionally, the IIS defective *daf-2(e1370)* mutant was shown to have a decreased fat phenotype when stained using the vital Nile Red and BODIPY-FA staining, the opposite of what was observed with biochemical analysis which indicated increased fat levels in the *daf-2(e1370)* mutants. Starvation also produced contrasting results; as expected, triglyceride

levels fell with fasting, but Nile Red signal intensity increased in wild type animals. Some other metabolic mutants also showed similar discrepancies (O'Rourke et al. 2009b; Soukas et al. 2009). Moreover, mutants defective for gut granule formation show almost nil staining using Nile Red with normal levels of fat stores (Schroeder et al. 2007). This means that fat stored outside of gut granules might not be correctly quantified using vital Nile Red. This would make it necessary to confirm the observed phenotype with additional measures of quantification of lipids.

Irrespective of this controversy, over 45 papers have used vital Nile Red as a proxy stain for fat stores and have implicated over 400 genes in lipid regulation. This includes usage in high-throughput screens (Ashrafi et al. 2003) designed to identify gene inactivations that cause fat reduction or accumulation. This thesis has utilised the vital Nile Red staining to identify signalling pathways required for the reduced NR staining phenotype observed upon PHB depletion.

4.1.2.2 Fixed staining methods

The very first method employed for histochemical assessment of fat in *C. elegans* was done by fixation using the dye- Sudan Black B (Kimura et al. 1997). Since then several other dyes such as Oil- Red-O (ORO)(Soukas et al. 2009) and fluorescent dyes such as LipidTox (O'Rourke et al. 2009b), BODIPY (Klapper et al. 2011) and Nile Red (Brooks et al. 2009) have been utilized as a proxy for fat content. This thesis has utilised the dye, ORO to determine triglyceride levels in worms. Fixative staining technique involves fixation of the worms using isopropanol or paraformaldehyde and staining with ORO (or any of the above listed dyes). The fixative based treatment is followed by image-based quantification of the amount of bound dye. ORO dye produces results representative of biochemical determination of fat stores (O'Rourke et al. 2009b; Wahlby et al. 2014). Lipid droplets in the intestine, hypodermis and germline can be visualised using this dye (Figure 17). As the worm has a thick cuticle, even after fixation, worms are not uniformly permeable to staining. Therefore, they are subjected to rapid free/thaw cycles to disrupt the cuticle for permeabilisation and penetration of the dye. This technique often disturbs lipid droplet morphology after fixation. Also, fixed staining methods often

result in broken/destroyed worm bodies, making this method difficult for forward genetic approaches.

The methods discussed above are not without their liabilities regarding both execution and analysis. It is always better to use more than one method in order to correctly analyse a metabolic phenotype in an organism.

4.1.3 Fat synthesis and storage

Fatty acids are known to have roles in selective permeability, membrane fluidity and signalling (Watts 2009) and are mostly obtained from the bacterial diet. But, *C. elegans* can also synthesize them *de novo* from acetyl CoA. In *de novo* synthesis of fatty acids - Acetyl-CoA is carboxylated by acetyl-CoA carboxylase (ACC, encoded by *pod-2* gene in *C. elegans*) to form malonyl-CoA. Malonyl- CoA provides 2 carbon units to fatty acid synthase (FAS) to generate fatty acids of different lengths, mainly chains of sixteen carbons (C16:0) (Rappleye et al. 2003; Ashrafi 2007). Palmitic acid (C16:0) can be integrated into TAGs or phospholipids or can be modified by fatty acid elongases and desaturases to form a variety of saturated, monounsaturated (MUFAs) and polyunsaturated fatty acids (PUFAs) of different lengths (Watts and Browse 2002; Watts and Ristow 2017). For storage of fatty acids, fatty acyl-CoAs derived from exogenous or endogenous sources are converted to phosphatidic acid, diacylglycerol and eventually to triacylglycerols (TAGs)(Salway 2004) that are then stored as lipid droplets and yolk. TAGs are a vital energy source during embryogenesis, during low food availability and during the dauer stage

4.1.4 Fat oxidation/breakdown

The flux of lipids through β-oxidation pathways determines how stored lipids are moved. Homologs of mitochondrial and peroxisomal genes encoding proteins involved in β-oxidation of fatty acids are present in the nematodes. Though many of these are encoded by many different family members, studies do suggest that different family members might function under different circumstances. Stored triacylglycerides are mobilized by lipolytic enzymes called lipases that breakdown triacylglycerides to liberate fatty acids. Nematode lipases have homologues for many mammalian lipases including the hormone sensitive lipase (C46C11.1), phospholipase A2 (C07E3.9 and C03H5.4) and the adipose triglyceride lipase (ATGL). The *C. elegans* ATGL is regulated by

AMP-activated kinase and modulates lipid mobilization during the dauer stage (Narbonne and Roy 2009). Another lipase, LIPase Like-4 *(lipl-4)* is known to act downstream of the signals from the germline to regulate fat storage in *C. elegans* (Wang et al. 2008).

Fatty acids that are liberated are then activated to their respective acyl-CoA derivatives by acyl-CoA synthases. There exist short and medium/long chain acyl-CoA synthetases for activation of short and medium/long chain fatty acids. There are at least 7 members of the long chain acyl-CoA synthetases in *C. elegans*. Activation of free fatty acids is important for efficient uptake of nutrients into cells so that it can be utilized by catabolic or anabolic pathways (Mashek and Coleman 2006). Activated fatty acyl-CoA are oxidised depending on their size within mitochondria (short/medium/long chain fatty acids) or peroxisomes (very long chain fatty acids). Activated short chain fatty acids can translocate freely between the cytosol and the mitochondria of cells, however, activated medium- or long chain free fatty acids require the aid of CPT-1 (the nematode ortholog of the human carnitine palmitoyltransferase I) to proceed to β- oxidation. A bulk of these degradation related enzymes have been shown to be expressed in the intestine, hypodermis or both (Mullaney and Ashrafi 2009). Acyl CoA dehydrogenases involved in β-oxidation pathways breakdown fatty acyl-CoAs to acetyl-CoA which can enter the TCA. β-oxidation occurs in the mitochondrial matrix and yields reduced electron carriers, whereas peroxisomal β-oxidation of long-chain fatty acids is not linked directly to energy metabolism as the reduced electron carrier is directly oxidized by molecular oxygen yielding hydrogen peroxide.

4.2 *C. elegans* carbohydrate

Carbohydrates are hydrated organic molecules consisting of carbon, hydrogen and oxygen and are classified based on their structural complexity. The simplest being a monosaccharide, which then form polymers referred to as di-, tri-, oligo- and polysaccharides consisting of repeated monosaccharide moieties with acetal type linkages. Carbohydrates are a major energy source and worms store it as glycogen. Although the bulk of the worm's carbohydrate stores is glycogen (3.3% of the dry body mass) (Cooper and Van Gundy 1970), significant amounts of trehalose and glucose stores are also found (Hanover et al. 2005). Glycogen consists of thousands of glucose molecules and

is broken down by an enzymatic process called glycogenolysis. On the other hand, excess glucose is stored as glycogen by activation of glycogen synthase. There is evidence for glycogen storage as well as glucose mobilization from glycogen in the nematodes. It has been observed that dauers not only accumulate significant amounts of lipids but also glycogen. Glycogen is preferentially mobilized in the dauer state, while glycogen synthesis is downregulated (Holt and Riddle 2003; Depuydt et al. 2014). Since glucose can be used to generate ATP in the absence of oxygen by means of anaerobic glycolysis (Braeckman et al. 2009),it has been shown that increased glycogenolysis can mediate survival in states of anoxia and hypo-osmotic stress (Frazier and Roth 2009; LaRue and Padilla 2011; Depuydt et al. 2014; LaMacchia and Roth 2015).

4.2.1 Visualization and quantification of glycogen

Iodine staining is a simple method, wherein the color of the stain ranges from light brown to dark brown indicating presence of glycogen. But quantitative iodine staining is an issue, as the staining is sensitive to the concentration of iodine used. Moreover, the color is unstable after staining (Morris 1946; Wilson et al. 2002). Effective glycogen staining can be done on whole worms by exposing unfixed worms to iodine vapor or a diluted (1:10-1:20) Lugol's iodine solution (2% I2 in 4% KI) (Frazier and Roth 2009). Both methods are easy and fast but, the Lugol's method has lower contrast than the vapor method.

Figure   18: Iodine staining for visualising glycogen stores.A wild-type and a *daf-2 (e1370)* mutant (top and bottom respectively) stained with iodine and photographed simultaneously. Glycogen can be seen under the pharynx, hypodermis and gut. *daf- 2 (e1370)* adults exhibit increased glycogen storage as shown (Frazier and Roth 2009).

Glycogen stores are observed in early embryos. L1 larvae have little glycogen, but as larval stages progress, glycogen accumulation is observed in the head, tail, hypodermis, or gut in L2/L3 animals. L4 and very young adult animals (Figure 18) had maximal glycogen concentration, which shows a decrease as the animals begin reproduction (consistent with this process exhausting their

stored carbohydrates). In adult males, glycogen is localized in the anterior of the worm and absent from the tail hypodermis (Frazier and Roth 2009).

To validate iodine staining, a histological method - Best's Carmine was tested which gave similar results to the iodine method (Frazier and Roth 2009). A means of observing glycogen stores via vital staining is by using Carminic acid. But, this method of staining has been observed to stain carbohydrate stores only in the intestinal cells or gut of the worms (Hanover et al. 2005; Forsythe et al. 2006; LaRue and Padilla 2011).

4.2.2 Carbohydrate synthesis and storage

Gluconeogenesis is responsible for synthesizing glucose from noncarbohydrate precursors. One of the substrates for gluconeogenesis is glycerol that is derived from triacylglyceride breakdown. Excess carbohydrates may be stored as glycogen. While most of the enzymes in gluconeogenesis catalyze reversible reactions, few non-reversible reactions of gluconeogenesis are catalyzed by phosphoenolpyruvate carboxykinase (PEPCK), pyruvate carboxylase, fructose 1, 6-bisphosphatase and glucose 6-phosphatase. Worms also possess the glyoxylate shunt that allows the synthesis of carbohydrates via gluconeogenesis from acetyl-CoA obtained from fatty acid β- oxidation. The glyoxylate pathway is also known in bacteria, fungi, protists and plants. The main glyoxylate cycle enzymes in *C. elegans*, isocitrate lyase and malate synthase, are contained as two separate structural domains in a single protein, ICL-1 (Liu et al. 1995). An active glyoxylate pathway (Kahn and McFadden 1980; Vanni et al. 1990) has been shown to be required for the survival of long –lived *daf-2* and several ETC-defective mutants (Mit mutants) as well as the mitochondrial mutant *clk-1(qm30)* (Murphy et al. 2003; Cristina et al. 2009; Gallo et al. 2011)

4.2.3 Carbohydrate oxidation

Carbohydrates are broken down by glycolytic enzymes to pyruvate and ultimately to acetylCoA. They can then be converted to and stored as fats. Most enzymes in glycolysis catalyze reversible reactions. The irreversible steps in glycolysis are catalyzed by hexokinase, phosphofructokinase-1 and pyruvate kinase.

5. Protein kinases

Kinases are enzymes that by phosphorylation can alter other proteins. These control key biochemical pathways by phosphorylation of substrate proteins and account for ~2% of genes in several eukaryotic genomes making them one of the largest gene families. Kinases are known to modify the activities of up to 30% of all cellular proteins (Manning 2005). Protein phosphorylation regulates basic functions of all eukaryotes such as DNA replication, cell cycle control, gene transcription, protein translation, signal transduction, growth, differentiation, apoptosis and energy metabolism (Plowman et al. 1999).

Kinases are also a part of several conserved signalling pathways that are known to modulate ageing. Also, several of these signalling pathways have been described to cross-talk via their kinase components. Kinases are evolutionarily conserved and *C. elegans* has homologs for over 80% of the human kinome. The fact that 53 kinase families are conserved amongst yeast, invertebrate and mammalian kinomes shows the diversity of essential functions mediated by kinases (Figure 19A)(Manning 2005).
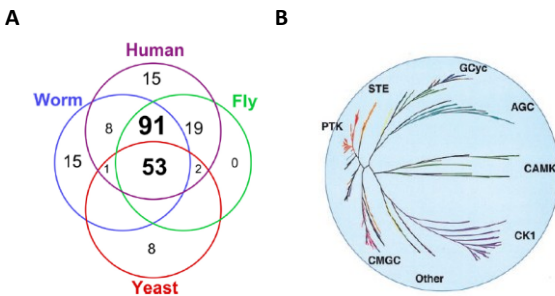
Figure 19: *C. elegans* kinome **A**. Distribution of 212 kinase subfamilies throughout four kinomes (Manning 2005) **B.** Hyperbolic tree representation of *C. elegans* protein kinases with the major protein kinase groups are labelled in different colours (Plowman et al. 1999).

Based on the current accepted classification of protein kinases (as per the KinBase resource - http://www.kinase.com/kinbase/ (Manning et al. 2002a)), the *C. elegans* kinome is divided into two groups –the atypical protein kinases (aPKs) and the conventional eukaryotic protein kinases (ePKs). aPKs are a small set of protein kinases that do not share clear sequence similarity with ePKs, but have been shown experimentally to have protein kinase activity (Manning et al. 2002b). ePKs are the largest group and share a conserved catalytic domain. ePKs have been further classified into eight families (Plowman et al. 1999; Manning et al. 2002a; Manning et al. 2002b)(Figure 19B)

1. AGC family (including cyclic-nucleotide and calcium-phospholipid dependent kinases, ribosomal S6-phosphorylating kinases, G protein-coupled kinases, and all close relatives of these groups)
2. CAMKs (calmodulin-regulated kinases)
3. CK1 family (casein kinase 1, and close relatives)
4. CMGC family (including cyclin-dependent kinases, mitogen-activated protein kinases, CDK-like kinases, and glycogen synthase kinase)
5. RGC family (receptor guanylate cyclase kinases, which are similar in domain sequence to tyrosine kinases, TKs)
6. STE family (including many kinases functioning in MAP kinase cascades)
7. TK family (tyrosine kinases)
8. TKL family (tyrosine kinase- like kinases (TKLs), a diverse group resembling TK but which are in fact serine-threonine kinases)
9. Other group consisting of a mixed collection of kinases that could not be classified easily into the previous families.

In *C. elegans*, kinome wide screenings have been employed to enhance the current understanding of kinases in different processes. For example, to understand the influence of kinases in muscle protein degradation, a kinase screening for over 90% of the kinome was initiated (Lehmann et al. 2013) wherein 40% of kinases studied were found to be of importance in establishing or maintaining muscle cell health, with most kinases required for both. Also, kinases from the Ahringer and the ORFeome library were screened to identify kinases involved in germline hyperplasia (Qi et al. 2017).

5.1 Glycogen Synthase Kinase -3 (GSK-3)

GSK-3 is an evolutionarily conserved serine-threonine kinase. It was first identified as one of the several protein kinases capable of phosphorylating and inactivating glycogen synthase, an enzyme that catalyses the last step in glycogen synthesis. This was reported in rabbit skeletal muscles and was the third such kinase to be discovered, hence named GSK-3 (Embi et al. 1980; Woodgett and Cohen 1984). GSK-3 was later on identified as a major tau protein kinase (Ishiguro et al. 1993).These findings showed the importance of GSK-3 in glucose metabolism and neurodegeneration, which remain major areas of GSK-3 research. Despite its original name, the functions of this kinase extend far beyond its role in glycogen metabolism. GSK-3 has been implicated

in a wide range of biological scenarios including signalling pathways and processes such as cell fate determination, metabolism, transcriptional control across several species (reviewed in (Cohen and Frame 2001; Woodgett 2001). Later on, it was shown through studies using L6 myotubes that insulin signalling through protein kinase B inhibits GSK-3 (Parker et al. 1983; Cross et al. 1995) resulting in the dephosphorylation of substrates of GSK-3, including glycogen synthase and eIF2B (eukaryotic initiation factor 2B). This leads to the insulin-induced stimulation of glycogen and protein synthesis (Cohen and Frame 2001).

5.1.1 GSK-3 isoforms, orthologues and expression

GSK-3 is ubiquitously expressed and is composed of 2 highly homologous genes, GSK-3α (51 kDa) and GSK-3β (47 kDa) (Woodgett 1990) which have similar biological functions and belong to the CMGC group of protein kinases. Both isoforms have 11 exons and share 98% similarilty within their kinase domains, with substantial differences in their N- and C-terminal domains (Lau et al. 1999; Yao et al. 2002). Immunoelectron microscopy and sub fractionation studies in rat cerebellum showed that GSK-3β locates in the cytoplasm, with small amounts detected in the mitochondria and nucleus; while GSK-3α is not detected in the mitochondria (Hoshi et al. 1995). The Drosophila orthologue of GSK-3 is Zeste-White3 or Shaggy (Bourouis et al. 1990; Siegfried et al. 1990) and is known to regulate segment polarity and wing organization. GSK-3 homologues are conserved through eukaryotic evolution (Ali et al. 2001). Many species like fish, amphibians, lizards have both isoforms, while birds have only GSK-3β and appear to have selectively lost GSK-3α (Plyte et al. 1992; Bianchi et al. 1993; Alon et al. 2011). GSK-3α KO mice are viable (MacAulay et al. 2007) whereas, GSK-3β KO mice are inviable (Hoeflich et al. 2000). This distinct phenotype difference between GSK-3α and -β KO mice prompted further study of their individual roles. So far, no isoform-selective inhibitors exist. However, GSK-3 conditional KO models have been generated that allow for tissue-specific deletion of isoforms.

5.1.2 GSK-3 regulation

In contrast to other kinases, GSK-3 is unusual in that it is typically active under basal conditions and is inhibited in response to a variety of inputs (Dorn and

Force 2005). GSK-3 mediated phosphorylation of substrates usually leads to inhibition of those substrates, hence, the inhibition of GSK-3 leads to functional activation of its downstream substrates. Regulation of pathways in which GSK-3 is involved may occur through inactivating phosphorylation by other protein kinases on serine-21 of GSK-3α or serine-9 of GSK-3β. In vitro studies have shown that insulin, growth factors, or certain amino acids inactivate GSK-3 through phosphorylation at serine 21 (GSK-3α) or serine 9 (GSK-3β) through the action of kinases such as AKT/PKB, p90rsk, and p70rsk (Cross et al. 1995; Eldar-Finkelman et al. 1995). Also through changes in tyrosine phosphorylation of GSK-3α at Tyr-279/GSK-3β at Tyr-216 (Cole et al. 2004). More than 50 targets have been reported to be phosphorylated by GSK-3, including metabolic enzymes, signalling molecules, structural proteins, and transcription factors. GSK-3 also exerts a strong influence on several signalling pathways that regulate various cellular functions (Doble and Woodgett 2003; Force and Woodgett 2009; Xu et al. 2009; Cheng et al. 2011; Kaidanovich-Beilin and Woodgett 2011) and is downstream of several signalling pathways such as IIS, Wnt, Hedgehog and Notch (Doble and Woodgett 2003; Sutherland 2011).

Here, we will limit the discussion to insulin and Wnt signalling pathway, as they are more relevant to this thesis. As mentioned earlier for insulin signalling, GSK-3 also plays a key inhibitory role in the Wnt pathway, however, the molecular mechanism of this is still unclear. The Wnts are a family of secretory glycoproteins functioning in diverse developmental processes (Miller 2002). Wnt signalling can be either the canonical or the noncanonical pathway. Here we focus on canonical Wnt signalling. A cytoplasmic destruction complex consisting of GSK-3, Casein Kinase 1 (CK1), Adenomatous Polyposis Coli (APC) and Axin mediate the phosphorylation of β-Catenin, targeting it for polyubiquitinylation and degradation in proteasomes. In the presence of Wnt, the destruction complex becomes inactivated. Wnt triggers signalling by binding to Frizzled and LDL-receptor related protein 6 (LRP6), causing the aggregation of Dishevelled (Dvl) and Axin on the plasma membrane (Bilic et al. 2007; Zeng et al. 2008; Wu and Pan 2010), unphosphorylated β-catenin accumulates in the cytoplasm and translocates to the nucleus, where it can associate with the TCF/LEFs and become a transcriptional transactivator. A model to explain how GSK-3 is inhibited in canonical Wnt signalling suggests that Wnt signalling initiates sequestration of GSK-3 from the cytosol into multi-

vesicular endosomes, thus reducing its cytosolic levels. Though β-Catenin also translocates into the endosomes with GSK-3, once cytosolic GSK-3 is sufficiently degraded, newly translated β-Catenin is not phosphorylated and accumulates in the nucleus (Taelman et al. 2010).

5.1.3 Therapeutic perspectives

Deregulation of GSK-3 function has been implicated in many age related pathophysiological processes such as diabetes, Alzheimer's disease, bipolar disorder and cancer, making GSK-3, a tempting therapeutic target. Lithium was one of the first inhibitors of GSK-3 to be discovered (Klein and Melton 1996) and shown to work in intact cells (Stambolic et al. 1996). Lithium activates glycogen synthase and stimulates glucose synthesis in primary rat adipocytes (Cheng et al. 1983) and in muscle. Stronger inhibitors like, SB 216763 and SB 415286, exhibit high rates of glycogen synthesis in HeLa cells (Coghlan et al. 2000). Since then many chemical inhibitors of GSK-3 have been developed. Lithium has been used for the past several years for treatment of bipolar disorder, Alzheimer's disease, depression and stroke (Chiu and Chuang 2010).

5.1.4 GSK-3 in nematodes

The *C. elegans* orthologue of mammalian *gsk-3*β is *gsk-3 (*previously called, *sgg-1).* In *C. elegans*, the function of Wnt genes, including GSK-3 is required for endoderm specification and mitotic spindle orientation (Schlesinger et al. 1999). GSK-3 also influences C blastomere differentiation during embryonic development independently of its well documented role in Wnt signalling. It restricts the specification of mesendodermal tissue to a single blastomere (Maduro et al. 2001). Wnt signalling regulates diverse biological processes, but, how such varied responses are produced is not yet clear (Sawa and Korswagen 2013). In worms, loss of BAR-1 reduces the activity of the FOXO ortholog DAF-16 in dauer formation and lifespan (Essers et al. 2005). BAR-1 also has a role in vulval precursor cell specification, with *bar-1(ga80)* mutants exhibiting delayed development (van der Bent et al. 2014) along with an incomplete vulva, a protruding vulva and egg-laying defects (Eisenmann et al. 1998). Additionally, Wnt signalling contributes to spindle orientation, cell corpse clearance, and gonadal migration. These depend on a common process of cell cytoskeleton modification. Wnt pathway signals to CED-10/Rac (engulfment pathway) via

two separate branches to regulate modulation of the cytoskeleton in different scenarios. Cell corpse clearance and gonadal migration require the MOM-5 /Fz receptor, GSK-3, and APC/APR-1, that activates the CED-2/5/12 branch of the engulfment machinery. Rearrangement of mitotic spindles requires the MOM-5/Fz receptor, GSK-3, and β-catenins, but not the downstream factors LIT-1/NLK or POP-1/Tcf (Cabello et al. 2010). The canonical Wnt pathway also mediates anteroposterior axon guidance in motor neurons (Maro et al. 2009). GSK-3 dynamics also include regulating oocyte to embryo transition along with KIN-19 (Nishi and Lin 2005; Shirayama et al. 2006). *gsk-3* also inhibits the RAS/ERK pathway function and regulates oocyte growth (Arur et al. 2009). It has been proposed that GSK-3 phosphorylates SKN-1 under normal conditions, and prevents it from accumulating in intestinal nuclei, whereas in conditions of oxidative stress, p38 pathway signalling and PMK-1phosphorylation of SKN-1 are dramatically increased that counteracts inhibition of SKN-1 by GSK-3 (An et al. 2005).A kinome wide screening has also indicated GSK-3 as being essential in protein homeostasis, autophagy and in maintaining mitochondrial network and sarcomere structure in muscle (Lehmann et al. 2013)

5.1.5 GSK-3 in ageing and metabolism

GSK-3α KO mice have a short lifespan (Zhou et al. 2013). In worms, *gsk-3 (nr2047)* mutants have been shown to have a 36% reduction in median lifespan compared with wild type. Hence, loss of GSK-3 is detrimental to lifespan (McColl et al. 2008). Inhibition of GSK-3 via administration of lithium has been observed to extend lifespan, in yeast, flies, humans and *C. elegans* (McColl et al. 2008; Zarse et al. 2011; Sofola-Adesakin et al. 2014; Tam et al. 2014; Castillo-Quan et al. 2016). Lithium addition in the diet can also modulate resistance to stress and metabolism in *Drosophila*, via inhibition of GSK-3 (Castillo-Quan et al. 2016). Recently, there is evidence from studies during late oogenesis in *Drosophila,* that decreased insulin signalling initiates ETC remodeling and mitochondrial respiratory quiescence through GSK3 (Sieber et al. 2016). GSK-3 was also implicated in inhibition of AMPK activity - a key kinase that regulates cellular energy homeostasis (Suzuki et al. 2013; Saldivia et al. 2016)**.**

Depletion of prohibitins (PHBs) reduces lifespan in wild type worms, while, under compromised insulin signalling it extends lifespan. PHB depletion also alters Nile Red (NR) staining *in vivo* both, in wild type and IIS mutants early in adulthood while the phenotype is retained only in IIS mutants during ageing. Thus, loss of PHBs influences ageing and metabolism in a genetic background specific manner. The unique phenotype of PHBs can help to better understand how mitochondrial function regulates lifespan in reponse to different cues. Therefore, the main objective of this thesis is to reveal novel regulators involved in the metabolic response to PHB deletion in wild type and IIS mutants. The specific objectives towards the achievement of this goal are:

1. Characterise *C. elegans* prohibitin deletion mutants.

2. Establish an automated sorting and imaging strategy to screen for genetic interactions of essential genes.

3. Identify signalling pathways mediating the response to PHB depletion by performing a kinase RNAi screen.

4. Investigate the role of GSK-3, a candidate identified in the RNAi screen, in ageing and metabolism.

1. Characterisation of mitochondrial PHB deletion mutants

Prohibitin proteins are essential for embryonic development and for somatic and germline differentiation in the larval gonad of *C. elegans* (Artal-Sanz et al. 2003). In line with that homozygous mutants having a null *phb-1* allele develop into gametogenesis-defective sterile adults due to maternal effect (Artal-Sanz and Tavernarakis 2009b). This makes PHBs part of the approximately 30% of the genes in the worm genome, that have been categorized as essential genes - based on information from screens for lethal or sterile mutants (Brenner 1974; Kemphues 2005). A bulk of these was associated with developmental processes, and hence, the study of such lethal mutations may disclose new information about essential biological processes.Lethal mutations can be propagated and stably maintained in heterozygosis, by introduction of balancer chromosomes. Briefly, these are chromosomal rearrangements that allow lethal or sterile mutations to be maintained in a stable way in heterozygosis. They carry chromosomal errors like inversions or translocations that suppress recombination and thus, prevent loss of terminal alleles in a population. About 85% of the worm genome has been successfully balanced by this manner, with ongoing efforts aimed at covering the whole genome. A bulk of the balancers carry fluorescent transgenes (commonly, GFP) that enable easy identification of heterozygous animals. Homozygous animals are identified with ease as they lack fluorescent transgene expression (Edgley et al. 2006; Chen et al. 2015; Iwata et al. 2016).

Homozygous PHB deletion mutants resulting from heterozygous mothers exhibit sterility and hence, need to be maintained as balanced heterozygous to be viable. The *phb-2* deletion was balanced using an inversion on chromosome II - *mln1[dpy-10(e128) mls14 (myo-2::GFP)],* which carries an integrated pharyngeal GFP. Balancer homozygotes are Dumpy and sterile (because of the *dpy-10(e128)* allele) having two copies of GFP (Figure 20, left), heterozygotes are phenotypically wild type having a single copy of GFP (Figure 20, middle) and homozygous PHB deletion mutants lack GFP (Figure 20, right) and are sterile. As we intended to study PHB deletion mutants in an IIS depleted *daf-2(e1370)* mutant background, *phb-2(tm2998);daf-2(e1370)* double mutants were generated. Since the same allleles are used all through this thesis, mutants can be referred just by the gene name for simplicity.
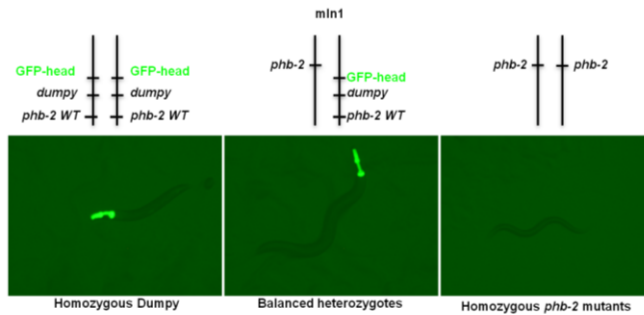
Figure 20: Mitochondrial deletion mutant, *phb-2(tm2998).* Balanced *phb-2(tm2998)* deletion mutants containing the chromosomal inversion *mIn1*[*dpy-10(e128)mIs14(myo-2::GFP)*]*.* Homozygous *phb-2* mutants are smaller in size and lack GFP (right). All worm images were acquired at the Young Adult stage using an Olympus Stereoscope.

On the other hand, *phb-1* deletion was balanced by a reciprocal translocation between chromosomes I and III - *hT2[bli-4(e937)qIs48(myo-2::*GFP*)](I;III)*. However, the *qIs48* element housing the GFP transgene is not very stable (Fernandez et al. 2012) and is often lost, making the task of distinguishing the homozygous *phb-1* worms from the heterozygous wild type difficult and thus, not suitable for large scale experiments. In *C. elegans*, the phenotypes elicited by knockdown of either *phb-1* or *phb-2* via RNAi are the same (Artal-Sanz and Tavernarakis 2009b; Lourenco et al. 2015). Also, both subunits of the PHB complex have been confirmed as absent in both *phb-1 (tm2571)* and *phb-2(tm2998)* mutants (Hernando-Rodriguez et al. 2018). Therefore, we focused on *phb-2* deletion mutants.

1.1 Development is severely delayed in PHB mutants

As mentioned earlier, *C. elegans* develops through four larval stages (L1, L2, L3 and L4) before exiting as a reproductive young adult (YA). All the larval stages are separated by periods of molting (M1, M2, M3 and M4). We utilised a recently developed technique to precisely measure the duration of each larval developmental stage. Briefly, we use *C. elegans* expressing the firefly luciferase (LUC) constitutively and ubiquitously throughout development (Lagido et al. 2008). The luciferase enzyme catalyses oxidation of luciferin generating light. As *C. elegans* is transparent, the LUC-marked strains emit light when provided with exogenous luciferin. The absence of luciferin intake during the molts provokes a decrease in the bioluminescence signal (Olmedo et al. 2015).

Luminescence signal can be determined in single animals. For this purpose, LUC::GFP was introduced in *daf-2* and *phb-2* mutants, as well as *phb-2; daf-2* double mutants. Development from arrested L1s was measured at 20°C. *phb-2* and *phb-2; daf-2* mutants exhibit a strong delay in development in comparison with wild-type and *daf-2* mutants (Figure 21A).
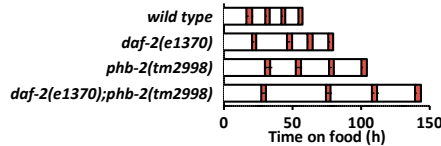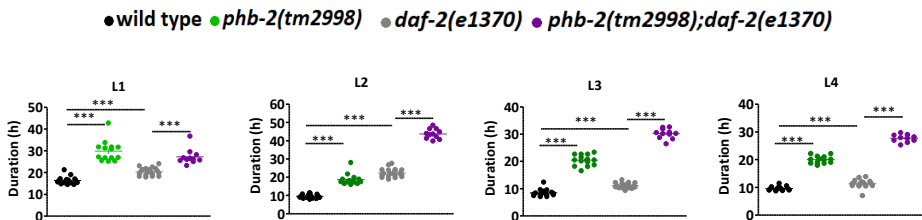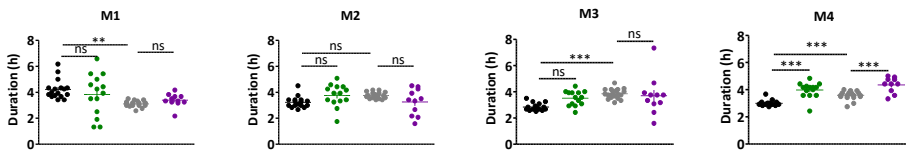

Figure 21: Quantification of the duration of larval stages and periods of molting, using the LUC::GFP bioluminescent reporter. **A**. Average duration of development for wild type (n = 17), *daf-2* (n=19), *phb-2* (n = 14) and *phb-2; daf-2* (n= 11) at 20 ºC. Red represents the molts as inferred by low LUC signal. Error bars represent the SD of the duration of each interval. **B.** Duration of all larval stages (L1-L4). **C.** Duration of all molting cycles. Scatter plot representative of one of two independent experiments (***P ≤ 0.001, **P ≤ 0.01, ns- not significant; 1 way ANOVA, Bonferroni's multiple comparison test).

When comparing each larval stage, we observe that *phb-2* deletion extends the duration of all larval stages, both in wild type and in *daf-2* mutants (Figure 21B). However, the duration of the molting cycles are not significantly affected by *phb-2* deletion, with the exception of the M4, which is extended in both genetic backgrounds (Figure 21C).Additionally, we also note that the duration of larval and molting stages is longer in *daf-2* mutants, when compared against

the wild type, especially the L2 stage, as previously established (Ruaud et al. 2011; Olmedo et al. 2015).

1.2 Pharyngeal pumping is reduced in PHB mutants

Alterations in physiological processes such as delayed development, altered defecation, feeding and pharyngeal pumping rates, reduction in mobility, low brood size, etc. often accompany scenarios wherein mitochondrial function has been compromised (Tsang and Lemire 2003). Pharyngeal pumping was observed to be reduced in wild type animals when subjected to *phb-1/-2* RNAi (Artal-Sanz et al. 2003). PHB deletion in both wild type and *daf-2* mutants significantly reduced the rate of pharyngeal pumping (Figure 22).

Pharynx pumps/min	Day 1
Wild type	243.5 ± 24.84
phb-2	198.6 ± 29.08
daf-2	220.5 ± 23.53
phb-2;daf-2	148.9 ± 32.25
Pharynx pumps/min	Day 5
Wild type	178.4 ± 50.11
phb-2	100.2 ± 49.70
daf-2	129.4 ± 55.06
phb-2;daf-2	59.60 ± 35.32
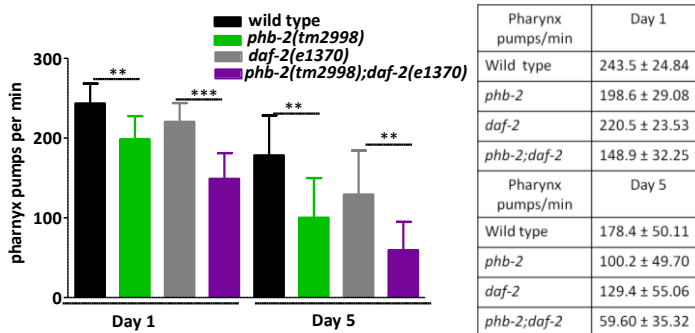
Figure 22: Pharyngeal pumping rates in wild type, *phb-2, daf-2* and *phb-2;daf-2* mutants. Bar graph representative of one of two independent experiments (n>10, Mean ± SD, 1 way ANOVA, Dunn's multiple comparison test, ***P ≤ 0.001, **P ≤ 0.01)

We also observed *daf-2* mutants displayed lower rates of pumping in comparison to wild type animals on both day 1 and day 5. *daf-2* mutants have been previously shown to have reduced pharyngeal contractions albeit at a lower temperature of 15°C (Bansal et al. 2015; Dillon et al. 2016). Pharyngeal pumping decreases during ageing (Huang et al. 2004; Bansal et al. 2015). We observed the same from day 1 to day 5 across all genetic backgrounds (Figure 22).

1.3 Lifespan of the PHB mutants

PHB mutants, *phb-1(tm2571), phb-2(tm2998)* and *phb-2(tm2998);daf-2(e1370)* were subjected to lifespan analysis on *E.coli* OP50 to verify whether they recapitulate the results obtained using RNAi against *phb-1* and *phb-2* (Artal-Sanz and Tavernarakis 2009b). Similar to the lifespan phenotype observed

upon RNAi, both *phb-1* and *phb-2* deletion mutants lived shorter than wild type animals. On the other hand, *phb-2;daf-2* double mutants exhibited increased longevity in comparison to *daf-2* mutants (Figure 23, Table 3).
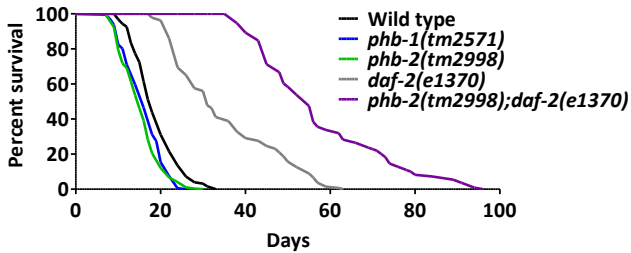

Figure 23: Lifespan of *phb-1, phb-2* and *phb-2;daf-2* mutants on *E.coli* OP50. Survival curves are representative of two independent longevity assays.
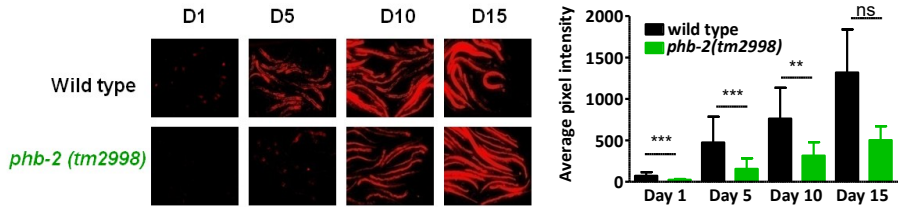
1.4 Nile Red staining is reduced in PHB mutants

It has been previously shown that prohibitin depletion reduces Nile Red staining both, in wild type and *daf-2* mutants early in adulthood. However, as animals age, this phenotype is retained only by *daf-2* mutants on *phb-1/2* RNAi (Artal-Sanz and Tavernarakis 2009b). We assayed the same using PHB mutants to evaluate if Nile Red could be used for screening purposes. The *phb-2* mutants show reduced Nile Red staining (Figure 24A) in comparison to wild type, but reach wild type levels on day 15.

However, *phb-2* deletion in *daf-2* mutants exhibited low staining all throughout ageing up to day 25 (Figure 24B,C), thus, recapitulating the Nile Red phenotype observed upon *phb-1/-2* RNAi. Nile Red staining accumulates through the course of ageing in all genetic backgrounds.

A

B
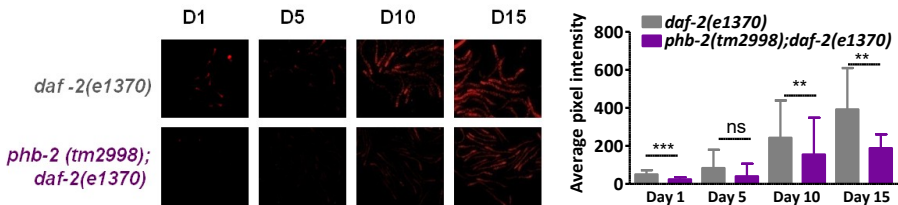
C
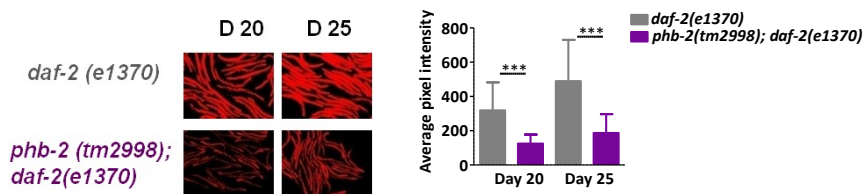
Figure 24: Reduced Nile Red staining in mitochondrial PHB mutants. **A-B** Comparion of Nile Red staining during the course of ageing (day 1 to 15) in **A**. wild type and *phb-2* mutants - images (left panel), the quantification of the same (right panel) and in **B.** *phb-2;daf- 2* mutants as compared to the *daf-2* mutants (left) and bar graph representing average pixel intensity (right). The bar graphs are representative of two independent experiments in both **A** and **B** (n>70 for day 1 & 5, n>50 for day 10 and n>25 for day 15 - all conditions, Mean ± SD, 1 way ANOVA , Dunn's multiple comparison test, ***P ≤0.001, **P ≤ 0.01, ns >0.05; D-Day). **C.** Nile Red staining of *daf-2* and *phb-2;daf-2* mutants on day 20 and 25. Bar graph representative of two independent experiments (n>60, Mean ± SD, 1 way ANOVA, Dunn's multiple comparison test, ***P ≤ 0.001; D-Day).

1.5 Triglyceride levels are increased in PHB mutants

Vital dyes have been strongly debated over what exactly they are staining within the nematode in the recent past. Hence, we analyzed the lipid status of PHB mutants using Oil-Red-O, a fixative based staining method more reliable for analysing fat content. We observed increased Oil-Red-O staining in PHB

mutants (Figure 25). In accordance with previously published data, *daf-2* mutants showed increased triglycerides (Yen et al. 2010) in comparison to wild type animals. Moreover, *phb-2;daf-2* mutants displayed more triglyceride content in comparison to *daf-2* mutants (Figure 25).
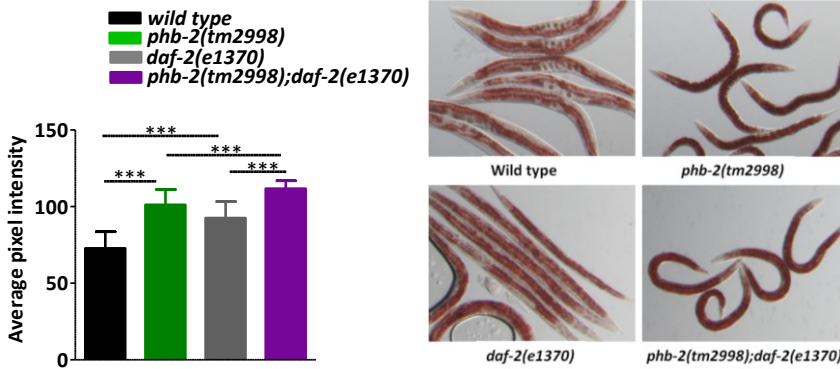
Figure 25: Oil-Red-O staining of mitochondrial PHB mutants compared to wild type and *daf-2* mutant backgrounds on first day of adulthood (Day1). Worms were stained using the quick Oil-Red-O method (wild type (n=52), *phb-2* (n =38), *daf-2* (n =67), *phb-2;daf-2* (n =34), Mean ± SD, ***P < 0.001; 1 way ANOVA, Bonferroni's multiple comparison test). Representative images are shown).

2. Automated worm-sorting and image analysis for the study of essential genes

2.1 Sorting conditions for homozygous PHB deletion mutants

The worm sorter, COPAS, was used to facilitate sorting of the mitochondrial PHB mutants. Previously, similar sorting conditions have been reported for selection of homozygous worms that lack pharyngeal GFP from a mixed population at the L3 (Latorre et al. 2015)and L4 (Ruegger et al. 2015)larval stages. In this thesis, worms were sorted at the L1 larval stage in order to facilitate RNAi from the start of larval development.

In order to select the population of interest lacking pharyngeal GFP, we initially acquired data from over 200-500 worms in order to gate a proper region of worms hence, excluding unhatched eggs, dead corpses within the samples, curled worms etc. The data of acquired worms can be stored as.txt or in an excel format for review, in order to set proper conditions and also for future references. Based on that, we drew a gating region within a particular area on Extinction PeakHeight (Ext PH) vs Extinction PeakWidth (Ext PW)(see Figure 26, upper dot plot). This aids in selection of worms that have a certain maximal optical density and a certain length above the set threshold avoiding unwanted objects. Next, we viewed green PeakWidth vs green PeakHeight parameters in the sort dot plot that enabled us to view the different populations of worms: homozygous *phb-2* worms (non - GFP in the pharynx), heterozygous wild type (GFP expression in the pharynx) and dumpy worms (GFP expression in the pharynx)(see Figure 26, lower dot plot). This reflects the relative green fluorescence within the earlier gated population. We select and sort the nonGFP homozygous worms (Figure 27, A and B) from the mixed population.

Once, sorting parameters were successfully established, we sorted around 40 PHB homozygous larvae per well in a 96-well microtitre plate. Under ideal working conditions, one plate took approximately 40 minutes. Worms were grown till the young adult stage in bacteria producing dsRNA supplemented with Nile Red. In order to quantify the intensity of Nile Red staining, we designed a customized protocol for worm segmentation.
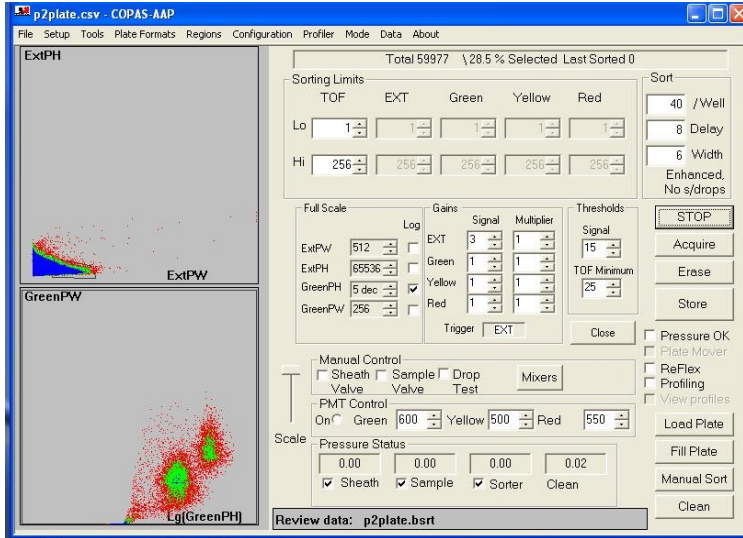
Figure 26: Screenshot of the dot plot view with the established gating (upper) and sorting (lower) conditions for *phb-2(tm2998)* mutants. The scale, gains, thresholds, photomultiplier tube (PMT) control levels, the sort delay and width are values that were adjusted based on several sorting tests and specific values were chosen that are best for the sample being analyzed.
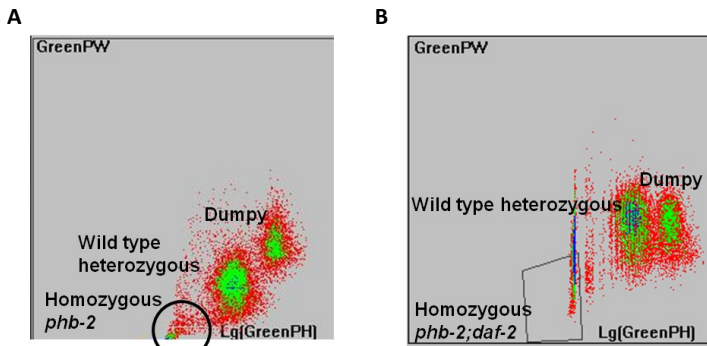

Figure 27: Screenshot of the sorting regions. Sorting dot plot of **A.** *phb-2(tm2998)/mIn1* balanced animals, where the population of *phb-2(tm2998)* homozygous L1 larvae that are sorted is marked by a circle and **B.** *phb-2(tm2998);daf-2(e1370)/mIn1* balanced animals, where the *phb-2(tm2998);daf-2(e1370)* homozygous L1 larvae is marked by a square.

2.2 High-throughput imaging strategies

2.2.1 Image acquisition and analysis

Image acquisition was done using the IN Cell Analyzer 2000, an inverted microscope designed for automated fluorescent imaging and analysis of cells. We optimized imaging and segmentation protocols to be applied to *C. elegans*.

Building an imaging protocol starts with an acquisition protocol that establishes the plates and selection of wells to be imaged, amongst other parameters such as wavelengths and exposure times to use. Once an established protocol is run, the system works without user input to complete the imaging. Once worms reached the desired stage, here, the young adult (YA) stage, images were acquired by utilizing the 2x objective, in three different channels – brightfield, FITC/GFP and Cy3/Red at identical settings and exposure times (see Materials and Methods). Image analysis for quantification of Nile Red intensity was performed with a user-defined protocol created using the Developer Toolbox software (version 1.9.2) (GE Healthcare). This software accompanies the IN Cell Analyzer 2000 and enables direct upload and automated analysis of image stacks. The FITC/GFP channel was added for well segmentation and to spot accidently sorted heterozygous worms with pharyngeal GFP expression which were then removed from the data analysis.

The segmentation protocol was built from individual sets of targets which were then linked together to obtain all the required measurement regions in one target. Each target was created step by step -1) pre-processing to enhance the image prior to segmentation, 2) segmentation of the target to generate a mask, after which post processing operations were added to clean up the target mask. Once the targets had been created and optimized, measurements were made in the individual targets or the linked target sets. The following targets were created: thewell edge (used to subtract out any well debris), the worm and the dilated worm (used to calculate background intensities adjacent to the worm). First, intensity based well segmentation was done using the auto fluorescence of the well edge in the FITC/GFP channel and after post-processing refinement steps, the resultant segmentation mask was inverted to give the well edge (Figure 28A). Next, the bright field image was enhanced using a pre-processing step to achieve better segmentation of worms in the brightfield channel (Figure 28B). After post processing, refinement of the worm mask and subtraction of the well edge to remove well artefacts, acceptance criteria based on morphological parameters were applied to remove unwanted worms and debris (Figure 28C). The worm mask was transferred sequentially to the Cy3/Red channel which enabled additional acceptance criteria based on intensity measures to be applied if necessary to further refine the final worm target set (Figure 28D).The final worm mask was then copied and dilated to

generate a region around the worm to enable calculation of immediate backgroundintensity (Figure 28E).
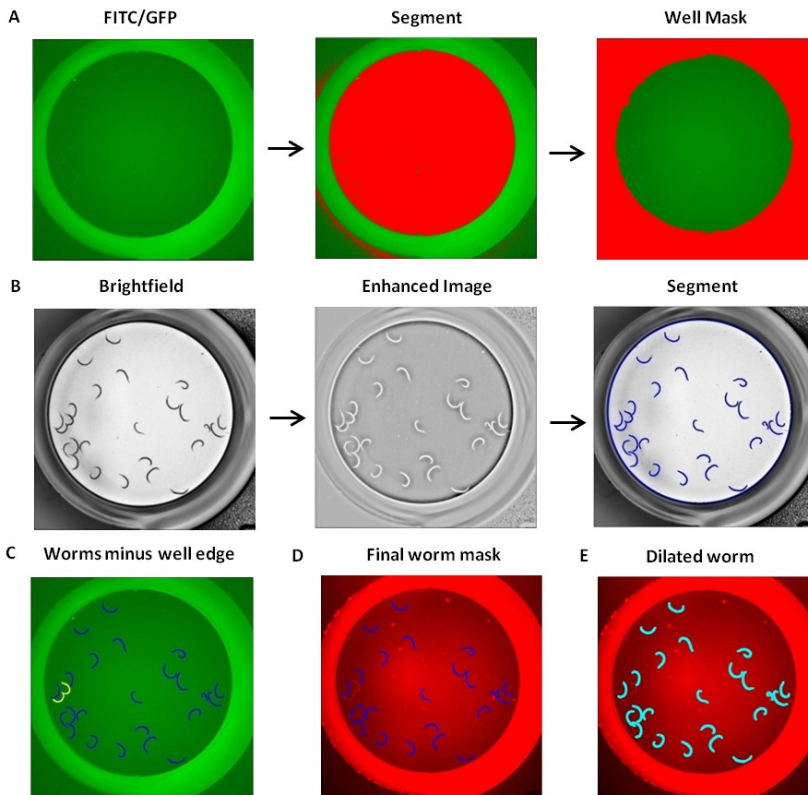

Figure 28: Outline of the image segmentation protocol for balanced mutants. **A.** Well segmentation was done in the GFP channel based on intensity and then the image was inverted. **B.** The image in the brightfield channel was subjected to pre-processing to enhance the contrast, to enable ease of segmentation. The segmented worms were tagged in blue. To select worms and to exclude artefacts/debris, acceptance criteria based on morphological parameters were applied (these can be modulated as per user requirement).**C.** Next, the well edge was subtracted from the segmented worms (blue) and overlapping worms (yellow) were excluded. **D.** This segmented worm mask was transferred to the Cy3/Red channel. **E.** For background subtraction, the segmented worms were dilated in order to measure theintensity of the immediate background.

In the final sequence, the targets, worm and background, were linked together to get both measurements together in one target. The software links two targets at a time and there must be at least one pixel overlap to achieve a linkage. Thus, the final Worm Mask was linked to Dilated Worm Mask, to result

in a target which has both measurement regions - worm mask and dilated worm mask (Figure 29A). By the dilation of the worm, we can measure and subtract the intensity of the immediate background. This feature is very useful when screenings require usage of dyes (such as the one used in this thesis), as dyes can stain plastic and can cause different background intensities depending on the area of the well being measured. A comprehensive list of measures for each worm was collected covering morphological and Intensity based measures from the Cy3/Red channels (Figure 29B).

For experiments that involved older worms, the analysis protocol was checked at each step and the segmentation parameters, post processing steps and acceptance criteria were re-optimized.

A
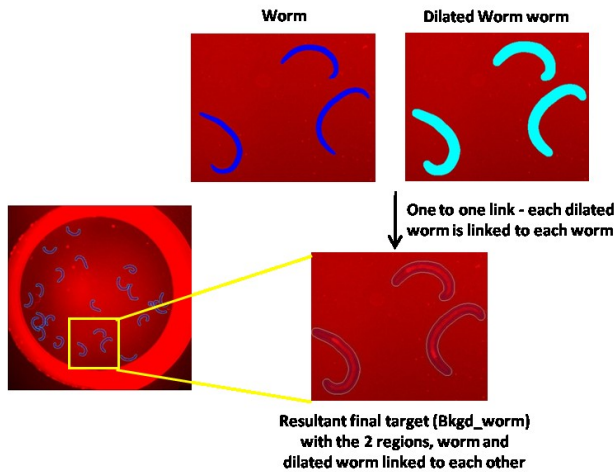
B

Target	Fiber Length Worm	Int Worm	Int Bkgd Cy3	Int Worm - Bkgd	area
1	827.500	295.587	276.694	18.893	30681.552
2	715.362	294.108	265.131	28.978	25161.612
3	841.149	315.978	304.674	11.305	32681.332

Figure 29: Target linking and background subtraction **A.** Target linking to compose a final target. Worm mask and dilated worm were linked together. The final target shows the two measurement regions: the worms outlined in blue, the immediate background outlined in cyan. **B.** Identified targets with the corresponding measurements. The output sheet from the Developer toolbox with the segmented worms and their measures such as fiber length (Fiber length worm), Intensity of the worm (Int Worm), intensity of the immediate background (Int Bkgd Cy3), background subtraction (Int Worm - Bkgd) and the area of the worm (area). Additional measures like major axis length, X/Y position, form factor can be added as per user requirement during target linking.

2.2.2 Improved image analysis incorporating identification of heterozygous worms using Developer Toolbox

The above image acquisition and segmentation protocol has been modified to incorporate a step that correctly identifies unwanted heterozygous worms with green pharynx. This was required as the sorting with the COPAS might not always be efficient, resulting in eventual heterozygous worms with pharyngeal GFP expression in the screening plates. This modified protocol follows the same initial steps of well segmentation in the green channel image and segmentation of worms in the brightfield image, followed by subtraction of the well edge (Figure 28). Once worms were well delineated, green heads of the heterozygous worms with pharyngeal GFP were segmented in the FITC/GFP channel image and acceptance criteria based in area and intensity were used to better define green heads (Figure 30 and 31A). In the final sequence, the targets were linked together to get all three measurement regions together in one target. Here, Final Worm Mask was linked to Dilated Worm Mask, Worm-Green Head was linked to Dilated Worm Mask, then using a composed link these two groups were linked together to result in a target which has all three measurement regions, final worm mask,the dilated worm and the worm minus green head linked together (Figure 30 and 31B). User defined morphological and intensity based measurementswere collected for each worm from both green and red channels (Figure 31C).
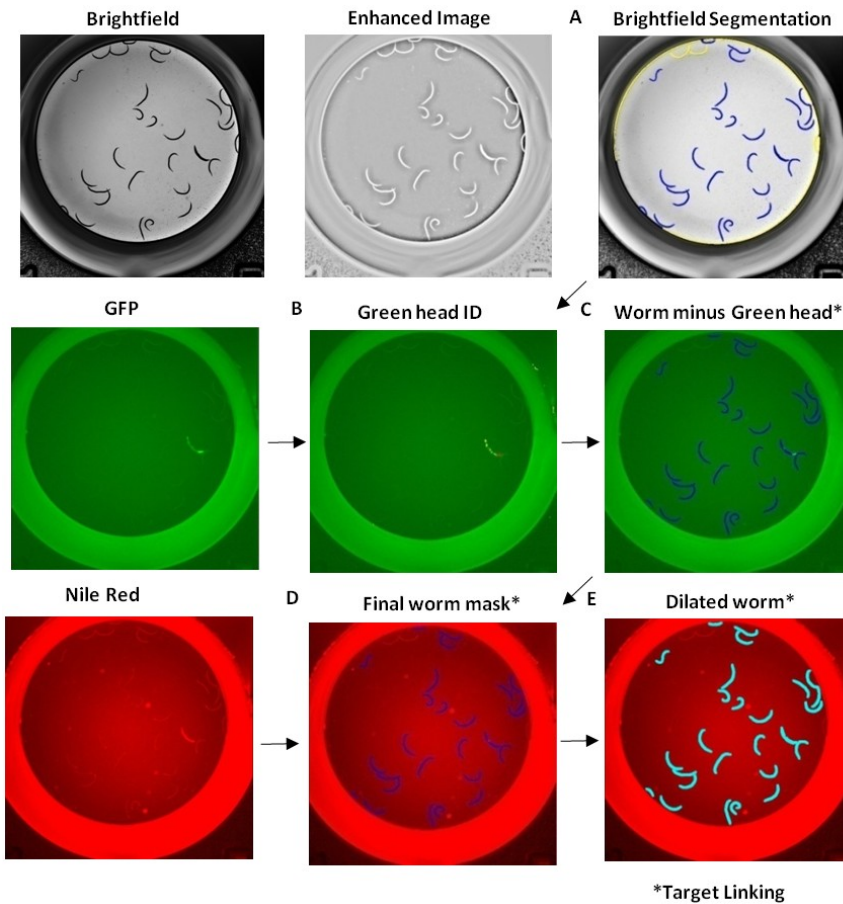
Figure 30: Outline of the protocol for identification of heterozygous worms with GFP expression in the pharynx. Briefly, post well segmentation in the green channel, the worms were segmented after enhancing the contrast in the Brightfield Channel (Image A). Acceptance criteria were applied to remove artefacts (Blue accepted, Yellow rejected). The worm mask was transferred to the green image to identify, if needed, worms with green heads based on the green head ID (Image B and C). The final worm mask dilated (Image E), the dilated region around the worm, was used to calculate the immediate background intensity. Finally, the targets labelled by asterisks are linked together to get all three measurement regions, i.e, Dilated worm, Worm minus Green Head and Final Worm Mask, together in one target.

A
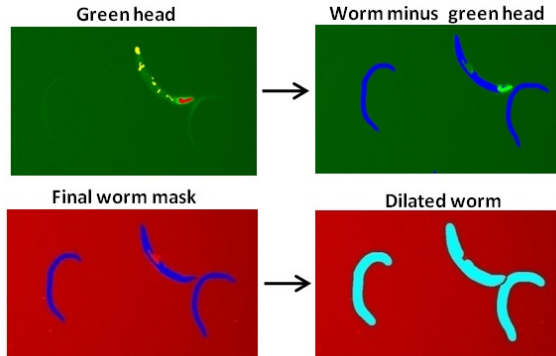
B
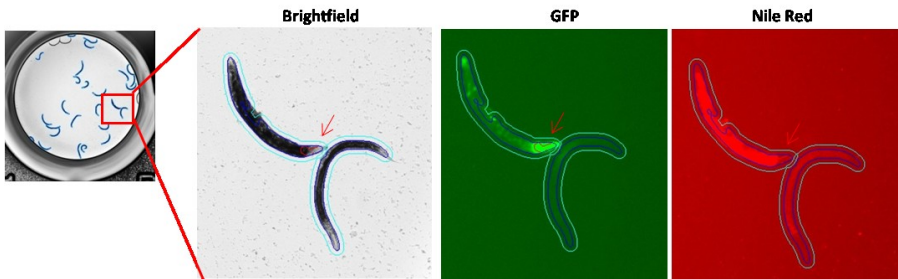
C

Target	Int Worm-Bkgd FITC	Green Head ID	Int Worm-Bkgd Red
12	212.897	9.318	206.398
13	1.506	0.000	11.484
14	2.313	0.000	15.546

Figure 31: Identification of heterozygous animals (Green Head ID). **A.** After worm delineation in the brightfield channel, green heads were segmented and tagged in red. In the next step, the identified green heads were subtracted from the worm bodies. As a result, segmented worms appear blue without the green heads, thus, "worm minus green head".Segmented worms are dilated (bottom panel) in order to facilitate measurement of the intensity of the immediate background. **B.** A balanced heterozygous animal expressing pharyngeal GFP has been identified (red arrow) within a population of homozygous *phb-2* mutants. The heterozygous animal exhibits increased Nile Red staining in comparison to the homozygous *phb-2* mutants.**C.** Segmentation analysis output of the analysis for balanced mutants. Intensity of the worm subtracting the background intensity in the green image (Int Worm - Bkgd FITC), identification of green head (green head ID) and intensity of the worm subtracting the background intensity in the red image (Int Worm - Bkgd Red) are depicted in the analysis output. Target 12 is the correctly identified heterozygous worm with a green head ID greater than 0.

2.3 Open-sourcing of the segmentation protocol through CellProfiler

These segmentation protocols built via the Developer toolbox limits their usage to researchers with access to the GE Healthcare platform. To get around this disadvantage, we implemented the protocol in the free and open source CellProfiler software (Hernando-Rodriguez et al. 2018), thus, providing an analysis pipeline to identify green head worms, and capable of measuring intensities in both green and red channels.

We compared worm segmentation outputs resulting from the Developer Toolbox and CellProfiler and found them comparable (Figure 32B). We evaluated wild type and *phb-2* mutants after Nile Red staining and observed lower Nile Red staining in *phb-2* mutants irrespective of the software used for segmentation (Figure 32C), hence, validating this method. The image analysis protocol generated through the CellProfiler software is easily adaptable to the user's needs in terms of different fluorescent markers, image formats and image resolutions.
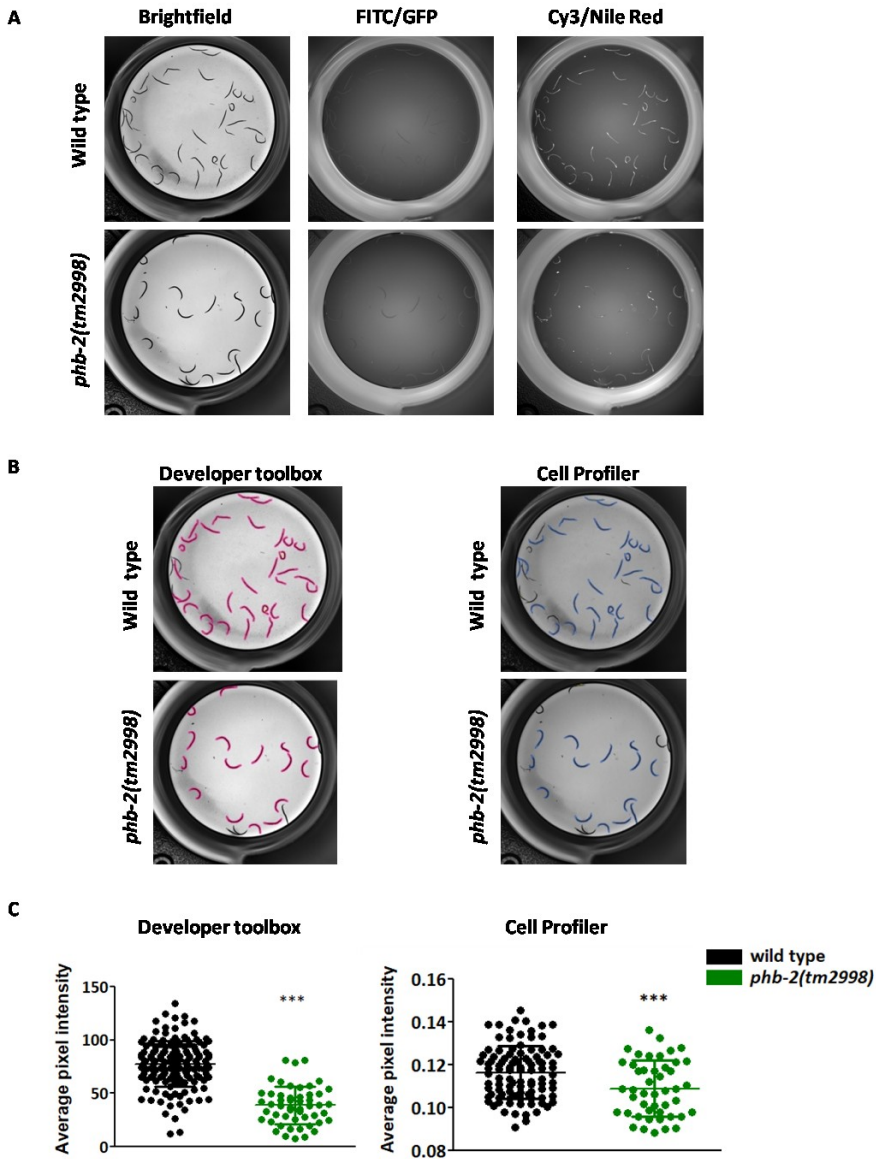
Figure 32: Open sourced segmentation protocol (CellProfiler).**A.**Representative images of wild type and *phb-2(tm2998)* mutants taken sequentially in the brightfield, GFP and Cy3 channels using the IN Cell Anlayzer 2000.**B.**Comparison of the image segmentation output for wild type and *phb-2(tm2998)* mutants generated from Developer toolbox (GE Heathcare) versus CellProfiler. **C.** Quantification ofNile Red staining of *phb-2(tm2998)* mutants versus wild type animals. Graphical representation of data obtained from the Developer toolbox and CellProfiler protocols. As previously shown, depletion of *phb-2* reduces Nile Red staining using both of the protocols (*** P value < 0.0001; Unpaired t-Test)

3. A kinase RNAi screen to identify genetic interactors of mitochondrial prohibtins

The opposing ageing phenotypes elicited by lack of PHBs provided an opportunity to understand which cellular signalling pathways may differentially regulate ageing depending on external or internal energy demands (Artal-Sanz and Tavernarakis 2009b). This project was aimed at identifying genes that might play a role in regulating metabolic responses to prohibitin depletion under conditions in which PHB depletion affects ageing in an opposite manner.

We performed an RNAi screen to identify relevant signalling pathways involved in PHB-mediated phenotypes, by screening the contribution of all kinases represented in the ORFeome RNAi library (Rual et al. 2004). Kinases are conserved signalling molecules modulating cellular processes and popular targets for drug discovery. Moreover, the *C. elegans* kinome has 81% homology with human kinases (Manning 2005). We utilised *phb-2* and *phb-2; daf-2* mutants for the screening and exploited the reduced Nile Red staining phenotype observed upon PHB depletion in wild type and IIS mutants (Figure 24) (Artal-Sanz and Tavernarakis 2009b) as a read out. Despite the discrepancies surrounding vital Nile Red staining (O'Rourke et al. 2009b; Soukas et al. 2013; Wang et al. 2014) it is extremely convenient for screening strategies and has helped identify gene inactivations that modulate fat metabolism (Ashrafi et al. 2003).

As mentioned earlier, the PHB mutants are balanced strains and require a laborious selection of homozygous PHB mutants. Hence, we grew worms in liquid cultures to scale up the worm populationand employed the worm sorter, COPAS, for sorting worms of interest. The ORFeome kinase sub-library contained 264 kinases, 32 clones did not grow and hence, the total number of analyzed kinases is 232. The 232 kinases are housed in three 96 well plates where the last row has been left empty to house controls. For quantification of the Nile Red staining, a worm segmentation protocol was developed for the imaging platform IN Cell Analyzer 2000 (GE Healthcare) (Figure 33).
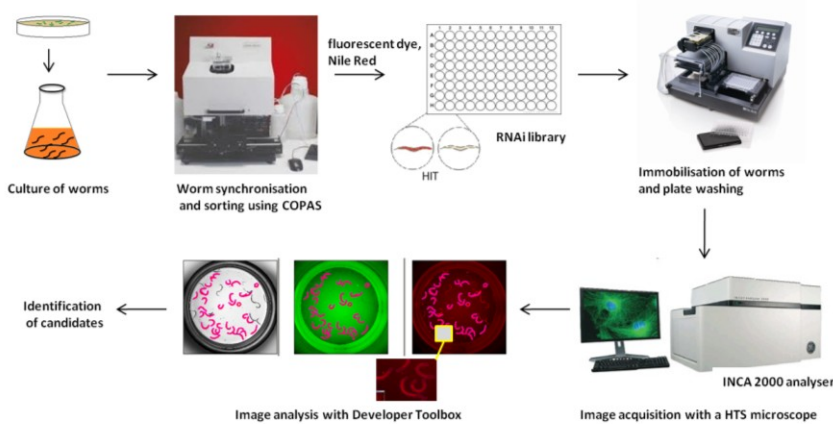
Figure 33: Overview of the RNAi screening strategy. Worms are grown in liquid media to generate large populations. Homozygous PHB mutants are sorted at L1 stage from a mixed population of balanced heterozygous animals into multiwell plates using the COPAS Biosort "worm sorting". Next, bacteria containing the ORFeome kinase RNAi sublibrary are added to the wells, supplemented with Nile Red and worms are incubated at 20°C. When worms reach the desired stage, plates are washed to clear bacteria and they are imaged in brightfield and fluorescent channels using an automated microscope, IN Cell Analyzer (GE Healthcare). A user-defined image segmentation protocol is used to define potential hits based on the intensity of Nile Red staining of worms in comparison with the control.

We screened for RNAi clones that increase Nile Red staining and, thus, suppress the reduced Nile Red phenotype of *phb-2* deletion in otherwise wild type animals and in *daf-2* insulin receptor mutants. The empty vector pL4440 stained with 100nM was run in all the plates as negative control. In order to ensure the effectiveness of the RNAi screen, additionally a positive control was established -*sgk-1(RNAi)* that increases Nile Red staining (Jones et al. 2009).

The primary screen comprised two biological replicates using *phb-2* and *phb-2; daf-2* mutants. 4-6 wells with empty vector and 2 wells with positive control were run in the primary screen. 41 RNAi clones that were above the range representing +1SD from the mean of the control (empty vector) and were recurring in both sets of biological repeats were chosen to be screened a third and final time. The 41 candidates were re-tested in a liquid format and resulted in a final list of 26 significant candidates (Figure 34).
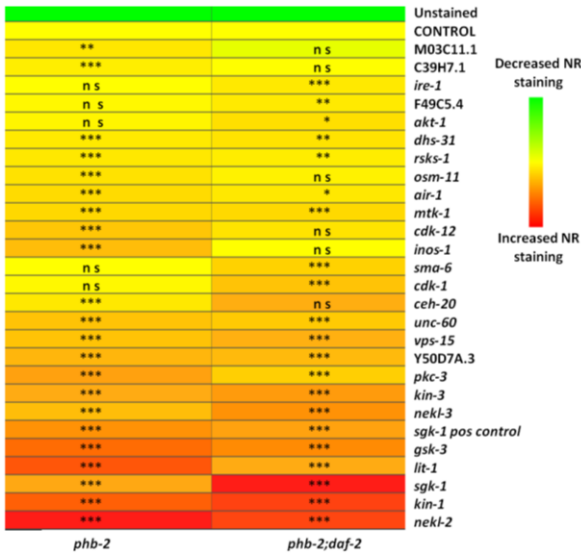
Figure 34: Heatmap depicting the behaviour of the 26 kinases identified from the RNAi screen upon Nile Red staining in PHB deficient backgrounds. These clones cause a significant difference in Nile Red staining with respect to the control, in any of the two genetic backgrounds (One way ANOVA, Dunn's multiple comparison test, ns = not significant $p>0.05$, *=$p<0.01$, ** = $p<0.01$, *** = $p< 0.001$)

We only recovered kinases that suppressed the reduced Nile Red staining phenotype of PHB mutants. We did not observe any kinases enhancing this phenotype. The identified kinases could be put into 18 functional groups with a bulk related to phosphorylation (Figure 35), followed by kinases whose function is related to reproduction and development, where PHB has been shown to be essential (Artal-Sanz et al. 2003). We also observed kinases related to lipid storage and the Wnt signalling pathway. Amongst the candidates, we also encountered kinases that have been previously shown to modulate longevity and fat metabolism and previously shown to interact with PHB, such as SGK-1, the serum and glucocorticoid kinase 1,regulates fat metabolism in *C. elegans* (Jones et al. 2009; Soukas et al. 2009) and interacts with PHB to regulate lifespan and the mitochondrial unfolded protein response (UPR[mt])(Gatsi et al. 2014). Apart from this, we also identified the S6 kinase/RSKS-1, a conserved substrate of the mechanistic Target of Rapamycin (mTOR) complex 1 (Laplante and Sabatini 2012) that regulates fat (Shi et al. 2013) and interacts with PHB to regulate lifespan in yeast (Schleit et al. 2013). Another kinase that was identified in the screening was MTK-1, an ortholog of human MAP3K4 (mitogen activated protein kinase kinase kinase 4) that also interacts with PHB. PHB mutants subjected to *mtk-1* RNAi exhibit increased UPR[mt] (Villringer and Artal-Sanz, unpublished data). Among the kinases related to Wnt signalling, a strong candidate was the glycogen synthase kinase-3, GSK-

3. GSK-3 is a conserved serine/threonine kinase that is phosphorylated upon prohibitin depletion in mice hippocampus (Merkwirth et al. 2012). Here, we observed that lack of *gsk-3* suppresses the reduced Nile Red staining phenotype of PHB mutants.
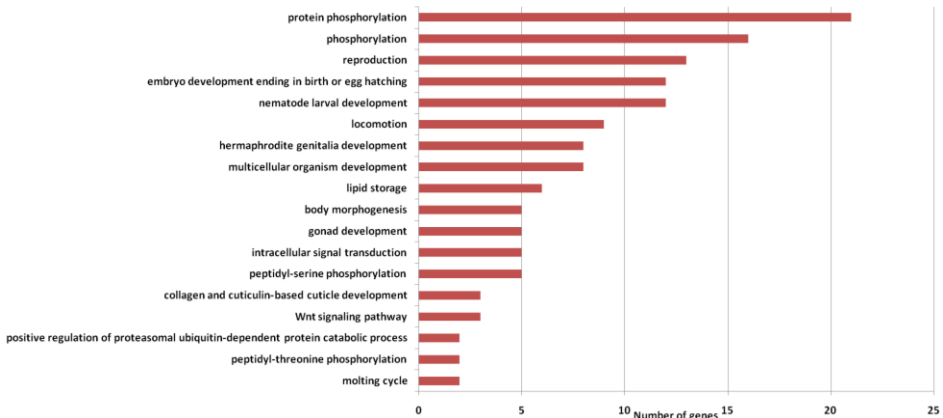

Figure 35: Classification of the identified 26 kinases according to function built using DAVID Bioinformatics Resource 6.8. Significantly enriched GO terms (p<0.05) have been represented.

As our goal was to ultimately identify genes involved in the lifespan phenotype conferred by PHB depletion, we pre-selected certain candidates to ascertain their role in longevity upon mitochondrial prohibitin depletion (Appendix 1, A1.2-A1.5).

4. Establishing the role of GSK-3 in longevity and metabolism

Among the pre-selected candidates, GSK-3 was chosen for further analysis. GSK-3 is a multifaceted conserved kinase and a known target of AKT that regulates systemic metabolism (Cross et al. 1995; Cohen and Frame 2001). GSK-3 has many substrates and is involved in many other processes including in Wnt signalling and in disease pathologies (Kaidanovich-Beilin and Woodgett 2011; Sutherland 2011; Patel and Woodgett 2017). Additionally, the role of GSK-3 has been studied immensely in early nematode development (Schlesinger et al. 1999; Maduro et al. 2001; Nishi and Lin 2005; Arur et al. 2009; Maro et al. 2009; Cabello et al. 2010) and while GSK-3 has established functions in metabolic regulation in other organisms (MacAulay et al. 2007; Alon et al. 2011; Zimmermann et al. 2013; Castillo-Quan et al. 2016; Chen et al. 2016; Sieber et al. 2016; Markussen et al. 2018), a role for GSK-3 in metabolism in *C. elegans* is unknown. Based on these observations, we decided to ascertain the role of GSK-3 with a focus on how its depletion might alter the longevity and metabolism seen upon mitochondrial prohibitin depletion and also compromised IIS signalling.

4.1 GSK-3 differentially regulates lifespan in *C. elegans* depending on the metabolic status

Previously, *gsk-3*(*nr2047*) mutants have been shown to exhibit reduced lifespan at 25°C (McColl et al. 2008). Wild type animals on *gsk-3* RNAi showed a mild reduction in lifespan (Figure 36) as observed in *gsk-3*(*nr2047*) mutants, while the long lifespan of IIS mutants was almost fully suppressed upon GSK-3 depletion, showing for the first time that GSK-3 is essential for the long lived phenotype of insulin mutants (Figure 36, Table 4). The lifespan of *phb-2* mutants on *gsk-3* RNAi was only very mildly affected, while the double *phb-2; daf-2* mutants showed a strong reduction, similar to *daf-2* mutants. Thus, GSK-3 depletion resulted in a differential reduction in lifespan across all genetic backgrounds. This phenotype was similar irrespective of addition of FUdR, to prevent progeny production (Refer Appendix 2.1, Table 4). We also inhibited GSK-3 by addition of lithium (a chemical compound previously shown to inhibit GSK-3 (Stambolic et al. 1996)) in wild type and *daf-2(e1370)* mutants, and observed suppression of lifespan at 20°C, contrary to published data (Refer Appendix 2.2, Table 4).

All genetic backgrounds exhibited vulval bursting on *gsk-3(RNAi)*, the phenotype being more severe in wild type animals (Table 4). Though we censored worms that exhibited vulval explosion during lifespan assays (like most laboratories), this phenomenon has been described in detail as age associated vulval integrity defects (Avid) by the Kaeberlein Lab and has been proposed as a marker for healthspan in nematodes (Leiser et al. 2016).
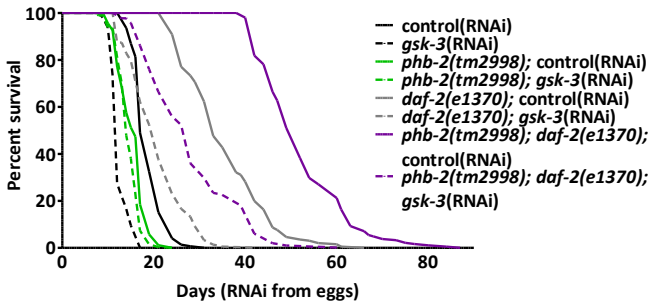

Figure 36: Lifespan analysis of wild type, *daf-2*, *phb-2*, and *phb-2;daf-2* subjected to *gsk-3(RNAi)* post embryogenesis. Average of two independent lifespan curves has been represented here.

GSK-3 function is essential during early embryonic development (Maduro et al. 2001; Nishi and Lin 2005; Shirayama et al. 2006). We noticed a slight developmental delay in worms grown on *gsk-3(RNAi)* from the L1 larval stage. In order to avoid deleterious developmental effects and to monitor whether GSK-3 functions during ageing, we assayed the effect of GSK-3 depletion from adulthood. We observed that mean lifespans wereincreased when worms weresubjected to *gsk-3(RNAi)* from adulthood (Figure 37) in comparison to post embryogenesis confirming a role for GSK-3 during development.
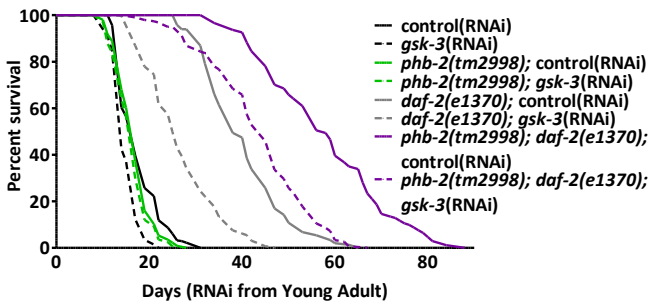

Figure 37: Lifespan analysis of wild type, *daf-2*, *phb-2* and *phb-2; daf-2* mutants subjected to *gsk-3(RNAi)* during adulthood. Average of two independent lifespan curves has been represented here.

Wild type animals subjected to *gsk-3* RNAi exhibited significantly reduced lifespan (17%), whereas GSK-3 depletion in IIS *daf-2* mutants led to a pronounced decrease (34%) in lifespan, confirmingthat GSK-3 is essential for the extended longevity of *daf-2* mutants. Interestingly, depletion of GSK-3 did not affect *phb-2* mutants, while the lifespan of *phb-2; daf-2* mutants decreased by 22 % upon *gsk-3(RNAi)* (Figure 37 and Table 4).

Remarkably, we observed that prohibitin deletion conferred a survival benefit to GSK-3 depleted animals, both in wild type and *daf-2* mutant backgrounds, regardless of whether gene knockdown via RNAi treatment was initiated post embryogenesis or from adulthood (Figure 36 and 37, Table 4).

4.1.1 Loss of Wnt components, KIN-19 and BAR-1 elicits a similar lifespan phenotype as seen upon *gsk-3(RNAi)*

GSK-3 is a component of the destruction complex in canonical Wnt signalling in *C. elegans,* whereit functions along with Axin, the tumor suppressor gene product APC, and the casein kinase CK1 to degrade β-catenin and thus, suppresses the expression of specific target genes. In worms, the kinase CK1 and β-catenin are encoded by *kin-19* and *bar-1*. We investigated the role of KIN-19 and BAR-1 in lifespan regulation to determine if the GSK-3 phenotypes were mediated by Wnt signalling.

Loss of KIN-19 elicited a similar response as GSK-3 depletion during ageing, as inhibiting *kin-19* from adulthood by using RNAi led to a lifespan decrease across all backgrounds with the exception of *phb-2* mutants and being the effect stronger in *daf-2* mutant backgrounds (Figure 38, upper panel, Table 5). Moreover, the beneficial effect in lifespan seen upon loss of GSK-3 in mitochondrial mutants was also observed upon loss of KIN-19. Similarly, loss of BAR-1 significantly reduced lifespan in IIS mutant backgrounds (Figure 38, lower panel), though the observed decreases were much milder than those observed upon loss of GSK-3 and KIN-19 (Table 4 and 5).Consistent with the role of BAR-1 in vulval cell specification, we observed vulval rupture in worms grown on *bar-1(RNAi)*. Loss of KIN-19 also led to vulval ruptures, similar to the loss of GSK-3 phenotype. Worms that were lost from the analyses due to this reason were censored from the lifespan analyses (see Table 5).
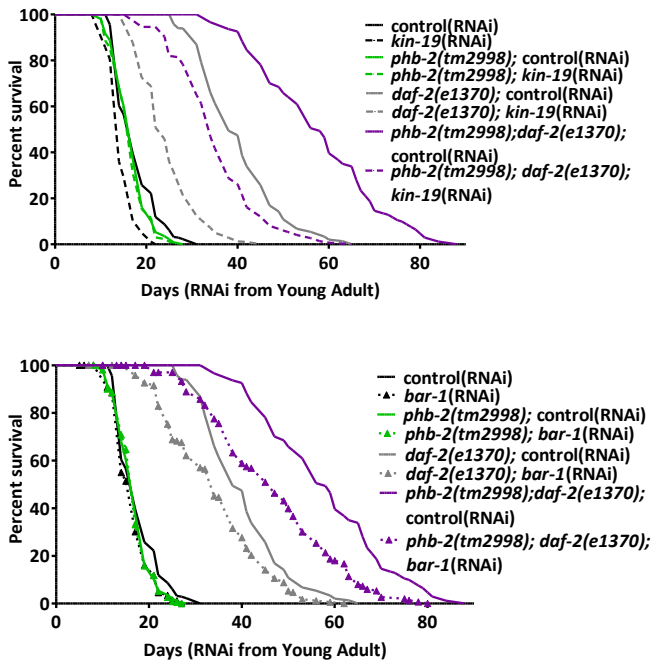
Figure 38: Knockdown of components of the Wnt signalling pathway, KIN-19 and BAR-1. Survival curves of mutant animal populations subjected to *kin-19 (RNAi)* (upper panel) and *bar-1(RNAi)* (lower panel) are shown. Average of two independent lifespan curves has been represented here.

4.2 Knockdown of GSK-3 leads to embryonic lethality in wild type and IIS mutants

It had been noted previously that reducing *gsk-3* expression by RNAi causes embryonic lethality, though this phenotype has not been quantified (An et al. 2005). More recently, it has been shown that GSK-3 promotes adult germline stem and progenitor cells (GSCs) proliferation in a germline autonomous and kinase-dependent manner. Adult GSCs support gamete production and sustain germline development in the worm. Not only do adult *gsk-3* mutant germlines contain lower GSCs, compared to wild type, it is so from early larval stages such as L3 and L4. As this occurs throughout development, it is indicative that the germline output would also be reduced (Furuta et al. 2018).

Post embryonic depletion of GSK-3 by means of RNAi in wild type animals was characterised by a reduced brood size and embryonic lethality post day 1 of egg-laying. On the other hand, *daf-2* mutants upon *gsk-3(RNAi)* exhibited a stronger reduction in brood size and 100% embryonic lethality (Figure 39).These stronger phenotypes are in accordance with the more severe lifespan reduction observed in *daf-2* mutants as compared to wild type. Also,

daf-2(e1370) mutants produced fewer progeny in comparison to wild type animals (Kenyon et al. 1993).
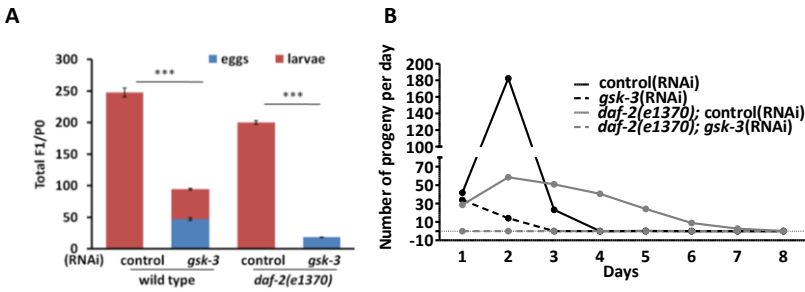

Figure 39: Effect of GSK-3 depletion on brood size and embryonic lethality. **A.** Comparison of total brood size (unhatched eggs and larvae) in wild type and *daf-2 (e1370)* mutants on control*(RNAi)* and *gsk-3(RNAi)* (The blue portions of the bars represent unhatched eggs; the red portions indicate hatched eggs or larvae, Mean±SD) **B.** Number of progeny per day in wild type and *daf-2* mutants upon GSK-3 depletion. One of two independent reproductive brood size assays has been represented here (n ≥ 8 worms for all conditions).

4.3 Ubiquitous expression of GSK-3

In order to study the expression pattern of *gsk-3*, we constructed the strain, P*gsk-3*::GFP::*gsk-3,* using the SapTrap methodology for CRISPR-Cas9 (Schwartz and Jorgensen 2016) system. The advantage of this technique is that it reduces the time for assembling repair templates and sgRNAs and utilizes a combined tag and selectable marker that aids in direct identification of modified worms. To build a translational reporter of GSK-3, we utilized a tag plus marker plasmid (Munoz-Jimenez et al. 2017) that incorporates FLP-mediated gene knockout. Hence, this reporter strain we generated can be used to study tissue-specific inhibition of gene expression by crossing it with transgenic strains that express FLP in a tissue specific manner.

GSK-3 is ubiquitously expressed and showed a tissue dependent sub-cellular localisation. GSK-3 was detected in embryos both, in the nucleus and the cytoplasm (Figure 40A). At the adult stage, expression was prominent in head and tail neurons (Figure 40B,C), intestine (Figure 40D), muscles (Figure 40E) and in the P-granules in the germ line (Figure 40G). Apart from these, the sperm (Figure 40F) and vulval precursor cells (Figure 40H) also exhibited strong expression of GSK-3.

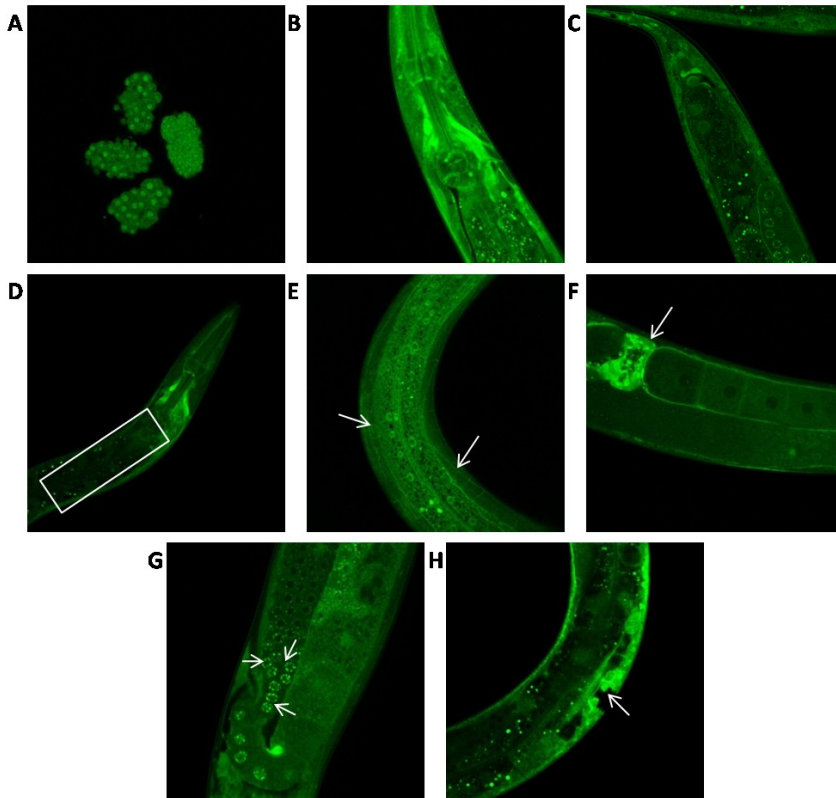Figure 40: Expression pattern of GFP::GSK-3 transgenic worms. Expression can be observed in **A.** embryos, **B.**and **C.** the nervous system – head and tail neurons respectively, **D.** the intestine (white rectangle) and **E.**muscles (white arrows).In the germline, GSK-3 is expressed strongly in **F.** sperm (white arrow), **G.**within P granules (white arrow) in the germline and **H.** in vulval precurcor (refer white arrow) cells. *Images were taken by Dr.F J Garcia.

We checked if the expression pattern of GSK-3 was altered in IIS defective animals or upon *phb-1(RNAi)*. We did not observe obvious changes in the expression pattern (Figure 41A), while, quantification of total GSK-3::GFP revealed that GSK-3 levels are increased in PHB depleted worms and *daf-2* mutants (Figure 41B). These increased levels of GSK-3 might not be indicative of increased activity of GSK-3 as it is a kinase whose activity is regulated by phosphorylation.
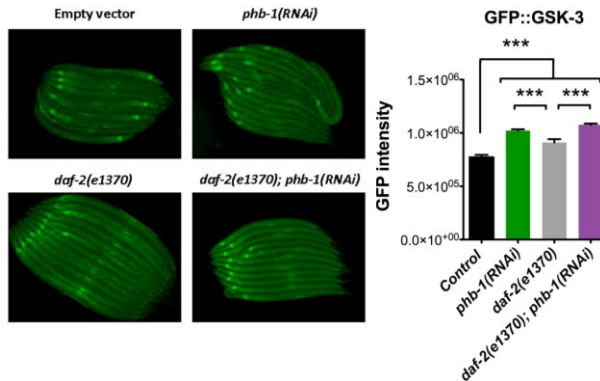
A
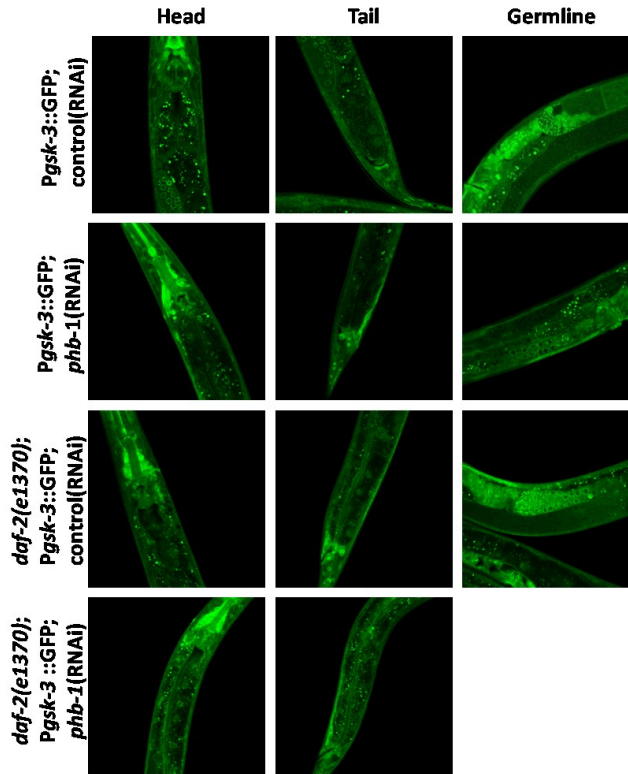
B

Figure 41: Expression of GSK-3. **A.**GSK-3 expression in the head, tail and germline of wild type and *daf-2* mutants transgenic for GFP::*gsk-3* on control*(RNAi)* and *phb-1(RNAi)*.**B.** Quantification of GSK-3 expression levels in insulin *daf-2(e1370)* and PHB depleted backgrounds. One of two independent experiments is represented. *Images were taken by Dr.F J Garcia.

4.4 Metabolic alterations upon GSK-3 depletion

Studies in both mammals and nematodes have suggested that age related modulations in carbohydrate and lipid metabolism can influence the ageing process and optimal usage of energy stores is critical for organismal survival (Hansen et al. 2013; Watts and Ristow 2017). Moreover, GSK-3 is expressed strongly in the intestine, the major metabolic organ in worms. This prompted us to investigate whether metabolic changes are associated with the decreased longevity phenotype observed under conditions of GSK-3 depletion across wild type animals and worms with compromised insulin signalling and mitochondrial function. We looked at metabolic stores and key genes involved in carbohydrate and triglyceride metabolism.

4.4.1 Glycogen stores are differentially altered in insulin and mitochondrial mutants upon GSK-3 depletion

GSK-3 is a key regulator of glycogen metabolism (Embi et al. 1980). Briefly, IIS signalling inhibits GSK-3, dephosphorylating glycogen synthase responsible for glycogen synthesis (Parker et al. 1983; Cross et al. 1995). In *Drosophila*, it has been observed that insulin signalling represses mitochondrial quiescence and glycogen accumulation by inhibiting the AKT target gene, GSK3 (Sieber et al. 2016). In order to analyse glycogen content in worms upon *gsk-3(RNAi)*, we utilized iodine vapor staining. As reported by others, we also observed increased glycogen content in *daf-2* mutants compared to wild type worms (Frazier and Roth 2009; Depuydt et al. 2014). GSK-3 depletion in wild type animals did not alter glycogen content, whereas, in *daf-2* mutants, we observed a further increase in glycogen content upon GSK-3 depletion (Figure 42A,B).

On the contrary, GSK-3 depletion reduces glycogen content in PHB mutant backgrounds, both in *phb-2* and *phb-2;daf-2* double mutants (Figure 42A,B). PHB-2 deletion resulted in decreased glycogen content, both in otherwise wild type worms and in *daf-2* mutants, a likely consequence of a higher reliance on glycolytic metabolism due to defective mitochondrial functioning. As the reduced glycogen content observed upon GSK-3 depletion occurs specifically upon PHB deletion, it is plausible that the benefits of depleting PHB in GSK-3 deficient worms could be linked to an increased reliance on glycogen for energy production. However, reduced glycogen content could also be

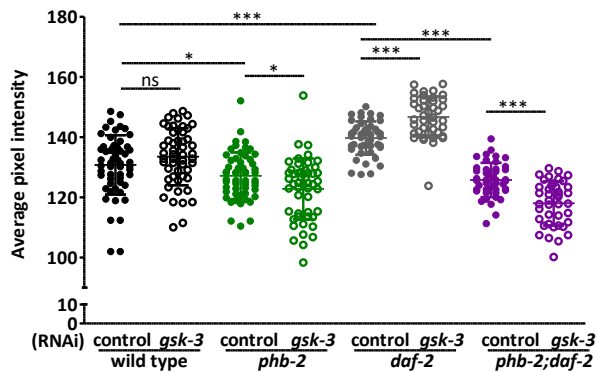reflecting impaired glycogen storage.

A
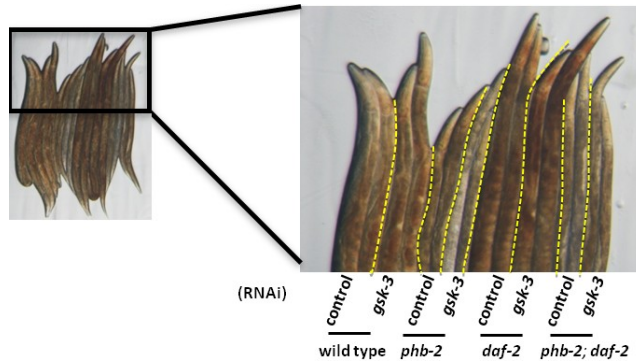
B

Figure 42: Glycogen storage in *C. elegans* viewed using iodine vapor staining **A.** Representative images of glycogen stores across wild type, *daf-2*, *phb-2* and *phb-2;daf-2* mutants subjected to control and *gsk-3(RNAi)* **B.** Scatter plot representing quantification of glycogen stores (Animals were imaged at Day1 of adulthood in all conditions, Mean±SD, Unpaired t- test, ns = not significant p>0.05, * = p<0.05, ** = p<0.01, *** = p< 0.001, n ≥ 41 worms for all conditions, average of three independent experiments represented).

In order to distinguish the latter from the former, we looked at the expression of fructose 1, 6 - biphosphatase, encoded by *fbp-1* in *C. elegans*, a non-reversible enzyme involved in gluconeogenesis. We observed that upon GSK-3 depletion, the expression of P*fbp-1*::GFP is reduced in both, wild type and PHB mutants (Figure 43A). Additionally, PHB depletion was observed to also have less expression of FBP-1 in comparison to wild type worms. This low expression of the FBP-1 reporter in PHB depleted worms on control and on *gsk-3(RNAi)*, thus, indicates less glucose generation in these animals and hence, the low

glycogen phenotype observed. Despite the fact that glycogen stores were unaltered in wild type animals depleted of GSK-3 (Figure 42), we observed reduced expression of *fbp-1*(Figure 43A). In order to confirm whether *gsk-3* depletion reduces the expression of gluconeogenic genes we looked at the mRNA levels of other genes involved in gluconeogenesis, *mdh-1* and *icl-1*, both of which appear reduced (Figure 43B).
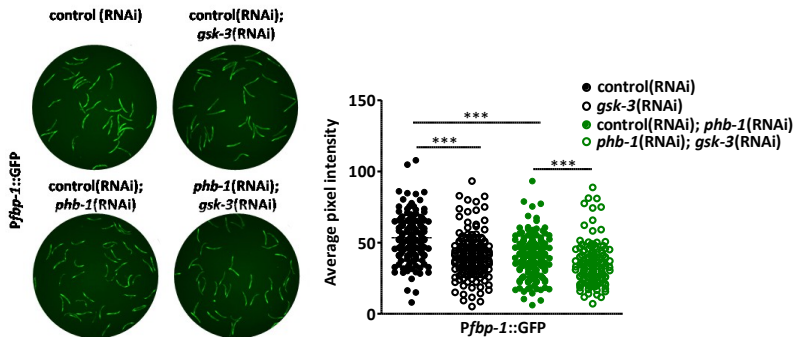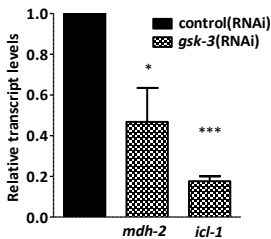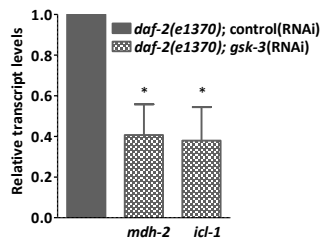

Figure 43: Reduced gluconeogenesis upon GSK-3 knockdown. **A.** Quantification of expression of the transgenic strain, P*fbp-1*::GFP , in wild type and PHB depleted wild type animals grown on control*(RNAi)* and *gsk-3(RNAi)* (Animals were imaged at Day1 of adulthood in all conditions, Mean±SD, One way ANOVA, *** = p< 0.001, n >130 worms for all conditions, scatter plot representative of three independent experiments) **B-C.** qRT-PCR of gluconeogenic genes, *mdh-2* and *icl-1* in **B.** wild type and **C.** IIS mutants grown on control*(RNAi)* and *gsk-3(RNAi)* (Mean±SEM, Unpaired t-test, * = p<0.05,*** = p< 0.001, graph representative of three independent experiments, each with 2-3 technical repeats)

Additionally, we found that *daf-2* mutants grown on *gsk-3(RNAi)* also exhibit low expression of *mdh-2* and *icl-1* (Figure 43C). As both genes are part of the glyoxylate shunt that allows carbohydrate synthesis via gluconeogenesis, this is indicative of the shunt in these animals being less active. The further increase

in glycogen stores in IIS mutants grown on *gsk-3(RNAi)* might result from increased glycogen synthase activity instead.

4.4.2 Triglyceride content is reduced upon *gsk-3(RNAi)*, except in *daf-2 (e1370)* mutants

Apart from glycogen/carbohydrates, triglycerides constitute the major energy storage in nematodes. Also, they are efficient energy storage molecules due to their reduced state (Ashrafi 2007; Watts and Ristow 2017). Using fixative Oil-Red-O staining, we assessed triglyceride content across all genetic backgrounds.
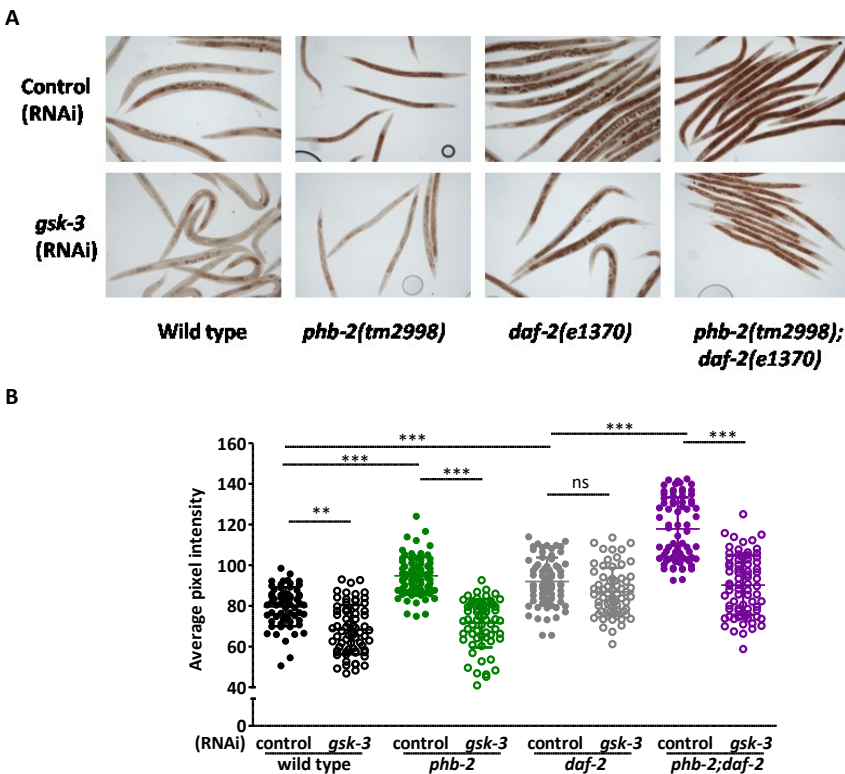
Figure 44: Whole body triglyceride levels in wild type, *daf-2, phb-2* and *phb-2;daf-2* mutants subjected to *gsk-3(RNAi)* **A.** Representative images of worms subjected to fixative Oil-Red-O staining **B.** Quantification of Oil-Red-O staining (Animals were imaged at Day1 of adulthood in all conditions, Mean±SD, One way ANOVA, ns = not significant p>0.05, ** = p<0.01, *** = p< 0.001, n ≥ 60 worms for all conditions, average of two independent experiments represented)

As reported earlier, *daf-2 (e1370)* mutants exhibited increased triglycerides (Yen et al. 2010). We observed that *phb-2(tm2998)* deletion mutants contain higher triglyceride levels compared to wildtype and *phb-2* deletionfurther increases the triglyceride content of *daf-2(e1370)* mutants. Interestingly, depletion of GSK-3 reduced triglycerides in all genetic backgrounds except in *daf-2(e1370)* mutants (Figure 44). The reduced Oil-Red-O staining observed in wild type upon loss of GSK-3 is similar to the decreased whole-body triglyceride levels in *Drosophila* upon addition of lithium - a known inhibitor of GSK-3 (Castillo-Quan et al. 2016).

4.4.3 Knockdown of GSK-3 leads to increased lipolysis

Mobilization of stored fat through β-fatty acid oxidation is dependent on liberated fatty acids from triacylglycerides through the activity of lipases. Since, we observed decreased ORO staining, we investigated if that indicates increased lipid breakdown. We checked for alterations in expression of adipose triglyceride lipase, ATGL-1(Zimmermann et al. 2004; Gronke et al. 2005; Kershaw et al. 2006), known to localize to lipid droplets (Zhang et al. 2010a; Lee et al. 2014). Depletion of GSK-3 results in increased ATGL-1::GFP levels (Figure 45A,B)across all genetic backgroundsexcept in PHB depleted otherwise wildtype animals, where *agtl-1* expression levels are unaltered. PHB depleted animals already show increased *atgl-1* expression compared to wild type worms (Figure 45).
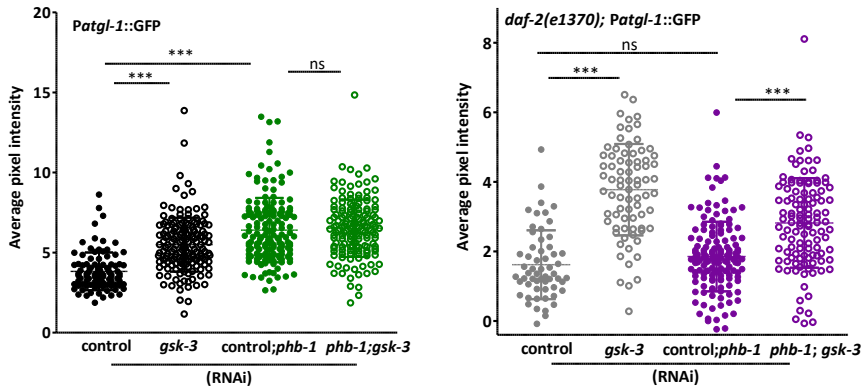
A
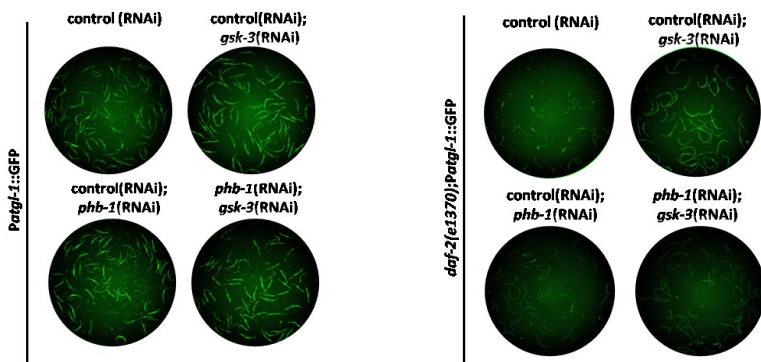
B

Figure 45: GSK-3 deficient animals exhibit increased hydrolysis of lipids. **A.** Representative images of alteration in ATGL-1 protein levels upon loss of GSK-3 across different genetic backgrounds. **B.**Scatter plots represent mean fluorescence of ATGL-1::GFP as seen in wild type (left panel) and IIS depleted animals (right panel) grown on control*(RNAi)*, *gsk-3(RNAi)*,*phb-1(RNAi)* or a combination (Animals were imaged at Day1 of adulthood in all conditions, Mean±SD, One way ANOVA, Dunn's multiple comparison test, ns = not significant p>0.05, *** = p< 0.001, n ≥ 58 worms for all conditions, one of two independent experiments represented).

The increased expression levels of ATGL upon *gsk-3(RNAi)* is in accordance with the reduced Oil -Red-O staining observed earlier. Being an exception *daf-2* mutants that exhibit increased expression of ATGL-1 upon GSK-3 depletion, although no alterations in triglyceride content was observed.
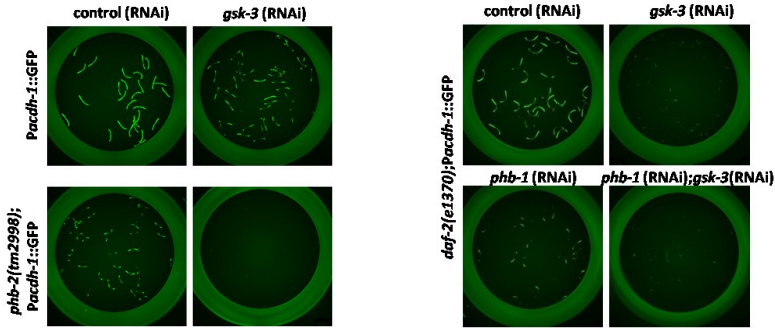
4.4.4 Fatty acid oxidation is reduced upon *gsk-3(RNAi)*

In order to get insight on whether GSK-3 depleted worms utilised energy from β-fatty acid oxidation from triglycerides, we looked at the expression of certain genes involved in fatty acid oxidation (Figure 46A,B). *acdh-1* encodes for a short-chain acyl-CoA dehydrogenase, a mitochondrial enzyme that catalyzes the first step of fatty acid β-oxidation. We looked at the expression of *acdh-1* by utilising a transgenic strain, P*acdh-1*::GFP. We found that the GFP expression is dramatically reduced upon GSK-3 depletion in wild type (Figure 46A,B; left panel). Additionally, we crossed the *phb-2(tm2998)* mutants to the metabolic reporter *Pacdh-1*::GFP, and observed a strong repression in GFP signal, which intensified upon *gsk-3(RNAi)* (Figure 46, left panel). Similarly, in conditions of reduced IIS signalling, GSK-3 depletion caused a decrease in
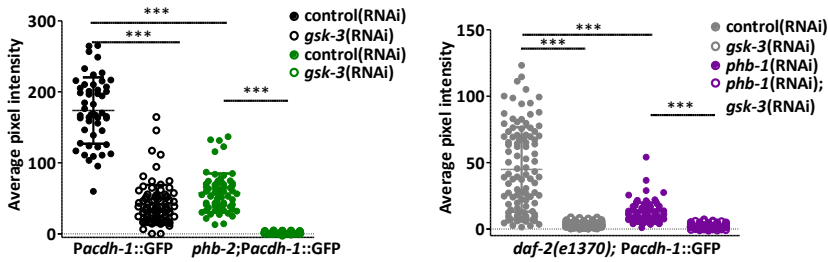
P*acdh-1*::GFP expression both, in the presence and absence of PHB (Figure 46, A and B, right panel).

A
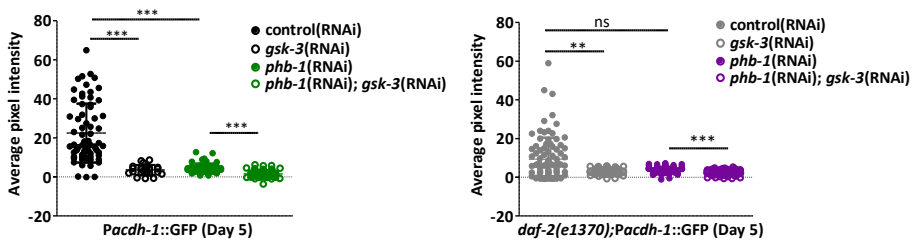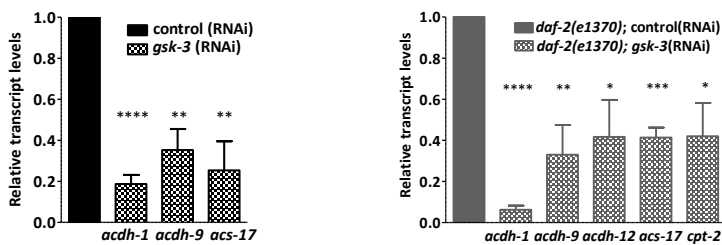

B

C

D

Figure 46: Reduced fatty acid β-oxidation upon *gsk-3(RNAi)* **A.**Expression of P*acdh-1*::GFP in wildtype and *phb-2* mutants upon *gsk-3(RNAi)* (left panel); and in IIS depleted worms on *gsk-3*

and *phb-1;gsk-3* double RNAi (right panel) **B**. Scatter plot representing quantification of P*acdh-1*::GFP levels from images shown in **A**. Animals were imaged at Day1 of adulthood in all conditions, in **A**- n≥51 for all conditions, one of two independent experiments represented; in **B**- n≥85, one of two independent experiments, each having two biological repeats has been represented **C**. Expression of *acdh-1* at day 5 of adulthood. Scatter plots represent the quantification of P*acdh-1*::GFP levels in otherwise wild type and PHB depleted worms grown on control and *gsk-3(RNAi)* (left panel) and in *daf-2(e1370)* mutants upon GSK-3 or PHB depletion or when both GSK-3 and PHB-1 are depleted using double RNAi (right panel), n≥23 for all conditions, average of two independent experiments (For **B, C** Mean±SD, One way ANOVA, Dunn's multiple comparison test, ns = not significant, **=p<0.01, *** = p< 0.001) **D**. Expression of *acdh-1,-9, -12; acs-17; cpt-2* in wild type and IIS mutants grown on *gsk-3(RNAi)* compared to control*(RNAi)* (Mean ±SEM, Unpaired t-test, *=p<0.05, **=p<0.01, *** = p< 0.001, **** = p< 0.0001, graph representative of three independent experiments, each with 2-3 technical repeats).

This experiment was continued until day 5 of adulthood and similar reductions were observed (Figure 46C). Thus, nematodes depleted of GSK-3 or PHB might be averse to utilising energy derived from breakdown of short chain fatty acids.

In addition, we observed a downregulation of other genes involved in fatty acid oxidation in wild type worms and IIS defective *daf-2* mutants upon loss of GSK-3 (Figure 46D). In particular, expression of acyl-CoA dehydrogenases - *acdh-1*, -9, *-12*; acyl-CoA synthetase - acs-*17* and the carintine pamiltoyltransferase *cpt-2* were found to be reduced (Figure 46D, left and right panel).

Thus, despite the increased rate of lipolysis (Figure 45) upon loss of GSK-3, the fatty acids are not being utilised in fatty acid oxidation as observed by the reduced expression of the genes above. This is of significance as nematodes obtain major dietary requirements from bacterial diet and not from *de novo* fatty acid synthesis. Several of the genes involved in fatty acid metabolism are expressed in the intestine, epidermis or both. Also, there are multiple family members that encode for the genes involved in fat metabolism. Additional metabolic genes involved in fatty acid oxidation and in *de novo* fat synthesis were analysed in conditions of loss of GSK-3 or PHB-1, and many were found to be differentially regulated (Appendix 3, A3.2,A3.3). We were able to conclude that while loss of GSK-3 led to a strong downregulation of short-/medium-/ long- chain oxidation of fatty acids in all backgrounds tested, loss of PHB-1 led to strong decreases only in genes involved in short chain fatty acid degradation, indicating selective utilisation. Moreover, genes involved in *de*

novo fat synthesis were also found to be repressed upon *gsk-3(RNAi)* (Appendix 3, A3.4) which can be a potential cause of reduced lipid storage in GSK-3 depleted worms.

Thus, the extensive modulations in several core genes involved in fatty acid metabolism upon *gsk-3(RNAi)* across genetic backgrounds and specifically in wild type animals implicate GSK-3 as having a prominent role in metabolism in *C. elegans* in lipid synthesis and degradation, the latter being essential for energy generation.

**4.4.5 Vitellogenesis is reduced when GSK-3 is depleted**

Reproduction has a complex interplay with metabolism and ageing (Hansen et al. 2013), as it is an energy consuming process causing alterations in lipid metabolism, thus influencing organismal survival. Lipids are mobilised in worms during reproduction in a process called vitellogenesis, wherein vitellogenins (VIT) transport stored lipids in the form of yolk to the oocytes from the intestine. VIT genes are expressed in the intestine in adult hermaphrodites (Kimble and Sharrock 1983). Analysis of the long-lived IIS *daf-2* mutants has shown that these animals accumulate substantially less VIT (DePina et al. 2011) and their long lifespan is compromised upon over expression of VIT (Seah et al. 2016). GSK-3 depletion is characterised by a reduction in lifespan, along with defective reproduction leading to embryonic lethality (Figure 36,37,39) as well as modulations in fat metabolism (Figure 44). Hence, we investigated if vitellogenesis was altered upon GSK-3 knockdown by checking the expression levels of a member of the vitellogenin family, VIT-6. The expression of VIT-6 was observed to be decreased upon GSK-3 depletion across all genetic backgrounds (Figure 47A, B). As shown earlier, we observed low vitellogenesis in *daf-2(e1370)* mutants compared to wild type (DePina et al. 2011). Incidentally, the PHB depletion in otherwise wild type animals led to decreased VIT-6 expression (Figure 47A), whereas the same in IIS depleted worms had no significant effect (Figure 47B).

As VIT proteins mediate transport of lipids from the intestine to the gonad, the reduction in vitellogenesis is consistent with the low lipid content seen using ORO staining upon loss of GSK-3. The reduced vitellogenesis in wildtype and IIS mutants on *gsk-3(RNAi)* is also in accordance with GSK-3 depleted animals exhibiting a low brood size. Despite the fact that they are sterile, the

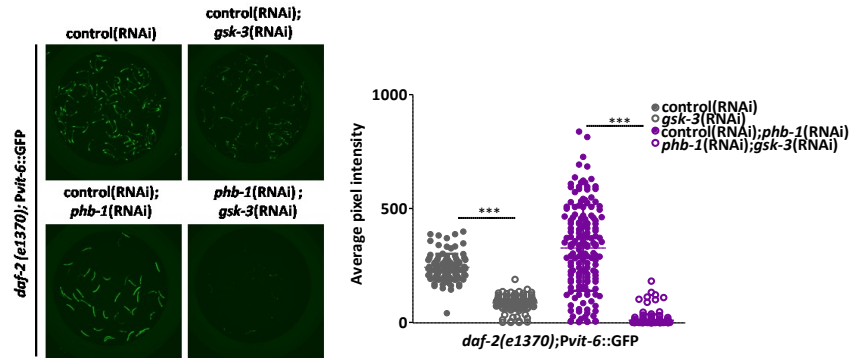mitochondrial PHB mutants do not exhibit significant changes in expression of
vit-6.

A
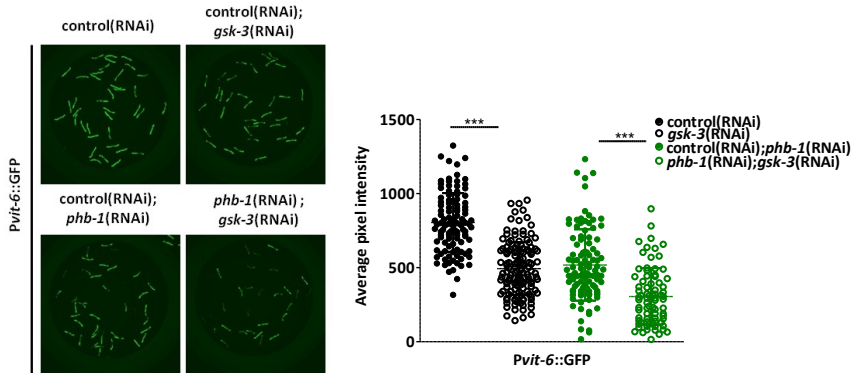
B

Figure 47 : Decreased vitellogenesis upon GSK-3 depletion. **A.** The transgenic strain P*vit-6*::GFP
and **B.** *daf-2(e1370)*;P*vit-6*::GFP were utilized to check for alterations in *vit-6* expression upon
GSK-3 knockdown in worms grown on control and *phb-1(RNAi)*. The scatter plot to the right of **A.**
and **B.** represents the quantification of GFP intensity (Animals were imaged at Day1 of
adulthood in all conditions, Mean±SD, One way ANOVA - Dunn's multiple comparison test, *** =
p< 0.001. In **A.** n ≥ 78 worms for all conditions, one of three independent experiments. In **B.** n ≥
98 worms for all conditions, one of two independent experiments)

4.5 GSK-3 depletion compromises mitochondrial respiration

Depletion of GSK-3 leads to alterations in energy stores and decreased fatty
acid oxidation. We decided to directly measure mitochondrial metabolic
activity in whole worms by utilizing the Seahorse XFp Analyzer (Luz et al. 2015;
Koopman et al. 2016; Fong et al. 2017). This provides real-time measures of the

oxygen consumption rate (OCR) of worms, the result of mitochondrial respiration through oxidative phosphorylation.

Key mitochondrial parameters, basal and maximal respiration were determined by means of OCR measurements. To interpret the data and compare strains or RNAi treatments, the OCR per well was converted to OCR per worm (by directly counting the number of worms after the assay). In our case, the mitochondrial mutants and the *gsk-3(RNAi)* treated worms were smaller than their controls at the YA stage and at Day 5. As worm size was significantly different among the studied genetic backgrounds both at YA and at day 5 (Figure 48 A, B), we corrected OCR per worms for worm area.

We observed that compared to wild type nematodes, *daf-2* mutants exhibited less basal respiration at the YA stage (Figure 48C), while *phb-2* deletion did not affect basal respiration neither in wild type nor in *daf-2* mutants. However, the *phb-2* mutants exhibit increased OCR compared to the *phb-2; daf-2* double mutants. No alterations were detected in basal respiration upon GSK-3 depletion across the different genetic backgrounds except a decrease in *phb-2; daf-2*mutants (Figure 48C).

Respiration changes significantly during development and ageing. We observed that at day 5, basal respiration decreased in the wild type (Figure 48D) (Braeckman et al. 2002a; Braeckman et al. 2002b), but not in IIS defective *daf-2* mutants, which at day 5 respired at par with wild type. *phb-2* mutants exhibited increased OCR compared to wild type animals probably a result of accumulating faulty mitochondria through ageing, whereas the IIS defective mutants depleted of PHB exhibit decreased OCR compared to *daf-2* mutants. GSK-3 depletion, however, reduced respiration during ageing as observed at day 5 exclusively in *daf-2* mutants (Figure 48D).

We also examined maximal respiratory capacity by addition of the mitochondrial uncoupler, carbonyl cyanide 4-(trifluoromethoxy) phenylhydrazone (FCCP)(Figure 48E,F). FCCP is added to fully uncouple mitochondrial respiration, i.e., it dissipates the proton gradient in the mitochondrial membrane and hence, in an attempt to re-establish the proton gradient, the worm increases oxygen consumption. This is a reflection of mitochondrial-specific respiration at maximum capacity. We observed that

maximal respiration is significantly higher than basal respiration in all genetic backgrounds at the YA stage and at Day 5 (Appendix 4, Figure A4.1).
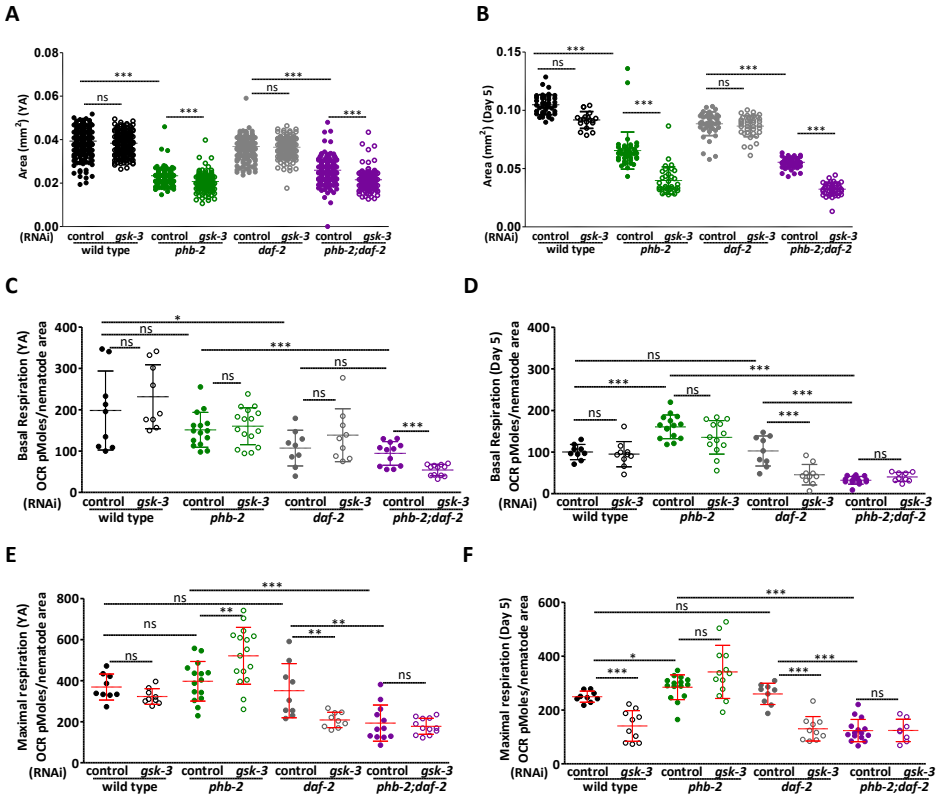

Figure 48: Alterations in mitochondrial metabolism upon depletion of GSK-3. **A-B** Comparison of worm area in wild type, *daf-2, phb-2* and *phb-2;daf-2* during ageing, **A.** Young adult, **B.** Day 5, grown on control*(RNAi)* and *gsk-3(RNAi)* (1 way ANOVA, Dunn's multiple comparison test, ns = not significant p>0.05, *** = p< 0.001, Mean± SD, n > 190 worms at YA stage and n >18 worms at day 5 for all conditions represented). **C-F** Variations in consumption rate (OCR) across all four genetic backgrounds grown on control*(RNAi)* and *gsk-3(RNAi)*. Basal respiration at young adult (YA) stage(**C.**) and during ageing, at day 5 of adulthood (**D.**) and maximal oxygen consumption rate (OCR) as observed by treatment using FCCP at YA stage (**E**)and at day 5 (**F**). Data has been depicted normalised to worm area in all cases (Unpaired t-test, ns=not significant p>0.05, * = p<0.05, ** = p<0.01, *** = p< 0.001, mean±SD, n = at least 3 independent experiments consisting of 3-4 wells each of control*(RNAi)* and *gsk-3(RNAi)* for each genetic background tested).

The deletion of PHB in otherwise wild type animals had no significant effect on maximal respiration, while the same in IIS defective mutants led to a decrease already at YA stage (Figure 48E). *daf-2* mutants, despite their low basal rate of

respiration (Figure 48C), respired at par with wild type indicating they are capable of responding to external stress (Figure 48E). GSK-3 depletion caused an increase in maximal OCR in *phb-2* mutants and a strong decrease in *daf-2* mutants not affecting wild type animals or *phb-2;daf-2* mutants (Figure 48E).

During ageing PHB depletion modulates OCR differentially in wild type and IIS defective mutants, increasing and decreasing respectively, similar to basal respiration at day 5 (Figure 48F), while no significant differences were observed for d*af-2* mutants compared to wild type. Mitochondrial mutants on *gsk-3(RNAi)* were unaffected upon FCCP addition, although a tendency to increase maximal OCR is observed. Maximal respiration upon GSK-3 depletion wasstrongly reduced again in *daf-2* mutants at day 5, just like at the YA stage (Figure 48F). Loss of GSK-3 also compromised maximal respiration in wild type animals at day 5.

A
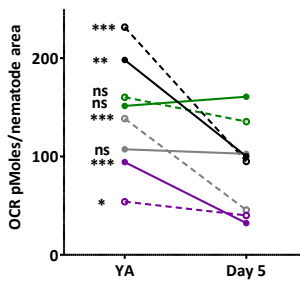
Figure 49: Change in rate of respiration of all genetic backgrounds grown in *control(RNAi)*and *gsk-3(RNAi)*, through ageing, from young adult to day 5 of adulthood, **A**.basal and **B.** maximal. (The ***, **, *, ns indicate significant changes from YA to day 5 n each genetic background. Unpaired t-test, ns=not significant p>0.05, * = p<0.05, ** = p<0.01, *** = p< 0.001)

B
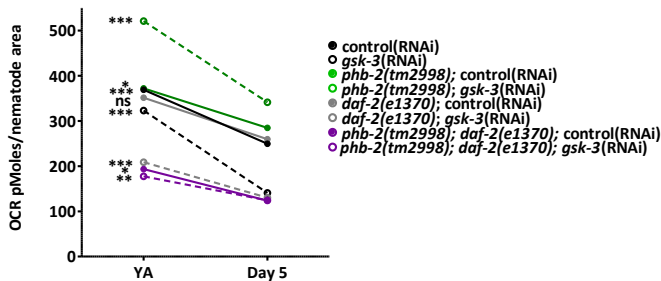
To summarise, IIS mutants tend to not change their basal or maximal rate of respiration from young adult to day 5, unlike wild type that exhibit a reduction (Figure 49A,B). While the *phb-2* mutants also show unaltered respiration patterns during ageing, the respiration of the double mutant *phb-2;daf-2* is

slightly decreased. Loss of GSK-3, prominently reduced basal and maximal respiration in wild type and IIS mutants, while having no effect on mitochondrial *phb-2* mutants. Interestingly, the basal and maximal OCR of IIS mutants on *gsk-3(RNAi)* are quite similar through the course of ageing (Figure A4.1). Upon addition of FCCP, only *phb-2* mutants on *gsk-3(RNAi)* show a strong increase in OCR during ageing. An increased capacity to respond to external stress might be of importance as these are the only mutants that are unaffected in terms of survival (Figure 36,37) upon GSK-3 depletion.

4.6 Selective induction of the mitochondrial unfolded protein response (UPR^mt) upon *gsk-3(RNAi)*

The observed altered mitochondrial bioenergetics upon *gsk-3* depletion might be associated with additional signs of mitochondrial stress. Mitochondrial dysfunction is detected by a surveillance pathway specific to the mitochondria, the UPR^mt, that involves induction of mitochondrial chaperone genes such as *hsp-6* or *hsp-60*. Prohibitins have a prominent role in maintenance of mitochondrial structure and function, and prohibitin depletion strongly induces the UPR^mt. This is accompanied by increased mitochondrial content in wildtype animals on *phb-1(RNAi)*, whereas the same is suppressed in PHB depleted IIS *daf-2* mutants (Artal-Sanz and Tavernarakis 2009b; Gatsi et al. 2014).

We assayed the expression of P*hsp-6*::GFP reporter in wildtype, *daf-2* mutants on control and *gsk-3(RNAi)* and upon PHB depletion. As observed earlier with *phb-1(RNAi)* (Gatsi et al. 2014) and *phb-2(RNAi)* (Schleit et al. 2013), *phb-2* deletion strongly induced the UPR^mt (Hernando-Rodriguez et al. 2018), while the UPR^mt was suppressed in the double mutant *phb-2;daf-2* (Figure 50B). Depletion of GSK-3 strongly induces the UPR^mt in wildtype (Figure 50A) worms, while metabolically compromised *daf-2* mutants were unaffected upon GSK-3 depletion. The *phb-2* mutants do not further induce the UPR^mt upon GSK-3 loss (Figure 50B), while *daf-2* mutants depleted of PHB show a slight, albeit significant induction of the UPR^mt upon GSK-3 depletion.
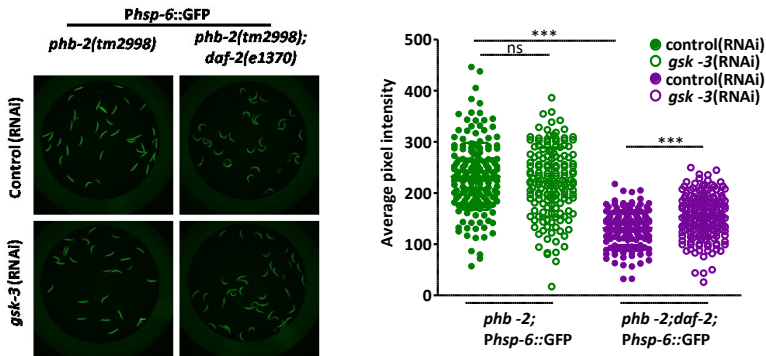
A
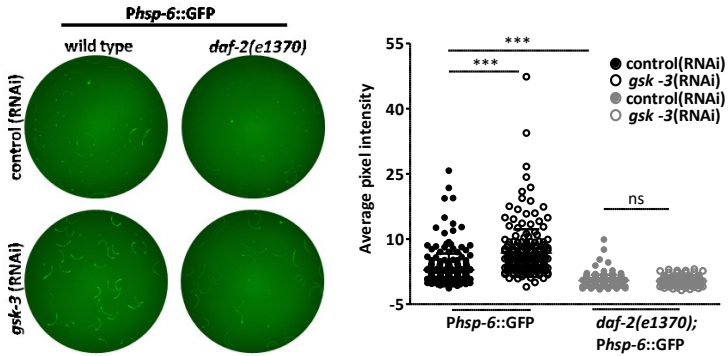
B

Figure 50: Induction of UPR^mt reporter, P*hsp-6*::GFP. Fluorescent microscopy images of transgenic animals grown on control*(RNAi)* and *gsk-3(RNAi)* **A.** P*hsp-6*::GFP and *daf-2(e1370)*;P*hsp-6*::GFP (left panel), quantification of *hsp-6*::GFP expression (right panel) and **B.** *phb-2(tm2998)*;P*hsp-6*::GFP and *phb-2(tm2998);daf-2(e1370)*;P*hsp-6*::GFP (left panel) and quantification of *hsp-6*::GFP expression (right panel) (Mean ± SD; n > 135 in all conditions, 1 way ANOVA, Dunn's multiple comparison test, ns = not significant p>0.05, *** = p< 0.001. Average of two independent experiments has been shown)

4.7 GSK-3 is essential for ER homeostasis and mitochondrial membrane lipid composition

Like the mitochondria, the endoplasmic reticulum also synthesizes, folds and secretes proteins. The unfolded protein response of the endoplasmic reticulum (UPR^ER), is a stress response specific to the ER, allowing it to adapt to proteostatic imbalances. Moreover, the ER is also a site of lipid synthesis, in particular phospholipids and sterols. We wondered whether GSK-3 might also be essential in maintaining ER stabililty. In metazoans, activation of the IRE-1 branch of the UPR^ER results in increased splicing of the mRNA encoding the transcription factor X-box binding protein 1 (XBP1), which activates UPR^ER

target genes such as the ER-specific chaperone and heat-shock protein hsp-4/BiP (Ron and Walter 2007). We found that loss of GSK-3 via RNAi resulted in activation of UPR[ER], as indicated by an increase in P*hsp-4*::GFP expression levels (Figure 51).
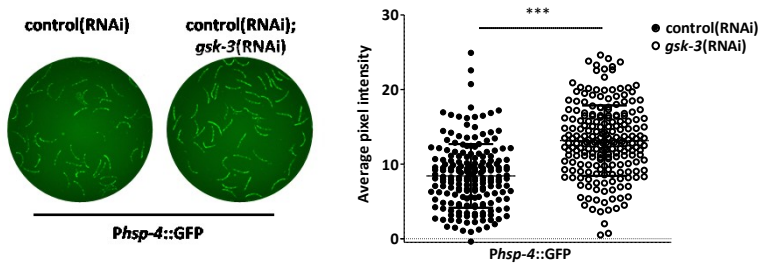

Figure 51: Induction of UPR[ER] reporter, P*hsp-4*::GFP. Representative images of P*hsp-4*::GFP transgenic strain on control*(RNAi)* and *gsk-3(RNAi)* (left panel). Scatterplot represents the GFP quantification (right panel) (Mean ± SD; n > 190 in both conditions, Unpaired t-test, *** = p< 0.001. Average of three independent experiments has been shown)

This activation of the UPR[ER], while an indication of imbalance in proteostasis, might also be a reflection of perturbations in membrane lipid composition. Mitochondria synthesize some lipids on their own, particularly, phosphatidylglycerol (PG), cardiolipin (CL), phosphatidylethanolamine (PE), and phosphatidic acid (PA). They depend also on the transfer and assembly of lipids mainly formed in the endoplasmic reticulum (ER) like phosphatidylinositol (PI), phosphatidylserine (PS) and phosphatidylcholine (PC), sterols and sphingolipids and hence, a continuous supply and exchange of lipids is required for maintaining mitochondrial membrane integrity and overall cellular function (Horvath and Daum 2013).

In light of this, we found alterations in the amount and composition of membrane lipids, especially the most abundant phospholipids – PE, PC, PS, when GSK-3 was depleted both, in wild type and in *daf-2* mutants (Figure 52). *phb-2* mutants displayed increased levels of phospholipids compared to wild type, whereas in the double mutant *phb-2;daf-2* some phospholipid species were decreased in comparison to *daf-2* mutants. Interestingly, we also detected alterations in cardiolipin levels, a unique phospholipid exclusively located in the inner mitochondrial membrane (Paradies et al. 2014). Cardiolipin is involved in mitochondrial dynamics and biogenesis, cristae organization,

apoptosis and mitophagy. Loss of GSK-3 tends to increase CL levels particularly in wild type and *daf-2* mutants (Figure 52). Similarly, sphingolipids such as ceramides were also upregulated upon loss of GSK-3 in wild type animalsand *daf-2* mutants, with milder increases in the other backgrounds.
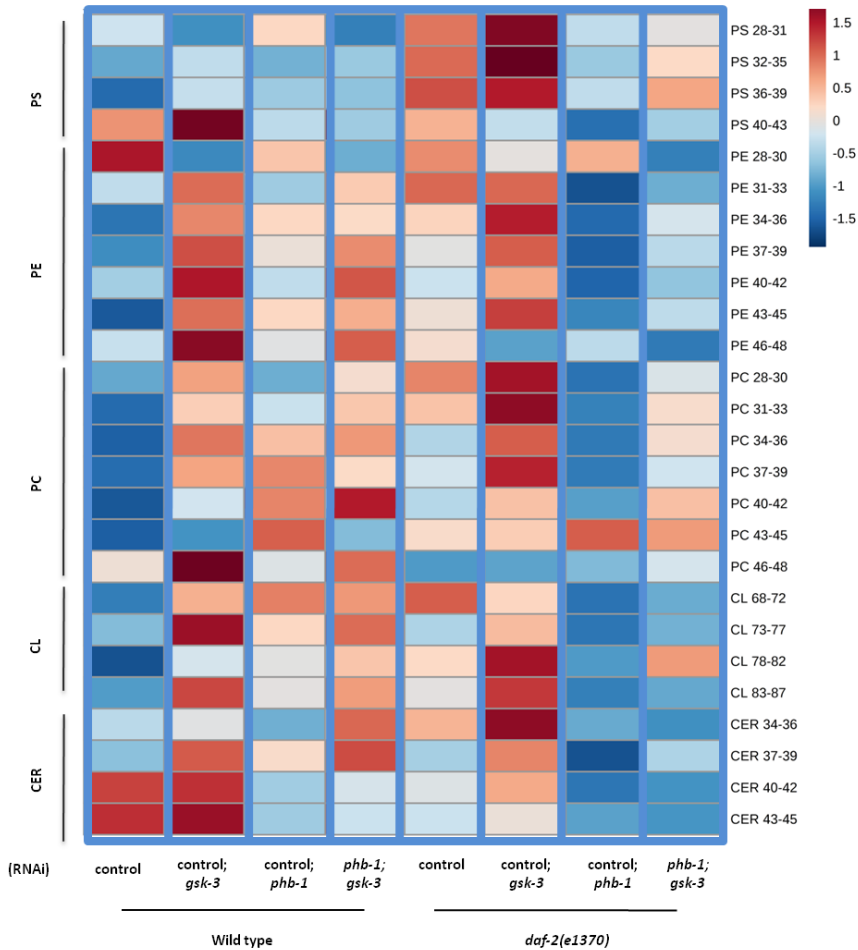
Figure 52: Altered membrane lipid compostitions across genetic backgrounds. Worms were grown in control*(RNAi)* and *gsk-3(RNAi)* or a combination of both at the young adult stage. PS - phosphatidylserine; PE -phosphatidylethanolamine; PC -phosphatidylcholine; CL - cardiolipin; CER- Ceramide (Phospholipids are designated as phospholipid(AB-CD), where AB-CD denotes the total number of carbon atoms in the fatty acyl chains, n = at least 3-4 independent samples were collected for each condition, data analysed by Dr. Lourenco)

These membrane perturbations are despite the fact that mitotracker analysis revealed no significant alterations in mitochondrial content when GSK-3 is depleted across these genetic backgrounds (Appendix 4, Figure A4.3).

4.8 Intestinal GSK-3 is essential for the longevity *daf-2(e1370)* mutants

The *C. elegans* intestine is a central metabolic organ in the nematode, mainly responsible for digestion of food, nutrient uptake and synthesis and storage of macromolecules. There are several evidences that implicate the intestine as having a major role in healthy ageing and lifespan regulation (Rera et al. 2013). The intestine is a major site of fat storage and modulations in the same have been observed in mutants of the IIS signalling pathway. For example, reestablishment of DAF-16 expression only in the intestine of*daf-2;daf-16* mutants, extends lifespan (Libina et al. 2003).Dietary restriction increases lifespan in *C. elegans* as in other organisms and autophagy in the intestine has been shown to have a role in ensuring this lifespan extension in the worm(Gelino et al. 2016).

Based on the expression pattern of GSK-3 and the observable expression in the intestine, an intestine specific RNAi system was used to knockdownGSK-3 solely in the intestine. For this, we used an RNAi DEfective, *rde-1* mutant strain, where*rde-1*has been rescued only in the intestine. Hence, these animals are refractory to RNAi in all tissues expect the intestine (Espelt et al. 2005).

We observed that depletion of GSK-3 in the gut alone was sufficient to cause a significant reduction in lifespan across all backgrounds (Figure 53 A-D). We observed that there was an average decrease in mean lifespan of 7% for wild type, 58% for *daf-2*, 22% for *phb-2*and 20% for *phb-2;daf-2* (Table 4) upon *gsk-3(RNAi)*. The IIS mutant lifespan was reduced below that of wild type on GSK-3 attenuation (Figure 53A, B; also Refer Table 4), indicating that active GSK-3 in the intestine was absolutely essential to the long lived phenotype of *daf-2 (e1370)* mutants.
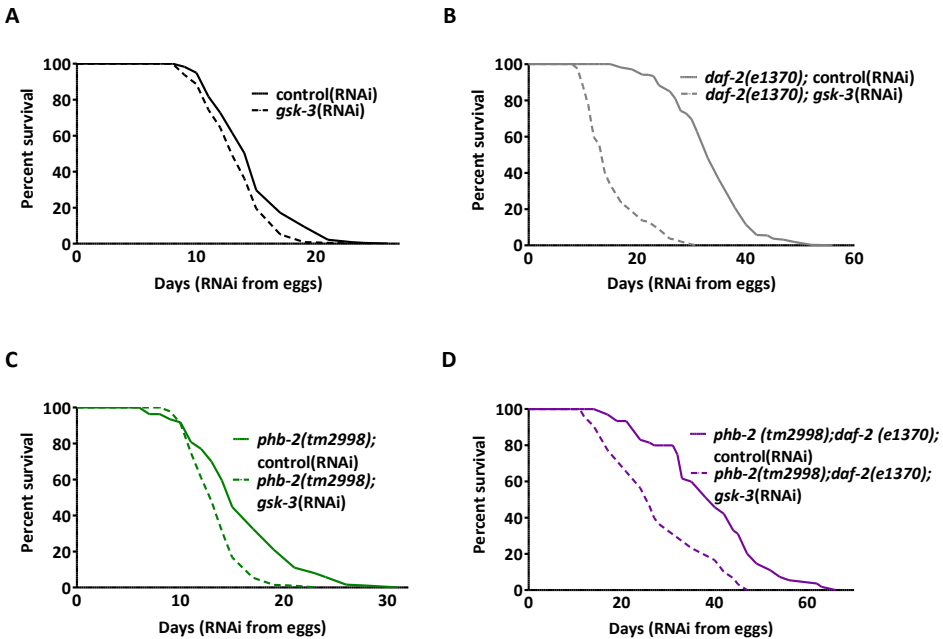
Figure 53: Intestine-specific GSK-3 depletion accelerates ageing in **A.** wild type **B.** *daf-2(e1370)* **C.** *phb-2(tm2998)* and **D.** *phb-2(tm2998);daf-2(tm2998)* mutants. Lifespan analysis carried out using an intestine specific RNAi system, *rde-1(ne219);kbIs7*. Average of at least two independent lifespan curves has been represented here.

The intestine of the worm is also a major site for responses to stress. The transcription factor SKN-1, is known to regulate intestinal genes that are involved in detoxifications and protect against ROS.

4.9 SKN-1 activity measured via expression of P*gst-4*::GFP

The *C. elegans* SKN-1 (ortholog of the mammalian Nuclear factor E2-related factor (Nrf) protein family) is a key transcription factor involved in the protection against oxidative and xenobiotic stresses (Blackwell et al. 2015). It has been proposed that under normal conditions, GSK-3 inhibits SKN-1 localization and subsequent target gene induction, whereas, in response to oxidative stress, SKN-1 is phosphorylated by PMK-1/p38 MAPK in the cytoplasm, after which it goes to the nucleus and induces the expression of a wide range of antioxidant and detoxifying enzymes such as *gst-4* (encoding for the drug-metabolizing enzyme glutathione S-transferase 4). The SKN-1 transcriptional response to oxidative stress is well-conserved between species (An et al. 2005).

The transcriptional activity of SKN-1 can be indirectly assayed via a transcriptional reporter of the *gst-4* promoter which shows increased GFP levels when transcription is activated *in vivo*. We examined expression of GST-4 when GSK-3 was inhibited across otherwise wildtype and PHB depleted worms. Additionally, we crossed the P*gst-4*::GFP reporter strain to *daf-2* mutants.We observed induction of P*gst-4*::GFP upon *gsk-3(RNAi)*in wildtype and PHB depleted animals. On the contrary,GSK-3 attenuation reduces GST-4 expression in *daf-2* and *daf-2;phb-2*mutants (Figure 54A, B). The induction of *gst-4* in wildtype animals upon GSK-3 depletion is in accordance with earlier reports (An et al. 2005), and hence, an indication that SKN-1 is active. While it is known that SKN-1responsive genes, such as *gst-4* are upregulated in *daf-2* L4 larvae (Tullet et al. 2008), we refrain from commenting on this as wild type and IIS mutants were not compared in the same experiment, and we looked at Day1 animals. The mitochondrial PHB mutants, *phb-2* and *phb2;daf-2* exhibited a mild reduction to no effect respectively in terms of GST-4::GFP expression. The suppression of P*gst-4*::GFP upon *gsk-3(RNAi)* in *daf-2*mutant backgrounds (Figure 54B), might indicate regulation of GST-4 or SKN-1 from other inputs.
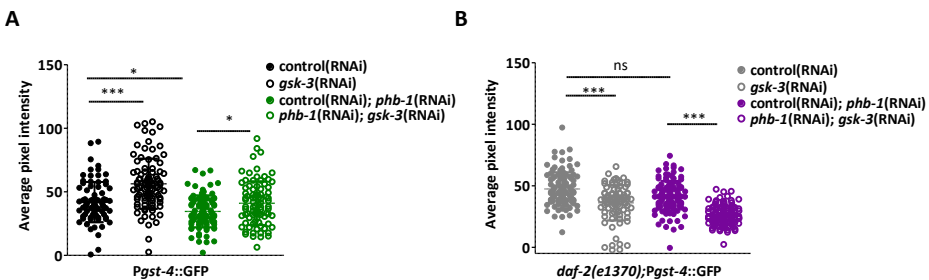
Figure 54: P*gst-4*::GFP expression(mean GFP intensity) in **A.**Wild type and **B.** *daf-2(e1370)* mutants upon PHB and GSK-3 depletion (Animals imaged at Day 1 of adulthood, Mean±SD, One way ANOVA, Dunn's multiple comparison test, ns =not significant, *=p<0.05,*** = p< 0.001 , for **A**. n≥80, average of two independent experiments and for **B**. n≥85, one of two independent experiments has been represented)

Nonetheless, recent studies have revealed that the use of GST-4 as a sole readout for SKN-1 activation and subsequent interpretation of results should be done with caution as *gst-4* can also be transcriptionally activated by EOR-1, a transcription factor mediating effects of the epidermal growth factor (EGF) pathway (Detienne et al. 2016).

Although this result cannot contribute to an explanation of the differential ageing phenotype observed upon depletion of GSK-3, utilizing the SKN-1::GFP transgenic strain in the future might help confirm whether SKN-1 is actually localized to intestinal nuclei across PHB-1 and/or IIS depleted animals on *gsk-3 (RNAi)*. This might better indicate any potential modulation of oxidative stress responses.

Automated image acquisition and analysis for essential genes

Caenorhabditis elegans is an exceptional genetically tractable organism that is easy to maintain and has a short, well defined life cycle. More importantly, the worm genome shares high homology with that of humans. These features make it an amenable platform for high-throughput and high-content screens (Boutros and Ahringer 2008; O'Rourke et al. 2009a; O'Reilly et al. 2016). Despite these significant advantages, large-scale studies in *C. elegans* with respect to investigation of essential genes are still not well developed. Though there exist temperature-sensitive alleles that allow the temporal suppression of gene function; very few essential genes have a ts allele (Housden et al. 2017; Mok et al. 2017). A way out, is the use of chromosome balancers, which already cover 85% of the genome, with additional efforts aimed at having fluorescently labelled balancers for all *C. elegans* essential genes via CRISPR (Iwata et al. 2016).

The conserved mitochondrial prohibitin (PHB) complex composed of two subunits, PHB-1 and PHB-2, is located in the inner mitochondrial membrane and both subunits are interdependent for the formation of the complex. Phenotypes observed upon either *phb-1* or *phb-2* via RNAi are similar. Also, both subunits of the PHB complex have been confirmed as absent in both *phb-1(tm2571)* and *phb-2(tm2998)* mutants (Hernando-Rodriguez et al. 2018). Prohibitin proteins are essential for embryonic development in *C. elegans* (Artal-Sanz et al. 2003) and homozygous *phb-1* and *phb-2* deletion mutants are sterile due to maternal contribution. Therefore, deletion mutants need to be maintained as balanced heterozygous.

As the task of distinguishing the homozygous *phb-2* worms from the heterozygous wild type is difficult, these mutants are not suitable for large scale experiments, such as for the purpose of RNAi screenings. Hence, we developed and present here a successful strategy in this regard, for automated whole animal image-based RNAi screening that can be applied to essential genes when carrying a fluorescently labelled balancer. Developing this automated pipeline involved two major steps. First, sorting non GFP homozygous mutant animals from a GFP-marked balanced population at the first larval stage (L1) in order to identify genes acting during early larval development, and second, developing a robust automated imaging and

segmentation protocol using a microscopy platform not previously utilized for *C. elegans*. COPAS is a convenient approach for high-throughput analysis involving balanced strains, as it facilitates a task that manually would be impracticable. In the past, GFP balanced strains have been sorted at older larval stages such as L3,L4 (Latorre et al. 2015; Ruegger et al. 2015); but not for the purposes of screening.

Previously, high-throughput imaging strategies specific to *C. elegans* have been designed using various microscopy platforms (Moy et al. 2009; Gosai et al. 2010; Wahlby et al. 2012; Maia et al. 2015). Similar to others, the IN Cell Analyzer (GE Healthcare) used in this thesis utilizes a combination of brightfield- and fluorescence-based imaging. Image acquisition has been optimised to include an entire well of a 96-well plate in a single image, ensuring even brightfield illumination by sealing the plate with a transparent seal. The optimised autofocus and scanning times of the IN Cell Analyzer enable image acquisition of an entire 96-well plate in three channels in less than 15 min. We have designed an automated segmentation protocol for balanced strains in *C. elegans*. This user-defined, user-friendly protocol was built using the Developer Toolbox (GE Healthcare) software that allows intensity based measurements apart from other measures defined by the user like area, length, curvature, etc. It can be used for any strain without the need of transgenesis, as segmentation is done in the brightfield image. A novelty of this segmentation protocol is the measurement of the background surrounding each target. By dilating the targeted worm, we can easily measure and subtract the intensity of the immediate background. This is very appropriate in the cases of dyes, such as Nile Red in this thesis, that stain plastic and can cause different background intensities depending on the area of the well. Another feature of the improved image analysis protocol is the successful identification of worms carrying a pharyngeal GFP element. When COPAS sorting is not 100% efficient, heterozygous worms will develop into fertile adults and lay progeny in the wells; hence, the need of distinguishing worms carrying the GFP balancer from homozygous mutants.

As mentioned, segmentation of worms is done in the brightfield and the protocol can be adapted for any strain. These protocols are not restricted to only RNAi screenings and can also be utilised for regular imaging experiments

involving dyes or transgenic GFP strains as image acquisition and analysis is faster and surpasses the traditional time consuming manner of mounting worms on slides and of manually segmenting worms. This thesis has also utilised the segmentation protocols built using the Developer toolbox for image analyses in additional experiments.

Though COPAS can serve as an alternative to microscopy based measurements, as it can measure length, optical density and fluorescence emission of single worms (Squiban et al. 2012; Zugasti et al. 2016), image-based microscopy platforms are far more advantageous. They are faster and images are stored, making them accessible for re-analysis. Also, a much smaller number of animals can be used for image based assays as compared to the COPAS, allowing exploration of a large number of different treatments in parallel, such as RNAi or drug screens. Image-based screens also ensure that multiple outputs can be examined from the image, e.g. fluorescent intensities in different channels, size and shape measurements. This could also be used to detect other phenotypes such as sterility by classifying the small worms as progeny based on worm length measurement, or to distinguish between thin and fat worms based on worm width measurement. We have translated the image analysis protocol for Cell-Profiler (Carpenter et al. 2006), a free and open source image analysis software, making the protocol available to the scientific community. In doing so, we broaden the features of the CellProfiler "WormToolbox" for high-throughput screening of image-based *C. elegans* phenotypes (Wahlby et al. 2012; Wahlby et al. 2014). We provide validation that both protocols produce comparable results. Although the segmentation output is not exactly the same in terms of number of worms being segmented, the level of stringency in the segmentation criteria can be modulated with ease for both protocols.

A kinase RNAi screen reveals potential mediators of the effect of PHB depletion on metabolism and longevity.

We performed an RNAi screen utilising a kinase RNAi library looking for PHB genetic interactors. We used vital Nile Red staining as a read out for the RNAi screen, as a strong metabolic feature exhibited by PHB deletion both, in wild type and IIS mutants, is low Nile Red accumulation (Figure 24). Using this technique, we obtained 26 RNAi clones (Figure 34) that suppressed the

reduced NR staining phenotype of the mitochondrial PHB mutants, but did not encounter any that further enhanced the low NR phenotype.

With respect to the NR staining method used as a readout for the RNAi screen, the status of this vital stain as to whether it stains true fat reserves or infact lysosomal related organelles (LROs) has been debated. Vital NR, when fed to nematodes was believed to indicating fat stores (Ashrafi et al. 2003), though now it has been shown that the compartments within the worm being stained by NR are different from netrual lipid stores in *C. elegans* (O'Rourke et al. 2009b; Yen et al. 2010; Klapper et al. 2011). Infact, staining with Oil-Red-O revealed that depletion of PHB resulted in increased accumulation of triglycerides in both wild type and IIS defective *daf-2* mutants (Figure 25). As mitochondria are involved in fat oxidation, mitochondrial dysfunction may lead to accumulation of lipids. The ORO staining is in accordance with data from metabolomic studies (unpublished data, Lourenço et.al). Previously, Sudan Black staining for triglycerides in aged worms devoid of PHB has revealed decreased staining (Artal-Sanz and Tavernarakis 2009b), but as the Oil-Red-O staining is done in younger worms, it is probable that the differences are a result of age based changes in fat accumulation.

NR co-localises with autofluorescent intestinal granules, thus it is believed that LRO are the site of age pigment/lipofuscin accumulation (Hermann et al. 2005; Schroeder et al. 2007). High levels of lipofuscin might indicate a physiologically aged state (it is not yet clear whether high levels cause ageing or are a symptom of ageing), as seen from many mutants with altered LRO biology that have altered lifespan. Example, short-lived strains such as *daf-16, rict-1, kat-1* have increased LRO autofluorescence and NR, and long-lived strains such as *daf-2, daf-7, eat-2* tend to have lower levels of both (O'Rourke et al. 2009b; Soukas et al. 2009). But, this is not the case for all long-lived or short lived mutants, and hence, cannot be taken as a co-relation (Samuelson et al. 2007). But if lysosomal function is impacted due to increased age pigment buildup, it might lead to alterations in vesicular trafficking and autophagy, both of which can contribute to accelerated ageing. However, other reports suggest that rather than lipofuscin (Brunk and Terman 2002; Gerstbrein et al. 2005), the autofluorescent substance in *C.elegans* LROs is anthranilate, a breakdown product of tryptophan (Coburn et al. 2013). It has also been suggested that NR

stained LRO's are sites of zinc or cholesterol storage (Roh et al. 2012; Wang et al. 2014). Alterations in zinc have been linked to lifespan (Kumar et al. 2016), and stored zinc can aid in detoxification and be a source of zinc during dietary deficiency (Roh et al. 2012). However, regardless of the stain status, vital NR staining is reproducible and sensitive to genetic manipulations that are expected to alter staining and thus, provides a useful tool to screen for genetic interactors. Previously, vital Nile Red has been utilized in different model systems to identify genes that alter fat and to identify pathways involved in fat regulation (Greenspan et al. 1985; Ashrafi et al. 2003; McKay et al. 2003; Van Gilst et al. 2005a; Jones et al. 2008; Lemieux et al. 2011).

Amongst the identified kinases in the screening, a majority are involved in phosphorylation (except *dhs-31, osm-11, inos-1, ceh-20, unc-60*) and in organism development, signal transduction, reproduction, Wnt signalling, lipid storage, locomotion, etc (Figure 35). Though we did not encounter any GO terms relate to ageing, *ire-1, akt-1, rsks-1, osm-11, ceh-20, unc-60, gsk-3, sgk-1* (Hertweck et al. 2004; Hamilton et al. 2005; Hansen et al. 2007; Samuelson et al. 2007; McColl et al. 2008; Henis-Korenblit et al. 2010; Walter et al. 2011; Dresen et al. 2015) are genes that have been shown previously to influence worm lifespan. In addition to finding genes previously shown to be involved in metabolism such as *vps-15, kin-1, ire-1, inos-1, akt-1, sgk-1*, we also found genes that have been previously described to interact with PHBs in the past such as *rsks-1, sgk-1, mtk-1* and *gsk-3*. While both SGK-1 and RSKS-1 have been shown to interact with PHBs to regulate lifespan (Schleit et al. 2013; Gatsi et al. 2014), we show here that depletion of MTK-1 leads to an opposing longevity phenotype in *phb-2* and *phb-2;daf-2* mutants (Figure A1.2). Thus, the presence of these known genes previously implicated in metabolism and longevity regulation and/or showing an interaction with PHB validates the screening. Further study of these PHB interacting genes found in this study will yield additional insight into the diverse functions of the mitochondrial prohibitins.

GSK-3 deficiency causes differential shortening of lifespan and defective reproduction

The focus of this thesis is GSK-3, a kinase that when knocked down produces an increase in the NR staining phenotype of *phb-2* and *phb-2;daf-2* mutants. As we used the Nile Red phenotype only as a visual readout for screeing purposes

to point us towards potential interactors of PHBs, probing if and why GSK-3 is involved in regulating LRO biology is beyond the scope of this thesis. However, we did observe from transciptomic analyses done in the lab (data not shown), that the expression of *kat-1*, a mitochondrial ketothiolase, a key gene involved in the regulation of LRO biology (Soukas et al. 2013) was downregulated upon *gsk-3(RNAi)* in the mitochondrial PHB mutants. Interestingly, KAT-1 is a highly conserved enzyme in the mitochondrial fatty acid β-oxidation pathway and is known to act in the intestine (Mak et al. 2006).

This multifunctional serine threonine kinase is highly conserved in evolution and has been described to regulate several signalling cascades. Besides its prominent role in glycogen metabolism, GSK-3 has been implicated in diseases such as diabetes, Alzheimer's disease, bipolar disorder and cancer, making it a tempting therapeutic target. Importantly, GSK-3 is regulated in response to PHB deficiency in Phb2[KO] mice, where GSK-3β was inactivated by phosphorylation at Ser position 9 in hippocampal tissue lysates (Merkwirth et al. 2012). While the function of GSK-3 in *C. elegans* has been studied majorly during early development, it has not been well elaborated in *C. elegans* with emphasis on ageing and metabolism. Herein, we investigated how *gsk-3(RNAi)* impacts ageing and metabolism under conditions of reduced IIS signalling and in mitochondrial prohibitin mutants.

We present evidence that loss of GSK-3 accerelates ageing differentially depending on the metabolic status of the animal. Published studies in the past have established that loss of the conserved GSK-3 shortens lifespan in maternally rescued *gsk-3* null *C. elegans* (McColl et al. 2008) and in mice (Zhou et al. 2013). In accordance, we observed that *gsk-3(RNAi)* reduces wild type lifespan significantly; however, the same does not impact *phb-2* mutant survival. GSK-3 function is essential for the long lived IIS *daf-2* and *phb-2; daf-2* double mutants (Figure 36). Particularly, the impact of decrease upon *gsk-3(RNAi)* is striking for *daf-2* mutant, implying that GSK-3 is essential for the extended longevity of IIS mutants. The shortening of the *phb-2;daf-2* mutants on loss of GSK-3 can be attributed to DAF-2,as PHB-2 is unaffected. What was intriguing about the effect of *gsk-3(RNAi)* was that its effect on shortening survival of wildtype worms was significantly higher than its effect on shortening survival of *phb-2* mutants and similarly amongst *daf-2* and *phb-2;*

daf-2 mutants. As GSK-3 is implicated in metabolism in other systems, it is quite possible that the ageing phenotype seen in worms is subject to metabolic perturbations.

GSK-3 loss results in embryonic lethality and reduced brood size in wild type worms, (Figure 39) indicating reduced fitness, in line with reports of lethality and developmental defects in mice, *Drososphila* (Bourouis et al. 1990; Hoeflich et al. 2000) and in worms upon GSK-3 disruption. In worms, lethality is attributed to abnormal C blastomere differentiation and Wnt signalling (An et al. 2005; Gleason et al. 2006). Worms devoid of the GSK-3 and the Wnt component, APR-1 also exhibit distorted gonads (Cabello et al. 2010). GSK-3 is required for OMA-1 degradation, a regulator of oocyte to embryo transition (Nishi and Lin 2005) and the phenotype *oma-1(zu405)* mutant embryos are similar to that of GSK-3 depleted embryos (Schlesinger et al. 1999; Maduro et al. 2001; Lin 2003). Thus, embryonic defects upon loss of GSK-3 could be due to failure of timely degradation of OMA-1. Also, adult *gsk-3* mutant germlines have lower GSCs essential for germline development (Furuta et al. 2018), further implicating GSK-3 in early development. A more drastic lethal phenotype is exhibited by *daf-2(e1370)* mutants upon depletion of GSK-3 (Figure 39). Based on IIS signalling inhibition of GSK-3, *daf-2* mutants are likely to have active GSK-3, and hence, an active GSK-3 is required for normal reproduction in these worms. In *Drosophila,* late stage oocytes (conditions when IIS signalling is lost) subjected to *gsk-3(RNAi)*, were inviable (Sieber et al. 2016), similar to the effect seen by us in *daf-2(e1370)* mutants, implying the importance of GSK-3 in conditions of low IIS signalling. Additionally, a developmental role for GSK-3 across all genetic backgrounds is also confirmed by the fact the mean lifespans are increased when worms are exposed to *gsk-3(RNAi)* from adulthood (Figure 37) rather than from embryos.

In addition to the described dynamics of GSK-3, we observe expression of GSK-3 in the sperm. The worm embryo has distinct embryonic anteroposterior (AP) asymmetries. The sperm, probably via its associated centrosome, establishes the AP axis through the control of cytoplasmic rearrangement and final polarization of the zygote requires basic elements of the cytoskeleton (Goldstein and Hird 1996). Additionally, Wnt signalling is involved in inducing polar changes in cellular morphology via remodelling of the cytoskeleton.

Hence, there might be a link with sperm expression of GSK-3 to the observed embryonic defects.

A major role for GSK-3 is as a key negative regulator of Wnt signalling, as a member of the destruction complex. Other components of the destruction complex include *kin-19* and *pry-1.* Loss of KIN-19 elicits a similar acceleration of ageing across all backgrounds, as observed upon *gsk-3(RNAi)* (Figure 38A). Incidently, *pry-1* mutants have a low brood size much like GSK-3 depleted worms and are short-lived (Ranawade et.al, bioRxiv, pre-print). Interestingly, we found that decreasing Wnt signalling via loss of BAR-1, also elicits the same lifespan phenotype (Figure 38B) as observed upon *gsk-3(RNAi)* and *kin-19 (RNAi)* (Table 4,5). It has been shown previously that upon loss of BAR-1, the Wnt-signalling pathway is activated implying a compensation mechanism (van der Bent et al. 2014). Additionally, experiments in the lab showed that *bar-1 (RNAi)* downregulates GSK-3. This could indicate why loss of Wnt components leads to a similar reduced longevity phenotype across the four genetic backgrounds.

GSK-3 is a well-documented target of lithium (Stambolic et al. 1996; Ryves and Harwood 2001; De Sarno et al. 2002) and the effects of lithium on ageing have been studied in yeast and *C. elegans*, with lithium extending lifespan (McColl et al. 2008; Zarse et al. 2011; Sofola-Adesakin et al. 2014; Tam et al. 2014). Though effects of lithium on *Drosophila* ageing were previously inconclusive (Matsagas et al. 2009; Zhu et al. 2015), now there is evidence of lifespan extension (Castillo-Quan et al. 2016). Lithium concentration in the drinking water of a large Japanese population has been associated with reduced overall mortality (Zarse et al. 2011), suggesting that lithium may be a bona fide anti-ageing drug. Lithium is a popular drug used to treat mood affect disorders, but has a narrow therapeutic range beyond which there is risk of tissue damage (Malhi and Tanious 2011). Evidence from work in flies and worms suggest the same is true for lifespan extension; lower doses extend lifespan, whereas higher concentrations are detrimental (McColl et al. 2008; Zhu et al. 2015; Castillo-Quan et al. 2016). We used a concentration of lithium previously shown to extend lifespan in both worms and flies with contradictory results (Figure A2.2). Importantly, in our experiments done at 20 °C, lithium addition to wild type and conditions of compromised IIS signalling strongly shortens

lifespan against the previous observation where lithium extended wild type and *daf-2(e1368)* median lifespan by 36 % and 19% respectively (McColl et al. 2008). The authors had concluded that the effect of lithium on lifespan was not due to reduced IIS signalling, as *daf-16(mu86)* mutants show a 50% extension in lifespan upon LiCl addition. In this work, we used the *daf-2(e1370)* strain, and temperature is different, so results are not comparable. Though, our reduced longevity upon lithium addition is in accordance with our results using *gsk-3(RNAi)*. Therefore, our results call for caution regarding the use of lithium as an anti-ageing agent, more so as lithium is the only GSK-3 inhibitor approved for human use (Williams and Harwood 2000; Meijer et al. 2004; Martinez et al. 2011). Incidentally, in studies wherein the authors performed lithium experiments at 20 °C but exposed worms to a lower concentration of LiCl - wild type worms exhibit only a mild increase in survival (Zarse et al. 2011); and there was downregulation of metabolic genes including *fasn-1, acs-17, acdh-8, ech-9* and vitellogenin genes including *vit-5, vit-6* (Inokuchi et al. 2015), the latter being similar to our metabolic observations upon *gsk-3(RNAi)* in wild type animals, and points to lithium targeting GSK-3. Ofcourse, we will need further evidence to back our preliminary claim and explore the possibility of lithium having an additional target apart from GSK-3.

Altered carbohydrate metabolism upon loss of GSK-3

In order to understand the differential effect of GSK-3 on lifespan regulation we looked at energy stores and metabolism. Reduced GSK-3 activity results in increased activity of glycogen synthase, leading to increase in glycogen (Embi et al. 1980; Parker et al. 1983; Woodgett and Cohen 1984; Cross et al. 1995), hence, in order to ascertain whether loss of GSK-3 alters glycogen stores, we measured glycogen stores using iodine vapor staining. While this technique is easier than biochemical assays as it allows detection of whole body glycogen in vivo, it involves simultaneous exposure of worms of interest to the iodine vapors (Frazier and Roth 2009; LaMacchia et al. 2015; Gusarov et al. 2017; Seo et al. 2018). This method can stain more than one population of animals at a time and one can control the time of exposure. The glycogen content revealed by iodine vapor staining correlates well with biochemical methods as reported by others. Iodine vapor staining is better than vital staining via carminic acid as

it only stains glycogen in the gut (Hanover et al. 2005; Forsythe et al. 2006; LaRue and Padilla 2011).

Here, we noted that lack of GSK-3 does not affect the whole body glycogen content in wild type contrary to the expected increase on the basis of the role established for GSK-3 (active insulin signalling inhibits GSK-3 and activates glycogen synthase). Inhibiting GSK-3 via lithium addition in flies also resulted in unaltered levels of glycogen (Castillo-Quan et al. 2016). However, *daf-2* mutants have increased glycogen stores (Figure 42) as observed by us and others (Depuydt et al. 2014) and GSK-3 loss led to a further increase of glycogen. *daf-2* mutants are metabolically different to wild type and have many metabolic pathways like glycolysis and gluconeogenesis upregulated (Depuydt et al. 2014). Glycogen synthesis impairment via glycogen synthase - 1 (*gsy-1)* RNAi suppresses the enhanced survival of *daf-2* mutants in a hypoosmotic-anoxic environment, while RNAi against glycogen phosphorylase (*pyg*-1 or T22F3.3) does not affect their survival (LaMacchia et al. 2015). Also, *gsy-1(RNAi)* reduces longevity in *daf-2* mutants (Gusarov et al. 2017), while *pyg-1(RNAi)* leading to increased glycogen mildly extends *daf-2* longevity. However, lifespan of wild type animals is mildly increased upon RNAi against both *gsy-1* and *pyg-1*. These reports imply that alterations in glycogen synthesis and storage are more vital in case of reduced *daf-2* signalling than glycogen breakdown, unlike wild type worms. If glycogen synthesis and storage upon low insulin signalling is controlled by GSK-3, probably via inhibition of glycogen synthase, which upon GSK-3 depletion becomes activated, then a further increase in glycogen than what is required by *daf-2* mutants might also be detrimental.

Interestingly, in wild type animals, GSK-3 loss downregulates gluconeogenesis as per low expression of *fbp-1* (Figure 43A), and this is supported by RNA-seq analysis as *fbp-1* and additionally, *pck-1* were also downregulated upon *gsk-3 (RNAi)*. However, despite this, glycogen stores are not affected in these animals. Also, glyoxylate shunt genes, *icl-1 and mdh-2* upon *gsk-3(RNAi)* in wild type and *daf-2* mutants are decreased*,* implying decreased metabolism of fatty acids to promote gluconeogenesis.

On the other hand, PHB depletion led to decreased glycogen in otherwise wild type and IIS mutants, and *gsk-3(RNAi)* further reduced glycogen in these

worms. Analysis from RNA-seq data in our lab has revealed that upon *phb-1 (RNAi)*, there is an upregulation of glycolytic pathways, and hence, the reduced glycogen is likely a reflection of increased glycolytic metabolism as mitochondria in these animals is impaired. Moreover, we also observed that expression levels of *fbp-1,* a gluconeogenic enzyme was downregulated in worms grown on *phb-1(RNAi)* and *phb-1;gsk-3(RNAi)* (Figure 43A). As less glucose is generated, the result is less glycogen. This is supported by RNA-seq analysis that revealed that upon *gsk-3(RNAi)*, there is significant decrease of key gluconeogenic genes including *fbp-1* in *phb-2* and *phb-2;daf-2* mutants.

A major effector of glycogen in several organisms is AMPK and it has a complex regulation. Acute activation of AMPK inhibits glycogen synthase (GS) to suppress glycogen biosynthesis (Carling and Hardie 1989; Wojtaszewski et al. 2002; Jorgensen et al. 2004; Miyamoto et al. 2007), while chronic activation of AMPK results in glycogen accumulation (Luptak et al. 2007; Hunter et al. 2011). However, glycogen does not shorten lifespan on a normal diet, as seen in *daf-2* mutants that store more glycogen, have an active AMPK and live longer (Apfeld et al. 2004). Our efforts to check whether AMPK is active upon *gsk-3(RNAi)* were unsuccessful owing to variability amongst experiments (Appendix 5). Wild type, *daf-2* and the mitochondrial PHB mutants on control and *gsk-3(RNAi)* were analysed with an antibody that recognizes the phosphorylated T172 on AMPK, an important response to cellular metabolic stress (Hardie 2004; Hardie et al. 2012). The general trend was that AMPK was active in all genetic backgrounds except wild type upon *gsk-3(RNAi)*. Previously, AMPK has been shown to be activated in *phb-2* mutants (Zubovych et al. 2010).

gsk-3(RNAi) strongly downregulates fat degradation

Additonally, we observed reductions in whole body triglycerides (Figure 44) upon depletion of GSK-3 except in *daf-2* mutants. Accordingly, reducing GSK-3 activity via lithium addition has been observed to decrease whole body triglycerides, the main lipid storage in flies, in a dose-dependent manner (Castillo-Quan et al. 2016). Low triglyceride content could be due to either decreased lipogenesis or increased fatty acid oxidation. Using the *atgl-1p*::*atgl-1*::*gfp* translational reporter, we found that gsk-3*(RNAi)* increased ATGL-1::GFP levels, across all genetic backgrounds suggesting increased hydrolysis of lipids.

Despite the availability of fatty acids as inferred by increased ATGL-1 levels, expression of several acyl CoA synthases, *acs-19* and *acs-13* and dehydrogenases *acdh-1/-2/-7*, also the mitochondrial *cpt-2* involved in transfer of medium- /long- chain fatty acids from cytosol to mitochondria, (Figure 46, A3.2, A3.3, A3.3) were downregulated upon *gsk-3(RNAi)*. Acyl CoA synthases and dehydrogenases are amongst the most abundant proteins identified in purified lipid droplets (Zhang et al. 2012), indicating a physical association between organelles of fat storage and mobilization. Specifically, the mitochondrial *acdh-1* exhibited a decrease across all genetic backgrounds upon GSK-3 loss (Figure 46). The decreases in β-oxidation genes upon loss of GSK-3 found in our study are also reflected at the transcript level.

Previously, PHB loss in wild type animals has been shown to have increased content of short chain and saturated fatty acids, with a decrease of long chain and unsaturated fatty acids (Lourenco et al. 2015). In line with this, we observed that PHB depleted nematodes only showed strong decrease of short chain fatty acid oxidation, *acdh-1* and *-2* and *acs-19*; whereas, genes involved in medium-/long- chain fat oxidation, *acdh-7*, *acs-13* were unaffected. Also unaffected was the expression of *cpt-2,* suggesting no issues with regard to import of medium-/long- chain fatty acids into the mitochondria (Figure 46, A3.2, A3.3, A3.3)*.* This implies that there is a preference for the β-oxidation of medium and long chain fatty acids for energy production rather than short chain fatty acids when PHB is depleted.

Fatty acid oxidation occurs in the mitochondria and peroxisomes, the major metabolic organelles, and is a conserved mechanism of energy generation. While at the moment we lack information about oxidation processes in the peroxisomes upon *gsk-3(RNAi)*, the consequences of the reduced levels of the different genes tested indicate reduced fat breakdown upon loss of GSK-3 and such a deregulation in fat oxidation could cause energetic deficits. However, these observations do not explain the reduced ORO staining.

ACDH-1 is involved in β-oxidation of short chain fatty acids (human homolog, SCAD) (Van Gilst et al. 2005b) and also in branched chain amino acid (BCAA) breakdown (human homolog, ACADSB) (Murphy et al. 2003). Based on sequence comparison, ACDH-1 more closely resembles the latter (Watson et al.

2013). The transgenic strain, P*acdh-1*::GFP, used in this thesis has strong expression in the intestine and hypodermis (Arda et al. 2010; MacNeil et al. 2013). As P*acdh-1*::GFP levels were very low upon both GSK-3 and/or PHB-1 depletion in both wild type and *daf-2* backgrounds, we were concerned whether this strain can reflect changes in oxidation of short chain fatty acids. Hence, additionally we show that *acdh-2* (homologous to *acdh-1)* (MacNeil et al. 2013), also exhibits a reduction in expression levels similar to *acdh-1* when worms are subjected to *gsk-3* or *phb-1(RNAi)* (Figure A3.2). In addition, P*acdh-1*::GFP levels are increased in animals with low glycogen stores indicating a change in response. Though we will need to further verify whether this increased P*acdh-1*::GFP expression in worms grown on *gsy-1(RNAi)* indicates increased short chain fatty acid oxidation (Figure A3.1,A).

Indeed, the transgenic strain *Pacdh-1*::GFP is an established reporter of dietary vitamin B12 status, as GFP is highly expressed when vitamin B12 is low (such as in *E. coli* OP50 and HT115) and is repressed when vitamin B12 is high (such as in *Comamonas* DA1877)(MacNeil et al. 2013; Watson et al. 2013; Watson et al. 2014; Watson et al. 2016). *acdh-1* is at the top of the alternate propionate shunt that includes *ech-6, hach-1, hphd-1* and *alh-8.* This shunt is transcriptionally activated when vitamin B12 is in low supply (Watson et al. 2016). An active propionate shunt prevents toxic build up of propionate, a byproduct of fat and protein breakdown and enables survival on a vitamin B12 deficient diet. Based on this, we can speculate that the very low expression of P*acdh-1*::GFP upon loss of GSK-3 and/or PHB-1, indicates a compromised propionate shunt. This is backed with evidence from RNA-seq analyses in our lab that all the genes involved in the propionate shunt are significantly downregulated in wildtype and mitochondrial PHB mutants upon *gsk-3(RNAi)*. Incidentally, some genes involved in vitamin B12 dependent propionyl CoA breakdown, *pcca-1, pccb-1, mce-1, mmcm-1* were also downregulated upon GSK-3 loss. As these worms are grown on HT115 bacteria lacking vitamin B12, it is possible that active ACDH-1 indicates breakdown of fat or proteins as seen in wild type and IIS mutants. However, in worms devoid of GSK-3, there is compromised fat or protein breakdown as indicated by a low *acdh-1* expression. Previously, PHB depleted worms have been observed to show alteration in amino acid metabolism (Lourenco et al. 2015), hence, altered *acdh-1* upon PHB depletion could be indicating that as well.

Intriguingly, knockdown of *acdh-1* in wild type animals does not affect lifespan. (Yuan et al. 2012) and there is evidence that *daf-2* mutant has increased levels of propionate and exhibit significantly increased abundance of the propionate catabolic enzymes MCE-1, MMCM-1, PCCA-1 and PCCB-1(Depuydt et al. 2014). Hence, an activation of this breakdown pathway indicates increased catabolism of fatty acids or branched chain amino acids in the *daf-2* mutant.

Interestingly, the human homolog of *acdh-1*, ACADSB was found amongst metabolic proteins that associate specifically with GSK3β1. Hence, it could be a potential mediator in the atypical functions of GSK3β1 (Gao et al. 2013).

Fat synthesis is a key requirement of growth and GSK-3 depletion reduces *de novo* fat synthesis in wild type as seen from the expression levels of the transgenic strain P*pod-2*:GFP (Figure A3.5), but not in PHB depleted animals. This behavior might be linked to the ageing phenotype but we miss information about *daf-2* and *phb-2;daf-2* mutants. However, RNA seq analyses done in the lab indicate that *pod-2* is unaffected in *phb-2;daf-2* mutants on *gsk-3(RNAi).* In wild type and IIS defective *daf-2* mutants, upon *gsk-3(RNAi)* expression levels of *fasn-1* and *fat-7* were downregulated respectively. Thus, the reduction in whole body ORO staining upon loss of GSK-3 could be a result of decrease in expression of *de novo* fat synthesis genes.

As proper breakdown of fats is required for the mitochondria to utilize in energy production, a deregulation of lipid breakdown as seen upon GSK-3 loss could fail to meet to the energy demands of these worms. Additionally, worms depleted of GSK-3 are less active phenotypically from control animals, especially *daf-2* mutants. While the consequences of GSK-3 depletion on mitochondrial function are not evident across genetic backgrounds while worms are young, on day 5 in aged worms, wild type and IIS mutants exhibit strong decreases in respiration, while PHB depleted animals modulate respiration differentially. Moreover, the accumulation of fatty acids as a result of irregular lipid breakdown during ageing could lead to lipotoxicity, often associated with age-related disorders and metabolic syndromes.

Similar to the altered fat metabolism seen in wild type worms on *gsk-3(RNAi)*, *pry-1* mutants (component of Wnt destruction complex) also exhibit drastically reduced lipid levels and downregulation of genes involved in *de novo* synthesis

such as the desaturases, *fasn-1*, *fat-5*, and *-6* and elongases, *elo-3* and *-6*; and also those involved in fatty acid oxidation such as *acdh-1*, -6, *-11*, *-23*; *acs-2*, -11, *-17*; *cpt-1*, *-4,* and *ech-9 (*Ranawade et.al, bioRxiv, pre-print). The authors also recorded that yolk lipoprotein vitellogenins (VITs), *vit-1*, *-2*, *-3*, *-4*, *-5*, and -6, important for lipid distribution were also differentially regulated. In line with this we also observed that loss of GSK-3 led to decreased expression of VIT-6 across all genetic backgrounds (Figure 47). Additional investigation of the other VITs and their alterations during ageing might yield more information on whether deregualtion of these contributes to the metabolic defects seen upon *gsk-3(RNAi)*. These observations indicate a possible mediation by Wnt signalling in lipid metabolism.

Lack of GSK-3 perturbs mitochondrial lipid composition

In yeast cells deficient of PHB, survival depends on lipid composition of mitochondrial membranes, especially alterations in CL and PE (Osman et al. 2009). Also, reduction in *fat-7* expression limits monounsaturated fatty acid synthesis that maintains fatty acid levels and could potentially alter cellular and membrane lipid composition, particularly, that of the mitochondria (Osman et al. 2011). In accordance with this, GSK-3 depletion leads to alterations in mitochondrial membrane lipids, i.e. strong increases in PLs in wild type and *daf-2* mutants (Figure 52). It has been described that increased accumulation of PLs in the mitochondria depends on lipid transport between the ER and mitochondria. Additionally this could involve intramitochondrial lipid trafficking (Osman et al. 2011). Mitochondrial phospholipid composition varies little among different cells, indicating that major changes might not be tolerated. Altered phospholipid levels and phospholipid damage have been linked to a variety of human disease states (Chicco and Sparagna, 2007; Joshi et al., 2009). In yeast, GSK-3 positively regulates Elo2 phosphorylation, a fatty acid elongase protein. Phophorylation of Elo2 is important for very long chain fatty acid (VLCFA) synthesis that in turn is essential for ceramide synthesis (Zimmermann et al. 2013).

With respect to the alterations in membrane lipids, of particular interest are two classes, Phosphatidylcholine (PC) and cardiolipins (CL). Regarding the former, PC are increased strongly across genetic backgrounds upon *gsk-3 (RNAi)*. PC synthesis requires the major methyl donor, S-adenosylmethionine,

SAM (encoded as *sams-1* in nematodes). In line with the increased PC levels, RNA seq analyses revealed that *sams-1* is upregulated in wild type, *phb-2* and *phb-2;daf-2* mutants upon loss of GSK-3. Moreover, SAMS-1 has been implicated in a conserved regulation involving the transcription factor SREBP-1/SBP-1 in lipogenesis, such that under conditions of low SAM or decreased PC, lipogenesis is promoted by nuclear accumulation of SBP-1(Walker et al. 2011; Ding et al. 2015). Also, knocking down *sams-1* extends longevity (Hansen et al. 2005). In our case, an increased *sams-1* and increase in the phospholipid PC, could potentially inhibit SBP-1 and block lipogenesis, as seen from the reduction in fat stores upon *gsk-3(RNAi).*

Cardiolipins have an important role in mitochondrial bioenergetic processes. Also, they have been shown to interact with a number of proteins, including the respiratory chain complexes, generation of the inner membrane potential and are essential for mitochondrial structure and integrity (Paradies et al. 2014). *gsk-3(RNAi)* alters CL composition more in wild type and in conditions of low IIS signalling in comparison to the PHB mutants. CL is required for mitochondrial fusion and fission, a key step in separating mitochondria that are not functional for mitophagy - selective degradation of mitochondria by autophagy. Incidentally, other PLs derived from the mitochondria like phosphatidylethanolamine (PE) and phosphatidylglycerol (PG) are also vital for the autophagy (Shatz et al. 2016; Hsu and Shi 2017). Thus, changes in PL compositions could be linked to autophagy dysregulation.

In agreement, *gsk-3(RNAi)* leads to an increase in autophagy (Lehmann et al. 2013) via observation of accumulation of the autophagic vesicle marker LGG-1. Autophagy is a conserved cellular homeostasis and stress response mechanism to degrade long-lived proteins, molecules and organelles. It is a multistep process that involves vesicular transport events leading to tethering and fusion of autophagic vesicles with several intracellular compartments (Megalou and Tavernarakis 2009; Amaya et al. 2015). Interestingly, we have evidence from RNAseq data that lack of GSK-3 upregulates processes related to membrane vesicle trafficking across all genetic backgrounds. In *C. elegans*, autophagy is involved in many processes through embryonic and larval development and also in stress responses. In long lived strains like *daf-2,* studies have shown that

ageing and longevity are dependent on autophagy (Melendez et al. 2003; Melendez and Levine 2009; Chen et al. 2017).

Altered mitochondrial membrane lipid composition has also been implicated in ageing in other systems. Broadly, alterations could be due to disturbance of enzymes involved in phospholipid remodeling, as well as changes in the dietary fatty acids and this can have bioenergetic costs, by affecting mitochondrial capacity and function (Schenkel and Bakovic 2014; Valencak and Azzu 2014; Medkour et al. 2017) .

Mitochondrial bioenergetics during ageing upon GSK-3 depletion

To investigate if GSK-3 affects mitochondrial function during ageing, we measured basal and maximal oxygen consumption rate (OCR). For assessing mitochondrial function, some time consuming methods are in use - biochemical analysis of extracts (Krijgsveld et al. 2003), in vivo ATP level analysis via transgenic reporter (Lagido et al. 2008), in vivo mitochondrial membrane potential analysis (Gaskova et al. 2007) and analysis of basal oxygen consumption (Braeckman et al. 2002a); but these measure one specific aspect of mitochondrial function and might not give a clear picture of overall mitochondrial health. Seahorse Extracellular Flux Analyzers (Luz et al. 2015; Koopman et al. 2016) offer real-time oxygen consumption measures and also of other parameters like maximal respiratory capacity, spare respiratory capacity, ATP coupled respiration and proton leak in whole worms in multi-well formats without the need for lysing cells or isolating mitochondria.

Our OCR data normalized by worm number and corrected for worm area show that it is under low *daf-2* signalling that GSK-3 loss strongly impairs basal respiration during ageing (Figure 48). Exposure to FCCP, a mitochondrial uncoupler revealed that maximal respiratory capacities in wild type and *daf-2* mutants were strongly compromised upon *gsk-3(RNAi)* (Figure 48), indicating that GSK-3 function is also important for mitochondrial function in wild type animals. Additionally, mRNA levels of *ucp-4,* an uncoupling protein was downregulated in IIS mutants grown on *gsk-3(RNAi)* (Figure A4.4), signifying a prospect that mitochondria might be compromised. Strong alterations in maximal OCR were only observed in *phb-2* mutants that exhibited an increase on *gsk-3(RNAi)* that could be linked to the ability to better modulate energetic

responses to GSK-3 loss. The long lived *phb-2;daf-2* mutants do not show changes in respiraton upon GSK-3 depletion except a significant decrease at YA stage, but oxygen consumption reduces during ageing slightly. Though, overall they always exhibit a low oxygen consumption rate.

We additionally normalised OCR data only to number of worms and observed that it changes result interpretation substantially owing to the size differences among the different genetic backgrounds (Annexure 4, Figure A4.2). Loss of GSK-3 in wild type and IIS mutants elicits similar effects with respect to basal and maximal OCR irrespective of normalisation as they do not exhibit significant changes in size. However, the decreased basal OCR in the mitochondrial mutants, *phb-2* and *phb-2;daf-2* with respect to wildtype and *daf-2* mutants at the YA stage (Annexure 4, Figure A4.2) might be attributed to faulty mitochondria but its more likely a result of the small size of these mutants as these are not observed when the data is corrected for worm area (Figure 48). Also, during ageing at day 5, the increased basal and maximal respiration of the short lived *phb-2* compared to wild type is missed when not corrected for area. The long lived double mutants *phb-2;daf-2* respire lower than the IIS depleted mutants irrespective of method of normalisation. *phb-2* and *phb-2;daf-2* mutants on *gsk-3(RNAi)* tend to respire less, without corrections for size differences (Annexure 4, Figure A4.2), implying that their low OCR is not because they have potentially faulty mitochondria upon GSK-3 loss but that in fact their respiration is unaffected. Similarly, GSK-3 depletion does not affect the maximal respiration of *phb-2* mutants, and decreases the same during ageing (Annexure 4, Figure A4.2) but area normalisation reveals that in fact these worms respire much more when younger and are unaffected at day 5.

These data present important points towards the fact that careful review is required with respect to results gathered from such metabolic analyses as they depend on the manner of normalisation, as shown here. Normalizing to size is essential for cases wherein the experimental backgrounds being tested show obvious and significant differences - such as ours (Figure 48). Nematode respiratory rates have been normalized by several ways, such as worm number, worm volume, worm length, total protein and mitochondrial copy number. For cases where mutants or RNAi treated worms are smaller than the

respective age-matched controls, correcting for protein levels provides extra information. Although it has been reported that mitochondrial dysfunction via RNAi led to reduced respiration with both worm number and protein normalization (Wu et al. 2014) and hence, one can normalize to mitochondrial DNA content to account for differences in mitochondrial activity (Weimer et al. 2014). Though our mitotracker staining at the YA stage (A4.3) reveals that the dysfunctional mitochondrial mutants, *phb-2* and *phb-2;daf-2* with respect to wildtype and *daf-2* mutants have less mitochondrial content and this is reflected at the basal OCR at YA stage irrespective of normalization. However, mitotracker staining is not indicative of mitochondrial activity and hence, it is better to use mitochondrial DNA copy number to normalize.

Reductions in size and alterations in oxygen consumption are potential consequences of mitochondrial stress. While we have been unable to check ATP levels in these backgrounds, we did observe that depletion of GSK-3 activates UPR^{mt} selectively (Figure 50). Loss of GSK-3, induces *hsp-6* expression in wild type animals while *daf-2* mutants are unaffected. The mitochondrial PHB mutants induce the UPR^{mt}, but loss of GSK-3 further induces *hsp-6* expression only in the *phb-2; daf-2* double mutants. Activation of UPR^{mt} is also known to cause metabolic restructuring, such as activating glycolytic genes and repressing those of oxidative phosphorylation (Nargund et al. 2012; Nargund et al. 2015). As we have evidence in the lab that atleast in *phb-2* and *phb-2;daf-2* mutants, glycolytic pathways are upregulated, cases where UPR^{mt} is active; one can contemplate that it is likely that GSK-3 depleted animals that are capable of inducing *hsp-6* expression could also potentially rely on glycolysis.

Tissue specific analysis of GSK-3 with a focus on ageing

Though GSK-3 has ubiquitous expression (Figure 40), in line with its impact on metabolism, depleting GSK-3 solely in the intestine leads to reduction in lifespan across all genetic backgrounds and strongly so in the *daf-2* mutants (Figure 53). This implies an important intestinal role for GSK-3, the major metabolic organ in worms. We also noted that loss of *gsk-3* in the intestine did not recapitulate the embryonic lethality observed in wild type animals subjected to whole animal *gsk-3(RNAi),* but the same worsened the lethal phenotype of*daf-2* mutants as they barely laid eggs (observation not quantified). This again indicates a strong role for GSK-3 in development, both

whole body and in the intestine, when IIS signalling is low.The genomic tagging of GSK-3 via CRIPSR-Cas9 utilising the SapTrap protocol (Schwartz and Jorgensen 2016) incorporates a compatible GFP KO cassette (Munoz-Jimenez et al. 2017). This has been further developed in the lab to generate tissue specific GSK-3 KO strains to observe the lifespan phenotype when this kinase is knocked out in three tissues, namely, intestine, muscles and neurons. We confirmed that wild type and PHB depleted animals exhibit decreased longevity only when GSK-3 is inactivated in the intestine, and are unaffected upon neuronal and muscle GSK-3 loss. IIS defective *daf-2* mutants exhibit a decrease when GSK-3 is knocked out in intestine andmuscles, whereas, *daf-2* mutants devoid of PHB exhibit a reduced lifespan upon GSK-3 KO in all tested tissues, intestine, neurons and muscles. These differential alterations in lifespanupon tissue specific GSK-3 KO across different genetic backgrounds imply relevance of GSK-3 function in specific tissues.

Recently, it was shown in dissected ovaries of *Drosophila* that during late oogenesis when IIS activity is reduced, GSK3 promotes mitochondrial quiescence and glycogen accumulation (Sieber et al. 2016). This is different from studies in whole *Drosophila* wherein no alterations in glycogen were seen when GSK-3 was inhibited via Lithium (Castillo-Quan et al. 2016). Previous data using in vitro experiments does indicate that not only there might be distinct roles for GSK-3α and GSK-3β, but also tissue-specific phenotypes associated with each of these isoforms (Ciaraldi et al. 2006; Patel et al. 2008). Hence, these tissue specific *C. elegans* GSK-3 KO strains can be utilised as new genetic tools in the future to further analyse tissue-specific roles of GSK-3 in regulation of development, ageing and lipid and carbohydrate metabolism.

Limitations of this study

GSK-3 is a kinase that is inactivated upon phosphorylation at Ser9 in GSK-3β in vertebrates (Sutherland et al. 1993; Cross et al. 1995; Frame et al. 2001; Afanas'ev 2010). This thesis is unable to demonstrate whether the acivity of GSK-3 is subject to a similar regulation in *vivo*, due to lack of a good antibody; and whether or not Ser9 is conserved in *C. elegans*. The status of phophorylation is of importance as it has been seen that PI3 kinase-resistant GSK3 (gsk3[KI]) mice with enhanced adiponectin production are protected against the development of metabolic syndrome as compared to gsk3[WT] mice

(Chen et al. 2016). Also, a recent paper established that active GSK-3 inhibits AMPK function, a key regulator of cellular homeostasis. Interestingly the authors showed that insulin signalling a conserved inhibitory pathway for GSK-3 promotes GSK3-dependent AMPK phosphorylation and inhibition (Suzuki et al. 2013),that leads to metabolic fluctuations resulting in catabolism of fatty acids in vitro. These reports highlight the importance of this unusual kinase, GSK-3 and its physiological relevance.

An area of research wherein GSK-3 has a role is tauopathies, including Alzheimer's disease (AD), Down syndrome, Parkinson's amongst others. Tau are microtubule-associated proteins (MAP) found in neuronal axons. Tau protein binds to microtubules (MTs) and stimulates MT polymerization and promotes stabilization. In diseased states, tau is hyperphosphorylated and dissociates from MTs and tau forms filaments that aggregate in neurons. In a genome wide screen carried out by Kraemer et. al, to identify potential modifiers of tau-induced pathologic phenotype, *gsk-3(RNAi)* was found to further enhance the tau-induced Unc phenotype (Kraemer et al. 2006). GSK-3 is a component of the canonical Wnt signalling pathway and is known to regulate MT stability, and hence, it is possible that certain functions are mediated through Wnt as well. While the role of kinases in tauopathies has been done using transgenic animal models, not all the results obtained were consistent. In mice, there are conflicting studies wherein conditional overexpression of GSK-3β has been detrimental or protective. On the other hand, in *Drosophila*, results were consistent with GSK-3β promoting tau-induced neurodegeneration and lack of GSK-3β or use of GSK-3β inhibitors supressing the tau phentoypes (Gotz et al. 2010). In the work done in *C. elegans*, RNAi of GSK-3 enhances tau-induced phenotypes, implying that at least in this system, GSK-3 is protective (Kraemer et al. 2006).

Incidentally, loss of PHB2 in the forebrain of mice leads to neurodegeneration and tau hyperphosphorylation, while GSK-3β was found to be inactivated by phosphorylation at Ser9, accompanied by the activation of the upstream kinase, AKT. This implied that GSK-3 might not be the cause for the increased tau pathology in Phb2[NKO] mice (Merkwirth et al. 2012). It will be interesting to check whether loss of GSK-3 in worms under conditions of reduced IIS function or upon PHB depletion, induces taupathies or leads to an alleviation.

Future directions

As the semi-automated screening strategy used by us was successful, the same can applied at a larger scale to an OrthoList RNAi library that has been built in the lab (Hernando-Rodriguez et al. 2018) utilising the automated data analysis platform. This can be of considerable advantage in the future for researchers to streamline RNAi screens by focusing on genes with translational potential to human health and provide insights into the mechanisms on biological processes in humans.

Given the stong reduction in lifespan and drastic embryonic lethality when GSK-3 is depleted in the intestine, especially in *daf-2* mutants, it would be worth to see if an intestine specific expression of GSK-3 could rescue these phenotypes. It would also help establish the intestine as a key site of GSK-3 function under impaired insulin signalling.

There are serveral lines of evidence linking GSK-3 to metabolism and ageing. However, in worms, the most known downstream effector of GSK-3 is SKN-1 (An et al. 2005). Identification of other downstream effectors of GSK-3 would be crucial for better understanding the hypometabolic phenotype and accerelated ageing observed upon GSK-3 loss. Another thing to investigate would be if there are possible mediations in these by components of Wnt signalling.

An observation that requires further exploration is the potential role of GSK-3 in LRO biology by checking the same in wild type and IIS deficient backgrounds. The fact that we observe downregulation of *kat-1* in PHB deletion mutants could be related to the premature ageing phenotype of GSK-3 depleted worms. Lack of *kat-1* shortens lifespan but was found dispensable for the long lived *daf-2(e1370)* mutants. Also, KAT-1 loss leads to increase in accumulation of lipofuscin pigment and also encodes for ketoacyl thiolase, a conserved metabolic enzyme that catalyzes the last step of fatty acid oxidation (Berdichevsky et al. 2010). The accerelation in ageing observed upon GSK-3 loss, could be a result of decreased fat oxidation, but one cannot rule out the the other possibility, such as due to increased accumulation of lipofuscin. Additionally, also investigate the Wnt components, KIN-19, BAR-1 in this regard.

As per downregulation of *acdh-1,* which could be indicating irregular BCAA breakdown, it would be worth to check level of protein aggregation in GSK-3 depleted conditions. Previously, a kinome screen has implicated GSK-3 being essential in proteostasis (Lehmann et al. 2013). The same authors also implied that lack of GSK-3 leads to accumulaton of autophagic vesicles. As autophagy involves lysosomes, we could potentially also utilize Electron Microscopy (EM) for a more reliable observation of the different autophagic structures such as autophagosomes or autolysosomes.

We observe strong alterations in mitochondrial lipid components and in respiration, despite the fact that mitochondrial content is not impacted upon loss of GSK-3. However, we might gain more information from studying mitochondrial structure. More so, as previously, PHB deficient worms have been shown to have abnormal mitochondrial morphology (Artal-Sanz et al. 2003)and GSK-3 was identified as required for normal maintenance of mitochondrial network structure in adult muscle (Lehmann et al. 2013).

Lithium addition elicits a response similar to *gsk-3(RNAi)* in our hands. Incidentally, in vitro studies indicate that lithium treatment results in nuclear translocation of β-catenin and hence, Wnt activation (Sinha et al. 2005). It is quite probable that Wnt components that elicit the same longevity phenotype could also be targets of lithium in worms as well.

Based on the indications that loss of GSK-3 could activate glycolysis, additional data can be gained by investigating in vitro enzymatic activities of genes involved in glycolysis/ gluconeogenesis to verify if indeed they are affected upon *gsk-3(RNAi)*.

1. Mitochondrial prohibitin (PHB) deletion mutants, *phb-2(tm2998)* and *phb-2 (tm2998);daf-2(e1370)* show an opposing longevity phenotype and low *in vivo* Nile Red staining. These mutants are developmentally delayed with reduced pharyngeal pumping and increased fat stores.

2. Customized imaging and segmentation protocols were created for the balanced prohibitin mutants for high throughput screening. These can be potentially exploited for any strain or dye as the segmentation is done in the brightfield channel.

3. A semi-automated kinase RNAi screen was performed using a kinase sub-library in *phb-2* and *phb-2;daf-2* mutants. This resulted in identification of 26 kinases that suppressed the low Nile Red staining phenotype of PHB mutants in either one or both backgrounds.

4. Amongst the candidates, we provide evidence for the function of GSK-3, whose loss causes a differential accerelation in ageing. GSK-3 is essential for the long lifespan of IIS defective *daf-2* and *phb-2;daf-2* mutants, while its depletion does not affect the lifespan of *phb-2* mutants and only mildly shortens wild type lifespan.

5. Depletion of KIN-19 and BAR-1, members of the Wnt signalling pathway elicits a similar differential ageing phenotype as seen upon loss of GSK-3.

6. GSK-3 depletion further increases the glycogen stores in the long-lived insulin signalling mutants, and further depletes glycogen in mitochondrial PHB mutants. Glycogen stores in wild type animals were not affected.

7. With respect to carbohydrate metabolism, GSK-3 loss downregulates gluconeogenesis in wild type and PHB-1 depleted worms.

8. GSK-3 loss reduces the main lipid storage - triglycerides across all genetic backgrounds except in IIS *daf-2* mutants.

9. GSK-3 influences lipid synthesis and breakdown pathways in *C. elegans.* Loss of GSK-3 reduced short chain fatty acid oxidation across all genetic backgrounds. Also, oxidation of medium-/long- chain fatty acids was decreased across wild type, *daf-2* and *phb-2* mutants devoid of GSK-3. *phb-2* mutants regulate fat oxidation differentially with a strong suppression specifically in

short chain fatty acid oxidation, while oxidation of medium-/long- chain fatty acids was unaffected.

10. Fat synthesis is reduced in wild type and *daf-2* mutants upon loss of GSK-3. However, PHB depleted worms were unaffected.

11. GSK-3 strongly decreases vitellogenesis across all genetic backgrounds.

12. GSK-3 loss impacts mitochondrial health through ageing. It deteriorates strongly in IIS *daf-2* mutants and wild type worms, whereas PHB depleted worms, show an increased capacity to respire upon GSK-3 depletion. *phb-2; daf-2* are unaffected by GSK-3 loss, keeping extremely low respiration levels.

13. Mitochondrial membrane lipid composition was altered upon loss of GSK-3 in a background specific manner, with significant alterations in wild type and IIS defective mutants.

14. Mitochondrial UPR is induced in a background specific manner upon GSK-3 loss. While it was strongly induced in wild type animals, *daf-2* mutants were unresponsive. The already active mitochondrial UPR in *phb-2* was unaffected and *phb-2;daf-2* mutants further induced UPR^{mt} on *gsk-3(RNAi)*.

15. Intestinal function of GSK-3 is required for normal lifespan across wild type and PHB deletion mutants but is indispensable for *daf-2(e1370)* lifespan, as intestinal depletion of GSK-3 fully suppresses the long lifespan of *daf-2* mutants.

16. GSK-3 is ubiquitously expressed in *C. elegans.* Strong expression is seen in the embryos, intestine, muscles and the nervous system. It is also seen in the germline, particularly, in sperm and vulval precursor cells

1. *C. elegans* maintainence

All nematode strains were maintained and cultured at 20°C on Nematode Growth Medium (NGM) plates seeded with *Escherichia coli* strain OP50, under standard conditions (Brenner 1974). *E. coli* OP50 is a uracil auxotroph whose growth is limited on NGM plates. This property allows worms to be visualized easily on the plates. The frequency with which various *C. elegans* strains should be transferred and maintained depends on their genotype, and also at the temperature at which they are being maintained. It is best to maintain them without starvation/ contamination of the OP50 bacteria.

Commonly used maintenance methods are picking and chunking. These can be carried out with ease under a stereomicroscope. Picking involves transferring worms with a worm picker. A worm picker/pick is a flame sterilized platinum wire looped into a Pasteur pipette. Chunking involves usage of a sterilized spatula to remove a chunk of agar from an old plate to a fresh plate with bacteria. The worms will crawl out of the old piece of agar (chunk) and onto the bacterial lawn of the new plate. Chunking works well for the transfer of homozygous populations but is not advisable for heterozygous stocks (Stiernagle 2006).

2. Strains used

The following strains were used in this study:

STRAIN	MRS NUMBER	GENOTYPE	SOURCE
Bristol N2	MRS1	N2(wild-type Bristol isolate)	CGC
CB1370	MRS 88	*daf-2(e1370) III*	CGC
BR6115	MRS 122	*phb-1(tm2571)I/hT2[bli-4(e937) qIs48] (I;III)*	NBRP, 10 times outcrossed before introducing the hT2 balancer
BR6108	MRS 56	*phb-2(tm2998); mIn1[mIs14 dpy-10 (e128)]II*	NBRP, 10 times outcrossed before introducing the mIn1 balancer
BR6206	MRS 49	*phb-2(tm2998);mIn1[mIs14 dpy-10(e128)]II; daf-2(e1370)III*	NBRP

VL749	MRS348	*wwIs24[acdh-1p::GFP + unc-119(+)]*	CGC
	MRS415	*daf-2(e1370) III; wwIs24[acdh-1p ::GFP + unc-119(+)]*	This study
	MRS444	*phb-2(tm2998);mIn1[mIs14 dpy-10 (e128)]II; wwIs24[acdh-1p::GFP + unc-119(+)]*	This study
	MRS458	*fpIs107(acdh-2p::GFP)*	Jarriault Lab
CL2166	MRS179	*dvIs19 [(pAF15)gst-4p::GFP::NLS] III*	CGC
	MRS482	*daf-2(e1370); dvIs19 [(pAF15)gst-4p::GFP: : NLS] III*	This study
SJ4005	MRS85	*zcIs4[hsp-4::GFP] V*	CGC
PE255	MRS 186	*feIs5[sur-5::luc+::gfp; rol-6(su1006)]V*	Dr. C.Lagido
	MRS 210	*daf-2(e1370)III ;feIs5[sur-5::luc+::gfp; rol-6 (su1006)]X*	Dr. M.Olmedo
	MRS 229	*phb-2(tm2998);mIn1[mIs14 dpy-10 (e128)]II;feIs5[sur-5::luc+::gfp; rol-6(su1006)]X*	This study
	MRS 230	*phb-2(tm2998);mIn1[mIs14 dpy-10 (e128)]II; daf-2(e1370)III;feIs5[sur-5::luc+::gfp; rol-6(su1006)]X*	This study
SJ4100	MRS 57	*zcIs13[Phsp-6::GFP]V*	CGC
BR6296	MRS 64	*daf-2(e1370)III, zcIs13[Phsp-6::GFP]V*	Dr. Artal-Sanz
	MRS106	*phb-2(tm2998);mIn1[mIs14 dpy-10 (e128)]II; zcIs13[Phsp-6::GFP]V*	Dr. Artal-Sanz
	MRS60	*phb-2(tm2998);mIn1[mIs14 dpy-10 (e128)]II; daf-2(e1370)III; zcIs13[Phsp-6::GFP]V*	Dr. Artal-Sanz
VP303	MRS198	*rde-1(ne219)V;kbIs7*	CGC
	MRS419	*daf-2(e1370)III; rde-1(ne219)V;kbIs7*	This study
	MRS418	*phb-2(tm2998);mIn1[mIs14 dpy-10 (e128)]II; rde-1(ne219)V;kbIs7*	This study
	MRS447	*phb-2(tm2998);mIn1[mIs14 dpy-10 (e128)]II; daf-2(e1370)III; rde-1(ne219)V;kbIs7*	This study
BC13916	MRS 452	*sEx13916 [rCesW09B6.1::GFP + pCeh361] -* pod-2::GFP	CGC
BC11281	MRS 453	*sEx11281 [rCes R07H5.2::GFP + pCeh361] -* cpt-2::GFP	CGC
BC12611	MRS 456	*sIs11096 [rCes T25G12.5::GFP + pCeh361] -* acdh-7::GFP	CGC
BC10604	MRS 450	*sIs10325 [rCesC36A4.9::GFP + pCeh361] - acs-19*::GFP	CGC
BC10191	MRS451	*sEx10191[rCesY65B4BL.5::GFP + pCeh361] -* acs-13::GFP	CGC
BC11264	MRS 455	*sIs11264 [rCesK07A3.1::GFP + pCeh361] - fbp-1*::GFP	CGC

	MRS 481	*Pgsk-3::GFP::gsk-3*	This study
	MRS 500	*daf-2(e1370); Pgsk-3::GFP::gsk-3*	This study
VS20	MRS 218	*hjIs67[atgl-1p::atgl-1::GFP+mec-7::RFP]*	CGC
	MRS 270	*daf2(e1370); hjIs67[atgl-1p::atgl-1::GFP+mec-7::RFP]*	Dr. Lourenço
BC12843	MRS 401	*sIs11286[rCesK07H8.6::GFP+pCeh361] - vit6::GFP*	CGC
	MRS 402	*daf-2(e1370); sIs11286 [rCesK07H8.6:: GFP+ pCeh361] - daf-2(e1370);vit6::GFP*	Dr. Lourenço

** From *Caenorhabditis* Genetics Center (CGC) and National BioResource Project (NBRP)*

3. Worm synchronization by alkaline hypochlorite treatment (Bleaching)

Alkaline hypochlorite solution, commonly called as bleach solution was made as follows - 6.5 ml H_2O, 0.5ml 5M KOH and 3ml 5% Bleach (This recipe is for 10 ml). The hypochlorite solution kills all worms not protected by the egg shell. A worm population with enough gravid adults was washed off using M9 buffer (3 g KH_2PO_4, 6 g Na_2HPO_4, 5 g NaCl, 1 ml 1 M $MgSO_4$, H_2O to 1 litre. Sterilize by autoclaving) into a 15ml tube. They were washed by centrifuging for 1min at 1300g and 5 ml bleach solution was added to the worm pellet. This was incubated for 2mins with vigorous vortexing/shaking. The pellet was centrifuged for 1 min at 1300g, supernatant removed and re-suspended in 5ml of M9 buffer. Next, the supernatant was removed and the worm pellet was incubated in 1ml M9 buffer plus 4ml bleach solution for 40-60 secs with periodic vortexing/shaking till only embryos remained.

Caution: Check the bleached worms under the stereoscope at this stage, if no worm cuticles are left, the sample should be centrifuged immediately.

The pellet with embryos was washed four times in 5ml of M9 buffer (1min, 1300g) to remove bleach, and finally re-suspended in M9. The eggs were taken and laid onto NGM or RNAi NGM plates, or left to hatch overnight at 20° C in M9 buffer (shaking incubator) to obtain synchronized L1 larvae.

4. Growing *C. elegans* in liquid medium

Large quantities of *C. elegans* can be grown on S Medium (20ml NaCl 5M, 50 ml Potassium phosphate 1M pH 6, 10 ml 1M potassium citrate pH 6, 10 ml trace metals solution, 3 ml 1M $CaCl_2$, 3 ml 1M $MgSO_4$. Components were added using sterile technique; this should not be autoclaved) using concentrated *E.*

coli OP50 as a food source (Stiernagle 2006). *E. coli* OP50 was inoculated in 1L of LB (500ml each in 2L flasks) and grown overnight at 37°C. The bacteria was pelleted down and concentrated by centrifuging at 3200 ×g for 20mins. The supernatant was discarded. The concentrated bacterial pellet was re-suspended in S Medium (30g/L) supplemented with cholesterol (1ml/L). This OP50 suspension in S Medium can be stored at 4°C for upto 4 weeks. Concentrated *E. coli* OP50 can be prepared in advance and stored such that bacteria can be added as per requirement.

To start a liquid culture of worms, worms from 1-2 large plates were washed out in M9 buffer / S Medium. The worm pellet was washed 2x times to clean out the bacteria from the plate. The clean worm pellet was now added to 50-100ml of S Medium OP50. The worm culture was monitored, and additional *E. coli* OP50 was added as required.

Cultures can be monitored by checking a drop of the culture under the microscope. If the food supply is depleted (the culture solution would no longer be visibly cloudy), one should add more concentrated *E. coli* OP50 suspended in S Medium. When many gravid adult animals are spotted in each drop, the culture is ready to be bleached.

Note: The amount of food needed will depend on the starting inoculum of worms and the genotype, and the length of time for which the worms are grown (2-3 generations).

5. RNAi assays

For RNAi assays on plate (Lifespan and imaging experiments), worms were placed on NGM plates seeded with HT115 (DE3) bacteria, either the pL4440 empty vector or the required RNAi construct. The RNAi bacterial cultures of interest supplemented with tetracycline (15 µg/ml) and ampicillin (100 µg/ml) were grown overnight at 37°C, 180 rpm in a shaking incubator. Next day, diluted cultures supplemented with only ampicillin (100 µl/ml) or carbenicillin (25 µg/ml) were grown at 37°C, 180 rpm for 3 hours. 2 mM IPTG was added to the cultures to induce expression of dsRNA. Plates were seeded with the bacterial cultures and left overnight at room temperature.

For mitochondrial fractions, the pre-inoculum and day culture was done as described above and then bacteria were induced in culture at 37°C, 180 rpm

for 2 hours. This was then pelleted down by centrifugation at 3200 ×g at 4 °C for 20 min. Pellets were re-suspended in S Basal (5.85 g NaCl, 1g K_2HPO_4, 6g KH_2PO_4 , H_2O to 1 litre. Sterilized by autoclaving) at 4 °C. Re-suspended pellets were centrifuged again at 3200×g for 20 min at 4°C. Bacterial stocks were prepared by re-suspending the pellets (30 g/L) in S Medium containing carbenicillin (25 µg/ml), IPTG (1 mM) and cholesterol (5 µg/ml). This can be stored 4 °C.

For the kinase RNAi screen, frozen bacteria containing the RNAi clones from the ORFeome kinase sub-library (96-well plate) was left to thaw at room temperature briefly and replicated onto LB agar supplemented with ampicillin (100 µg/ml) and tetracycline (15µg/ml) using a pin-replicator. Bacteria was grown overnight at 37°C. Growing the bacteria in solid media enables ease of visualization and identification of the clones where the bacteria did not grow. Bacteria was inoculated into 1ml of LB (100 µl/ml Amp; 15 µg/ml Tet) in deep well 96-well plates, grown overnight and next day induced using 2mM IPTG for 2 hrs at 37°C, 180 rpm. The induced culture was pelleted down at 4000rpm for 8mins. The bacterial pellet in each well, i.e., each RNAi clone was re-suspended in 250µl of S Medium with 2mM IPTG, 100nM Nile Red.

6. Selection of homozygous *phb-2* mutants using the COPAS worm sorter

Gravid adult worms were bleached from a liquid culture. Embryos were left to hatch into L1 larvae overnight in S Medium (shaking incubator at 20°C, 120 rpm). The COPAS was switched on left to stabilize and cleaned with MQ water and 70% EtOH before sorting. The L1 larvae were checked and filtered through 40 µm nylon cell strainer to exclude debris like unbroken corpses/clumped unhatched eggs that might remain in the sample from the bleaching. A clean L1 preparation aids in ease of sorting. Also, 0.01% Triton X-100 was added to avoid worms sticking within the tubes or the sample cup of the COPAS. The concentration of animals per milliliter was adjusted using a microscope. (Ideally 1worm/µL by diluting the sample). Sheath flow rate of 9.5 ml/min and worm concentration of 15–20 events per second was maintained during sorting. At the start of each experiment, a small sample was sorted and visually verified to confirm a correct sorting.

Approximately 40 sorted homozygous *phb-2* mutants per well were supplemented with 100µl RNAi bacteria plus Nile Red and incubated at 20°C (shaking) at 120 rpm till the desired imaging stage. Worms were imaged at the young adult (YA). Depending on the genotypes worms were grown on the RNAi plates for following times:

Wild type worms   - approximately 48 hrs
daf-2(e1370) mutants   - approximately 72 hrs
phb-2(tm2998) mutants   -approximately 96 hrs
phb-2(tm2998); daf-2(e1370)   - approximately 144 hrs

7. Oil Red O staining

Quick ORO (qORO) was performed as described in Wahlby, C. *et.al* (Wahlby et al. 2014). Approximately 50 worms were seeded on NGM RNAi plates. Worms were washed off at the desired developmental stage by washing the plates twice with 200µl of S-basal using glass Pasteur pipettes to minimize loss of worms that might stick to the surface of plastic tips. Worms were transferred to 1.5mL tubes. After the worms settled to the bottom of the tubes, the supernatant (approx 175µl) was aspirated as much as possible without disturbing the worm pellet. The fixative was immediately added.

For fixation, 200µl of high-quality 60% isopropanol was added to worms in the 1.5mL tubes. After the worms settled to the bottom of the tubes, the supernatant was aspirated. 200µl of freshly filtered ORO working solution (60%ORO) was added. Worms were stained at 25°C in a wet chamber (wet paper towels in a parafilm-wrapped plastic box) for over 6 hrs. Then the supernatant was washed out and 250µl of 0.01% Triton X-100 in S-basal was added. Stained worms can be kept in this solution at 4°C for at least a month without altering quantities or distribution of fat.

Long ORO staining was conducted as described previously in Soukas, A. *et.al* (Soukas et al. 2009) by washing synchronized 200–300 day 1 adult animals from plates. The worms were resuspended and washed twice with PBS and then suspended in 120 µL of PBS to which an equal volume of 2× MRWB buffer containing 2% paraformaldehyde was added (composition: 160 mM KCl, 40 mM NaCl, 14 mM Na_2EGTA, 1 mM Spermidine HCl, 0.4 mM Spermine, 30 mM Na PIPES at pH 7.4, 0.2% BME). The worms were taken through three freeze–

thaw cycles between dry-ice/ethanol and warm running tap water, followed by spinning at 14,000*g*, washing once in PBS to remove PFA, resuspension in 60% isopropanol to dehydrate, and addition of 60% Oil-Red-O stain (Oil-Red-O was prepared as follows: from 0.5 g/100 mL isopropanol stock solution equilibrated for several days, freshly diluted with 40% water, 60% stock, and allowed to sit 10 min and filtered using 0.2 to 0.4 μm).

8. Nile Red staining on plate

Nile Red was dissolved in DMSO at 5 mg/ml and diluted in M9 to a final concentration of 0.02 μg/ml. This was spread on top of nematode growth media (NGM) plates seeded with HT115 (DE3) *E. coli* bacteria containing the appropriate RNAi plasmids. Synchronized eggs obtained by bleaching were allowed to develop to the desired stage at 20°C. Worms were grown continuously on Nile Red-containing plates (Artal-Sanz and Tavernarakis 2009b). Nematodes were cultured at 20°C until the young adult /day 5/10/20/25.

9. Mitotracker staining

Mitotracker Deep Red was dissolved in DMSO to make a stock solution of 1 mM, which was diluted in water to a final concentration of 100 nM and spread on top of nematode growth media (NGM) plates seeded with HT115 (DE3) *E. coli* bacteria containing the appropriate RNAi plasmids. Synchronized animals were transferred to Mitotracker plates and stained overnight 20°C (Artal-Sanz and Tavernarakis 2009b) and imaged at YA stage.

10. Iodine Staining

Synchronized day 1 adult animals were transferred to 3% agarose pads and inverted over the opening in a 100g bottle of iodine crystals (Sigma) for 30-60 secs. Worms were stained simultaneously and manipulated on the pad before imaging. This was done without a coverslip (LaMacchia et al. 2015; LaMacchia and Roth 2015; Possik et al. 2015).

11. Worm imaging

For the RNAi screen, on the day of imaging, worms were anesthetized using 10mM (Tetramisole hydrochloride (Levamisole) and bacteria was washed off using the EL406 washer dispenser, BioTek using customised protocols. In order

to acquire clear images, plates were subjected to sequential flushes of water, shaking to disaggregate the bacteria, sedimentation of the worms and aspiration of the supernatant. Each well was filled to the brim and sealed with transparent SealPlate (Sigma-Aldrich) to ensure the horizontal meniscus required to give uniform brightfield illumination across each well. The imaging was done using the INCA Analyser 2000 (GE Healthcare). We took images by utilizing the 2x objective, in three different channels – bright field, FITC/GFP and Cy3/Nile Red at identical settings and exposure times (see below). Exposure settings for imaging PHB mutant RNAi screens stained with Nile Red.

Channel	Exposure	Offset	Magnification
Brightfield	0.015	40	2x
FITC (GFP)	0.500	40	2x
Cy3 (Nile Red)	1.300	-20	2x

Segmenation of worms was done using the protocol mentioned in the results section 2.2.1, of this thesis.

Analysis of worms expressing GFP (metabolic and stress reporters) was done using the INCA Analyser 2000 (GE Healthcare) as mentioned in Hernando-Rodriguez. *et.al.* (Hernando-Rodriguez et al. 2018). We took images utilizing the 2x objective, in two different channels – bright field, FITC/GFP at identical settings and exposure times (see below).
Exposure settings for imaging transgenic worms expressing GFP

Channel	Exposure	Offset	Magnification
Brightfield	0.015	50	2x
FITC (GFP)	0.800	100	2x

For worms stained using Mitotracker Red, images were obtained using the 2x objective with the INCA Analyser 2000 (GE Healthcare), in three different channels – bright field, FITC/GFP and Cy5/Red at identical settings and exposure times (see below). Segmenation of worms was done using the protocol mentioned in the results section 2.2.1, of this thesis.
Exposure settings for imaging PHB mutant RNAi screens stained with Mitotracker Red.

Channel	Exposure	Offset	Magnification
Brightfield	0.015	40	2x
FITC (GFP)	0.500	40	2x
Cy5	1.300	-35	2x

For worms fixed with Quick Oil-Red-O, images were acquired using an Olympus Stereoscope equipped with a color camera using identical settings utilizing the bright field (1.6x objective and 2.5 zoom). For those fixed with with long Oil-Red-O, images were acquired at 10x using a Zeiss microscope equipped with a color camera using identical settings utilizing the bright field. Images were saved in .tif format. For image analysis Image J was utilized. The saved .tif images were opened and split into its RGB components. The green channel was selected and inverted, and worms were segmented and measured. The background was also segmented and measured, in order to subtract the intensity of the worm from that of the background.

For worms subjected to Nile Red and grown on plates, worms were mounted in 2-3µl of 10mM Levamisole (anesthetic) on 2% agarose pads, covered with a coverslip and images were acquired at 5x using an AxioCam MRm camera on a Zeiss ApoTome Microscope. The following exposure settings were used – bright field: 1m/s, Texas Red (Nile Red): 197m/s, and GFP: 81m/s. More than 20 worms were sampled per condition. Image analysis was performed by quantifying the average pixel intensity using the ImageJ software.

For nematodes subjected to iodine staining, animals were rapidly imaged using identical settings on an Olympus stereoscope (colour camera) utilizing the bright field (1.6x objective and 2.5 zoom). Intensity of staining over the whole body was quantified using ImageJ software.

12. Lifespan assays

All lifespans were done at 20°C. Synchronized eggs were obtained by hypochlorite treatment of adult hermaphrodites grown on OP50 plates and placed on NGM plates containing OP50 *E. coli* or seeded with HT115 (DE3) bacteria, either the pL4440 empty vector or the required RNAi construct. During the course of the lifespan, adult animals were transferred every day during their reproductive period and afterwards every alternate day. In case of balanced strains, homozygous mutants were selected at the L3 stage and transferred every alternate day. Worms were scored as dead when they stopped responding to prodding, while censored worms included exploded animals, those exhibiting bagging (internal hatching), protruding gonad or worms that dried out on the edge of the plates/crawled off the plate. Prism

(GraphPad Software) was used to plot survival curves and significant increases or decreases in lifespan were determined by using the log-rank (Mantel–Cox) test.

For lifespans that required addition of FUdR, a synchronized embryo population was allowed to grow up to young adult stage in the absence of FUdR and then transferred on NGM/RNAi plates containing 50 µM FUdR.

For lifespans done on Lithium, wild type and *daf2(e1370)* mutants were cultured at 20°C until the L4 larval stage. L4 worms were then moved to NGM plates with or without 10mM LiCl (Sigma) and scored at 20 °C. For Lithium experiments at 25 °C, wild type and daf2*(e1370)* mutants were cultured at 20 °C until the L4 larval stage. L4 worms were then moved to NGM plates with or without 10mM LiCl (Sigma) and scored at 25 °C (McColl et al. 2008).

13. Egg laying/ fertility assay

Wild-type and *daf-2 (e1370)* worms at L4 stage were placed on individual plates containing either control or *gsk-3* RNAi (10 worms per condition) at 20°C. The worms were transferred to new plates every day for 5-7 days while undergoing reproduction. Bagged or ruptured worms were censored. The progeny were left to develop for 48 hrs before counting.

14. Luciferase assay

The reporter strains PE255 (MRS186), MRS 210, MRS229 and MRS230 were utilised to measure larval developmental timing. In order to ensure all animals start development at the same time, arrested L1s were first manually pipetted to a well of a white 96-well plate (1 worm per well) containing 100 µl of S-basal with 100 µM D-Luciferin. Development was resumed by addition of 100 µl of S-basal with 20 g/L *E. coli* OP50 and 100 µM D-Luciferin.Plates were sealed with a gas-permeable cover (Breathe Easier, Diversified Biotech). Luminescence was measured in a Berthold Centro LB960 XS3 for 1 sec, at 5-min intervals. Experiments were done inside temperature-controlled incubators (Panasonic MIR-154). The raw data from the luminometer was analyzed as described in Olmedo, M. *et.al.* (Olmedo et al. 2015). Briefly, the raw data was trend-corrected and used to generate heat maps. The trend corrected data was thresholded using 75% of the moving average to produce a binarized output in order to determine onset and offset of the molt. The data was evaluated for

onset and offset of molting by detecting the transitions in the binarized data. To assess statistics, one way ANOVA was performed using GraphPad Prism software. Note- for synchronization of L1s, the bleached eggs were left overnight without food at a concentration of 20worms/µl.

15. Seahorse Measurements

Respiratory rates were analysed in live nematodes using the Seahorse XFp Analyzer (8 well plates). The evening before the actual experiment, the seahorse instrument was switched on. It is necessary to hydrate the probes prior to the experiment. For this, an unused utility plate was taken, the lid and the green sensor cartridge was removed and placed upside down so as not to scrape the probe surface. 200µl of seahorse bioscience XF calibrant (pH7.4) was added into the wells of the utility plate. 400µl of the same on the sides of the wells in the plate. The sensor cartridge was placed back into the utility plate so probes dip into the wells. The lid was placed back and the cartridge was incubated overnight at 20°C.

The next day, *C. elegans* growing on the respective NGM RNAi plates were transferred to plates without food (2x) to remove bacteria. In the meantime, 25µM oligomycin, 50µM FCCP and 40 µM sodium azide were pipetted into the appropriate injection ports of the hydrated utility plate with the sensor cartridge and calibrated on the seahorse instrument (Port A - 20µl of 250µM Oligomycin, Port B - 22µl of 500µM FCCP, Port C- 25µl of 400µM Sodium Azide). EPA water (Luz et al. 2015)(60mg $MgSO_4$, $7H_2O$, 60mg $CaSO_4$.$2H_2O$, 4mg KCl, ddH_2O to 1L. Filtered in sterile conditions) was added to the seahorse cell culture microplate – 180µl within the wells and 400µl on the sides. Next, nematodes were picked to unbuffered EPA into an 8 well Seahorse microplate. 8 oxygen consumption measurements were taken for determination of basal OCR. After this, drugs were injected - 9, 8 and 4 cycles of measurements were taken after addition of oligomycin, FCCP and sodium azide. Each cycle is – 3min mix - wait for 30 secs -measured for 3 min.

All experiments were performed with synchronized YA animals and day 5 old adult animals. Animals in control or *gsk-3* RNAi were mounted side by side in the plate and on the same day. All drug stocks (10mM FCCP, 5mM Oligomycin) were made in EtOH. 1M sodium azide was in distilled water.

16. Pharyngeal pumping

Synchronized worms were placed on nematode growth media plates without food for 15 mins or so prior to counting pharyngeal pumping. Pumps per minute (ppm) were recorded for 1min under a regular stereomicroscope. At least 10 worms per condition were analyzed. Worms were analyzed for day 1 and day 5 of adulthood.

17. Mitochondrial Fractionation

L1 larvae were obtained by hypochlorite treatment from liquid cultures of worms of desired genotype fed with HT115 (DE3) *E. coli* bacteria with the appropriate RNAi plasmid constructs. These were grown in the respective RNAi conditions on RNAi NGM plates (600µl bacteria/plate). Approximately 40,000 (1000L1s/plate) worms were harvested at young adult (YA) stage. Worms were washed six times (3x with S Basal, 2x with double distilled water and 1x with MS-grade water, pelleted after each washing step by centrifugation at 800 ×g for 1 min at 20 °C and the final worm pellet was snap-frozen in liquid nitrogen and stored in the −80 °C freezer until further use.

Mitochondrial fractionation was carried out as per (Grad et al. 2007) by Dr. A B Lourenço. Instead of a Bead-Beater, a Polytron was used. The worms (in worm lysis buffer with protease inhibitor cocktail) were added to the chamber, and the chamber was filled to the top with cold worm lysis buffer. The rotor assembly was lowered into the chamber, displacing a small amount of liquid. All air should be excluded during the operation of the Polytron. The assembled chamber was surrounded with ice. Grinding/sonication was done at three pulses of 1 min each interspersed with 1-min intervals to allow for heat dissipation. A small aliquot of the supernatant was examined to assess the extent of breakage. The supernatant was recovered and homogenized by hand in a glass-Teflon homogenizer for 30 secs. Recovery was increased by rinsing the glass beads in worm lysis buffer and pooling the supernatants. The lysate was centrifuged at 2500g for 10 min at 4°C to pellet debris. The supernatant was centrifuged at 15,000g for 10 min at 4°C. The pellet was re-suspended in cold worm lysis buffer and centrifuged again at 15,000g for 30 min at 4°C. The pellet was re-suspended in a small volume of worm lysis buffer and homogenized briefly in a glass-Teflon homogenizer. The crude mitochondria

were aliquoted into micro centrifuge tubes, frozen in liquid N2, and stored at -80°C.

18. CRISPR-Cas9 tagging of GSK-3, Sap Trap cloning

For endogenous tagging of GSK-3, we utilised the CRISPR-Cas9 SapTrap technique by Schwartz et.al (Schwartz and Jorgensen 2016).

<u>Oligo Design for SapTrap Vectors</u>

First, an insertion site was identified (For N terminal tags, the tag should be inserted immediately after the start codon) (Figure 55A). 60 bases were acquired on each side of the DNA sequence flanking insertion site, and genomic sequence of the sgRNA binding site was checked to ensure that it does not contain a SapI recognition site.

Next, candidate sgRNA binding sites were identified. The selected sgRNA binding site should cut within 25 bases of the desired insertion site and it should be ensured that the repair template cannot be targeted by the selected sgRNA. Ideally, an sgRNA binding site should be selected that straddles the insertion site. sgRNA specificity was evaluated and selected using the Zhang lab's sgRNA design tool at http://crispr.mit.edu/.

To design Oligos (Figure 55),

a) Necessary mutations were introduced to the genomic sequence file, including PAM site or sgRNA binding site mutations required to immunize the repair template against the sgRNA. For *gsk-3*, we disrupted the PAM sequence with a silent G to C mutation to avoid re-cutting after repair (Figure 55B). b) To design 5' homology arm oligos, 57 bases immediately preceding the insertion site were selected. The "top" oligo is "TGG" followed by this 57 base sequence. The "bottom" oligo is "CAT" (N-terminal tag) followed by the reverse complement of the 57 base homology arm sequence. c) To design 3' homology arm oligos, 57 bases immediately following the insertion site were selected. The "top" oligo is "ACG" (N-terminal tag) followed by this 57 base sequence. The "bottom" oligo is "TAC" followed by the reverse complement of the 57 base homology arm sequence. d) sgRNA oligos were designed by copying the 20 bases immediately preceding the "NGG" PAM sequence. The "top" oligo is "TTG" followed by this 20 base

sequence. The "bottom" oligo is "AAC" followed by the reverse complement of the 20 base sequence. The PAM sequence was not included in the sgRNA construct.

Verifying the oligo sequences. It should be ensured that the oligo pairs will anneal to produce a product of 57 base-pairs flanked by the correct 3-base 5'-overhangs on each end (Figure 55B). Oligos will assemble with connector segments and tag segments from the SapTrap donor plasmid library to generate the desired repair templates (Figure 55C).

List of oligos for N-terminal tagging

MRS215	N TER sg RNA Top 5´-3	TTG –aatcaaatcaatcagtagtg
MRS216	N TER sg RNA Bottom 5´-3	AAC – cactactgattgatttgatt
MRS217	N TER 5´HA Top 5´-3	TGG-agagctcatatatacacacacacacacaagaatcaaatcaatcagtagtgtcgtgtg
MRS218	N TER 5´HA Bottom 5´-3	CAT –acacgacactactgattgatttgattcttgtgtgtgtgtgtgtatatatgagctct
MRS219	N TER 3´HA Top 5´-3	ACG-AATAAGCAGTTACTATCGTGCTCGCTGAAAAGCGGAAAACAAGTGACGATGGTCGTC
MRS220	N TER 3´HA Bottom 5´-3	TAC-GACGACCATCGTCACTTGTTTTCCGCTTTTCAGCGAGCACGATAGTAACTGCTTATT

Buffers and Reagents

10x Oligo Annealing Buffer (OAB) - 200 mM Tris-Cl pH 7.5, 500 mM NaCl,10 mM $MgCl_2$
SapTrap Donor and Destination Plasmids - all plasmid preps were diluted to 50 nM
SapTrap Enzyme Mix - prepared in advance and stored at -80°C in 2 µl aliquots.
Restriction enzymes for counter-selection of unreacted destination vector

Figure 55: Oligo Design for SapTrap Vectors **A.** *gsk-3* N-terminal insertion site. The native genomic sequence is shown for the desired insertion site flanked by 65 bases on each side. **B.** Oligo design. The same genomic region depicted in A is shown with theaddition of a PAM- site disrupting mutation for the selected sgRNA. The sequences used to generate the homology arm

and sgRNA oligos are marked. **C.** Sequence of the repair template generated from the oligos depicted in B.

<u>Anneal oligos</u>

Oligo stocks were resuspended to 100µM in water. Complementary oligo pairs were mixed to a final concentration of 10 µM each in 100 µl of 1x OAB. Oligo mixtures were heated to >95°C in a heat block and incubated for 2.5 mins. The heat block was turned off and the block was allowed to cool slowly to room temperature. The 10 µM annealed oligo stocks can be stored at -20°C for future use or diluted and used immediately. The annealed oligos were diluted in water to 150 nM. All 3 annealed oligo pairs for a given reaction were diluted in a single aliquot of water such that the final solution contained 150 nM of each of the 3 annealed oligo species.

<u>SapTrap Assembly</u>

The following were combined and mixed thoroughly by pipetting:

1 µl of 50nM Destination Vector   -pMLS256 (Dr.Askjaer's Lab 1491)
1 µl of 50nM connector vector   -pMLS288 (Dr.Askjaer's Lab 1511)
1 µl of 50nM tag and marker plasmid   - pBN312   (Dr.Askjaer's Lab 1519)
1 µl of annealed, diluted oligo mixture (150nM each oligo species)
1 µl of dH2O

A 2 µl aliquot of SapTrap Enzyme Mix (10x Cutsmart buffer, H_2O, 10 mM ATP, 1 M DTT, 400U/ µl T4DNA ligase, 10U/ µl T4 polynucleotide kinase, 10 U/ µl SapI) was thawed. To this, 0.5 µl of the above DNA mix was added and mixed thoroughly by pipetting up and down using a 2 µl pipette. The reaction was incubated at 25°C overnight. The following day, the T4 DNA ligase was heat inactivated by incubation at 65°C for 30 mins.

A solution of 1x Cutsmart buffer +1–2U/ µl of BamHI restriction enzyme was prepared (BamHI is an appropriate counter-selection restriction enzyme, as this does not cut the desired final product). 2.5 µl of the 1x Cutsmart + enzyme solution was added to the 2.5 µl SapTrap reaction and mixed. This was incubated at 37°C for 1 hr.

Transformation was performed using DH5α cells. To 50 µl of DH5α cells, 2 µl of the above Saptrap reaction solution was added. This was incubated for 20 mins on ice, and then at 42°C for 1 min. 250 µl of LB was added to the 52 µl reaction

mix and incubated at 37°C (shaking) for 30 mins. Approximately 150 µl of the solution was plated onto an LB plate supplemented with Ampicillin and grown at 37°C overnight. The next day, individual colonies were selected and inoculated. Plasmids were mini-prepped and sent for sequencing with M13F, M13R and oMLS471.

M13F (MRS 94): 5' –TGTAAAACGACGGCCAGT
M13R (MRS 95): 5' –CAGGAAACAGCTATGACCATG
oMLS471 (Dr.Askjaer's Lab 975)   :5'–TCCAAGAACTCGTACAAAAATGCTC

Injection and Isolation

unc-119(ed3) worms were cultured at 15°C on OP50 bacteria. L4 worms were picked the night prior to the injections and transferred to a fresh OP50 NGM plate. 30-40 animals were injected with the following injection mix (see table), animals were kept on individual plates and incubated at 25°C for 7-10 days. Plates were screened post 7 days to identify motile (*unc-119(+)*) animals that lacked the co-injection markers.

Insertion injection mix recipe

Component	Concentration	Comments
Combined repair template and sgRNA Expression vector	65ng/ µl	Nter5- confirmed through sequencing
Cas 9 Expression vector	25ng/ µl	Dr.Askjaer's Lab
Fluorescent co-injection markers	17.5ng/ µl	868 - pGH8- Plmn-1::mCherry::his-58 (neuronal red fluorescence)(10ng/ µl) 885 - pCFJ104 – Pmyo-3::mCherry (body wall muscle red fluorescence) (5 ng/ µl) 879 - pCJ90 - Pmyo-2::mCherry (pharyngeal muscle red fluorescence) (2.5ng/ µl)
Total	107.5 ng/ µl	-

Removing the Cbr-unc-119 marker

Worms selected from the above step have successful incorporation of the repair template containing the homology arms flanking the cleavage site and a genetic tag with a removable Cbr-unc-119 marker gene embedded in the intron. Insertions are selected by rescue of the Unc phenotype. The Cbr-unc-

119 can be excised by Cre recombinase- mediated site specific recombination, leaving a single LoxP site. For this purpose, homozygous young adult animals were injected with the following injection mix (see table). Array(+) F1 animals were selected. 5-10 array (+) worms were placed on up to 4 OP50 NGM plates. The F2 was screened and *unc-119(-)* animals were selected. The resultant strain was out crossed against the wild type to remove the *ed3* allele (This portion as done by Dr. FJ Garcia).

Removal of the Cbr-unc-119 marker - injection mix recipe

Component	Concentration	Comments
Cre expression plasmid	50ng/ µl	Dr.Askjaer's Lab -1493- pMLS328
Stuffer DNA	32.5 ng/ µl	Dr.Askjaer's Lab – 1478-pBN287
Fluorescent co-injection markers	17.5ng/ µl	868 - pGH8- Plmn-1::mCherry::his-58 (neuronal red fluorescence)(10ng/ µl) 885 - pCFJ104 – Pmyo-3::mCherry (body wall muscle red fluorescence) (5 ng/ µl) 879 - pCJ90 - Pmyo-2::mCherry (pharyngeal muscle red fluorescence) (2.5ng/ µl)
Total	100 ng/ µl	-

19. Quantitative RT-PCR

Total RNA was isolated from approximately 1500 synchronized wild type and *daf-2 (e1370)* mutants at the young adult stage grown on control and *gsk-3* RNAi. After harvest, the animals were flash frozen in liquid nitrogen. RNA was extracted based on a protocol modified from "easy RNA isolation from *C. elegans* : A TRIZOL based method" (Worm Breeder's Gazette 14:10). cDNA was prepared using INVITROGEN DNAse KIT reagents. Reverse transcription (1 µg per sample) was performed using Multiscribe reverse transcriptase and random 9-mer primers (Applied Biosystems). Quantitative PCR was performed using SYBR Green (Applied Biosystems) Master Mix in a CFX Connect Real Time System, Biorad at an annealing temperature of 60°C and 40 cycles. Relative gene expression, normalized to *pmp-3* and *cdc-42*, was determined between worms treated with control RNAi and *gsk-3* RNAi. Primers of target genes can be found in Table 7. Statistical difference was calculated with Student's t-test (Excel).

20. Western Blots

A synchronised population of worms was grown at 20°C until they reached the young adult stage. Worms were transferred to NGM plates without food and allowed to crawl for half an hour in order to remove excess of bacteria. 60 worms were collected in 10µl of M9 and flash frozen in liquid N2 and stored at -80°C. We added the same volume of sample buffer containing Ditiotreitol (DTT) and 2x LB (100mM Tris-HClph 6.8, 4% SDS, 0.005% Bromophenol Blue, 20% Glycerol), vortexed, heated the sample for 3 min and vortexed again. All samples were centrifuged before loading. 16 µl of each sample was run in a 4-20% pre-cast gradient gel (Mini-protean TGX Stain Free Precast gel, Biorad). Following electrophoresis, proteins were transferred to a PVDF membrane (Trans Blot turbo mini PVDF transfer pack Biorad) using a wet Trans-Blot system (Bio-Rad). The immunoblots were visualized by chemiluminescent detection (Molecular imager ChemiDoc XRS+ with image lab software Biorad). Independent assays repeated three times. The chemiluminescent signals were quantified using the software ImageLab (Bio-Rad) and normalized to actin signal levels. We incubated western blots with phospho-AMPKα Thr 172 (Santa Cruz Biotevhnology), diluted 1:300 (McQuary et al. 2016) and anti-actin (ICN, clone C4) diluted 1:1000. The data are represented as relative values normalized to the respective control.

Appendix 1

A1.1 Effect of FUdR on lifespan of wild type, IIS and mitochondrial mutants

As we were working with four different genetic backgrounds, we reasoned we could reduce the laborious task of transferring worms during the course of their egg laying period during lifespan assays by addition of FUdR (5-Fluoro-2'-deoxyuridine).FUdR supplementation helps to limit production and development of progeny by inhibiting DNA synthesis. It would also help to reduce the number of worms lost during egg laying due to internal hatching. While addition of FUdR to wild type animals has not been shown to affect their lifespan, there have been conflicting reports that FUdR has no effect on lifespan or can extend lifespan in certain mutants (Aitlhadj and Sturzenbaum 2010; Van Raamsdonk and Hekimi 2011; Rooney et al. 2014). Moreover, it can alter metabolic profiles in worms (Davies et al. 2012).

We observed a significant shift in the mean lifespans of wild type , *daf-2* and mitochondrial PHB mutants - a decrease in *daf-2* and *phb-2;daf-2* mutants and a increase in wild type and *phb-2* mutants (Figure A1.1, Table 6). The opposing phenotype of PHB depletion was still retained on FUdR, i.e, *phb-2(tm2998)* is short-lived and *phb-2(tm2998);daf-2(e1370)* mutants exhibited increased lifespan.
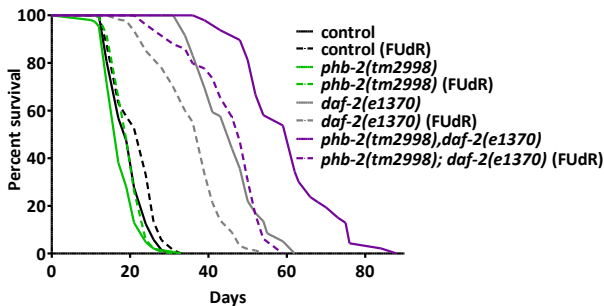
Figure A1.1: Lifespan analysis with and without FUdR. Wild type, *daf-2*, *phb-2* and *phb-2; daf-2* mutants were grown on HT115 (DE3) bacteria containing the empty vector pL4440. Curves represent one lifespan assay.

A1.2 *mtk-1 (*MTK-1/ MEKK-4 homolog)

While depletion of MTK-1 has been observed to induce the UPR[mt] and P*gst-4* ::GFP in the mitochondrial PHB mutants (data not shown), we observed that Nile Red staining is increased in the same upon *mtk-1(RNAi)*. *mtk-1* shares homology with yeast SSK2, a member of the MAP kinase kinase kinase family

of the HOG1 mitogen-activated signalling pathway known to regulate glycerol synthesis, osmoregulation and stress response genes (Gustin et al. 1998).
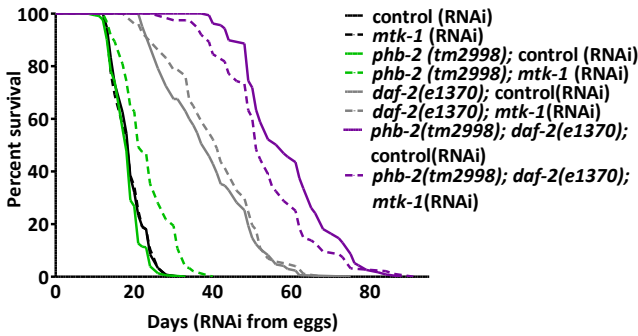
Figure A1.2: Lifespan analysis of wild type, *daf-2*, *phb-2* and *phb-2; daf-2* mutants subjected to *mtk-1 (RNAi)*. Average of two independent lifespan curves has been represented here.

mtk-1(RNAi) increased lifespan of the *phb-2 (tm2998)* mutants while it shortened the lifespan of the *phb-2(tm2998);daf-2(e1370)* mutants (Figure A1.2, Table 6). Wild type and *daf-2(e1370)* mutants were not affected upon loss of MTK-1. In order to further investigate this opposing effect upon *mtk-1(RNAi)*, we have performed a lipidomics study focussed on mitochondrial lipid alterations. Mitochondria are essential for organismal metabolism and physiology and it has been shown that composition of mitochondrial membrane lipids can influence the ageing process in yeast and in nematodes (Hulbert 2010; Valencak and Azzu 2014; Medkour et al. 2017; Nielson and Rutter 2018). Incidentally, *mtk-1(RNAi)* also induces UPR[mt] in both *phb-2* and *phb-2;daf-2* mutants. A recent worm paper observed that mitochondrial UPR might delay ageing in worms via global remodeling of lipid metabolism that includes increase in cardiolipins and fatty acids (Kim et al. 2016).

A1.3 S6 kinase/RSKS-1

Inhibition of RSKS-1(S6K), a key molecule in the target of rapamycin (TOR) pathway is known to extend lifespan in multiple species, including the worm (Laplante and Sabatini 2012). *daf-2(e1370);rsks-1 (ok1255)* double mutants also exhibit increased lifespan which requires DAF-16 (Chen et al. 2013). Also, the deficiency of PHB-2 in an *rsks-1(ok1255)* mutant leads to an extension in longevity (Schleit et al. 2013). Hence, we wanted to examine the effect of RSKS-1 depletion in *phb-2;daf-2* mutants.

We were only able to recapitulate the increase in longevity in *phb-2* mutants upon depletion of RSKS-1(Figure A1.3, A). Though we noticed a mild increase when *daf-2* mutants were subjected to *rsks-1(RNAi)*, but did not observe an increase in wild type animals when RSKS-1 is depleted, in stark contrast to the published extension (Chen et al. 2013; Schleit et al. 2013). We were unable to conclude the behaviour of *phb-2;daf-2* mutants upon *rsks-1(RNAi)* due to low "n"numbers, although a tendency to decrease was observed .

A
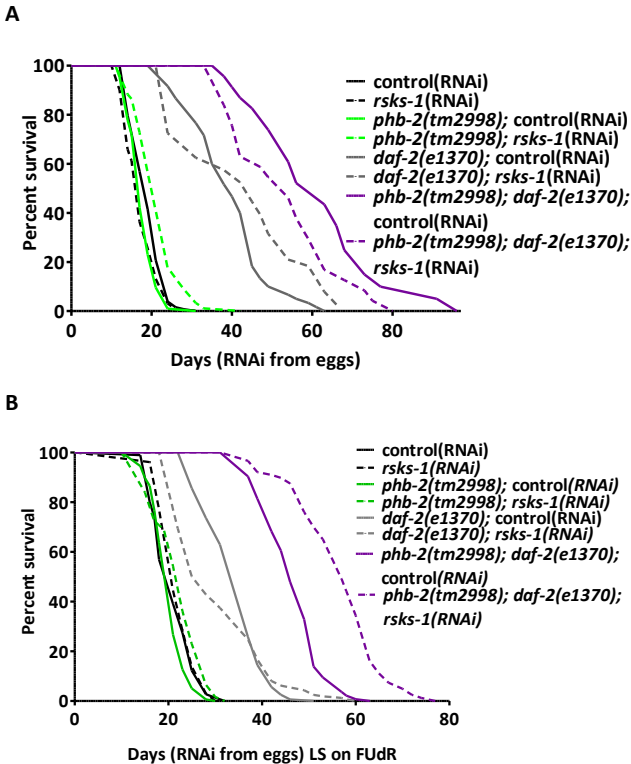
Figure A1.3: RSKS-1 depletion leads to increased longevity in *phb-2* mutants. Lifespan analysis of wild type, *daf-2, phb-2, phb-2; daf-2* subjected to *rsks-1 (RNAi)* **A**. without FUdR **B.**Upon addition of FUdR. Curves representative of one lifespan assay

B

The published extension of lifespan upon loss of RSKS-1 in wild type, IIS and PHB defective backgrounds was carried out in the presence of FUdR. Therefore, we assayed the effect of *rsks-1(RNAi)* in all genetic backgrounds in the presence of FUdR (Figure A1.3, B). While we were able to again recapitulate the extension seen upon PHB depletion, wild type worms remained unaffected. IIS mutants showed a mild decrease upon depletion of RSKS-1 in the presence of FUdR going against earlier published data using *daf-2 (e1370);rsks-1(ok1255)* double mutants (Chen et al. 2013). The mitochondrial

mutants, *phb-2 (tm2998); daf-2(e1370)* were observed to have an increase in lifespan upon *rsks-1(RNAi)*.

A1.4 KIN-1

kin-1 encodes multiple isoforms of a serine/threonine protein kinase that is orthologous to cAMP-dependent protein kinase (protein kinase A or PKA) catalytic subunits. They are involvedin several processes including lipid metabolism (Lee et al. 2014; Lee et al. 2016). Absence of *kin-1* has been shown to increase Oil-red-O staining, implying high triglycerides (Lee et al. 2014). The PKA pathway is well conserved and suppression of PKA in worms results in deleterious phenotypes - short lifespan, decreased egg laying, and reduced locomotion. *kin-1* is highly expressed in muscles, head and gonads (Lee et al. 2016). PKA signalling is important for oocyte maturation (Kim et al. 2012).

We found that despite starting the RNAi treatment at the L3/L4 stage, all genetic backgrounds depleted of *kin-1* exhibited strong vulval rupturing leading to a premature death of almost the whole experimental population, especially in the case of wild type and *daf-2(e1370)* mutants (Table 6). The *phb-2* mutants salvaged after the vulval bursting phenotype in *kin-1* RNAi lived an even more reduced lifespan (Figure A1.4), whereas, the long lived *phb-2;daf-2* mutants showed a sharp decline in lifespan.
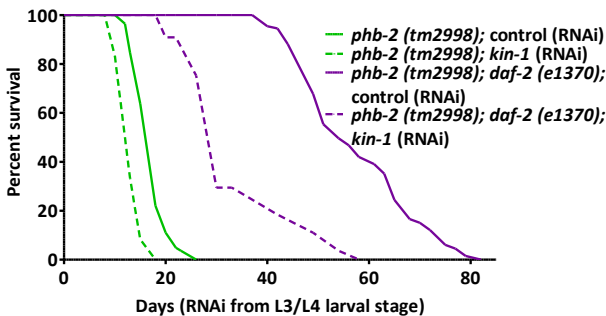
Figure A1.4: Lifespan analysis of PHB mutants, *phb-2* and *phb-2; daf-2*, subjected to *kin-1(RNAi)*. Curves represent one lifespan assay.

Recently, a role has been established for PKA pathway as a contributor to innate immunity in worms by signalling from the nervous system to periphery tissues to protect the host against pathogens (Xiao et al. 2017). This is of interest as exposure to the pathogen *Pseudomonas aeruginosa* causes mitochondrial dysfunction and activation of the UPR[mt] detects these

pathogens and initiates a protective innate immune response (Pellegrino et al. 2014).

A1.5 Y50D7A.3

Y50D7A.3 is orthologous to the human Phosphorylase Kinase Gamma-2 (PHKG2). Human PHKG2 phosphorylates and activates glycogen phosphorylase, which leads to the breakdown of glycogen. Mutations in PHKG2 are linked to cirrhosis and Glycogen storage disease. Not much is known about this gene in the nematode. Enzymes such as trehalose-6-phosphate synthase genes, related to carbohydrate metabolism have been known to modulate lifespan (Honda et al. 2010) in *C. elegans,* and we observed earlier that the kinase, GSK-3 known to phosphorylate and inhibit glycogen synthase also regulates lifespan. Hence, we investigated whether loss of this kinase could alter lifespan. However, we found that depletion of this kinase did not cause an alteration in lifespan (Figure A1.5, Table 6) in any of the genetic backgrounds.
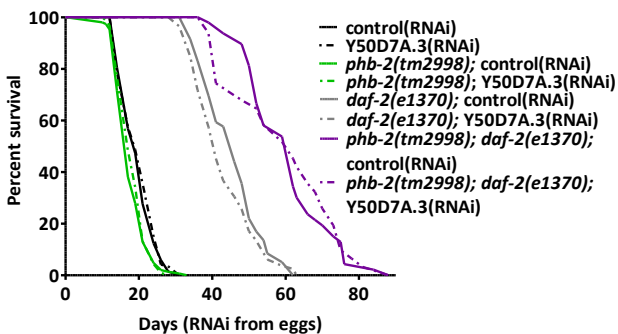
Figure A1.5: Lifespan analysis of wild type, *daf-2* and *phb-2, phb-2; daf-2* subjected to Y50D7A.3 *(RNAi).*One of two independent experiments is shown.

Appendix 2

A2.1 <u>Wild type, daf-2(e1370) and mitochondrial mutants – *phb-2(tm2998)* and *phb-2(tm2998);daf-2(e1370)* subjected to *gsk-3(RNAi)* in presence of 5-Fluoro-2'-deoxyuridine (FUdR)</u>

We observed that the reduction in lifespans across wild type, *daf-2(e1370)* and the mitochondrial PHB mutants upon GSK-3 depletion was unchanged upon FUdR addition (Figure A2.1, Table 4).
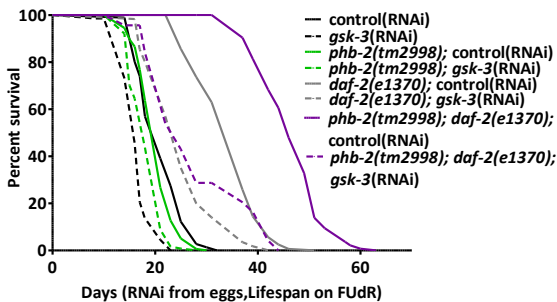
Figure A2.1: Survival curves of GSK-3 depleted worms in the presence of FUdR.

A2.2 <u>Inhibition of GSK-3 using Lithium</u>

Previously, it has been established that Lithium affects diverse biological processes, ranging from developmental effects to metabolic alterations. A known molecular target of lithium is GSK-3, and it has been suggested that lithium acts through inhibition of GSK-3 (Ryves and Harwood 2001; De Sarno et al. 2002). Hence, we investigated whether inhibiting GSK-3 through lithium addition in worms would reduce lifespans in a similar manner as *gsk-3(RNAi)* (Figure A2.2,A, Table 4). In accordance with our experiments with *gsk-3(RNAi)*, we observed reduced lifespan in wild type and IIS defective *daf-2(e1370)* mutants upon addition of Lithium Chloride.

However, previous work showed that exposure to lithium increased lifespan in worms, flies and humans (McColl et al. 2008; Zarse et al. 2011; Castillo-Quan et al. 2016). In particular, wild type and *daf-2(e1368)* mutants have been shown to have an increased lifespan in presence of LiCl (McColl et al. 2008). A key difference in how these experiments were performed is with respect to the temperature. McColl et al, performed experiments by moving L4 worms grown at 20°C on to NGM plates with LiCl and assayed at 25°C, as opposed to us that kept worms constantly at 20°C. However, further experiments would be

required to ascertain if indeed increased temperature is the cause for these differences, though we did see a tendency to increase lifespan at 25°C in wild type worms subjected to LiCl (Figure A2.2, B).
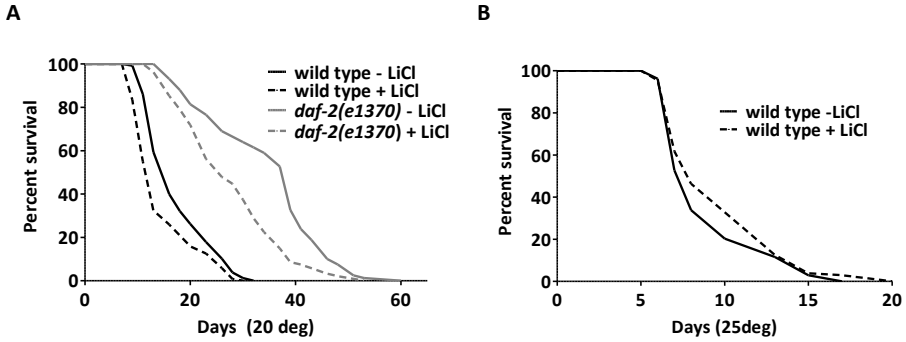
Figure A2.2: Effect of LiCl on the lifespan of wild type and *daf-2(e1370)* mutants. Survival curves of nematode populations at **A.** 20°C and at **B.** 25°C, exposed to 10 mM LiCl.

Appendix 3 - Analysis of additional metabolic genes upon depletion of GSK-3

A3.1 Increased expression of P*acdh-1*::GFP in worms with low glycogen stores.

In order to ascertain whether the P*acdh-1*::GFP reporter is capable of reflecting changes in fatty acid oxidation, we subjected wild type and *daf-2* mutants to *gsy-1(RNAi)*. Knockdown of glycogen synthase (*gsy-1*) reduces glycogen content in *C. elegans* (Frazier and Roth 2009; LaMacchia et al. 2015) , both in wild type and *daf-2* mutants (Figure A3.1,A). Knockdown of GSY-1 led to a strong induction of *Pacdh-1*::GFP in both wild type and IIS mutants (Figure A3.1,B)

A

B
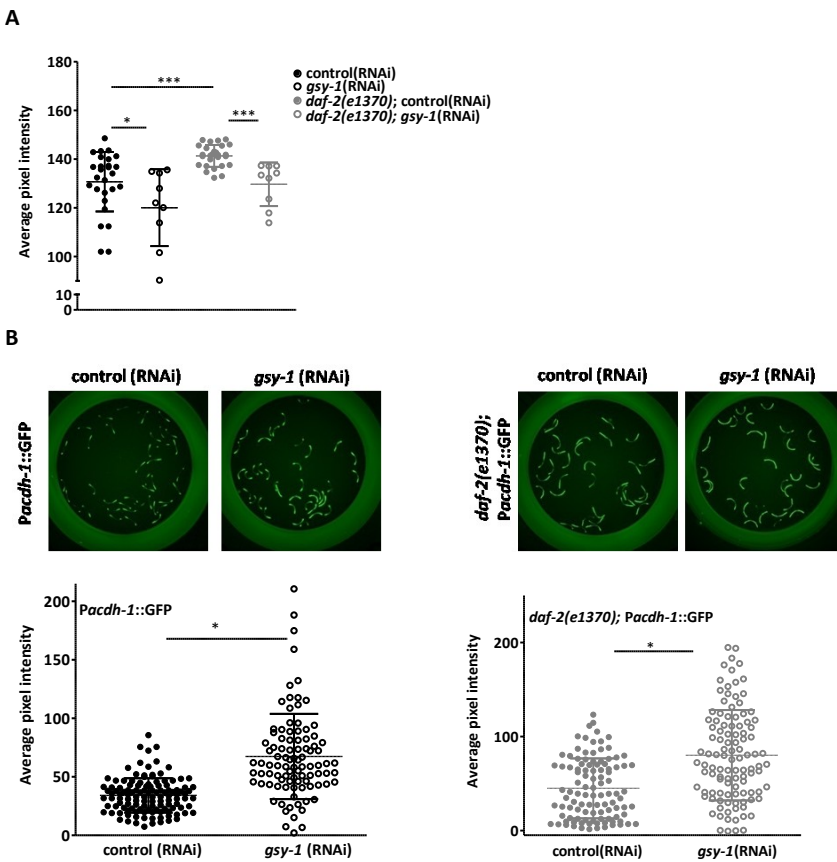
Figure A3.1: Worms with lower reserves of glycogen stores show increased short chain fatty acid oxidation **A**.Scatter plot representing quantification of glycogen stores in wild type and *daf-2* mutants depleted of GSY-1 viewed using iodine vapor staining (Mean±SD, Unpaired t- test, * = p<0.05,*** = p< 0.001, n ≥ 9 worms for all conditions) **B.**Expression of P*acdh-1*::GFP in wild type

and *daf-2* mutants upon *gsy-1(RNAi)* (top panel) and scatter plot representing quantification of P*acdh-1*::GFP levels of the respective images (bottom panel) (Mean±SD, One way ANOVA, Dunn's multiple comparison test,* = p<0.05) (Animals were imaged at Day1 of adulthood in all conditions in both **A** and **B**)

A3.2 <u>Short- and medium- chain dehydrogenases</u>

We assessed expression of an additional mitochondrial short chain acyl-CoA dehydrogenase, *acdh-2*, also predicted to catalyse the first step of β-fatty acid oxidation (MacNeil et al. 2013). We observed a repression in P*acdh-2*::GFP (similar to P*acdh-1*::GFP (Figure 46,A-B)), upon *gsk-3(RNAi)* and PHB depletion in wild type animals (Figure A3.2,A).
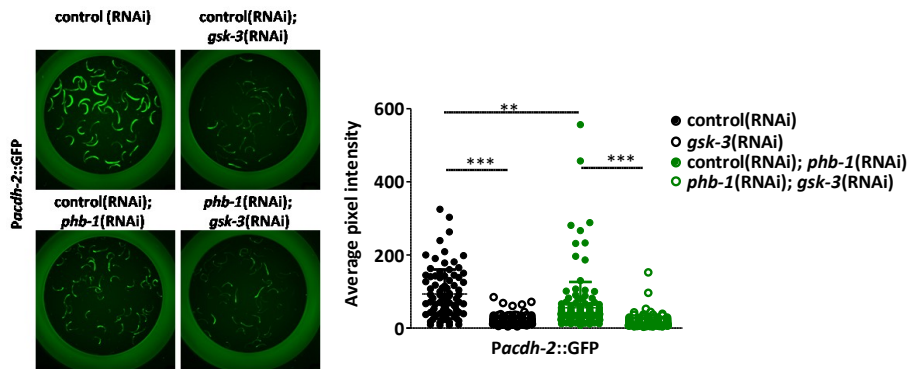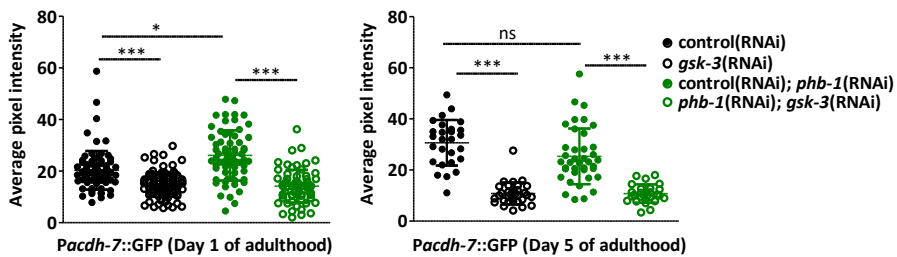
Figure A3.2: Reduced expression of *acdh-2* and *acdh-7* upon *gsk-3(RNAi)*. **A.** P*acdh-2*::GFP gene expression in otherwise wild type and PHB depleted worms grown on *gsk-3(RNAi)* versus control *(RNAi)* (left panel). Scatter plot (right panel) represents the quantification (Animals imaged at Day1 in all conditions, Mean±SD, One way ANOVA, Dunn's multiple comparison test, **=p<0.01, *** = p< 0.001, n≥86, one of two independent experiments represented).**B.** Scatter plots depicting the expression of P*acdh-7*::GFP on Day 1 (left panel, n≥64, one of two independent experiments) and Day 5 (right panel, n≥25) of adulthood upon loss of GSK-3 in otherwise wild

type and PHB depleted animals (Mean±SD, One way ANOVA, Dunn's multiple comparison test, ns = not significant, *=p<0.05, *** = p< 0.001)

Additionally, *acdh-7,* the nematode homolog of medium-chain acyl-CoA dehydrogenase as observed by P*acdh-7*::GFP (Figure A3.2, left panel) was also reduced in both wild type and PHB depleted worms grown on *gsk-3(RNAi)*. Interestingly, PHB depleted animals showed a mild increase in expression. During ageing (Figure 3.2, right panel), expression of *acdh-7* increased in wild type animals with no significant alterations in PHB depleted worms, but remained repressed in wild type and PHB depleted worms grown on *gsk-3(RNAi)*.

A3.3 Short- and long- chain acyl CoA synthetases

Lipid metabolism involves lipases that breakdown triglycerides to free fatty acids. These are then activated by acyl-CoA synthetases to their acyl-CoA derivates which are then oxidised in the mitochondria by acyl CoA dehydrogenases or the peroxisomes by acyl CoA oxidases (Watkins and Ellis 2012; Watts and Ristow 2017). As we observed reduction in expression of the acyl CoA dehydrogenases, *acdh-1/-2/-7*, we investigated whether acyl CoA synthatases are also downregulated. Consistent with our observation of decreased expression of short chain dehydrogenases, *acdh-1* and *-2* in PHB depleted worms and also upon *gsk-3* depletion, we observed that these worms also exhibited low expression of ACS-19 (an ortholog of human ACSS2 (acyl-CoA synthetase short-chain family member 2) (Figure A3.3, A-B, further indicating reduced fatty acid oxidation.

Similarly, P*acs*-13::GFP expression analysis (Figure A3.3, C) revealed that lackof GSK-3, both in wildtype and PHB depleted worms, results in low expression of the reporter. *acs-13* encodes an ortholog of human ACSL5 (acyl-CoA synthetase long-chain family member 5).Interestingly, PHB depleted animals were unaffected. These results indicate that while GSK-3 depletion reduces expression of both short and long-chain acyl CoA synthethases (Figure 46, A3.2, A3.3), PHB depletion only affects short chain acyl CoA synthethases and dehydrogenases.

A
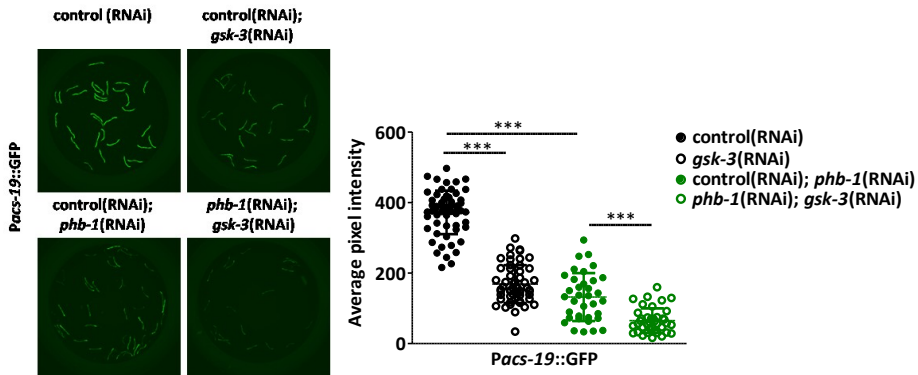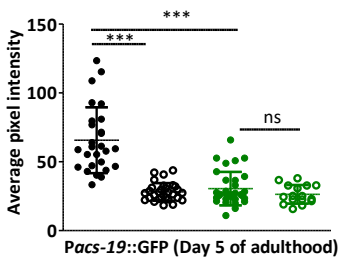
B   **C**
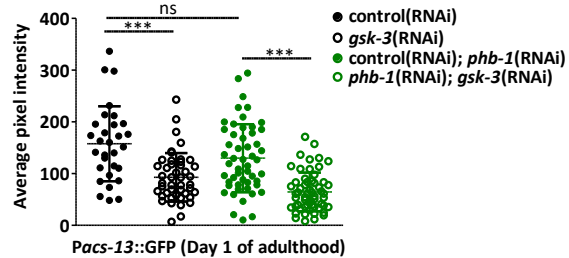
Figure A3.3: Expression of acyl CoA synthatases, *acs-19* and *acs-13*. **A.** Representative images of *acs-19* gene expression upon PHB and GSK-3 depletion (left panel) and quantification (right panel) at Day1 of adulthood (Mean±SD, One way ANOVA, Bonferroni's multiple comparison test, *** = p< 0.001, n≥35, one of three independent experiments represented). **B – C.** Scatter plot of P*acs-19* ::GFP expression on Day 5 (n≥16) and P*acs-13*::GFP expression on Day1 upon PHB and GSK-3 depletion (n≥30, one of two independent experiments represented) (Mean±SD, One way ANOVA, Dunn's multiple comparison test, ns = not significant, *** = p< 0.001)

A3.4 Carnitine palmitoyltransferase, *cpt-2*

Short-chain fatty acids are able to freely translocate between the cytosol and mitochondria, whereas medium- or long- chain fatty acids require the function of carnitine palmitoyltransferases, such as CPT-2 (Watts 2009; Yuan et al. 2012). Consistent with our observation of decreased medium-chain fatty acid degradation upon GSK-3 depletion, we observed decreased *Pcpt-2*::GFP expression (Figure A3.4), implying low import of medium-/long-chain fatty acids into the mitochondria. However, PHB depleted worms do not exhibit any changes in P*cpt-2*::GFP expression compared to wild type. This is consistent

with the fact that medium chain dehydrogenase *acdh-7* and long chain acyl CoA synthethase, *acs-13,* are not affected upon PHB depletion (Figure A3.2,B and A3.3,C)
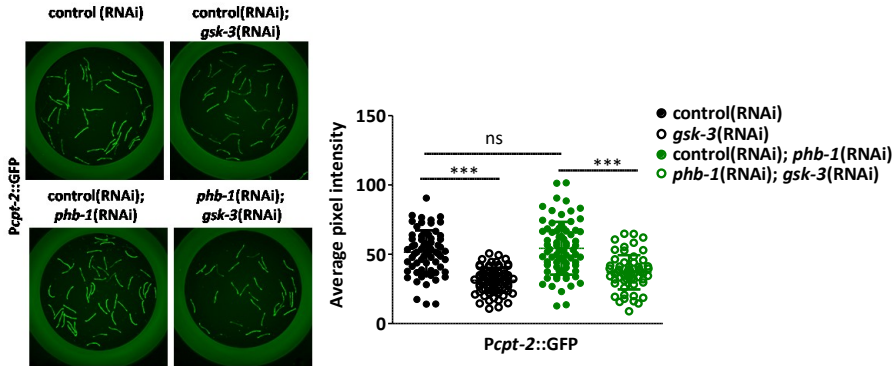
Figure A3.4: Expression of the carnitine palmitoyltransferase reporter, P*cpt-2*::GFP. Representative images are shown for wild type worms upon GSK-3 and PHB depletion (left panel) and the scatter plot (right panel) represents GFP quantification (Worms were imaged at Day1 of adulthood, Mean±SD, One way ANOVA, Dunn's multiple comparison test, *** = p< 0.001, ns=not significant,n≥61, one of two independent experiments has been represented).

A3.5 *de novo* fat synthesis

About 7–20% of *C. elegans* fatty acids are synthesized *de novo* from acetyl-CoA, with the exception of the monomethyl fatty acids, which are synthesized when worms feed on *E. coli* OP50 (Perez and Van Gilst 2008). The remaining are incorporated or modified from diet. The *de novo* synthesis of fatty acyl chains using the two carbon subunit acetyl-CoA is achieved by the activity of fatty acid synthase (FAS), encoded by *fasn-1*. The rate-limiting step of de novo fatty acid synthesis is the generation of malonyl-CoA by acetyl-CoA carboxylase (ACC),encoded by the *pod-2* gene in *C. elegans* (Watts and Ristow 2017). In addition to POD-2 and FASN-1 we looked at FAT-7 (an essential delta-9 fatty acid desaturase required for synthesis of monostaurated fatty acids, along with FAT-6, responsible for producing oleic acid, 18C:1n-9).

De novo fat synthesis based on the expression levels of P*pod-2*::GFP was downregulated only upon GSK-3 depletion, whereas PHB depleted animals, which show reduced *pod-2* expresssion (Figure A3.5,A) were not further affected by loss of GSK-3. Additionally, expression of *fasn-1* and *fat-7* was also repressed (Figure A3.5, B-C) when GSK-3 is depleted in wild type and *daf-*

2(e1370) mutants respectively. In particular, *fat-7* downregulation indicates lower levels of oleic acid, a known precursor for the synthesis of polyunsaturated fatty acids and triacylglycerides.
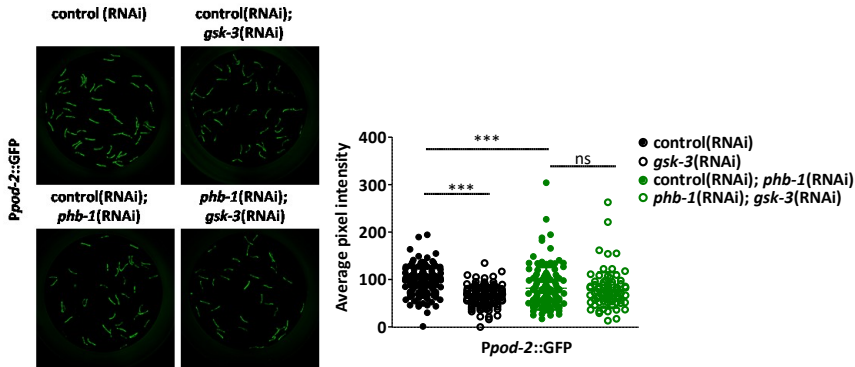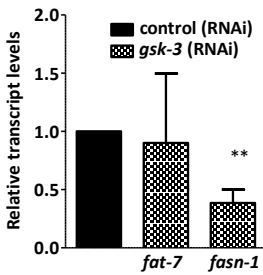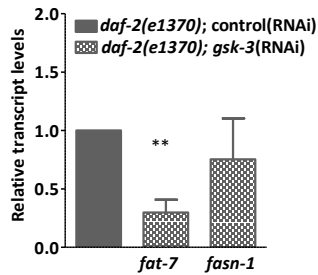
Figure A3.5: Altered *de novo* fatty acid metabolism upon *gsk-3(RNAi)*. **A.** *pod-2* gene expression in otherwise wild type and upon PHB depletion grown on *gsk-3(RNAi)* compared to control*(RNAi)* (left panel).The scatter plot (right panel) represents the respective GFP quantification (Animals were imaged at Day1 of adulthood in all conditions, Mean±SD, One way ANOVA, Dunn's multiple comparison test, *** = p< 0.001, ns=not significant , n≥87, one of two independent experiments has been represented) **B**-**C.** Expression of *fasn-1* and *fat-7* in wild type (**B**) and IIS mutants (**C**) grown on *gsk-3(RNAi)* compared to control*(RNAi)* (Mean ±SEM, Unpaired t-test, **=p<0.01, graph representative of three independent experiments, each with 2-3 technical repeats).

## Appendix 4 - Assessing metabolic activity using Seahorse XFp Analyzer
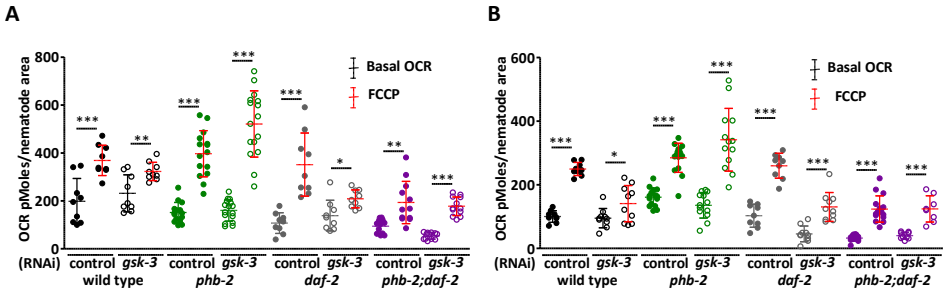
Figure A4.1: FCCP treatment caused an increase in OCR across all conditions tested **A.** at young adult stage, **B.** day 5 of ageing (Unpaired t-test, * = p<0.05, ** = p<0.01, *** = p< 0.001, bars represent ± SD, n = at least 3 independent experiments consisting of 3-4 wells each of control*(RNAi)* and *gsk-3(RNAi)* for each genetic background tested)
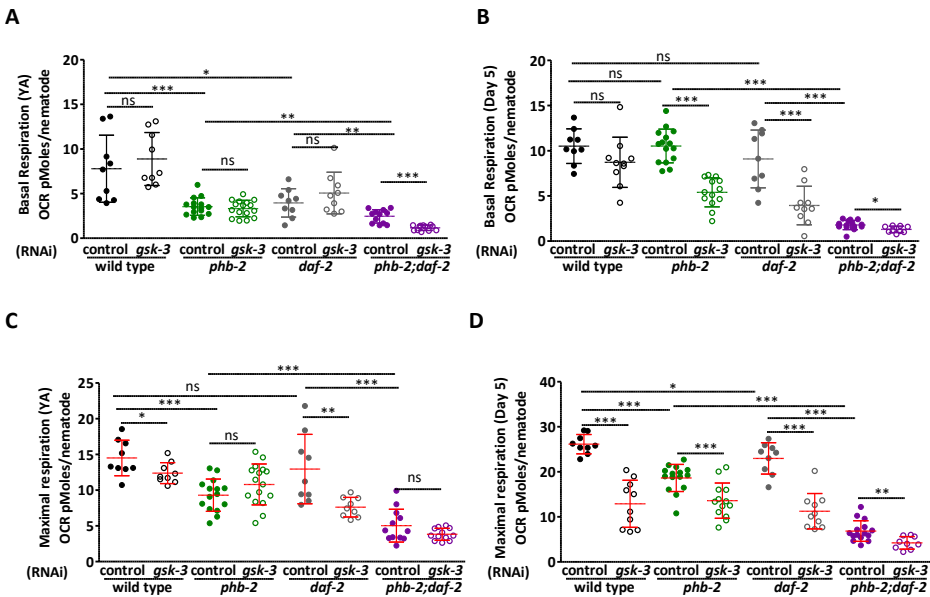
Figure A4.2: Basal and maximal oxygen consumption rates normalised to number of worms (**A-D**) across wild type, *daf-2 (e1370) and* the mitochondrial mutants – *phb-2(tm2998)* and *phb-2(tm2998);daf-2(e1370)*grown on control*(RNAi)* and *gsk-3(RNAi)* at young adult(YA) stage and during ageing, at day 5 of adulthood. **A-B**. Basal respiration at YA and at Day 5 respectively; basal respiration reduces during ageing in wild type **C-D**. Maximal respiration as observed by treatment using FCCP, at young adult stage and at day 5 of adulthood (Unpaired t-test, ns = not significant p>0.05, * = p<0.05, ** = p<0.01, *** = p< 0.001, bars represent ± SD, n = at least 3 independent experiments consisting of 3-4 wells each of control*(RNAi)* and *gsk-3(RNAi)* for each genetic background tested).
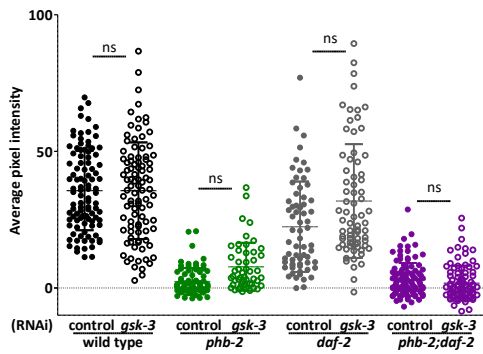
Figure A4.3: Mitochondrial content in animals devoid of GSK-3 (Animals were imaged at young adult stage in all conditions, Mean±SD, One way ANOVA, Dunn's multiple comparison test, ns=not significant , n≥50, one of two independent experiments has been represented)
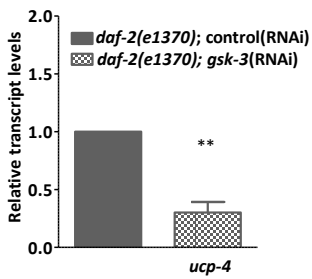
Figure A4.4: Expression of *ucp-4* in IIS mutants grown on *gsk-3(RNAi)* compared to control *(RNAi)* (Mean ±SEM, Unpaired t-test, **=p<0.01, graph representative of three independent experiments, each with 2-3 technical repeats).

Appendix 5 – AMPK status
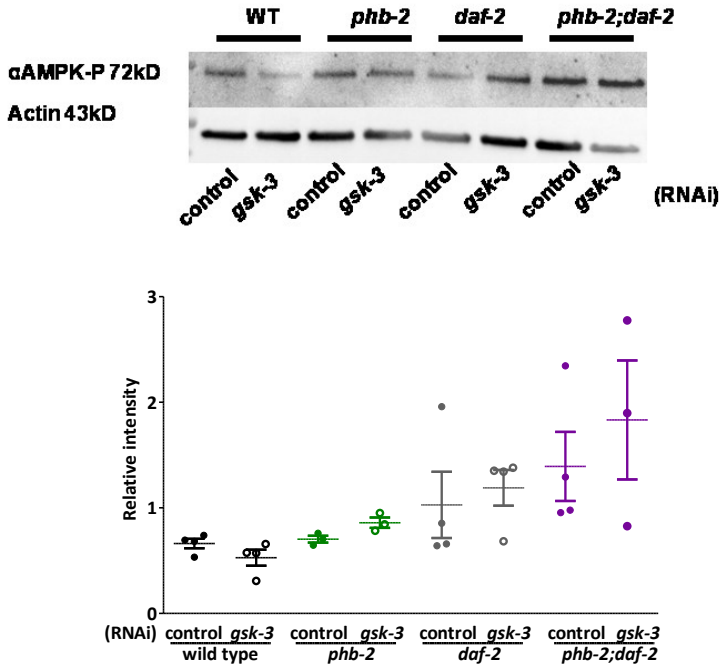
Figure A5.1: Levels of P-AMPK. Western blot analysis showing P-AMPK and actin protein levels in the different genetic backgrounds, in control and *gsk-3(RNAi)* (representative blot , top panel). Graphical representation of quantified P-AMPK intensity normalized to actin for the respective genetic backgrounds (atleast 3 independent experiments, lower panel).

LIST OF TABLES

Tables

Table 1: Pathways that regulate ageing

Pathway	Description
Nutrient sensing pathways An intervention to interrupt ageing is the process of dietary restriction (DR), a means of restricting food intake without malnutrition. DR has been shown to extend lifespan in various species. Longevity responses to dietary restriction are regulated by several conserved signalling pathways.	TOR signalling: TOR is a mechanistic or mammalian target of rapamycin responsible for regulation of cell growth, proliferation, motility and survival, protein synthesis, autophagy and transcription. This serine threonine kinase is a major amino acid and nutrient sensor that supports growth and blocks autophagy when food is present in abundance (Wullschleger et al. 2006). Inhibition of this pathway increases lifespan in yeast, flies, mice and in worms where it is mediated by the transcription factor PHA-4/FOXA. PHA-4 also regulates autophagy, a process that has a role in lifespan regulation (Sheaffer et al. 2008). Lifespan in worms is extended upto 150% upon inhibition of TOR (Vellai et al. 2003; Hansen et al. 2007). Additionally, the mutation of raptor, DAF-15 (regulatory associated protein of mTOR), leads to lifespan extension in worms. This is regulated by FOXO/DAF- 16, thus, there is cross-talk between IIS and TOR pathways (Jia et al. 2004). Apart from this, TOR regulates translation by activating p70S6K (ribosomal subunit S6 kinase, RSKS-1) and inhibiting the translation repressor eIF4EBP. Inhibition of translational regulators or p70S6K (RSKS-1) in *C. elegans* extends worm lifespan (Hansen et al. 2007). AMP-activated protein kinase (AMPK): It is a conserved nutrient and energy sensor that will activate catabolic pathways and repress anabolic pathways in an attempt to restore homeostasis (Hardie and Hawley 2001). Upon over expression of AMP kinase, lifespan is extended in *C. elegans*. AMP kinase is required for insulin/IGF-1 mutations to be able to extend worm lifespan (Apfeld et al. 2004). Also, the anti-diabetic drug metformin that activates AMP kinase can increase lifespan in mice(Onken and Driscoll 2010). Lately, neuronal AMPK activation was shown to regulate lifespan via catecholamine signalling in *C. elegans* (Burkewitz et al. 2015) It can also extend lifespan in a response to dietary restriction but is dispensable for chronic dietary restriction (*eat-2* mutants) (Greer et al. 2007a). AMPK acts partly via FOXO transcription factors to extend lifespan in worms (Greer et al. 2007a) Sirtuins: These are nicotinamide adenine dinucleotide (NAD) - dependent protein deacetylases, and are directly linked to cellular nutrient signalling through NAD$^+$(Imai et al. 2000). In worms,
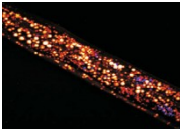
	over expression of the sirtuin gene *sir-2.1* increases lifespan (Tissenbaum and Guarente 2001) in a DAF-16/FOXO-dependent manner (Berdichevsky et al. 2006). Lifespan extension was also seen in flies (Rogina and Helfand 2004), indicating evolutionary conservation of sirtuins. However, on re-examining the effects of sirtuin overexpression on the lifespan in worms and flies abolished the pro-longevity observed earlier. The extension in lifespan was attributed to a background mutation in the transgenic animals used in these experiments (Burnett et al. 2011)
Signals from the reproductive system	The germline of *C. elegans* also influences ageing. When the worm germline is removed or through genetic manipulation, extension of lifespan is seen by 60% which requires DAF-16 activity, however, this effect is abolished when the somatic gonad is removed, suggesting that opposing signalling pathways might exist (Hsin and Kenyon 1999; Arantes-Oliveira et al. 2002). The extended lifespan upon germline removal is a result of signalling from the reproductive system to the intestine as DAF-16 accumulates within intestinal nuclei and functions in the intestine to increase life span when the germline is removed (Berman and Kenyon 2006). Signals from the reproductive system have been shown to mediate lifespan in flies and mice as well (Kenyon 2010a).
Epigenetic mechanisms	Epigenetic mechanisms like DNA methylation, histone modification and noncoding RNAs also regulate ageing. Histone-modifying enzymes such as the SET domain proteins, SET-9 and SET-15 accelerate ageing (Hamilton et al. 2005; Greer et al. 2010), while inhibition of members of the histone H3K4 methylation complex, ASH-2, WDR-5 and SET-2 and overexpression of RBR-2 (enzyme that mediates H3K4 demethylation) are known to extend lifespan (Greer et al. 2010). Depletion of the histone demethylase, UTX-1 increases longevity by genetically interacting with the IIS pathway (Jin et al. 2011; Maures et al. 2011). Also, microRNA (miRNA), a class of noncoding RNA molecules also function in lifespan regulation, example, miRNA *lin-4* and its target LIN-14. This was mediated by the IIS pathway in *C. elegans* (Boehm and Slack 2005).

Table 2: Methods for evaluating *C. elegans* fat stores. Adapted from (Elle et al. 2010; Lemieux and Ashrafi 2015)

Method	Subtype	Mechanism	Description
Vital dyes Nile Red	Nile Red	Dye partitions to live tissue depots	Benefits: Simple, fast, cheap; hence, ideal for screening experiments; uses standard microscopy techniques; allows live imaging. Drawbacks: fluorescence emission is sensitive to lipid composition; high variability; it stains gut granules that are not lipid droplets.
  BODIPY- FA	BODIPY-labelled fatty acids (BODIPY - FA)	Dye partitions to live tissue depots	Benefits: Simple, fast, cheap; stains hypodermal and intestinal lipid stores; allows live imaging. Drawbacks: gut granules stain strongest in the intestine; requires confocal microscopy.
Fixed staining Sudan Black	Colorimetric (Sudan black, Oil Red O)	Dye partitions to hydrophobic depots	Benefits: cheap, standard light microscopy. Drawbacks: requires fixation; time consuming; large variability; poor sensitivity; different fat depots not distinguishable.
  Oil Red O	Flourimetric (Nile Red, BODIPY, LipidTOX)	Dye partitions to hydrophobic depots	Benefits: cheap, standard light microscopy; improved sensitivity; better range than colorimetric stains Drawbacks: requires fixation and time consuming; large variability; different fat depots not distinguishable.
Electron Microscopy 	Osmium tetraoxide	-	Benefits: high resolution of cell structures Drawbacks: requires fixation with harmful substances like glutaraldehyde and/or paraformaldehyde; time consuming; advanced equipment required.
Analytical	Thin layer	Solvent based	Benefits: Direct quantification

Chemistry (Watts and Browse 2006; Srinivasan et al. 2008).	chromatography (TLC)	extraction and chromatography	of total TAG, Phospholipids, free fatty acids etc. Drawbacks: Reductive; is inconsiderate of cell biological complexities; large population based averages; low throughput method.
	Gas chromatography/ mass spectroscopy (GC/MS)	Solvent based extraction, high resolution chromatography and mass spectroscopy	Benefits: Can quantify the abundance of individual fatty acid chains. Drawbacks: Reductive; is inconsiderate of cell biological complexities; large population based averages; low throughput method.
Raman microscopy CARS (Hellerer et al. 2007; Le et al. 2010; Folick et al. 2011; Wang et al. 2011)	Coherent Anti-Stoke Raman Spectroscopy (CARS)	Raman-stimulated vibrational emission	Benefits: non invasive live animal staining, high resolution; microscopic detection of live tissue lipid depots; can be used to monitor the ratio of saturated to unsaturated fatty acids Drawbacks: Complex technique; is expensive ; more time consuming than fluorescence measurements; quantitation made difficult by non-resonant background and non-linear dependence of signal on underlying tissue; CARS signals arise from all lipid-rich structures (including cell membrane, cellular organelles, free lipids, yolk lipids, lipid droplets)
	Stimulated Raman Scattering (SRS)	Raman-stimulated vibrational emission	Benefits: Significant improvements over CARS in background signal and linear relationship between underlying sample and signal received. Drawbacks: Complex technique; is expensive; technically a more demanding optical setup than CARS; not easily available to researchers.
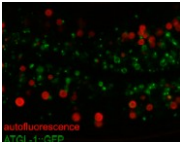
Transgenic strains (Mak 2012; Mak 2013; Liu et al. 2014)	Lipid droplet markers	Worms are genetically modified to express a GFP labeled, lipid droplet-associating protein	Benefits: live animal imaging; can be used to characterise lipid droplet size and number Drawbacks: requires confocal microscopy; may perturb the natural properties of lipid stores; not every lipid droplet expresses the same lipid droplet proteins
Dark field microscopy (Fouad et al. 2017)	-	Dark field images taken with ordinary light microscope are used to estimate fat levels in worms. This is done by defining a metric based on the amount of light scattered per area.	Benefits: no dyes or fixation. The light scattering metric is strongly correlated with worm fat levels as measured by ORO staining.

Table 3: Summary of lifespan data of PHB deletion mutants, on *E.coli* OP50.

* Maximum lifespan is the average of the longest-lived 10% of the animals assayed.
† Confirmed death events, divided by the total number of animals included in lifespan assays. Total equals the number of animals that died plus the number of animals that were censored. The number of independent lifespan assays for each strain is shown in parentheses.
‡ Compared to wild type animals.

Strains	Mean ± SEM	Maximum* ± SEM	Deaths/Total†	P-value‡
Wild type	18±0	29.45±1.45	137/326(2)	
phb-1(tm2571)	17±1	23.45±0.05	215/227(2)	< 0.0001
phb-2(tm2998)	14.5±0.5	25.30±1.307	302/313(2)	< 0.0001
daf-2(e1370)	30.5±2.5	57.31±1.312	134/333(2)	< 0.0001
phb-2(tm2998); daf-2(e1370)	55.5±0.5	85.41±8.41	110/162(2)	< 0.0001

Table 4: Summary of lifespan data upon depletion of GSK-3

compared to respective genetic background versus *gsk-3(RNAi)*
§ *phb-2(tm2998)* and *daf-2(e1370)* mutants compared to wild type
‡ *phb-2(tm2998);daf-2(e1370)* mutants compared to *daf-2(e1370)* mutants
‡ *phb-2(tm2998);gsk-3(RNAi)* versus wild type; *gsk-3(RNAi)*
‖ *phb-2(tm2998);daf-2(e1370);gsk-3(RNAi)* versus *daf-2(e1370);gsk-3(RNAi)*
ns no significant difference (P>0.05)

Strain	Median ±SEM (days)	Maximum* ±SEM (days)	Deaths/ Total†	% decrease upon loss of GSK-3 per trial	Vulval bursting	P value
RNAi from eggs						
Wild type, N2	18±1	25.23±0.45	300/369(2)	-	-	-
gsk-3(RNAi)	11.5±0.5	16.66±0.33	86/578(2)	35.29 %	491	< 0.0001#
				36.84 %		
phb-2(tm2998)	16.5±0.5	20.45±0.19	365/388(2)	-	-	< 0.0001§
phb-2(tm2998); gsk-3(RNAi)	14±1	18.75±0.06	294/396(2)	11.76 %	75	0.0015#
				18.75 %		< 0.0001‡
daf-2(e1370)	37.5±4.5	51.80±4.19	209/411(2)		-	< 0.0001§
daf-2(e1370); gsk-3(RNAi)	19±2	31.80±0.54	382/489(2)	36.36 %	92	< 0.0001#
				59.52 %		
phb-2(tm2998); daf-2(e1370)	50.5±1.5	71.24±0.35	189/332(2)		-	< 0.0001‡
phb-2(tm2998); daf-2(e1370); gsk-3(RNAi)	27.5±3.5	40.25±7.25	117/278(2)	53.84 %	87	< 0.0001#
				36.73 %		< 0.0001‖
RNAi from eggs (on FUdR)						
Wild type, N2	21	28.7	172/181(1)	-	-	-
gsk-3(RNAi)	16	21.8	53/206(1)	23.8 %	152	< 0.0001#
phb-2(tm2998)	21	26.6	159/178(1)	-	-	0.0377§
phb-2(tm2998); gsk-3(RNAi)	18	23.2	125/135(1)	14.2 %	-	<0.0001# <0.0001‡
daf-2(e1370)	37	43.9	159/179(1)	-	-	< 0.0001§

daf-2(e1370); gsk-3(RNAi)	25	38.2	172/177(1)	32.4 %	-	< 0.0001#
phb-2(tm2998); daf-2(e1370)	46	57.7	141/167(1)	-	-	< 0.0001‡
phb-2(tm2998); daf-2(e1370); gsk-3(RNAi)	25	42.6	30/80(1)	45.6 %	-	< 0.0001# 0.0244‖
RNAi from Adulthood (Young Adult stage)						
Wild type, N2	17±0	26.90±0.97	317/372(2)	-	-	-
gsk-3(RNAi)	14±0	19.57±0.12	271/503(2)	17.64 % / 17.64 %	220	< 0.0001#
phb-2(tm2998)	17±0	23.70±0.63	230/279(2)	-		0.0093§
phb-2(tm2998); gsk-3(RNAi)	17±0	22.82±0.17	290/378(2)	No change / No change	18	ns # / < 0.0001‡
daf-2(e1370)	39.5±1.5	57.58±0.70	151/385(2)	-	-	< 0.0001§
daf-2(e1370); gsk-3(RNAi)	26±1	41.37±0.50	318/384(2)	34.14 % / 34.21 %	6	< 0.0001#
phb-2(tm2998); daf-2(e1370)	58±2	80.66±1.46	180/281(2)	-	-	< 0.0001‡
phb-2(tm2998); daf-2(e1370); gsk-3(RNAi)	44±3	60.25±1.75	156/277(2)	31.66 % / 16.07 %	42	< 0.0001# / < 0.0001‖
Intestine specific RNAi system - *rde-1(ne219);kbIs7*						
rde-1(ne219); kbIs7	14.5±0.5	21.23±0.68	233/298(2)		-	
rde-1(ne219); kbIs7; gsk-3(RNAi)	13.5±0.5	18.3±0.69	238/298(2)	13.33 % / No change	13	< 0.0001#
phb-2(tm2998); rde-1(ne219); kbIs7	16±1	25.37±0.29	213/307(2)		-	
phb-2(tm2998); rde-1(ne219); kbIs7 ; gsk-3(RNAi)	12.5±0.5	18.38±1.72	214/286(2)	13.33 % / 29.41 %	7	< 0.0001#
daf-2(e1370); rde-1(ne219); kbIs7	34.7±1.1	44.7±2.39	363/615(4)		-	

Genotype						
daf-2(e1370); rde-1(ne219); kbIs7; gsk-3(RNAi)	14.5±2.2	25.8±1.74	230/716(4)	68.57 % 68.42 % 57.57 % 36.36 %	465	< 0.0001#
phb-2(tm2998); daf-2(e1370); rde-1(ne219); kbIs7	37±5	60.1±3.87	60/133(2)		-	
phb-2(tm2998); daf-2(e1370); rde-1(ne219); kbIs7; gsk-3(RNAi)	37±5	60.1±3.87	60/133(2)	16.66 % 25 %	-	< 0.0001#
Inhibition of GSK-3 by addition of Lithium Chloride, 20°C						
Wild type; LiCl-	16	28.7	94/147(1)	-	-	
Wild type; LiCl+	13	27.23	127/150(1)	18.75 %	-	< 0.0001#
daf-2(e1370); LiCl -	39	51.62	83/139(1)	-	-	
daf-2(e1370); LiCl +	26	45.7	96/150(1)	33.33 %	-	< 0.0001#
Inhibition of GSK-3 by addition of Lithium Chloride, 25°C						
Wild type; LiCl-	8	15.5	75/150(1)	-	-	
Wild type; LiCl+	8	16.54	106/152(1)	-	-	ns#

Table 5: Summary of lifespan data upon depletion of Wnt components

compared to respective genetic background versus test*(RNAi)*
§ *phb-2(tm2998)* and *daf-2(e1370)* mutants compared to wild type
‡ *phb-2(tm2998);daf-2(e1370)* mutants compared to *daf-2(e1370)* mutants
‡ *phb-2(tm2998);test(RNAi)* versus wild type; *test(RNAi)*
|| *phb-2(tm2998); daf-2(e1370); test(RNAi)* versus *daf-2(e1370);test(* RNAi)
ns no significant difference (P>0.05)

Strain	Median ±SEM (days)	Maximum* ±SEM (days)	Deaths/ Total†	% Change in lifespan	Vulval bursting	P value
Depletion of *kin-19* and *bar-1* (RNAi from Adulthood)						
Wild type, N2	17±0	26.9±0.97	317/372(2)	-	-	-
kin-19(RNAi)	14±0	19.7±1.09	355/411(2)	-17.64%	32	< 0.0001#
bar-1(RNAi)	17±0	23.4±0.1	384/493(2)	No change	38	< 0.0001#
phb-2(tm2998)	17±0	23.7±0.63	230/279(2)		-	< 0.0001§
phb-2(tm2998); kin-19(RNAi)	17±0	22.9±0.36	271/342(2)	No change	8	ns# < 0.0001‡
phb-2(tm2998); bar-1(RNAi)	17±0	23.56±0.1	350/397(2)	No change	10	ns# ns‡
daf-2(e1370)	39.5±1.5	57.58±0.7	151/385(2)		-	< 0.0001§
daf-2(e1370); kin-19(RNAi)	23±1	36.3±1.91	338/380(2)	-41.77%	-	< 0.0001#
daf-2(e1370); bar-1(RNAi)	33±5	51.61±2.0	179/423(2)	-16.45%	-	< 0.0001#
phb-2(tm2998); daf-2(e1370)	58±2	80.66±1.4	180/281(2)		-	< 0.0001‡
phb-2(tm2998); daf-2(e1370); kin-19(RNAi)	36±2	50.47±6.1	159/213(2)	-37.93%	15	< 0.0001# < 0.0001||
phb-2(tm2998); daf-2(e1370); bar-1(RNAi)	44.5±6.5	69.41±1.9	154/213(2)	-23.27%	40	< 0.0001# < 0.0001||

Table 6: Summary of lifespan data of additional screen candidates

compared to respective genetic background versus test*(RNAi)*

§ *phb-2(tm2998)* and *daf-2(e1370)* mutants compared to wild type

‡ *phb-2(tm2998);daf-2(e1370)* mutants compared to *daf-2(e1370)* mutants

‡ *phb-2(tm2998); test(RNAi)* versus wild type; *test(RNAi)*

|| *phb-2(tm2998); daf-2(e1370); test(RNAi)* versus *daf-2(e1370);test(* RNAi)

ns no significant difference (P>0.05)

Strain	Median ±SEM (days)	Maximum* ±SEM (days)	Deaths/ Total†	% Change in lifespan	Vulval bursting	P value
Depletion of *mtk-1* (RNAi from eggs)						
Wild type, N2	18.6±0.3	26.4±0.7	494/529(3)	-	-	-
mtk-1(RNAi)	19.3±0.8	26.4±1.0	479/498(3)	-	-	ns#
phb-2(tm2998)	18±0.5	24.8±0.6	405/464(3)	-	-	0.0018§
phb-2(tm2998); mtk-1(RNAi)	22.3±1.8	33.8±0.2	269/465(3)	+23.88%	-	<0.0001# < 0.0001‡
daf-2(e1370)	38±8	57.7±1.5	174/360(2)	-	-	< 0.0001§
daf-2(e1370); mtk-1(RNAi)	40.5±5.5	58.7±2.9	179/349(2)	-	-	ns#
phb-2(tm2998); daf-2(e1370)	58±4	78.1±1.95	146/233(2)	-	-	< 0.0001‡
phb-2(tm2998); daf-2(e1370); mtk-1(RNAi)	51.5±0.5	73.8±6.3	106/205(2)	-11.20%	-	0.0037# < 0.0001||
Depletion of *rsks-1* (RNAi from eggs)						
Wild type, N2	19	25.3	131/179(1)	-	-	
rsks-1(RNAi)	17	25	130/180(1)	-10.52%	-	0.0040#
phb-2(tm2998)	17	24.3	105/128(1)	-	-	0.0078§
phb-2(tm2998); rsks-1(RNAi)	21	32.3	94/149(1)	+23.52%	-	<0.0001#
daf-2(e1370)	40	57.8	60/210(1)	-	-	<0.0001§
daf-2(e1370); rsks-1(RNAi)	45	65.25	38/210(1)	+11.11%	-	0.0204#
phb-2(tm2998); daf-2(e1370)	63	93.5	22/111(1)	-	-	<0.0001‡

phb-2(tm2998); daf-2(e1370); rsks-1(RNAi)	54	77.5	24/163(1)	-14.28%	-	0.0675#
Depletion of rsks-1 (RNAi from eggs, LS on FUdR)						
Wild type, N2	21	28.7	172/181(1)	-	-	
rsks-1(RNAi)	21	28.55	178/180(1)	No effect	-	ns#
phb-2(tm2998)	21	26.62	159/178(1)	-	-	0.0377§
phb-2(tm2998); rsks-1(RNAi)	23	29.66	61/78(1)	+8.69%	-	0.0003#
daf-2(e1370)	37	43.93	159/179(1)	-	-	<0.0001§
daf-2(e1370); rsks-1(RNAi)	28	48.7	165/184(1)	-24.32%	-	0.0233#
phb-2(tm2998); daf-2(e1370)	46	57.71	141/167(1)	-	-	<0.0001‡
phb-2(tm2998); daf-2(e1370); rsks-1(RNAi)	57	71.12	83/100 (1)	+23.9%	-	<0.0001#
Depletion of Y50D7A.3 (RNAi from eggs)						
Wild type, N2	19±0	26.5±0.6	443/508(3)	-	-	-
Y50D7A.3 (RNAi)	17.6±0.6	26.1±0.8	469/510(3)	-7.36%	-	0.0240#
phb-2(tm2998)	17.6±0.6	25±0.4	428/489(3)	-	-	<0.0001§
phb-2(tm2998); Y50D7A.3 (RNAi)	18.3±0.6	26.5±1.0	400/536(3)	+3.97%	-	<0.0001#
daf-2(e1370)	43±3	58.5±0.6	119/377(2)	-	-	<0.0001§
daf-2(e1370); Y50D7A.3 (RNAi)	39.5±1.5	58±0.7	174/359(2)	-8.13	-	ns#
phb-2(tm2998); daf-2(e1370)	62.5±0.5	86.8±6.7	69/178(2)	-	-	<0.0001‡
phb-2(tm2998); daf-2(e1370); Y50D7A.3 (RNAi)	67.5±5.5	86.4±4.0	55/191(2)	+8%	-	ns#
Depletion of kin-1 (RNAi from L3/L4)						
Wild type, N2	18	24.9	182/200(1)	-	-	-
kin-1(RNAi)	population lost due to vulval bursting					
phb-2(tm2998)	18	23.6	82/103(1)	-	-	ns§
phb-2(tm2998); kin-1(RNAi)	13	18	24/136(1)	-27.77%	110	<0.0001#
daf-2(e1370)	30	56.16	115/193(1)	-	-	<0.0001§

daf-2(e1370); kin-1 (RNAi)	population lost due to vulval bursting				
phb-2(tm2998); daf-2(e1370)	54	76.1	99/166(1)	-	-	<0.0001‡
phb-2(tm2998); daf-2(e1370); kin-1 (RNAi)	30	54.3	31/158(1)	-44.44%	75	<0.0001#
Supplementation of FUdR						
Wild type, N2	19	27.5	138/149(1)	-	-	-
Wild type, N2; FUdR	24	30	144/151(1)	+26.31%	-	<0.0001#
phb-2(tm2998)	17	25.8	147/151(1)	-	-	-
phb-2(tm2998); FUdR	19	25.7	141/150(1)	+11.76%	-	<0.0001#
daf-2(e1370)	46	51.66	59/167(1)	-	-	-
daf-2(e1370); FUdR	39	49	162/180(1)	-15.21%	-	<0.0001#
phb-2(tm2998); daf-2(e1370)	62	80	47/67(1)	-	-	-
phb-2(tm2998); daf-2(e1370); FUdR	48	56	49/63(1)	-22.58%	-	<0.0001#

Table 7: Primer information for genes listed in this thesis

Gene	MRS code	Sequences (5'-3')
cpt-2	173	Forward - GCAAGATGGATTCGGTATTGG
	174	Reverse - TCACGTTTCGACTTATTGCTC
fat-7	181	Forward - GCTCTCTATGTGTTCTCAGG
	182	Reverse - CAATGATGTCGTTTTGAAGAGC
fasn-1	183	Forward - GGATAATACTGGAGAAGGATCG
	184	Reverse - ATGTTGTCCGAAGACTGAG
mdh-2	195	Forward - TTCCGAGCTTAAGGGACATGAC
	196	Reverse - GAGAATTTGGTGGATGGTTTGAC
icl-1	197	Forward - GCTGTCAGTCGTGCGGTTAC
	198	Reverse - GCGGTGAGCGAAAGGATTT
acdh-1	177	Forward - GCAAATGCAGATCCTAGCC
	178	Reverse - GTTTGTCTTTCCTCCTTATCTACAG
acdh-9	179	Forward - GGCAGACTTCCAGTATAACC
	180	Reverse - GCGTTTCTAACGATTAGTCTG
acdh-12	163	Forward - CCGATGTTTTCACTGTGTTTGC
	164	Reverse - CAAACGCTCTTTCGACAATGAAT
ucp-4	165	Forward - CGAACTTAAAGATAATTGGCTAACTCA
	166	Reverse - CGACATCTGATGGAAGTGATACAA
acs-17	161	Forward - GGAGACTATCACTGGAGAAGCTATG
	162	Reverse - GAACTGCTTCGTCTCCAAGAGTAG
cdc-42	Askjaer Lab	Forward - CTTTGAGCAATGATGCGAAA
		Reverse - TCATTCGAGAATGTCCGAGA
pmp-3	Askjaer Lab	Forward - TGGCCGGATGATGGTGTCGC
		Reverse - ACGAACAATGCCAAAGGCCAGC

References

Afanas'ev I. 2010. Signaling and Damaging Functions of Free Radicals in Aging-Free Radical Theory, Hormesis, and TOR. *Aging Dis* **1**: 75-88.

Ahn CS, Lee JH, Reum Hwang A, Kim WT, Pai HS. 2006. Prohibitin is involved in mitochondrial biogenesis in plants. *Plant J* **46**: 658-667.

Ahringer J. 2006. Reverse Genetics. *Wormbook*.

Aitlhadj L, Sturzenbaum SR. 2010. The use of FUdR can cause prolonged longevity in mutant nematodes. *Mech Ageing Dev* **131**: 364-365.

Ali A, Hoeflich KP, Woodgett JR. 2001. Glycogen synthase kinase-3: properties, functions, and regulation. *Chem Rev* **101**: 2527-2540.

Alon LT, Pietrokovski S, Barkan S, Avrahami L, Kaidanovich-Beilin O, Woodgett JR, Barnea A, Eldar-Finkelman H. 2011. Selective loss of glycogen synthase kinase-3alpha in birds reveals distinct roles for GSK-3 isozymes in tau phosphorylation. *FEBS Lett* **585**: 1158-1162.

Amaya C, Fader CM, Colombo MI. 2015. Autophagy and proteins involved in vesicular trafficking. *FEBS Lett* **589**: 3343-3353.

An JH, Vranas K, Lucke M, Inoue H, Hisamoto N, Matsumoto K, Blackwell TK. 2005. Regulation of the Caenorhabditis elegans oxidative stress defense protein SKN-1 by glycogen synthase kinase-3. *Proc Natl Acad Sci U S A* **102**: 16275-16280.

Antebi A. 2007. Genetics of aging in Caenorhabditis elegans. *PLoS Genet* **3**: 1565-1571.

Antoshechkin I, Sternberg PW. 2007. The versatile worm: genetic and genomic resources for Caenorhabditis elegans research. *Nat Rev Genet* **8**: 518-532.

Apfeld J, Kenyon C. 1998. Cell nonautonomy of C. elegans daf-2 function in the regulation of diapause and life span. *Cell* **95**: 199-210.

Apfeld J, O'Connor G, McDonagh T, DiStefano PS, Curtis R. 2004. The AMP-activated protein kinase AAK-2 links energy levels and insulin-like signals to lifespan in C. elegans. *Genes Dev* **18**: 3004-3009.

Arantes-Oliveira N, Apfeld J, Dillin A, Kenyon C. 2002. Regulation of life-span by germ-line stem cells in Caenorhabditis elegans. *Science* **295**: 502-505.

Arda HE, Taubert S, MacNeil LT, Conine CC, Tsuda B, Van Gilst M, Sequerra R, Doucette-Stamm L, Yamamoto KR, Walhout AJ. 2010. Functional modularity of nuclear hormone receptors in a Caenorhabditis elegans metabolic gene regulatory network. *Mol Syst Biol* **6**: 367.

Artal-Sanz M, de Jong L, Tavernarakis N. 2006. Caenorhabditis elegans: a versatile platform for drug discovery. *Biotechnol J* **1**: 1405-1418.

Artal-Sanz M, Tavernarakis N. 2009a. Prohibitin and mitochondrial biology. *Trends Endocrinol Metab* **20**: 394-401.

-. 2009b. Prohibitin couples diapause signalling to mitochondrial metabolism during ageing in C. elegans. *Nature* **461**: 793-797.

Artal-Sanz M, Tsang WY, Willems EM, Grivell LA, Lemire BD, van der Spek H, Nijtmans LG. 2003. The mitochondrial prohibitin complex is essential for embryonic viability and germline function in Caenorhabditis elegans. *J Biol Chem* **278**: 32091-32099.

Arur S, Ohmachi M, Nayak S, Hayes M, Miranda A, Hay A, Golden A, Schedl T. 2009. Multiple ERK substrates execute single biological processes in Caenorhabditis elegans germ-line development. *Proc Natl Acad Sci U S A* **106**: 4776-4781.

Ashrafi K. 2007. Obesity and the regulation of fat metabolism. *WormBook*: 1-20.

Ashrafi K, Chang FY, Watts JL, Fraser AG, Kamath RS, Ahringer J, Ruvkun G. 2003. Genome-wide RNAi analysis of Caenorhabditis elegans fat regulatory genes. *Nature* **421**: 268-272.

Atwell K, Qin Z, Gavaghan D, Kugler H, Hubbard EJ, Osborne JM. 2015. Mechano-logical model of C. elegans germ line suggests feedback on the cell cycle. *Development* **142**: 3902-3911.

Back JW, Sanz MA, De Jong L, De Koning LJ, Nijtmans LG, De Koster CG, Grivell LA, Van Der Spek H, Muijsers AO. 2002. A structure for the yeast prohibitin complex: Structure prediction and evidence from chemical crosslinking and mass spectrometry. *Protein Sci* **11**: 2471-2478.

Bansal A, Zhu LJ, Yen K, Tissenbaum HA. 2015. Uncoupling lifespan and healthspan in Caenorhabditis elegans longevity mutants. *Proc Natl Acad Sci U S A* **112**: E277-286.

Barriere A, Felix MA. 2014. Isolation of C. elegans and related nematodes. *WormBook*: 1-19.

Barsyte D, Lovejoy DA, Lithgow GJ. 2001. Longevity and heavy metal resistance in daf-2 and age-1 long-lived mutants of Caenorhabditis elegans. *FASEB J* **15**: 627-634.

Benedetti C, Haynes CM, Yang Y, Harding HP, Ron D. 2006. Ubiquitin-like protein 5 positively regulates chaperone gene expression in the mitochondrial unfolded protein response. *Genetics* **174**: 229-239.

Benson JA, Cummings EE, O'Reilly LP, Lee MH, Pak SC. 2014. A high-content assay for identifying small molecules that reprogram C. elegans germ cell fate. *Methods* **68**: 529-535.

Benyoucef S, Surinya KH, Hadaschik D, Siddle K. 2007. Characterization of insulin/IGF hybrid receptors: contributions of the insulin receptor L2 and Fn1 domains and the alternatively spliced exon 11 sequence to ligand binding and receptor activation. *Biochem J* **403**: 603-613.

References

Berdichevsky A, Nedelcu S, Boulias K, Bishop NA, Guarente L, Horvitz HR. 2010. 3-Ketoacyl thiolase delays aging of Caenorhabditis elegans and is required for lifespan extension mediated by sir-2.1. *Proc Natl Acad Sci U S A* **107**: 18927-18932.

Berdichevsky A, Viswanathan M, Horvitz HR, Guarente L. 2006. C. elegans SIR-2.1 interacts with 14-3-3 proteins to activate DAF-16 and extend life span. *Cell* **125**: 1165-1177.

Berger KH, Yaffe MP. 1998. Prohibitin family members interact genetically with mitochondrial inheritance components in Saccharomyces cerevisiae. *Mol Cell Biol* **18**: 4043-4052.

Berman JR, Kenyon C. 2006. Germ-cell loss extends C. elegans life span through regulation of DAF-16 by kri-1 and lipophilic-hormone signaling. *Cell* **124**: 1055-1068.

Bianchi MW, Plyte SE, Kreis M, Woodgett JR. 1993. A Saccharomyces cerevisiae protein-serine kinase related to mammalian glycogen synthase kinase-3 and the Drosophila melanogaster gene shaggy product. *Gene* **134**: 51-56.

Bieri T, Blasiar D, Ozersky P, Antoshechkin I, Bastiani C, Canaran P, Chan J, Chen N, Chen WJ, Davis P et al. 2007. WormBase: new content and better access. *Nucleic Acids Res* **35**: D506-510.

Bilic J, Huang YL, Davidson G, Zimmermann T, Cruciat CM, Bienz M, Niehrs C. 2007. Wnt induces LRP6 signalosomes and promotes dishevelled-dependent LRP6 phosphorylation. *Science* **316**: 1619-1622.

Blackwell TK, Steinbaugh MJ, Hourihan JM, Ewald CY, Isik M. 2015. SKN-1/Nrf, stress responses, and aging in Caenorhabditis elegans. *Free Radic Biol Med* **88**: 290-301.

Blumenthal T, Squire M, Kirtland S, Cane J, Donegan M, Spieth J, Sharrock W. 1984. Cloning of a yolk protein gene family from Caenorhabditis elegans. *J Mol Biol* **174**: 1-18.

Boehm M, Slack F. 2005. A developmental timing microRNA and its target regulate life span in C. elegans. *Science* **310**: 1954-1957.

Bogenhagen DF, Rousseau D, Burke S. 2008. The layered structure of human mitochondrial DNA nucleoids. *J Biol Chem* **283**: 3665-3675.

Bourouis M, Moore P, Ruel L, Grau Y, Heitzler P, Simpson P. 1990. An early embryonic product of the gene shaggy encodes a serine/threonine protein kinase related to the CDC28/cdc2+ subfamily. *EMBO J* **9**: 2877-2884.

Boutros M, Ahringer J. 2008. The art and design of genetic screens: RNA interference. *Nat Rev Genet* **9**: 554-566.

References

Braeckman BP, Houthoofd K, De Vreese A, Vanfleteren JR. 2002a. Assaying metabolic activity in ageing Caenorhabditis elegans. *Mech Ageing Dev* **123**: 105-119.

Braeckman BP, Houthoofd K, Vanfleteren JR. 2002b. Assessing metabolic activity in aging Caenorhabditis elegans: concepts and controversies. *Aging Cell* **1**: 82-88; discussion 102-103.

-. 2009. Intermediary metabolism. *WormBook*: 1-24.

Brenner S. 1974. The genetics of Caenorhabditis elegans. *Genetics* **77**: 71-94.

Brock TJ, Browse J, Watts JL. 2007. Fatty acid desaturation and the regulation of adiposity in Caenorhabditis elegans. *Genetics* **176**: 865-875.

Brooks KK, Liang B, Watts JL. 2009. The influence of bacterial diet on fat storage in C. elegans. *PLoS One* **4**: e7545.

Brunk UT, Terman A. 2002. Lipofuscin: mechanisms of age-related accumulation and influence on cell function. *Free Radic Biol Med* **33**: 611-619.

Buchser W, Collins M, Garyantes T, Guha R, Haney S, Lemmon V, Li Z, Trask OJ. 2004. Assay Development Guidelines for Image-Based High Content Screening, High Content Analysis and High Content Imaging. in *Assay Guidance Manual* (eds. GS Sittampalam, NP Coussens, K Brimacombe, A Grossman, M Arkin, D Auld, C Austin, J Baell, B Bejcek, TDY Chung, et al.), Bethesda (MD).

Buckingham SD, Sattelle DB. 2009. Fast, automated measurement of nematode swimming (thrashing) without morphometry. *BMC Neurosci* **10**: 84.

Burkewitz K, Morantte I, Weir HJ, Yeo R, Zhang Y, Huynh FK, Ilkayeva OR, Hirschey MD, Grant AR, Mair WB. 2015. Neuronal CRTC-1 governs systemic mitochondrial metabolism and lifespan via a catecholamine signal. *Cell* **160**: 842-855.

Burnett C, Valentini S, Cabreiro F, Goss M, Somogyvari M, Piper MD, Hoddinott M, Sutphin GL, Leko V, McElwee JJ et al. 2011. Absence of effects of Sir2 overexpression on lifespan in C. elegans and Drosophila. *Nature* **477**: 482-485.

Cabello J, Neukomm LJ, Gunesdogan U, Burkart K, Charette SJ, Lochnit G, Hengartner MO, Schnabel R. 2010. The Wnt pathway controls cell death engulfment, spindle orientation, and migration through CED-10/Rac. *PLoS Biol* **8**: e1000297.

Carling D, Hardie DG. 1989. The substrate and sequence specificity of the AMP-activated protein kinase. Phosphorylation of glycogen synthase and phosphorylase kinase. *Biochim Biophys Acta* **1012**: 81-86.

Carpenter AE, Jones TR, Lamprecht MR, Clarke C, Kang IH, Friman O, Guertin DA, Chang JH, Lindquist RA, Moffat J et al. 2006. CellProfiler: image

analysis software for identifying and quantifying cell phenotypes. *Genome Biol* **7**: R100.

Cassada RC, Russell RL. 1975. The dauerlarva, a post-embryonic developmental variant of the nematode Caenorhabditis elegans. *Dev Biol* **46**: 326-342.

Castillo-Quan JI, Li L, Kinghorn KJ, Ivanov DK, Tain LS, Slack C, Kerr F, Nespital T, Thornton J, Hardy J et al. 2016. Lithium Promotes Longevity through GSK3/NRF2-Dependent Hormesis. *Cell Rep* **15**: 638-650.

Chalfie M, Tu Y, Euskirchen G, Ward WW, Prasher DC. 1994. Green fluorescent protein as a marker for gene expression. *Science* **263**: 802-805.

Chang HW, Shtessel L, Lee SS. 2015. Collaboration between mitochondria and the nucleus is key to long life in Caenorhabditis elegans. *Free Radic Biol Med* **78**: 168-178.

Chen D, Li PW, Goldstein BA, Cai W, Thomas EL, Chen F, Hubbard AE, Melov S, Kapahi P. 2013. Germline signaling mediates the synergistically prolonged longevity produced by double mutations in daf-2 and rsks-1 in C. elegans. *Cell Rep* **5**: 1600-1610.

Chen H, Fajol A, Hoene M, Zhang B, Schleicher ED, Lin Y, Calaminus C, Pichler BJ, Weigert C, Haring HU et al. 2016. PI3K-resistant GSK3 controls adiponectin formation and protects from metabolic syndrome. *Proc Natl Acad Sci U S A* **113**: 5754-5759.

Chen JC, Jiang CZ, Reid MS. 2005. Silencing a prohibitin alters plant development and senescence. *Plant J* **44**: 16-24.

Chen X, Li M, Feng X, Guang S. 2015. Targeted Chromosomal Translocations and Essential Gene Knockout Using CRISPR/Cas9 Technology in Caenorhabditis elegans. *Genetics* **201**: 1295-1306.

Chen Y, Scarcelli V, Legouis R. 2017. Approaches for Studying Autophagy in Caenorhabditis elegans. *Cells* **6**.

Cheng H, Woodgett J, Maamari M, Force T. 2011. Targeting GSK-3 family members in the heart: a very sharp double-edged sword. *J Mol Cell Cardiol* **51**: 607-613.

Cheng K, Creacy S, Larner J. 1983. 'Insulin-like' effects of lithium ion on isolated rat adipocytes. II. Specific activation of glycogen synthase. *Mol Cell Biochem* **56**: 183-189.

Chiu CT, Chuang DM. 2010. Molecular actions and therapeutic potential of lithium in preclinical and clinical studies of CNS disorders. *Pharmacol Ther* **128**: 281-304.

Ciaraldi TP, Oh DK, Christiansen L, Nikoulina SE, Kong AP, Baxi S, Mudaliar S, Henry RR. 2006. Tissue-specific expression and regulation of GSK-3 in human skeletal muscle and adipose tissue. *Am J Physiol Endocrinol Metab* **291**: E891-898.

Clancy DJ, Gems D, Harshman LG, Oldham S, Stocker H, Hafen E, Leevers SJ, Partridge L. 2001. Extension of life-span by loss of CHICO, a Drosophila insulin receptor substrate protein. *Science* **292**: 104-106.

Coates PJ, Jamieson DJ, Smart K, Prescott AR, Hall PA. 1997. The prohibitin family of mitochondrial proteins regulate replicative lifespan. *Curr Biol* **7**: 607-610.

Coburn C, Allman E, Mahanti P, Benedetto A, Cabreiro F, Pincus Z, Matthijssens F, Araiz C, Mandel A, Vlachos M et al. 2013. Anthranilate fluorescence marks a calcium-propagated necrotic wave that promotes organismal death in C. elegans. *PLoS Biol* **11**: e1001613.

Coghlan MP, Culbert AA, Cross DA, Corcoran SL, Yates JW, Pearce NJ, Rausch OL, Murphy GJ, Carter PS, Roxbee Cox L et al. 2000. Selective small molecule inhibitors of glycogen synthase kinase-3 modulate glycogen metabolism and gene transcription. *Chem Biol* **7**: 793-803.

Cohen P, Frame S. 2001. The renaissance of GSK3. *Nature Reviews Molecular Cell Biology* **2**: 769- 776.

Cole A, Frame S, Cohen P. 2004. Further evidence that the tyrosine phosphorylation of glycogen synthase kinase-3 (GSK3) in mammalian cells is an autophosphorylation event. *Biochem J* **377**: 249-255.

Collins JJ, Huang C, Hughes S, Kornfeld K. 2008. The measurement and analysis of age-related changes in Caenorhabditis elegans. *WormBook*: 1-21.

Cooper AF, Van Gundy SD. 1970. Metabolism of Glycogen and Neutral Lipids by Aphelenchus avenae and Caenorhabditis sp. in Aerobic, Microaerobic and Anaerobic Environments. *J Nematol* **2**: 305-315.

Corsi AK, Wightman B, Chalfie M. 2015. A Transparent window into biology: A primer on Caenorhabditis elegans. *WormBook*: 1-31.

Cristina D, Cary M, Lunceford A, Clarke C, Kenyon C. 2009. A regulated response to impaired respiration slows behavioral rates and increases lifespan in Caenorhabditis elegans. *PLoS Genet* **5**: e1000450.

Cross DA, Alessi DR, Cohen P, Andjelkovich M, Hemmings BA. 1995. Inhibition of glycogen synthase kinase-3 by insulin mediated by protein kinase B. *Nature* **378**: 785-789.

Davies SK, Leroi AM, Bundy JG. 2012. Fluorodeoxyuridine affects the identification of metabolic responses to daf-2 status in Caenorhabditis elegans. *Mech Ageing Dev* **133**: 46-49.

De Sarno P, Li X, Jope RS. 2002. Regulation of Akt and glycogen synthase kinase-3 beta phosphorylation by sodium valproate and lithium. *Neuropharmacology* **43**: 1158-1164.

DePina AS, Iser WB, Park SS, Maudsley S, Wilson MA, Wolkow CA. 2011. Regulation of Caenorhabditis elegans vitellogenesis by DAF-2/IIS

through separable transcriptional and posttranscriptional mechanisms. *BMC Physiol* **11**: 11.

Depuydt G, Xie F, Petyuk VA, Smolders A, Brewer HM, Camp DG, 2nd, Smith RD, Braeckman BP. 2014. LC-MS proteomics analysis of the insulin/IGF-1-deficient Caenorhabditis elegans daf-2(e1370) mutant reveals extensive restructuring of intermediary metabolism. *J Proteome Res* **13**: 1938-1956.

Detienne G, Van de Walle P, De Haes W, Schoofs L, Temmerman L. 2016. SKN-1-independent transcriptional activation of glutathione S-transferase 4 (GST-4) by EGF signaling. *Worm* **5**: e1230585.

Dillin A, Hsu AL, Arantes-Oliveira N, Lehrer-Graiwer J, Hsin H, Fraser AG, Kamath RS, Ahringer J, Kenyon C. 2002. Rates of behavior and aging specified by mitochondrial function during development. *Science* **298**: 2398-2401.

Dillon J, Holden-Dye L, O'Connor V, Hopper NA. 2016. Context-dependent regulation of feeding behaviour by the insulin receptor, DAF-2, in Caenorhabditis elegans. *Invert Neurosci* **16**: 4.

Ding W, Smulan LJ, Hou NS, Taubert S, Watts JL, Walker AK. 2015. s-Adenosylmethionine Levels Govern Innate Immunity through Distinct Methylation-Dependent Pathways. *Cell Metab* **22**: 633-645.

Doble B, Woodgett JR. 2003. GSK-3: tricks of the trade for a multi-tasking kinase. *Journal of Cell Science*: 1175-1186.

Doitsidou M, Flames N, Lee AC, Boyanov A, Hobert O. 2008. Automated screening for mutants affecting dopaminergic-neuron specification in C. elegans. *Nat Methods* **5**: 869-872.

Dorn GW, 2nd, Force T. 2005. Protein kinase cascades in the regulation of cardiac hypertrophy. *J Clin Invest* **115**: 527-537.

Doudna JA, Charpentier E. 2014. Genome editing. The new frontier of genome engineering with CRISPR-Cas9. *Science* **346**: 1258096.

Dresen A, Finkbeiner S, Dottermusch M, Beume JS, Li Y, Walz G, Neumann-Haefelin E. 2015. Caenorhabditis elegans OSM-11 signaling regulates SKN-1/Nrf during embryonic development and adult longevity and stress response. *Dev Biol* **400**: 118-131.

Dupuy D, Bertin N, Hidalgo CA, Venkatesan K, Tu D, Lee D, Rosenberg J, Svrzikapa N, Blanc A, Carnec A et al. 2007. Genome-scale analysis of in vivo spatiotemporal promoter activity in Caenorhabditis elegans. *Nat Biotechnol* **25**: 663-668.

Durieux J, Wolff S, Dillin A. 2011. The cell-non-autonomous nature of electron transport chain-mediated longevity. *Cell* **144**: 79-91.

Duverger Y, Belougne J, Scaglione S, Brandli D, Beclin C, Ewbank JJ. 2007. A semi-automated high-throughput approach to the generation of transposon insertion mutants in the nematode Caenorhabditis elegans. *Nucleic Acids Res* **35**: e11.

Edgley ML, Baillie DL, Riddle DL, Rose AM. 2006. Genetic balancers. *WormBook*: 1-32.

Eisenmann DM, Maloof JN, Simske JS, Kenyon C, Kim SK. 1998. The beta-catenin homolog BAR-1 and LET-60 Ras coordinately regulate the Hox gene lin-39 during Caenorhabditis elegans vulval development. *Development* **125**: 3667-3680.

Eldar-Finkelman H, Seger R, Vandenheede JR, Krebs EG. 1995. Inactivation of glycogen synthase kinase-3 by epidermal growth factor is mediated by mitogen-activated protein kinase/p90 ribosomal protein S6 kinase signaling pathway in NIH/3T3 cells. *J Biol Chem* **270**: 987-990.

Elle IC, Olsen LC, Pultz D, Rodkaer SV, Faergeman NJ. 2010. Something worth dyeing for: molecular tools for the dissection of lipid metabolism in Caenorhabditis elegans. *FEBS Lett* **584**: 2183-2193.

Embi N, Rylatt DB, Cohen P. 1980. Glycogen synthase kinase-3 from rabbit skeletal muscle. Separation from cyclic-AMP-dependent protein kinase and phosphorylase kinase. *Eur J Biochem* **107**: 519-527.

Espelt MV, Estevez AY, Yin X, Strange K. 2005. Oscillatory Ca2+ signaling in the isolated Caenorhabditis elegans intestine: role of the inositol-1,4,5-trisphosphate receptor and phospholipases C beta and gamma. *J Gen Physiol* **126**: 379-392.

Essers MA, de Vries-Smits LM, Barker N, Polderman PE, Burgering BM, Korswagen HC. 2005. Functional interaction between beta-catenin and FOXO in oxidative stress signaling. *Science* **308**: 1181-1184.

Feng J, Bussiere F, Hekimi S. 2001. Mitochondrial electron transport is a key determinant of life span in Caenorhabditis elegans. *Dev Cell* **1**: 633-644.

Fernandez AG, Bargmann BO, Mis EK, Edgley ML, Birnbaum KD, Piano F. 2012. High-throughput fluorescence-based isolation of live C. elegans larvae. *Nat Protoc* **7**: 1502-1510.

Finkel T. 2015. The metabolic regulation of aging. *Nat Med* **21**: 1416-1423.

Fire A, Xu S, Montgomery MK, Kostas SA, Driver SE, Mello CC. 1998. Potent and specific genetic interference by double-stranded RNA in Caenorhabditis elegans. *Nature* **391**: 806-811.

Folick A, Min W, Wang MC. 2011. Label-free imaging of lipid dynamics using Coherent Anti-stokes Raman Scattering (CARS) and Stimulated Raman Scattering (SRS) microscopy. *Curr Opin Genet Dev* **21**: 585-590.

Fong S, Ng LF, Ng LT, Moore PK, Halliwell B, Gruber J. 2017. Identification of a previously undetected metabolic defect in the Complex II Caenorhabditis elegans mev-1 mutant strain using respiratory control analysis. *Biogerontology* **18**: 189-200.

Force T, Woodgett JR. 2009. Unique and overlapping functions of GSK-3 isoforms in cell differentiation and proliferation and cardiovascular development. *J Biol Chem* **284**: 9643-9647.

Forsythe ME, Love DC, Lazarus BD, Kim EJ, Prinz WA, Ashwell G, Krause MW, Hanover JA. 2006. Caenorhabditis elegans ortholog of a diabetes susceptibility locus: oga-1 (O-GlcNAcase) knockout impacts O-GlcNAc cycling, metabolism, and dauer. *Proc Natl Acad Sci U S A* **103**: 11952-11957.

Fouad AD, Pu SH, Teng S, Mark JR, Fu M, Zhang K, Huang J, Raizen DM, Fang-Yen C. 2017. Quantitative Assessment of Fat Levels in Caenorhabditis elegans Using Dark Field Microscopy. *G3 (Bethesda)* **7**: 1811-1818.

Frame S, Cohen P, Biondi RM. 2001. A common phosphate binding site explains the unique substrate specificity of GSK3 and its inactivation by phosphorylation. *Mol Cell* **7**: 1321-1327.

Fraser AG, Kamath RS, Zipperlen P, Martinez-Campos M, Sohrmann M, Ahringer J. 2000. Functional genomic analysis of C. elegans chromosome I by systematic RNA interference. *Nature* **408**: 325-330.

Frazier HN, 3rd, Roth MB. 2009. Adaptive sugar provisioning controls survival of C. elegans embryos in adverse environments. *Curr Biol* **19**: 859-863.

Friedland AE, Tzur YB, Esvelt KM, Colaiacovo MP, Church GM, Calarco JA. 2013. Heritable genome editing in C. elegans via a CRISPR-Cas9 system. *Nat Methods* **10**: 741-743.

Friedman DB, Johnson TE. 1988. A mutation in the age-1 gene in Caenorhabditis elegans lengthens life and reduces hermaphrodite fertility. *Genetics* **118**: 75-86.

Frokjaer-Jensen C. 2013. Exciting prospects for precise engineering of Caenorhabditis elegans genomes with CRISPR/Cas9. *Genetics* **195**: 635-642.

Frokjaer-Jensen C, Davis MW, Hopkins CE, Newman BJ, Thummel JM, Olesen SP, Grunnet M, Jorgensen EM. 2008. Single-copy insertion of transgenes in Caenorhabditis elegans. *Nat Genet* **40**: 1375-1383.

Furuta T, Joo HJ, Trimmer KA, Chen SY, Arur S. 2018. GSK-3 promotes S phase entry and progression in C. elegans germline stem cells to maintain tissue output. *Development*.

References

Fusaro G, Dasgupta P, Rastogi S, Joshi B, Chellappan S. 2003. Prohibitin induces the transcriptional activity of p53 and is exported from the nucleus upon apoptotic signaling. *J Biol Chem* **278**: 47853-47861.

Gallo M, Park D, Riddle DL. 2011. Increased longevity of some C. elegans mitochondrial mutants explained by activation of an alternative energy-producing pathway. *Mech Ageing Dev* **132**: 515-518.

Gamerdinger M, Hanebuth MA, Frickey T, Deuerling E. 2015. The principle of antagonism ensures protein targeting specificity at the endoplasmic reticulum. *Science* **348**: 201-207.

Gao X, Wang JY, Gao LM, Yin XF, Liu L. 2013. Identification and analysis of glycogen synthase kinase 3 beta1 interactome. *Cell Biol Int* **37**: 768-779.

Gaskova D, DeCorby A, Lemire BD. 2007. DiS-C3(3) monitoring of in vivo mitochondrial membrane potential in C. elegans. *Biochem Biophys Res Commun* **354**: 814-819.

Gatsi R, Schulze B, Rodriguez-Palero MJ, Hernando-Rodriguez B, Baumeister R, Artal-Sanz M. 2014. Prohibitin-mediated lifespan and mitochondrial stress implicate SGK-1, insulin/IGF and mTORC2 in C. elegans. *PLoS One* **9**: e107671.

Gelino S, Chang JT, Kumsta C, She X, Davis A, Nguyen C, Panowski S, Hansen M. 2016. Intestinal Autophagy Improves Healthspan and Longevity in C. elegans during Dietary Restriction. *PLoS Genet* **12**: e1006135.

Gershon H, Gershon D. 2002. Caenorhabditis elegans--a paradigm for aging research: advantages and limitations. *Mech Ageing Dev* **123**: 261-274.

Gerstbrein B, Stamatas G, Kollias N, Driscoll M. 2005. In vivo spectrofluorimetry reveals endogenous biomarkers that report healthspan and dietary restriction in Caenorhabditis elegans. *Aging Cell* **4**: 127-137.

Gerstein MB Lu ZJ Van Nostrand EL Cheng C Arshinoff BI Liu T Yip KY Robilotto R Rechtsteiner A Ikegami K et al. 2010. Integrative analysis of the Caenorhabditis elegans genome by the modENCODE project. *Science* **330**: 1775-1787.

Gill MS, Olsen A, Sampayo JN, Lithgow GJ. 2003. An automated high-throughput assay for survival of the nematode Caenorhabditis elegans. *Free Radic Biol Med* **35**: 558-565.

Girard LR, Fiedler TJ, Harris TW, Carvalho F, Antoshechkin I, Han M, Sternberg PW, Stein LD, Chalfie M. 2007. WormBook: the online review of Caenorhabditis elegans biology. *Nucleic Acids Res* **35**: D472-475.

Gleason JE, Szyleyko EA, Eisenmann DM. 2006. Multiple redundant Wnt signaling components function in two processes during C. elegans vulval development. *Dev Biol* **298**: 442-457.

References

Goldstein B, Hird SN. 1996. Specification of the anteroposterior axis in
    Caenorhabditis elegans. *Development* **122**: 1467-1474.
Gosai SJ, Kwak JH, Luke CJ, Long OS, King DE, Kovatch KJ, Johnston PA, Shun TY,
    Lazo JS, Perlmutter DH et al. 2010. Automated high-content live animal
    drug screening using C. elegans expressing the aggregation prone
    serpin alpha1-antitrypsin Z. *PLoS One* **5**: e15460.
Gotz J, Gladbach A, Pennanen L, van Eersel J, Schild A, David D, Ittner LM. 2010.
    Animal models reveal role for tau phosphorylation in human disease.
    Biochim Biophys Acta **1802**: 860-871.
Grad LI, Sayles LC, Lemire BD. 2007. Isolation and functional analysis of
    mitochondria from the nematode Caenorhabditis elegans. *Methods
    Mol Biol* **372**: 51-66.
Greenspan P, Fowler SD. 1985. Spectrofluorometric studies of the lipid probe,
    nile red. *J Lipid Res* **26**: 781-789.
Greenspan P, Mayer EP, Fowler SD. 1985. Nile red: a selective fluorescent stain
    for intracellular lipid droplets. *J Cell Biol* **100**: 965-973.
Greer EL, Dowlatshahi D, Banko MR, Villen J, Hoang K, Blanchard D, Gygi SP,
    Brunet A. 2007a. An AMPK-FOXO pathway mediates longevity induced
    by a novel method of dietary restriction in C. elegans. *Curr Biol* **17**:
    1646-1656.
Greer EL, Maures TJ, Hauswirth AG, Green EM, Leeman DS, Maro GS, Han S,
    Banko MR, Gozani O, Brunet A. 2010. Members of the H3K4
    trimethylation complex regulate lifespan in a germline-dependent
    manner in C. elegans. *Nature* **466**: 383-387.
Greer KA, Canterberry SC, Murphy KE. 2007b. Statistical analysis regarding the
    effects of height and weight on life span of the domestic dog. *Res Vet
    Sci* **82**: 208-214.
Griparic L, van der Wel NN, Orozco IJ, Peters PJ, van der Bliek AM. 2004. Loss of
    the intermembrane space protein Mgm1/OPA1 induces swelling and
    localized constrictions along the lengths of mitochondria. *J Biol Chem*
    279: 18792-18798.
Grishok A. 2005. RNAi mechanisms in Caenorhabditis elegans. *FEBS Lett* **579**:
    5932-5939.
Gronke S, Mildner A, Fellert S, Tennagels N, Petry S, Muller G, Jackle H,
    Kuhnlein RP. 2005. Brummer lipase is an evolutionary conserved fat
    storage regulator in Drosophila. *Cell Metab* **1**: 323-330.
Gruber J, Chen CB, Fong S, Ng LF, Teo E, Halliwell B. 2015. Caenorhabditis
    elegans: What We Can and Cannot Learn from Aging Worms. *Antioxid
    Redox Signal* **23**: 256-279.

References

Gusarov I, Pani B, Gautier L, Smolentseva O, Eremina S, Shamovsky I, Katkova-Zhukotskaya O, Mironov A, Nudler E. 2017. Glycogen controls Caenorhabditis elegans lifespan and resistance to oxidative stress. *Nat Commun* **8**: 15868.

Gustin MC, Albertyn J, Alexander M, Davenport K. 1998. MAP kinase pathways in the yeast Saccharomyces cerevisiae. *Microbiol Mol Biol Rev* **62**: 1264-1300.

Hamilton B, Dong Y, Shindo M, Liu W, Odell I, Ruvkun G, Lee SS. 2005. A systematic RNAi screen for longevity genes in C. elegans. *Genes Dev* **19**: 1544-1555.

Hannon GJ. 2002. RNA interference. *Nature* **418**: 244-251.

Hanover JA, Forsythe ME, Hennessey PT, Brodigan TM, Love DC, Ashwell G, Krause M. 2005. A Caenorhabditis elegans model of insulin resistance: altered macronutrient storage and dauer formation in an OGT-1 knockout. *Proc Natl Acad Sci U S A* **102**: 11266-11271.

Hansen M, Flatt T, Aguilaniu H. 2013. Reproduction, fat metabolism, and life span: what is the connection? *Cell Metab* **17**: 10-19.

Hansen M, Hsu AL, Dillin A, Kenyon C. 2005. New genes tied to endocrine, metabolic, and dietary regulation of lifespan from a Caenorhabditis elegans genomic RNAi screen. *PLoS Genet* **1**: 119-128.

Hansen M, Taubert S, Crawford D, Libina N, Lee SJ, Kenyon C. 2007. Lifespan extension by conditions that inhibit translation in Caenorhabditis elegans. *Aging Cell* **6**: 95-110.

Hardie DG. 2004. The AMP-activated protein kinase pathway--new players upstream and downstream. *J Cell Sci* **117**: 5479-5487.

Hardie DG, Hawley SA. 2001. AMP-activated protein kinase: the energy charge hypothesis revisited. *Bioessays* **23**: 1112-1119.

Hardie DG, Ross FA, Hawley SA. 2012. AMPK: a nutrient and energy sensor that maintains energy homeostasis. *Nat Rev Mol Cell Biol* **13**: 251-262.

Haynes CM, Petrova K, Benedetti C, Yang Y, Ron D. 2007. ClpP mediates activation of a mitochondrial unfolded protein response in C. elegans. *Dev Cell* **13**: 467-480.

Hellerer T, Axang C, Brackmann C, Hillertz P, Pilon M, Enejder A. 2007. Monitoring of lipid storage in Caenorhabditis elegans using coherent anti-Stokes Raman scattering (CARS) microscopy. *Proc Natl Acad Sci U S A* **104**: 14658-14663.

Henis-Korenblit S, Zhang P, Hansen M, McCormick M, Lee SJ, Cary M, Kenyon C. 2010. Insulin/IGF-1 signaling mutants reprogram ER stress response regulators to promote longevity. *Proc Natl Acad Sci U S A* **107**: 9730-9735.

Hermann GJ, Schroeder LK, Hieb CA, Kershner AM, Rabbitts BM, Fonarev P, Grant BD, Priess JR. 2005. Genetic analysis of lysosomal trafficking in Caenorhabditis elegans. *Mol Biol Cell* **16**: 3273-3288.

Hernando-Rodriguez B, Erinjeri AP, Rodriguez-Palero MJ, Millar V, Gonzalez-Hernandez S, Olmedo M, Schulze B, Baumeister R, Munoz MJ, Askjaer P et al. 2018. Combined flow cytometry and high-throughput image analysis for the study of essential genes in Caenorhabditis elegans. *BMC Biol* **16**: 36.

Hertweck M, Gobel C, Baumeister R. 2004. C. elegans SGK-1 is the critical component in the Akt/PKB kinase complex to control stress response and life span. *Dev Cell* **6**: 577-588.

Hoeflich KP, Luo J, Rubie EA, Tsao MS, Jin O, Woodgett JR. 2000. Requirement for glycogen synthase kinase-3beta in cell survival and NF-kappaB activation. *Nature* **406**: 86-90.

Holt SJ, Riddle DL. 2003. SAGE surveys C. elegans carbohydrate metabolism: evidence for an anaerobic shift in the long-lived dauer larva. *Mech Ageing Dev* **124**: 779-800.

Honda Y, Tanaka M, Honda S. 2010. Trehalose extends longevity in the nematode Caenorhabditis elegans. *Aging Cell* **9**: 558-569.

Horvath SE, Daum G. 2013. Lipids of mitochondria. *Prog Lipid Res* **52**: 590-614.

Hoshi M, Sato M, Kondo S, Takashima A, Noguchi K, Takahashi M, Ishiguro K, Imahori K. 1995. Different localization of tau protein kinase I/glycogen synthase kinase-3 beta from glycogen synthase kinase-3 alpha in cerebellum mitochondria. *J Biochem* **118**: 683-685.

Housden BE, Muhar M, Gemberling M, Gersbach CA, Stainier DY, Seydoux G, Mohr SE, Zuber J, Perrimon N. 2017. Loss-of-function genetic tools for animal models: cross-species and cross-platform differences. *Nat Rev Genet* **18**: 24-40.

Houthoofd K, Braeckman B, Vanfleteren J. 2003. Metabolism and life span determination in C. elegans. *Advances in Cell Aging and Gerontology* **14**: 143–175.

Hsin H, Kenyon C. 1999. Signals from the reproductive system regulate the lifespan of C. elegans. *Nature* **399**: 362-366.

Hsu AL, Murphy CT, Kenyon C. 2003. Regulation of aging and age-related disease by DAF-16 and heat-shock factor. *Science* **300**: 1142-1145.

Hsu P, Shi Y. 2017. Regulation of autophagy by mitochondrial phospholipids in health and diseases. *Biochim Biophys Acta* **1862**: 114-129.

Hsu PD, Lander ES, Zhang F. 2014. Development and applications of CRISPR-Cas9 for genome engineering. *Cell* **157**: 1262-1278.

Hu PJ. 2007. Dauer. *WormBook*: 1-19.

Huang C, Xiong C, Kornfeld K. 2004. Measurements of age-related changes of physiological processes that predict lifespan of Caenorhabditis elegans. *Proc Natl Acad Sci U S A* **101**: 8084-8089.

Hubbard EJ. 2014. FLP/FRT and Cre/lox recombination technology in C. elegans. *Methods* **68**: 417-424.

Hulbert AJ. 2010. Metabolism and longevity: is there a role for membrane fatty acids? *Integr Comp Biol* **50**: 808-817.

Hunter RW, Treebak JT, Wojtaszewski JF, Sakamoto K. 2011. Molecular mechanism by which AMP-activated protein kinase activation promotes glycogen accumulation in muscle. *Diabetes* **60**: 766-774.

Hwangbo DS, Gershman B, Tu MP, Palmer M, Tatar M. 2004. Drosophila dFOXO controls lifespan and regulates insulin signalling in brain and fat body. *Nature* **429**: 562-566.

Imai S, Armstrong CM, Kaeberlein M, Guarente L. 2000. Transcriptional silencing and longevity protein Sir2 is an NAD-dependent histone deacetylase. *Nature* **403**: 795-800.

Inokuchi A, Yamamoto R, Morita F, Takumi S, Matsusaki H, Ishibashi H, Tominaga N, Arizono K. 2015. Effects of lithium on growth, maturation, reproduction and gene expression in the nematode Caenorhabditis elegans. *J Appl Toxicol* **35**: 999-1006.

Iser WB, Wolkow CA. 2007. DAF-2/insulin-like signaling in C. elegans modifies effects of dietary restriction and nutrient stress on aging, stress and growth. *PLoS One* **2**: e1240.

Ishiguro K, Shiratsuchi A, Sato S, Omori A, Arioka M, Kobayashi S, Uchida T, Imahori K. 1993. Glycogen synthase kinase 3 beta is identical to tau protein kinase I generating several epitopes of paired helical filaments. *FEBS Lett* **325**: 167-172.

Ising C, Koehler S, Brahler S, Merkwirth C, Hohne M, Baris OR, Hagmann H, Kann M, Fabretti F, Dafinger C et al. 2015. Inhibition of insulin/IGF-1 receptor signaling protects from mitochondria-mediated kidney failure. *EMBO Mol Med* **7**: 275-287.

Iwata S, Yoshina S, Suehiro Y, Hori S, Mitani S. 2016. Engineering new balancer chromosomes in C. elegans via CRISPR/Cas9. *Sci Rep* **6**: 33840.

Jia K, Chen D, Riddle DL. 2004. The TOR pathway interacts with the insulin signaling pathway to regulate C. elegans larval development, metabolism and life span. *Development* **131**: 3897-3906.

Jin C, Li J, Green CD, Yu X, Tang X, Han D, Xian B, Wang D, Huang X, Cao X et al. 2011. Histone demethylase UTX-1 regulates C. elegans life span by targeting the insulin/IGF-1 signaling pathway. *Cell Metab* **14**: 161-172.

Jinek M, Chylinski K, Fonfara I, Hauer M, Doudna JA, Charpentier E. 2012. A programmable dual-RNA-guided DNA endonuclease in adaptive bacterial immunity. *Science* **337**: 816-821.

Johnson TE. 2003. Advantages and disadvantages of Caenorhabditis elegans for aging research. *Exp Gerontol* **38**: 1329-1332.

Jones KS, Alimov AP, Rilo HL, Jandacek RJ, Woollett LA, Penberthy WT. 2008. A high throughput live transparent animal bioassay to identify non-toxic small molecules or genes that regulate vertebrate fat metabolism for obesity drug development. *Nutr Metab (Lond)* **5**: 23.

Jones KT, Greer ER, Pearce D, Ashrafi K. 2009. Rictor/TORC2 regulates Caenorhabditis elegans fat storage, body size, and development through sgk-1. *PLoS Biol* **7**: e60.

Jorgensen SB, Nielsen JN, Birk JB, Olsen GS, Viollet B, Andreelli F, Schjerling P, Vaulont S, Hardie DG, Hansen BF et al. 2004. The alpha2-5'AMP-activated protein kinase is a site 2 glycogen synthase kinase in skeletal muscle and is responsive to glucose loading. *Diabetes* **53**: 3074-3081.

Jupe ER, Liu XT, Kiehlbauch JL, McClung JK, Dell'Orco RT. 1996a. The 3' untranslated region of prohibitin and cellular immortalization. *Exp Cell Res* **224**: 128-135.

-. 1996b. Prohibitin in breast cancer cell lines: loss of antiproliferative activity is linked to 3' untranslated region mutations. *Cell Growth Differ* **7**: 871-878.

Kahn FR, McFadden BA. 1980. Embryogenesis and the glyoxylate cycle. *FEBS Lett* **115**: 312-314.

Kaidanovich-Beilin O, Woodgett JR. 2011. GSK-3: Functional Insights from Cell Biology and Animal Models. *Front Mol Neurosci* **4**: 40.

Kaletsky R, Murphy CT. 2010. The role of insulin/IGF-like signaling in C. elegans longevity and aging. *Dis Model Mech* **3**: 415-419.

Kamath RS, Ahringer J. 2003. Genome-wide RNAi screening in Caenorhabditis elegans. *Methods* **30**: 313-321.

Kamath RS, Martinez-Campos M, Zipperlen P, Fraser AG, Ahringer J. 2001. Effectiveness of specific RNA-mediated interference through ingested double-stranded RNA in Caenorhabditis elegans. *Genome Biol* **2**: RESEARCH0002.

Kasashima K, Ohta E, Kagawa Y, Endo H. 2006. Mitochondrial functions and estrogen receptor-dependent nuclear translocation of pleiotropic human prohibitin 2. *J Biol Chem* **281**: 36401-36410.

Kasashima K, Sumitani M, Satoh M, Endo H. 2008. Human prohibitin 1 maintains the organization and stability of the mitochondrial nucleoids. *Exp Cell Res* **314**: 988-996.

References

Keating CD, Kriek N, Daniels M, Ashcroft NR, Hopper NA, Siney EJ, Holden-Dye L, Burke JF. 2003. Whole-genome analysis of 60 G protein-coupled receptors in Caenorhabditis elegans by gene knockout with RNAi. *Curr Biol* **13**: 1715-1720.

Kemphues K. 2005. Essential genes. *WormBook*: 1-7.

Kenyon C. 2005. The plasticity of aging: insights from long-lived mutants. *Cell* **120**: 449-460.

-. 2010a. A pathway that links reproductive status to lifespan in Caenorhabditis elegans. *Ann N Y Acad Sci* **1204**: 156-162.

Kenyon C, Chang J, Gensch E, Rudner A, Tabtiang R. 1993. A C. elegans mutant that lives twice as long as wild type. *Nature* **366**: 461-464.

Kenyon CJ. 2010b. The genetics of ageing. *Nature* **464**: 504-512.

Kershaw EE, Hamm JK, Verhagen LA, Peroni O, Katic M, Flier JS. 2006. Adipose triglyceride lipase: function, regulation by insulin, and comparison with adiponutrin. *Diabetes* **55**: 148-157.

Kim HE, Grant AR, Simic MS, Kohnz RA, Nomura DK, Durieux J, Riera CE, Sanchez M, Kapernick E, Wolff S et al. 2016. Lipid Biosynthesis Coordinates a Mitochondrial-to-Cytosolic Stress Response. *Cell* **166**: 1539-1552 e1516.

Kim S, Govindan JA, Tu ZJ, Greenstein D. 2012. SACY-1 DEAD-Box helicase links the somatic control of oocyte meiotic maturation to the sperm-to-oocyte switch and gamete maintenance in Caenorhabditis elegans. *Genetics* **192**: 905-928.

Kimble J, Sharrock WJ. 1983. Tissue-specific synthesis of yolk proteins in Caenorhabditis elegans. *Dev Biol* **96**: 189-196.

Kimura KD, Tissenbaum HA, Liu Y, Ruvkun G. 1997. daf-2, an insulin receptor-like gene that regulates longevity and diapause in Caenorhabditis elegans. *Science* **277**: 942-946.

Klapper M, Ehmke M, Palgunow D, Bohme M, Matthaus C, Bergner G, Dietzek B, Popp J, Doring F. 2011. Fluorescence-based fixative and vital staining of lipid droplets in Caenorhabditis elegans reveal fat stores using microscopy and flow cytometry approaches. *J Lipid Res* **52**: 1281-1293.

Klein PS, Melton DA. 1996. A molecular mechanism for the effect of lithium on development. *Proc Natl Acad Sci U S A* **93**: 8455-8459.

Kojima T, Kamei H, Aizu T, Arai Y, Takayama M, Nakazawa S, Ebihara Y, Inagaki H, Masui Y, Gondo Y et al. 2004. Association analysis between longevity in the Japanese population and polymorphic variants of genes involved in insulin and insulin-like growth factor 1 signaling pathways. *Exp Gerontol* **39**: 1595-1598.

References

Koopman M, Michels H, Dancy BM, Kamble R, Mouchiroud L, Auwerx J, Nollen EA, Houtkooper RH. 2016. A screening-based platform for the assessment of cellular respiration in Caenorhabditis elegans. *Nat Protoc* **11**: 1798-1816.

Kraemer BC, Burgess JK, Chen JH, Thomas JH, Schellenberg GD. 2006. Molecular pathways that influence human tau-induced pathology in Caenorhabditis elegans. *Hum Mol Genet* **15**: 1483-1496.

Krijgsveld J, Ketting RF, Mahmoudi T, Johansen J, Artal-Sanz M, Verrijzer CP, Plasterk RH, Heck AJ. 2003. Metabolic labeling of C. elegans and D. melanogaster for quantitative proteomics. *Nat Biotechnol* **21**: 927-931.

Kujoth GC, Hiona A, Pugh TD, Someya S, Panzer K, Wohlgemuth SE, Hofer T, Seo AY, Sullivan R, Jobling WA et al. 2005. Mitochondrial DNA mutations, oxidative stress, and apoptosis in mammalian aging. *Science* **309**: 481-484.

Kumar J, Barhydt T, Awasthi A, Lithgow GJ, Killilea DW, Kapahi P. 2016. Zinc Levels Modulate Lifespan through Multiple Longevity Pathways in Caenorhabditis elegans. *PLoS One* **11**: e0153513.

Kuroyanagi H, Kobayashi T, Mitani S, Hagiwara M. 2006. Transgenic alternative-splicing reporters reveal tissue-specific expression profiles and regulation mechanisms in vivo. *Nat Methods* **3**: 909-915.

Kwok TC, Ricker N, Fraser R, Chan AW, Burns A, Stanley EF, McCourt P, Cutler SR, Roy PJ. 2006. A small-molecule screen in C. elegans yields a new calcium channel antagonist. *Nature* **441**: 91-95.

Lagido C, Pettitt J, Flett A, Glover LA. 2008. Bridging the phenotypic gap: real-time assessment of mitochondrial function and metabolism of the nematode Caenorhabditis elegans. *BMC Physiol* **8**: 7.

Lakowski B, Hekimi S. 1996. Determination of life-span in Caenorhabditis elegans by four clock genes. *Science* **272**: 1010-1013.

LaMacchia JC, Frazier HN, 3rd, Roth MB. 2015. Glycogen Fuels Survival During Hyposmotic-Anoxic Stress in Caenorhabditis elegans. *Genetics* **201**: 65-74.

LaMacchia JC, Roth MB. 2015. Aquaporins-2 and -4 regulate glycogen metabolism and survival during hyposmotic-anoxic stress in Caenorhabditis elegans. *Am J Physiol Cell Physiol* **309**: C92-96.

Laplante M, Sabatini DM. 2012. mTOR signaling in growth control and disease. *Cell* **149**: 274-293.

LaRue BL, Padilla PA. 2011. Environmental and genetic preconditioning for long-term anoxia responses requires AMPK in Caenorhabditis elegans. *PLoS One* **6**: e16790.

References

Latorre I, Chesney MA, Garrigues JM, Stempor P, Appert A, Francesconi M, Strome S, Ahringer J. 2015. The DREAM complex promotes gene body H2A.Z for target repression. *Genes Dev* **29**: 495-500.

Lau KF, Miller CC, Anderton BH, Shaw PC. 1999. Expression analysis of glycogen synthase kinase-3 in human tissues. *J Pept Res* **54**: 85-91.

Le TT, Duren HM, Slipchenko MN, Hu CD, Cheng JX. 2010. Label-free quantitative analysis of lipid metabolism in living Caenorhabditis elegans. *J Lipid Res* **51**: 672-677.

Lee JH, Han JS, Kong J, Ji Y, Lv X, Lee J, Li P, Kim JB. 2016. Protein Kinase A Subunit Balance Regulates Lipid Metabolism in Caenorhabditis elegans and Mammalian Adipocytes. *J Biol Chem* **291**: 20315-20328.

Lee JH, Kong J, Jang JY, Han JS, Ji Y, Lee J, Kim JB. 2014. Lipid droplet protein LID-1 mediates ATGL-1-dependent lipolysis during fasting in Caenorhabditis elegans. *Mol Cell Biol* **34**: 4165-4176.

Lee RY, Hench J, Ruvkun G. 2001. Regulation of C. elegans DAF-16 and its human ortholog FKHRL1 by the daf-2 insulin-like signaling pathway. *Curr Biol* **11**: 1950-1957.

Lee RYN, Howe KL, Harris TW, Arnaboldi V, Cain S, Chan J, Chen WJ, Davis P, Gao S, Grove C et al. 2018. WormBase 2017: molting into a new stage. *Nucleic Acids Res* **46**: D869-D874.

Lee SS, Lee RY, Fraser AG, Kamath RS, Ahringer J, Ruvkun G. 2003. A systematic RNAi screen identifies a critical role for mitochondria in C. elegans longevity. *Nat Genet* **33**: 40-48.

Lehmann S, Bass JJ, Szewczyk NJ. 2013. Knockdown of the C. elegans kinome identifies kinases required for normal protein homeostasis, mitochondrial network structure, and sarcomere structure in muscle. *Cell Commun Signal* **11**: 71.

Lehner B, Tischler J, Fraser AG. 2006. RNAi screens in Caenorhabditis elegans in a 96-well liquid format and their application to the systematic identification of genetic interactions. *Nat Protoc* **1**: 1617-1620.

Leiser SF, Jafari G, Primitivo M, Sutphin GL, Dong J, Leonard A, Fletcher M, Kaeberlein M. 2016. Age-associated vulval integrity is an important marker of nematode healthspan. *Age (Dordr)* **38**: 419-431.

Lejeune FX, Mesrob L, Parmentier F, Bicep C, Vazquez-Manrique RP, Parker JA, Vert JP, Tourette C, Neri C. 2012. Large-scale functional RNAi screen in C. elegans identifies genes that regulate the dysfunction of mutant polyglutamine neurons. *BMC Genomics* **13**: 91.

Lemieux GA, Ashrafi K. 2015. Insights and challenges in using C. elegans for investigation of fat metabolism. *Crit Rev Biochem Mol Biol* **50**: 69-84.

References

Lemieux GA, Liu J, Mayer N, Bainton RJ, Ashrafi K, Werb Z. 2011. A whole-organism screen identifies new regulators of fat storage. *Nat Chem Biol* **7**: 206-213.

Leung CK, Deonarine A, Strange K, Choe KP. 2011. High-throughput screening and biosensing with fluorescent C. elegans strains. *J Vis Exp*.

Libina N, Berman JR, Kenyon C. 2003. Tissue-specific activities of C. elegans DAF-16 in the regulation of lifespan. *Cell* **115**: 489-502.

Lin K, Dorman JB, Rodan A, Kenyon C. 1997. daf-16: An HNF-3/forkhead family member that can function to double the life-span of Caenorhabditis elegans. *Science* **278**: 1319-1322.

Lin R. 2003. A gain-of-function mutation in oma-1, a C. elegans gene required for oocyte maturation, results in delayed degradation of maternal proteins and embryonic lethality. *Dev Biol* **258**: 226-239.

Lithgow GJ, White TM, Melov S, Johnson TE. 1995. Thermotolerance and extended life-span conferred by single-gene mutations and induced by thermal stress. *Proc Natl Acad Sci U S A* **92**: 7540-7544.

Liu F, Thatcher JD, Barral JM, Epstein HF. 1995. Bifunctional glyoxylate cycle protein of Caenorhabditis elegans: a developmentally regulated protein of intestine and muscle. *Dev Biol* **169**: 399-414.

Liu X, Jiang N, Hughes B, Bigras E, Shoubridge E, Hekimi S. 2005. Evolutionary conservation of the clk-1-dependent mechanism of longevity: loss of mclk1 increases cellular fitness and lifespan in mice. *Genes Dev* **19**: 2424-2434.

Liu Z, Li X, Ge Q, Ding M, Huang X. 2014. A lipid droplet-associated GFP reporter-based screen identifies new fat storage regulators in C. elegans. *J Genet Genomics* **41**: 305-313.

Lopez-Otin C, Blasco MA, Partridge L, Serrano M, Kroemer G. 2013. The hallmarks of aging. *Cell* **153**: 1194-1217.

Lourenco AB, Munoz-Jimenez C, Venegas-Caleron M, Artal-Sanz M. 2015. Analysis of the effect of the mitochondrial prohibitin complex, a context-dependent modulator of longevity, on the C. elegans metabolome. *Biochim Biophys Acta* **1847**: 1457-1468.

Luptak I, Shen M, He H, Hirshman MF, Musi N, Goodyear LJ, Yan J, Wakimoto H, Morita H, Arad M et al. 2007. Aberrant activation of AMP-activated protein kinase remodels metabolic network in favor of cardiac glycogen storage. *J Clin Invest* **117**: 1432-1439.

Luz AL, Rooney JP, Kubik LL, Gonzalez CP, Song DH, Meyer JN. 2015. Mitochondrial Morphology and Fundamental Parameters of the Mitochondrial Respiratory Chain Are Altered in Caenorhabditis elegans

Strains Deficient in Mitochondrial Dynamics and Homeostasis Processes. *PLoS One* **10**: e0130940.

MacAulay K, Doble BW, Patel S, Hansotia T, Sinclair EM, Drucker DJ, Nagy A, Woodgett JR. 2007. Glycogen synthase kinase 3alpha-specific regulation of murine hepatic glycogen metabolism. *Cell Metab* **6**: 329-337.

MacNeil LT, Watson E, Arda HE, Zhu LJ, Walhout AJ. 2013. Diet-induced developmental acceleration independent of TOR and insulin in C. elegans. *Cell* **153**: 240-252.

Maduro MF, Meneghini MD, Bowerman B, Broitman-Maduro G, Rothman JH. 2001. Restriction of Mesendoderm to a Single Blastomere by the Combined Action of SKN-1 and a GSK-3beta Homolog Is Mediated by MED-1 and -2 in C. elegans. *Molecular Cell* **7**: 475-485.

Maglioni S, Arsalan N, Franchi L, Hurd A, Opipari AW, Glick GD, Ventura N. 2015. An automated phenotype-based microscopy screen to identify pro-longevity interventions acting through mitochondria in C. elegans. *Biochim Biophys Acta* **1847**: 1469-1478.

Maia AF, Tanenbaum ME, Galli M, Lelieveld D, Egan DA, Gassmann R, Sunkel CE, van den Heuvel S, Medema RH. 2015. Genome-wide RNAi screen for synthetic lethal interactions with the C. elegans kinesin-5 homolog BMK-1. *Sci Data* **2**: 150020.

Mak HY. 2012. Lipid droplets as fat storage organelles in Caenorhabditis elegans: Thematic Review Series: Lipid Droplet Synthesis and Metabolism: from Yeast to Man. *J Lipid Res* **53**: 28-33.

-. 2013. Visualization of lipid droplets in C. elegans by light and electron microscopy. *Methods Cell Biol* **116**: 39-51.

Mak HY, Nelson LS, Basson M, Johnson CD, Ruvkun G. 2006. Polygenic control of Caenorhabditis elegans fat storage. *Nat Genet* **38**: 363-368.

Malhi GS, Tanious M. 2011. Optimal frequency of lithium administration in the treatment of bipolar disorder: clinical and dosing considerations. *CNS Drugs* **25**: 289-298.

Manning G. 2005. Genomic overview of protein kinases. *WormBook*: 1-19.

Manning G, Plowman GD, Hunter T, Sudarsanam S. 2002a. Evolution of protein kinase signaling from yeast to man. *Trends Biochem Sci* **27**: 514-520.

Manning G, Whyte DB, Martinez R, Hunter T, Sudarsanam S. 2002b. The protein kinase complement of the human genome. *Science* **298**: 1912-1934.

Markussen LK, Winther S, Wicksteed B, Hansen JB. 2018. GSK3 is a negative regulator of the thermogenic program in brown adipocytes. *Sci Rep* **8**: 3469.

Maro GS, Klassen MP, Shen K. 2009. A beta-catenin-dependent Wnt pathway mediates anteroposterior axon guidance in C. elegans motor neurons. *PLoS One* **4**: e4690.

Martinez A, Gil C, Perez DI. 2011. Glycogen synthase kinase 3 inhibitors in the next horizon for Alzheimer's disease treatment. *Int J Alzheimers Dis* **2011**: 280502.

Mashek DG, Coleman RA. 2006. Cellular fatty acid uptake: the contribution of metabolism. *Curr Opin Lipidol* **17**: 274-278.

Mathew MD, Mathew ND, Ebert PR. 2012. WormScan: a technique for high-throughput phenotypic analysis of Caenorhabditis elegans. *PLoS One* **7**: e33483.

Matsagas K, Lim DB, Horwitz M, Rizza CL, Mueller LD, Villeponteau B, Rose MR. 2009. Long-term functional side-effects of stimulants and sedatives in Drosophila melanogaster. *PLoS One* **4**: e6578.

Maures TJ, Greer EL, Hauswirth AG, Brunet A. 2011. The H3K27 demethylase UTX-1 regulates C. elegans lifespan in a germline-independent, insulin-dependent manner. *Aging Cell* **10**: 980-990.

McClung JK, Danner DB, Stewart DA, Smith JR, Schneider EL, Lumpkin CK, Dell'Orco RT, Nuell MJ. 1989. Isolation of a cDNA that hybrid selects antiproliferative mRNA from rat liver. *Biochem Biophys Res Commun* **164**: 1316-1322.

McClung JK, Jupe ER, Liu XT, Dell'Orco RT. 1995. Prohibitin: potential role in senescence, development, and tumor suppression. *Exp Gerontol* **30**: 99-124.

McColl G, Killilea DW, Hubbard AE, Vantipalli MC, Melov S, Lithgow GJ. 2008. Pharmacogenetic analysis of lithium-induced delayed aging in Caenorhabditis elegans. *J Biol Chem* **283**: 350-357.

McKay RM, McKay JP, Avery L, Graff JM. 2003. C elegans: a model for exploring the genetics of fat storage. *Dev Cell* **4**: 131-142.

McQuary PR, Liao CY, Chang JT, Kumsta C, She X, Davis A, Chu CC, Gelino S, Gomez-Amaro RL, Petrascheck M et al. 2016. C. elegans S6K Mutants Require a Creatine-Kinase-like Effector for Lifespan Extension. *Cell Rep* **14**: 2059-2067.

Medkour Y, Dakik P, McAuley M, Mohammad K, Mitrofanova D, Titorenko VI. 2017. Mechanisms Underlying the Essential Role of Mitochondrial Membrane Lipids in Yeast Chronological Aging. *Oxid Med Cell Longev* **2017**: 2916985.

Megalou EV, Tavernarakis N. 2009. Autophagy in Caenorhabditis elegans. *Biochim Biophys Acta* **1793**: 1444-1451.

References

Meijer L, Flajolet M, Greengard P. 2004. Pharmacological inhibitors of glycogen synthase kinase 3. *Trends Pharmacol Sci* **25**: 471-480.

Melendez A, Levine B. 2009. Autophagy in C. elegans. *WormBook*: 1-26.

Melendez A, Talloczy Z, Seaman M, Eskelinen EL, Hall DH, Levine B. 2003. Autophagy genes are essential for dauer development and life-span extension in C. elegans. *Science* **301**: 1387-1391.

Mello CC, Kramer JM, Stinchcomb D, Ambros V. 1991. Efficient gene transfer in C.elegans: extrachromosomal maintenance and integration of transforming sequences. *EMBO J* **10**: 3959-3970.

Mengwasser J, Piau A, Schlag P, Sleeman JP. 2004. Differential immunization identifies PHB1/PHB2 as blood-borne tumor antigens. *Oncogene* **23**: 7430-7435.

Merkwirth C, Dargazanli S, Tatsuta T, Geimer S, Lower B, Wunderlich FT, von Kleist-Retzow JC, Waisman A, Westermann B, Langer T. 2008. Prohibitins control cell proliferation and apoptosis by regulating OPA1-dependent cristae morphogenesis in mitochondria. *Genes Dev* **22**: 476-488.

Merkwirth C, Langer T. 2009. Prohibitin function within mitochondria: essential roles for cell proliferation and cristae morphogenesis. *Biochim Biophys Acta* **1793**: 27-32.

Merkwirth C, Martinelli P, Korwitz A, Morbin M, Bronneke HS, Jordan SD, Rugarli EI, Langer T. 2012. Loss of prohibitin membrane scaffolds impairs mitochondrial architecture and leads to tau hyperphosphorylation and neurodegeneration. *PLoS Genet* **8**: e1003021.

Miedel MT, Graf NJ, Stephen KE, Long OS, Pak SC, Perlmutter DH, Silverman GA, Luke CJ. 2012. A pro-cathepsin L mutant is a luminal substrate for endoplasmic-reticulum-associated degradation in C. elegans. *PLoS One* **7**: e40145.

Miller JR. 2002. The Wnts. *Genome Biol* **3**: REVIEWS3001.

Miyamoto L, Toyoda T, Hayashi T, Yonemitsu S, Nakano M, Tanaka S, Ebihara K, Masuzaki H, Hosoda K, Ogawa Y et al. 2007. Effect of acute activation of 5'-AMP-activated protein kinase on glycogen regulation in isolated rat skeletal muscle. *J Appl Physiol (1985)* **102**: 1007-1013.

Mok CA, Au V, Thompson OA, Edgley ML, Gevirtzman L, Yochem J, Lowry J, Memar N, Wallenfang MR, Rasoloson D et al. 2017. MIP-MAP: High Throughput Mapping of Caenorhabditis elegans Temperature-Sensitive Mutants via Molecular Inversion Probes. *Genetics*.

Morris DL. 1946. Colorimetric determination of glycogen; disadvantages of the iodine method. *J Biol Chem* **166**: 199-203.

References

Moy TI, Conery AL, Larkins-Ford J, Wu G, Mazitschek R, Casadei G, Lewis K, Carpenter, A E and Ausubel, F M. 2009. High-Throughput Screen for Novel Antimicrobials using a Whole Animal Infection Model. *American Chemical Society Chemical Biology*.

Mullaney BC, Ashrafi K. 2009. C. elegans fat storage and metabolic regulation. *Biochim Biophys Acta* **1791**: 474-478.

Mullaney BC, Blind RD, Lemieux GA, Perez CL, Elle IC, Faergeman NJ, Van Gilst MR, Ingraham HA, Ashrafi K. 2010. Regulation of C. elegans fat uptake and storage by acyl-CoA synthase-3 is dependent on NR5A family nuclear hormone receptor nhr-25. *Cell Metab* **12**: 398-410.

Munoz-Jimenez C, Ayuso C, Dobrzynska A, Torres-Mendez A, Ruiz PC, Askjaer P. 2017. An Efficient FLP-Based Toolkit for Spatiotemporal Control of Gene Expression in Caenorhabditis elegans. *Genetics* **206**: 1763-1778.

Murphy CT, McCarroll SA, Bargmann CI, Fraser A, Kamath RS, Ahringer J, Li H, Kenyon C. 2003. Genes that act downstream of DAF-16 to influence the lifespan of Caenorhabditis elegans. *Nature* **424**: 277-283.

Nagarajan A, Ning Y, Reisner K, Buraei Z, Larsen JP, Hobert O, Doitsidou M. 2014. Progressive degeneration of dopaminergic neurons through TRP channel-induced cell death. *J Neurosci* **34**: 5738-5746.

Narbonne P, Roy R. 2009. Caenorhabditis elegans dauers need LKB1/AMPK to ration lipid reserves and ensure long-term survival. *Nature* **457**: 210-214.

Nargund AM, Fiorese CJ, Pellegrino MW, Deng P, Haynes CM. 2015. Mitochondrial and nuclear accumulation of the transcription factor ATFS-1 promotes OXPHOS recovery during the UPR(mt). *Mol Cell* **58**: 123-133.

Nargund AM, Pellegrino MW, Fiorese CJ, Baker BM, Haynes CM. 2012. Mitochondrial import efficiency of ATFS-1 regulates mitochondrial UPR activation. *Science* **337**: 587-590.

Nielson JR, Rutter JP. 2018. Lipid-mediated signals that regulate mitochondrial biology. *J Biol Chem* **293**: 7517-7521.

Nijtmans LG, Artal SM, Grivell LA, Coates PJ. 2002. The mitochondrial PHB complex: roles in mitochondrial respiratory complex assembly, ageing and degenerative disease. *Cell Mol Life Sci* **59**: 143-155.

Nijtmans LG, de Jong L, Artal Sanz M, Coates PJ, Berden JA, Back JW, Muijsers AO, van der Spek H, Grivell LA. 2000. Prohibitins act as a membrane-bound chaperone for the stabilization of mitochondrial proteins. *EMBO J* **19**: 2444-2451.

Nishi Y, Lin R. 2005. DYRK2 and GSK-3 phosphorylate and promote the timely degradation of OMA-1, a key regulator of the oocyte-to-embryo transition in C. elegans. *Dev Biol* **288**: 139-149.

Nuell MJ, Stewart DA, Walker L, Friedman V, Wood CM, Owens GA, Smith JR, Schneider EL, Dell' Orco R, Lumpkin CK et al. 1991. Prohibitin, an evolutionarily conserved intracellular protein that blocks DNA synthesis in normal fibroblasts and HeLa cells. *Mol Cell Biol* **11**: 1372-1381.

O'Neill C, Kiely AP, Coakley MF, Manning S, Long-Smith CM. 2012. Insulin and IGF-1 signalling: longevity, protein homoeostasis and Alzheimer's disease. *Biochem Soc Trans* **40**: 721-727.

O'Reilly LP, Knoerdel RR, Silverman GA, Pak SC. 2016. High-Throughput, Liquid-Based Genome-Wide RNAi Screening in C. elegans. *Methods Mol Biol* **1470**: 151-162.

O'Rourke EJ, Conery AL, Moy TI. 2009a. Whole-animal high-throughput screens: the C. elegans model. *Methods Mol Biol* **486**: 57-75.

O'Rourke EJ, Soukas AA, Carr CE, Ruvkun G. 2009b. C. elegans major fats are stored in vesicles distinct from lysosome-related organelles. *Cell Metab* **10**: 430-435.

Olmedo M, Geibel M, Artal-Sanz M, Merrow M. 2015. A High-Throughput Method for the Analysis of Larval Developmental Phenotypes in Caenorhabditis elegans. *Genetics* **201**: 443-448.

Onken B, Driscoll M. 2010. Metformin induces a dietary restriction-like state and the oxidative stress response to extend C. elegans Healthspan via AMPK, LKB1, and SKN-1. *PLoS One* **5**: e8758.

Osman C, Haag M, Potting C, Rodenfels J, Dip PV, Wieland FT, Brugger B, Westermann B, Langer T. 2009. The genetic interactome of prohibitins: coordinated control of cardiolipin and phosphatidylethanolamine by conserved regulators in mitochondria. *J Cell Biol* **184**: 583-596.

Osman C, Voelker DR, Langer T. 2011. Making heads or tails of phospholipids in mitochondria. *J Cell Biol* **192**: 7-16.

Paradies G, Paradies V, De Benedictis V, Ruggiero FM, Petrosillo G. 2014. Functional role of cardiolipin in mitochondrial bioenergetics. *Biochim Biophys Acta* **1837**: 408-417.

Park SE, Xu J, Frolova A, Liao L, O'Malley BW, Katzenellenbogen BS. 2005. Genetic deletion of the repressor of estrogen receptor activity (REA) enhances the response to estrogen in target tissues in vivo. *Mol Cell Biol* **25**: 1989-1999.

Parker PJ, Caudwell FB, Cohen P. 1983. Glycogen synthase from rabbit skeletal muscle; effect of insulin on the state of phosphorylation of the seven phosphoserine residues in vivo. *Eur J Biochem* **130**: 227-234.

Patel P, Woodgett JR. 2017. Glycogen Synthase Kinase 3: A Kinase for All Pathways? *Curr Top Dev Biol* **123**: 277-302.

Patel S, Doble BW, MacAulay K, Sinclair EM, Drucker DJ, Woodgett JR. 2008. Tissue-specific role of glycogen synthase kinase 3beta in glucose homeostasis and insulin action. *Mol Cell Biol* **28**: 6314-6328.

Pellegrino MW, Nargund AM, Kirienko NV, Gillis R, Fiorese CJ, Haynes CM. 2014. Mitochondrial UPR-regulated innate immunity provides resistance to pathogen infection. *Nature* **516**: 414-417.

Perez CL, Van Gilst MR. 2008. A 13C isotope labeling strategy reveals the influence of insulin signaling on lipogenesis in C. elegans. *Cell Metab* **8**: 266-274.

Petrascheck M, Ye X, Buck LB. 2007. An antidepressant that extends lifespan in adult Caenorhabditis elegans. *Nature* **450**: 553-556.

-. 2009. A high-throughput screen for chemicals that increase the lifespan of Caenorhabditis elegans. *Ann N Y Acad Sci* **1170**: 698-701.

Plowman GD, Sudarsanam S, Bingham J, Whyte D, Hunter T. 1999. The protein kinases of Caenorhabditis elegans: a model for signal transduction in multicellular organisms. *Proc Natl Acad Sci U S A* **96**: 13603-13610.

Plyte SE, Hughes K, Nikolakaki E, Pulverer BJ, Woodgett JR. 1992. Glycogen synthase kinase-3: functions in oncogenesis and development. *Biochim Biophys Acta* **1114**: 147-162.

Possik E, Ajisebutu A, Manteghi S, Gingras MC, Vijayaraghavan T, Flamand M, Coull B, Schmeisser K, Duchaine T, van Steensel M et al. 2015. FLCN and AMPK Confer Resistance to Hyperosmotic Stress via Remodeling of Glycogen Stores. *PLoS Genet* **11**: e1005520.

Praitis V, Casey E, Collar D, Austin J. 2001. Creation of low-copy integrated transgenic lines in Caenorhabditis elegans. *Genetics* **157**: 1217-1226.

Pulak R. 2006. Techniques for analysis, sorting, and dispensing of C. elegans on the COPAS flow-sorting system. *Methods Mol Biol* **351**: 275-286.

Pulliam DA, Bhattacharya A, Van Remmen H. 2013. Mitochondrial dysfunction in aging and longevity: a causal or protective role? *Antioxid Redox Signal* **19**: 1373-1387.

Qadota H, Inoue M, Hikita T, Koppen M, Hardin JD, Amano M, Moerman DG, Kaibuchi K. 2007. Establishment of a tissue-specific RNAi system in C. elegans. *Gene* **400**: 166-173.

Qi W, Yan Y, Pfeifer D, Donner VGE, Wang Y, Maier W, Baumeister R. 2017. C. elegans DAF-16/FOXO interacts with TGF-ss/BMP signaling to induce

germline tumor formation via mTORC1 activation. *PLoS Genet* **13**: e1006801.

Ramot D, Johnson BE, Berry TL, Jr., Carnell L, Goodman MB. 2008. The Parallel Worm Tracker: a platform for measuring average speed and drug-induced paralysis in nematodes. *PLoS One* **3**: e2208.

Rappleye CA, Tagawa A, Le Bot N, Ahringer J, Aroian RV. 2003. Involvement of fatty acid pathways and cortical interaction of the pronuclear complex in Caenorhabditis elegans embryonic polarity. *BMC Dev Biol* **3**: 8.

Rea SL, Ventura N, Johnson TE. 2007. Relationship between mitochondrial electron transport chain dysfunction, development, and life extension in Caenorhabditis elegans. *PLoS Biol* **5**: e259.

Rea SL, Wu D, Cypser JR, Vaupel JW, Johnson TE. 2005. A stress-sensitive reporter predicts longevity in isogenic populations of Caenorhabditis elegans. *Nat Genet* **37**: 894-898.

Rera M, Azizi MJ, Walker DW. 2013. Organ-specific mediation of lifespan extension: more than a gut feeling? *Ageing Res Rev* **12**: 436-444.

Riddle DL, Swanson MM, Albert PS. 1981. Interacting genes in nematode dauer larva formation. *Nature* **290**: 668-671.

Rieckher M, Kourtis N, Pasparaki A, Tavernarakis N. 2009. Transgenesis in Caenorhabditis elegans. *Methods Mol Biol* **561**: 21-39.

Rogina B, Helfand SL. 2004. Sir2 mediates longevity in the fly through a pathway related to calorie restriction. *Proc Natl Acad Sci U S A* **101**: 15998-16003.

Roh HC, Collier S, Guthrie J, Robertson JD, Kornfeld K. 2012. Lysosome-related organelles in intestinal cells are a zinc storage site in C. elegans. *Cell Metab* **15**: 88-99.

Ron D, Walter P. 2007. Signal integration in the endoplasmic reticulum unfolded protein response. *Nat Rev Mol Cell Biol* **8**: 519-529.

Rooney JP, Luz AL, Gonzalez-Hunt CP, Bodhicharla R, Ryde IT, Anbalagan C, Meyer JN. 2014. Effects of 5'-fluoro-2-deoxyuridine on mitochondrial biology in Caenorhabditis elegans. *Exp Gerontol* **56**: 69-76.

Rual JF, Ceron J, Koreth J, Hao T, Nicot AS, Hirozane-Kishikawa T, Vandenhaute J, Orkin SH, Hill DE, van den Heuvel S et al. 2004. Toward improving Caenorhabditis elegans phenome mapping with an ORFeome-based RNAi library. *Genome Res* **14**: 2162-2168.

Ruaud AF, Katic I, Bessereau JL. 2011. Insulin/Insulin-like growth factor signaling controls non-Dauer developmental speed in the nematode Caenorhabditis elegans. *Genetics* **187**: 337-343.

Ruegger S, Miki TS, Hess D, Grosshans H. 2015. The ribonucleotidyl transferase USIP-1 acts with SART3 to promote U6 snRNA recycling. *Nucleic Acids Res* **43**: 3344-3357.

Ryves WJ, Harwood AJ. 2001. Lithium inhibits glycogen synthase kinase-3 by competition for magnesium. *Biochem Biophys Res Commun* **280**: 720-725.

Saldivia M, Ceballos-Perez G, Bart JM, Navarro M. 2016. The AMPKalpha1 Pathway Positively Regulates the Developmental Transition from Proliferation to Quiescence in Trypanosoma brucei. *Cell Rep* **17**: 660-670.

Salway JG. 2004. *Metabolism at a Glance*.

Samuelson AV, Carr CE, Ruvkun G. 2007. Gene activities that mediate increased life span of C. elegans insulin-like signaling mutants. *Genes Dev* **21**: 2976-2994.

Sawa H, Korswagen HC. 2013. Wnt signaling in C. elegans. *WormBook*: 1-30.

Schenkel LC, Bakovic M. 2014. Formation and regulation of mitochondrial membranes. *Int J Cell Biol* **2014**: 709828.

Schleit J, Johnson SC, Bennett CF, Simko M, Trongtham N, Castanza A, Hsieh EJ, Moller RM, Wasko BM, Delaney JR et al. 2013. Molecular mechanisms underlying genotype-dependent responses to dietary restriction. *Aging Cell* **12**: 1050-1061.

Schlesinger A, Shelton CA, Maloof JN, Meneghini M, Bowerman B. 1999. Wnt pathway components orient a mitotic spindle in the early Caenorhabditis elegans embryo without requiring gene transcription in the responding cell. *Genes Dev* **13**: 2028-2038.

Schneider WJ. 1996. Vitellogenin receptors: oocyte-specific members of the low-density lipoprotein receptor supergene family. *Int Rev Cytol* **166**: 103-137.

Schroeder LK, Kremer S, Kramer MJ, Currie E, Kwan E, Watts JL, Lawrenson AL, Hermann GJ. 2007. Function of the Caenorhabditis elegans ABC transporter PGP-2 in the biogenesis of a lysosome-related fat storage organelle. *Mol Biol Cell* **18**: 995-1008.

Schwartz ML, Jorgensen EM. 2016. SapTrap, a Toolkit for High-Throughput CRISPR/Cas9 Gene Modification in Caenorhabditis elegans. *Genetics* **202**: 1277-1288.

Seah NE, de Magalhaes Filho CD, Petrashen AP, Henderson HR, Laguer J, Gonzalez J, Dillin A, Hansen M, Lapierre LR. 2016. Autophagy-mediated longevity is modulated by lipoprotein biogenesis. *Autophagy* **12**: 261-272.

References

Seo Y, Kingsley S, Walker G, Mondoux MA, Tissenbaum HA. 2018. Metabolic shift from glycogen to trehalose promotes lifespan and healthspan in Caenorhabditis elegans. *Proc Natl Acad Sci U S A* **115**: E2791-E2800.

Shatz O, Holland P, Elazar Z, Simonsen A. 2016. Complex Relations Between Phospholipids, Autophagy, and Neutral Lipids. *Trends Biochem Sci* **41**: 907-923.

Sheaffer KL, Updike DL, Mango SE. 2008. The Target of Rapamycin pathway antagonizes pha-4/FoxA to control development and aging. *Curr Biol* **18**: 1355-1364.

Shi X, Li J, Zou X, Greggain J, Rodkaer SV, Faergeman NJ, Liang B, Watts JL. 2013. Regulation of lipid droplet size and phospholipid composition by stearoyl-CoA desaturase. *J Lipid Res* **54**: 2504-2514.

Shirayama M, Soto MC, Ishidate T, Kim S, Nakamura K, Bei Y, van den Heuvel S, Mello CC. 2006. The Conserved Kinases CDK-1, GSK-3, KIN-19, and MBK-2 Promote OMA-1 Destruction to Regulate the Oocyte-to-Embryo Transition in C. elegans. *Curr Biol* **16**: 47-55.

Short KR, Bigelow ML, Kahl J, Singh R, Coenen-Schimke J, Raghavakaimal S, Nair KS. 2005. Decline in skeletal muscle mitochondrial function with aging in humans. *Proc Natl Acad Sci U S A* **102**: 5618-5623.

Sieber MH, Thomsen MB, Spradling AC. 2016. Electron Transport Chain Remodeling by GSK3 during Oogenesis Connects Nutrient State to Reproduction. *Cell* **164**: 420-432.

Siegfried E, Perkins LA, Capaci TM, Perrimon N. 1990. Putative protein kinase product of the Drosophila segment-polarity gene zeste-white3. *Nature* **345**: 825-829.

Sin O, Michels H, Nollen EA. 2014. Genetic screens in Caenorhabditis elegans models for neurodegenerative diseases. *Biochim Biophys Acta* **1842**: 1951-1959.

Sinha D, Wang Z, Ruchalski KL, Levine JS, Krishnan S, Lieberthal W, Schwartz JH, Borkan SC. 2005. Lithium activates the Wnt and phosphatidylinositol 3-kinase Akt signaling pathways to promote cell survival in the absence of soluble survival factors. *Am J Physiol Renal Physiol* **288**: F703-713.

Sofola-Adesakin O, Castillo-Quan JI, Rallis C, Tain LS, Bjedov I, Rogers I, Li L, Martinez P, Khericha M, Cabecinha M et al. 2014. Lithium suppresses Abeta pathology by inhibiting translation in an adult Drosophila model of Alzheimer's disease. *Front Aging Neurosci* **6**: 190.

Soukas AA, Carr CE, Ruvkun G. 2013. Genetic regulation of Caenorhabditis elegans lysosome related organelle function. *PLoS Genet* **9**: e1003908.

Soukas AA, Kane EA, Carr CE, Melo JA, Ruvkun G. 2009. Rictor/TORC2 regulates fat metabolism, feeding, growth, and life span in Caenorhabditis elegans. *Genes Dev* **23**: 496-511.

Spieth J, Blumenthal T. 1985. The Caenorhabditis elegans vitellogenin gene family includes a gene encoding a distantly related protein. *Mol Cell Biol* **5**: 2495-2501.

Squiban B, Belougne J, Ewbank J, Zugasti O. 2012. Quantitative and automated high-throughput genome-wide RNAi screens in C. elegans. *J Vis Exp*.

Srinivasan S, Sadegh L, Elle IC, Christensen AG, Faergeman NJ, Ashrafi K. 2008. Serotonin regulates C. elegans fat and feeding through independent molecular mechanisms. *Cell Metab* **7**: 533-544.

Stambolic V, Ruel L, Woodgett JR. 1996. Lithium inhibits glycogen synthase kinase-3 activity and mimics wingless signalling in intact cells. *Curr Biol* **6**: 1664-1668.

Steglich G, Neupert W, Langer T. 1999. Prohibitins regulate membrane protein degradation by the m-AAA protease in mitochondria. *Mol Cell Biol* **19**: 3435-3442.

Stiernagle T. 2006. Maintenance of C. elegans. *WormBook*: 1-11.

Stroustrup N, Ulmschneider BE, Nash ZM, Lopez-Moyado IF, Apfeld J, Fontana W. 2013. The Caenorhabditis elegans Lifespan Machine. *Nat Methods* **10**: 665-670.

Suh Y, Atzmon G, Cho MO, Hwang D, Liu B, Leahy DJ, Barzilai N, Cohen P. 2008. Functionally significant insulin-like growth factor I receptor mutations in centenarians. *Proc Natl Acad Sci U S A* **105**: 3438-3442.

Sun L, Liu L, Yang XJ, Wu Z. 2004. Akt binds prohibitin 2 and relieves its repression of MyoD and muscle differentiation. *J Cell Sci* **117**: 3021-3029.

Sutherland C. 2011. What Are the bona fide GSK3 Substrates? *Int J Alzheimers Dis* **2011**: 505607.

Sutherland C, Leighton IA, Cohen P. 1993. Inactivation of glycogen synthase kinase-3 beta by phosphorylation: new kinase connections in insulin and growth-factor signalling. *Biochem J* **296 (Pt 1)**: 15-19.

Sutphin GL, Kaeberlein M. 2009. Measuring Caenorhabditis elegans life span on solid media. *J Vis Exp*.

Suzuki T, Bridges D, Nakada D, Skiniotis G, Morrison SJ, Lin JD, Saltiel AR, Inoki K. 2013. Inhibition of AMPK catabolic action by GSK3. *Mol Cell* **50**: 407-419.

Swierczek NA, Giles AC, Rankin CH, Kerr RA. 2011. High-throughput behavioral analysis in C. elegans. *Nat Methods* **8**: 592-598.

Tabara H, Grishok A, Mello CC. 1998. RNAi in C. elegans: soaking in the genome sequence. *Science* **282**: 430-431.

Taelman VF, Dobrowolski R, Plouhinec JL, Fuentealba LC, Vorwald PP, Gumper I, Sabatini DD, De Robertis EM. 2010. Wnt signaling requires sequestration of glycogen synthase kinase 3 inside multivesicular endosomes. *Cell* **143**: 1136-1148.

Tam ZY, Gruber J, Ng LF, Halliwell B, Gunawan R. 2014. Effects of lithium on age-related decline in mitochondrial turnover and function in Caenorhabditis elegans. *J Gerontol A Biol Sci Med Sci* **69**: 810-820.

Tatar M, Kopelman A, Epstein D, Tu MP, Yin CM, Garofalo RS. 2001. A mutant Drosophila insulin receptor homolog that extends life-span and impairs neuroendocrine function. *Science* **292**: 107-110.

Taubert S, Van Gilst MR, Hansen M, Yamamoto KR. 2006. A Mediator subunit, MDT-15, integrates regulation of fatty acid metabolism by NHR-49-dependent and -independent pathways in C. elegans. *Genes Dev* **20**: 1137-1149.

Tavernarakis N, Wang SL, Dorovkov M, Ryazanov A, Driscoll M. 2000. Heritable and inducible genetic interference by double-stranded RNA encoded by transgenes. *Nat Genet* **24**: 180-183.

Tepper RG, Ashraf J, Kaletsky R, Kleemann G, Murphy CT, Bussemaker HJ. 2013. PQM-1 complements DAF-16 as a key transcriptional regulator of DAF-2-mediated development and longevity. *Cell* **154**: 676-690.

Terashima M, Kim KM, Adachi T, Nielsen PJ, Reth M, Kohler G, Lamers MC. 1994. The IgM antigen receptor of B lymphocytes is associated with prohibitin and a prohibitin-related protein. *EMBO J* **13**: 3782-3792.

Theiss AL, Sitaraman SV. 2011. The role and therapeutic potential of prohibitin in disease. *Biochim Biophys Acta* **1813**: 1137-1143.

Timmons L, Court DL, Fire A. 2001. Ingestion of bacterially expressed dsRNAs can produce specific and potent genetic interference in Caenorhabditis elegans. *Gene* **263**: 103-112.

Timmons L, Fire A. 1998. Specific interference by ingested dsRNA. *Nature* **395**: 854.

Tissenbaum HA. 2015. Using C. elegans for aging research. *Invertebr Reprod Dev* **59**: 59-63.

Tissenbaum HA, Guarente L. 2001. Increased dosage of a sir-2 gene extends lifespan in Caenorhabditis elegans. *Nature* **410**: 227-230.

Trifunovic A, Wredenberg A, Falkenberg M, Spelbrink JN, Rovio AT, Bruder CE, Bohlooly YM, Gidlof S, Oldfors A, Wibom R et al. 2004. Premature ageing in mice expressing defective mitochondrial DNA polymerase. *Nature* **429**: 417-423.

References

Tsang WY, Lemire BD. 2003. The role of mitochondria in the life of the nematode, Caenorhabditis elegans. *Biochim Biophys Acta* **1638**: 91-105.

Tullet JM, Hertweck M, An JH, Baker J, Hwang JY, Liu S, Oliveira RP, Baumeister R, Blackwell TK. 2008. Direct inhibition of the longevity-promoting factor SKN-1 by insulin-like signaling in C. elegans. *Cell* **132**: 1025-1038.

Twumasi-Boateng K, Berg M, Shapira M. 2014. Automated separation of C. elegans variably colonized by a bacterial pathogen. *J Vis Exp*.

Tzur YB, Friedland AE, Nadarajan S, Church GM, Calarco JA, Colaiacovo MP. 2013. Heritable custom genomic modifications in Caenorhabditis elegans via a CRISPR-Cas9 system. *Genetics* **195**: 1181-1185.

User Manual C. COPAS Biosort Operator's Manual.

Valencak TG, Azzu V. 2014. Making heads or tails of mitochondrial membranes in longevity and aging: a role for comparative studies. *Longev Healthspan* **3**: 3.

van der Bent ML, Sterken MG, Volkers RJ, Riksen JA, Schmid T, Hajnal A, Kammenga JE, Snoek LB. 2014. Loss-of-function of beta-catenin bar-1 slows development and activates the Wnt pathway in Caenorhabditis elegans. *Sci Rep* **4**: 4926.

Van Gilst MR, Hadjivassiliou H, Jolly A, Yamamoto KR. 2005a. Nuclear hormone receptor NHR-49 controls fat consumption and fatty acid composition in C. elegans. *PLoS Biol* **3**: e53.

Van Gilst MR, Hadjivassiliou H, Yamamoto KR. 2005b. A Caenorhabditis elegans nutrient response system partially dependent on nuclear receptor NHR-49. *Proc Natl Acad Sci U S A* **102**: 13496-13501.

Van Raamsdonk JM, Hekimi S. 2011. FUdR causes a twofold increase in the lifespan of the mitochondrial mutant gas-1. *Mech Ageing Dev* **132**: 519-521.

Vanni P, Giachetti E, Pinzauti G, McFadden BA. 1990. Comparative structure, function and regulation of isocitrate lyase, an important assimilatory enzyme. *Comp Biochem Physiol B* **95**: 431-458.

Vellai T, Takacs-Vellai K, Zhang Y, Kovacs AL, Orosz L, Muller F. 2003. Genetics: influence of TOR kinase on lifespan in C. elegans. *Nature* **426**: 620.

Waaijers S, Boxem M. 2014. Engineering the Caenorhabditis elegans genome with CRISPR/Cas9. *Methods* **68**: 381-388.

Wahlby C, Conery AL, Bray MA, Kamentsky L, Larkins-Ford J, Sokolnicki KL, Veneskey M, Michaels K, Carpenter AE, O'Rourke EJ. 2014. High- and low-throughput scoring of fat mass and body fat distribution in C. elegans. *Methods* **68**: 492-499.

References

Wahlby C, Kamentsky L, Liu ZH, Riklin-Raviv T, Conery AL, O'Rourke EJ, Sokolnicki KL, Visvikis O, Ljosa V, Irazoqui JE et al. 2012. An image analysis toolbox for high-throughput C. elegans assays. *Nat Methods* **9**: 714-716.

Walker AK, Jacobs RL, Watts JL, Rottiers V, Jiang K, Finnegan DM, Shioda T, Hansen M, Yang F, Niebergall LJ et al. 2011. A conserved SREBP-1/phosphatidylcholine feedback circuit regulates lipogenesis in metazoans. *Cell* **147**: 840-852.

Walter L, Baruah A, Chang HW, Pace HM, Lee SS. 2011. The homeobox protein CEH-23 mediates prolonged longevity in response to impaired mitochondrial electron transport chain in C. elegans. *PLoS Biol* **9**: e1001084.

Walther TC, Farese RV, Jr. 2012. Lipid droplets and cellular lipid metabolism. *Annu Rev Biochem* **81**: 687-714.

Wang MC, Min W, Freudiger CW, Ruvkun G, Xie XS. 2011. RNAi screening for fat regulatory genes with SRS microscopy. *Nat Methods* **8**: 135-138.

Wang MC, O'Rourke EJ, Ruvkun G. 2008. Fat metabolism links germline stem cells and longevity in C. elegans. *Science* **322**: 957-960.

Wang P, Liu B, Zhang D, Belew MY, Tissenbaum HA, Cheng JX. 2014. Imaging lipid metabolism in live Caenorhabditis elegans using fingerprint vibrations. *Angew Chem Int Ed Engl* **53**: 11787-11792.

Wang S, Fusaro G, Padmanabhan J, Chellappan SP. 2002. Prohibitin co-localizes with Rb in the nucleus and recruits N-CoR and HDAC1 for transcriptional repression. *Oncogene* **21**: 8388-8396.

Wang Y, Bogenhagen DF. 2006. Human mitochondrial DNA nucleoids are linked to protein folding machinery and metabolic enzymes at the mitochondrial inner membrane. *J Biol Chem* **281**: 25791-25802.

Watkins PA, Ellis JM. 2012. Peroxisomal acyl-CoA synthetases. *Biochim Biophys Acta* **1822**: 1411-1420.

Watson E, MacNeil LT, Arda HE, Zhu LJ, Walhout AJM. 2013. Integration of metabolic and gene regulatory networks modulates the C. elegans dietary response. *Cell* **153**: 253-266.

Watson E, MacNeil LT, Ritter AD, Yilmaz LS, Rosebrock AP, Caudy AA, Walhout AJM. 2014. Interspecies Systems Biology Uncovers Metabolites Affecting C. elegans Gene Expression and Life History Traits. *Cell* **156**: 1336-1337.

Watson E, Olin-Sandoval V, Hoy MJ, Li CH, Louisse T, Yao V, Mori A, Holdorf AD, Troyanskaya OG, Ralser M et al. 2016. Metabolic network rewiring of propionate flux compensates vitamin B12 deficiency in C. elegans. *Elife* **5**.

Watts JL. 2009. Fat synthesis and adiposity regulation in Caenorhabditis elegans. *Trends Endocrinol Metab* **20**: 58-65.

Watts JL, Browse J. 2002. Genetic dissection of polyunsaturated fatty acid synthesis in Caenorhabditis elegans. *Proc Natl Acad Sci U S A* **99**: 5854-5859.

-. 2006. Dietary manipulation implicates lipid signaling in the regulation of germ cell maintenance in C. elegans. *Dev Biol* **292**: 381-392.

Watts JL, Ristow M. 2017. Lipid and Carbohydrate Metabolism in Caenorhabditis elegans. *Genetics* **207**: 413-446.

Wei Y, Chiang WC, Sumpter R, Jr., Mishra P, Levine B. 2017. Prohibitin 2 Is an Inner Mitochondrial Membrane Mitophagy Receptor. *Cell* **168**: 224-238 e210.

Weimer S, Priebs J, Kuhlow D, Groth M, Priebe S, Mansfeld J, Merry TL, Dubuis S, Laube B, Pfeiffer AF et al. 2014. D-Glucosamine supplementation extends life span of nematodes and of ageing mice. *Nat Commun* **5**: 3563.

White AG, Lees B, Kao HL, Cipriani PG, Munarriz E, Paaby AB, Erickson K, Guzman S, Rattanakorn K, Sontag E et al. 2013. DevStaR: high-throughput quantification of C. elegans developmental stages. *IEEE Trans Med Imaging* **32**: 1791-1803.

Williams RS, Harwood AJ. 2000. Lithium therapy and signal transduction. *Trends Pharmacol Sci* **21**: 61-64.

Wilson WA, Wang Z, Roach PJ. 2002. Systematic identification of the genes affecting glycogen storage in the yeast Saccharomyces cerevisiae: implication of the vacuole as a determinant of glycogen level. *Mol Cell Proteomics* **1**: 232-242.

Wojtaszewski JF, Jorgensen SB, Hellsten Y, Hardie DG, Richter EA. 2002. Glycogen-dependent effects of 5-aminoimidazole-4-carboxamide (AICA)-riboside on AMP-activated protein kinase and glycogen synthase activities in rat skeletal muscle. *Diabetes* **51**: 284-292.

Wolkow CA, Kimura KD, Lee MS, Ruvkun G. 2000. Regulation of C. elegans life-span by insulinlike signaling in the nervous system. *Science* **290**: 147-150.

Wood WB, Johnson TE. 1994. Aging. Stopping the clock. *Curr Biol* **4**: 151-153.

Woodgett JR. 1990. Molecular cloning and expression of glycogen synthase kinase-3/factor A. *EMBO J* **9**: 2431-2438.

-. 2001. Judging a protein by more than its name: GSK-3. *Sci STKE* **2001**: re12.

Woodgett JR, Cohen P. 1984. Multisite phosphorylation of glycogen synthase. Molecular basis for the substrate specificity of glycogen synthase

kinase-3 and casein kinase-II (glycogen synthase kinase-5). *Biochim Biophys Acta* **788**: 339-347.

Wu D, Pan W. 2010. GSK3: a multifaceted kinase in Wnt signaling. *Trends Biochem Sci* **35**: 161-168.

Wu Y, Williams EG, Dubuis S, Mottis A, Jovaisaite V, Houten SM, Argmann CA, Faridi P, Wolski W, Kutalik Z et al. 2014. Multilayered genetic and omics dissection of mitochondrial activity in a mouse reference population. *Cell* **158**: 1415-1430.

Wullschleger S, Loewith R, Hall MN. 2006. TOR signaling in growth and metabolism. *Cell* **124**: 471-484.

Xiao Y, Liu F, Zhao PJ, Zou CG, Zhang KQ. 2017. PKA/KIN-1 mediates innate immune responses to bacterial pathogens in Caenorhabditis elegans. *Innate Immun* **23**: 656-666.

Xu C, Kim NG, Gumbiner BM. 2009. Regulation of protein stability by GSK3 mediated phosphorylation. *Cell Cycle* **8**: 4032-4039.

Xu X, Kim SK. 2011. The early bird catches the worm: new technologies for the Caenorhabditis elegans toolkit. *Nat Rev Genet* **12**: 793-801.

Yao HB, Shaw PC, Wong CC, Wan DC. 2002. Expression of glycogen synthase kinase-3 isoforms in mouse tissues and their transcription in the brain. *J Chem Neuroanat* **23**: 291-297.

Yen K, Le TT, Bansal A, Narasimhan SD, Cheng JX, Tissenbaum HA. 2010. A comparative study of fat storage quantitation in nematode Caenorhabditis elegans using label and label-free methods. *PLoS One* **5**.

Yoneda T, Benedetti C, Urano F, Clark SG, Harding HP, Ron D. 2004. Compartment-specific perturbation of protein handling activates genes encoding mitochondrial chaperones. *J Cell Sci* **117**: 4055-4066.

Yuan R, Tsaih SW, Petkova SB, Marin de Evsikova C, Xing S, Marion MA, Bogue MA, Mills KD, Peters LL, Bult CJ et al. 2009. Aging in inbred strains of mice: study design and interim report on median lifespans and circulating IGF1 levels. *Aging Cell* **8**: 277-287.

Yuan Y, Kadiyala CS, Ching TT, Hakimi P, Saha S, Xu H, Yuan C, Mullangi V, Wang L, Fivenson E et al. 2012. Enhanced energy metabolism contributes to the extended life span of calorie-restricted Caenorhabditis elegans. *J Biol Chem* **287**: 31414-31426.

Zarse K, Terao T, Tian J, Iwata N, Ishii N, Ristow M. 2011. Low-dose lithium uptake promotes longevity in humans and metazoans. *Eur J Nutr* **50**: 387-389.

Zeng X, Huang H, Tamai K, Zhang X, Harada Y, Yokota C, Almeida K, Wang J, Doble B, Woodgett J et al. 2008. Initiation of Wnt signaling: control of

Wnt coreceptor Lrp6 phosphorylation/activation via frizzled, dishevelled and axin functions. *Development* **135**: 367-375.

Zhang P, Judy M, Lee SJ, Kenyon C. 2013. Direct and indirect gene regulation by a life-extending FOXO protein in C. elegans: roles for GATA factors and lipid gene regulators. *Cell Metab* **17**: 85-100.

Zhang P, Na H, Liu Z, Zhang S, Xue P, Chen Y, Pu J, Peng G, Huang X, Yang F et al. 2012. Proteomic study and marker protein identification of Caenorhabditis elegans lipid droplets. *Mol Cell Proteomics* **11**: 317-328.

Zhang SO, Box AC, Xu N, Le Men J, Yu J, Guo F, Trimble R, Mak HY. 2010a. Genetic and dietary regulation of lipid droplet expansion in Caenorhabditis elegans. *Proc Natl Acad Sci U S A* **107**: 4640-4645.

Zhang SO, Trimble R, Guo F, Mak HY. 2010b. Lipid droplets as ubiquitous fat storage organelles in C. elegans. *BMC Cell Biol* **11**: 96.

Zhou J, Freeman TA, Ahmad F, Shang X, Mangano E, Gao E, Farber J, Wang Y, Ma XL, Woodgett J et al. 2013. GSK-3alpha is a central regulator of age-related pathologies in mice. *J Clin Invest* **123**: 1821-1832.

Zhu F, Li Q, Zhang F, Sun X, Cai G, Zhang W, Chen X. 2015. Chronic lithium treatment diminishes the female advantage in lifespan in Drosophila melanogaster. *Clin Exp Pharmacol Physiol* **42**: 617-621.

Zimmermann C, Santos A, Gable K, Epstein S, Gururaj C, Chymkowitch P, Pultz D, Rodkaer SV, Clay L, Bjoras M et al. 2013. TORC1 inhibits GSK3-mediated Elo2 phosphorylation to regulate very long chain fatty acid synthesis and autophagy. *Cell Rep* **5**: 1036-1046.

Zimmermann R, Strauss JG, Haemmerle G, Schoiswohl G, Birner-Gruenberger R, Riederer M, Lass A, Neuberger G, Eisenhaber F, Hermetter A et al. 2004. Fat mobilization in adipose tissue is promoted by adipose triglyceride lipase. *Science* **306**: 1383-1386.

Zubovych IO, Straud S, Roth MG. 2010. Mitochondrial dysfunction confers resistance to multiple drugs in Caenorhabditis elegans. *Mol Biol Cell* **21**: 956-969.

Zugasti O, Thakur N, Belougne J, Squiban B, Kurz CL, Soule J, Omi S, Tichit L, Pujol N, Ewbank JJ. 2016. A quantitative genome-wide RNAi screen in C. elegans for antifungal innate immunity genes. *BMC Biol* **14**: 35.

ACKNOWLEDGEMENTS

He vivido en C/ San Jacinto por mucho tiempo y me gustaría expresar mi gratitud a Maria P y su madre, Encarnación por ser absolutamente maravillosos y amables. Te extrañaré. The people I have lived with over the years in this flat and the fun I have had here will always be cherished fondly.

Davis, your sagely wisdom and goofiness continue to exasperate me. I am glad you are still around.

Lastly, Mom and Dad - thank you for supporting me through all my decisions. I do not think I will ever gather enough words to express how truly blessed I am to have you by my side. Joe, though our professions are as different as chalk and cheese, just like we are - thanks for having my back, always. I hope you guys are as proud of me as I am of you.